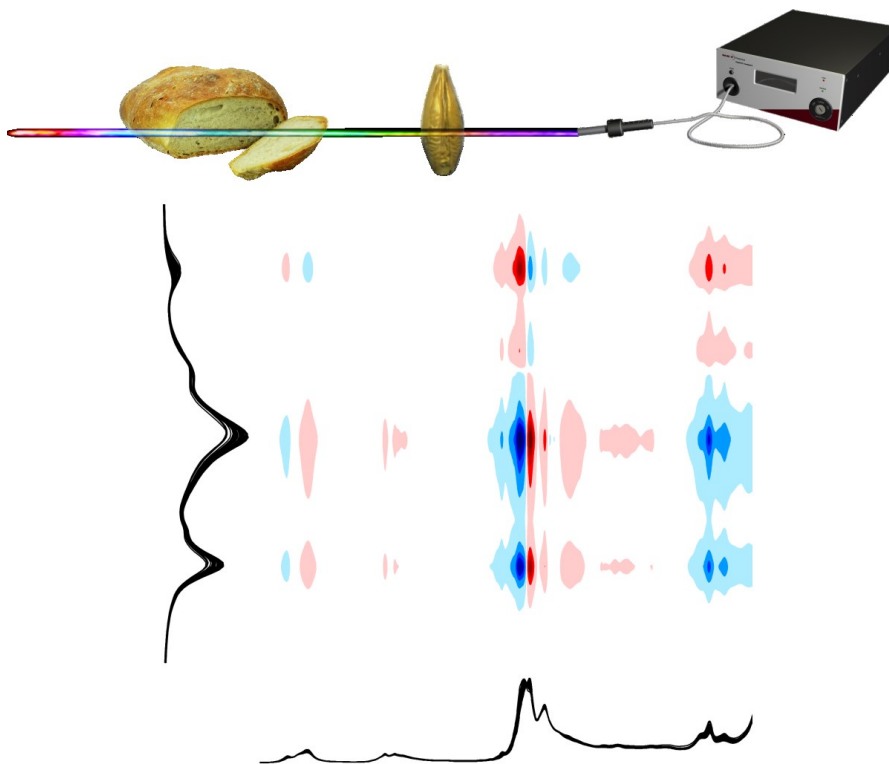




# Near infrared spectroscopy of food systems using a supercontinuum laser

PHD THESIS 2017 · TINE RINGSTED





# **Near infrared spectroscopy of food systems using a supercontinuum laser**

PhD thesis 2017

Tine Ringsted

Department of Food Science

Faculty of Science

University of Copenhagen

**Title**

Near infrared spectroscopy of food systems using a supercontinuum laser

**Submission**

March 31<sup>st</sup> 2017

**Defense**

June 19<sup>th</sup> 2017

**Supervisors**

Professor Søren Balling Engelsen

Department of Food Science, Faculty of Science, University of Copenhagen

Professor Søren Rud Keiding

Department of Chemistry, iNANO, Aarhus University

**Opponents**

Senior research scientist Jens Petter Wold

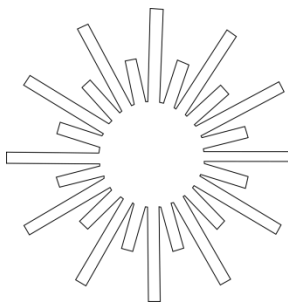
Nofima, Norway

Emeritus professor James Andries de Haseth

University of Georgia, Athens

Associate professor Frans van den Berg

Department of Food Science, Faculty of Science, University of Copenhagen



# Contents

---

<b>Preface</b>	<b>iii</b>
Acknowledgements .....	iii
List of publications .....	iv
List of abbreviations .....	vii
Abstract.....	viii
Dansk resumé.....	x
<b>1 Introduction</b>	<b>1</b>
1.1 Scope.....	1
1.2 Outline .....	2
<b>2 Theory</b>	<b>3</b>
2.1 Instrumental design of near- and mid-infrared spectrometers .....	3
2.1.1 The supercontinuum source.....	6
2.1.2 Dispersive Fourier transformation spectroscopy .....	8
2.2 Information in near- and mid-infrared spectroscopy .....	8
2.2.1 Chemical information in near and mid-infrared spectra.....	8
2.2.2 Physical information in near- and mid-infrared spectra .....	14
2.3 Multivariate modelling of near- and mid-infrared spectra .....	17
2.4 Preprocessing of near- and mid-infrared spectra .....	18
2.4.1 Noisy and irrelevant absorbance .....	19
2.4.2 Absolute absorbance variations (multiplicative effect) .....	20
2.4.3 Baseline offsets (additive effect).....	20
2.5 Near- or mid-infrared spectroscopy? That is the question .....	22
2.5.1 The influence of path-length.....	23
2.5.2 The influence of temperature.....	23
2.5.3 Comparison of near- and mid-infrared spectroscopy .....	24
2.6 Two-dimensional correlation spectroscopy.....	25
2.6.1 Calculations of two-dimensional correlation spectroscopy ...	25

2.6.2	Examples of two-dimensional correlation spectroscopy .....	28
2.6.3	Example of covarygram .....	33
2.7	Spectral interpretation with hydrogen–deuterium exchange.....	34
<b>3</b>	<b>Advantages of using a supercontinuum laser in food analysis</b>	<b>39</b>
3.1	Long-wavelength near-infrared spectroscopy of barley seeds .....	39
3.1.1	Aim .....	40
3.1.2	Experimental setup .....	40
3.1.3	Results.....	41
3.1.4	Discussion, concluding remarks and perspectives.....	41
3.2	Potential for supercontinuum gas measurements .....	46
3.3	Supercontinuum light and a wavelength separating fiber .....	48
3.3.1	Aim .....	48
3.3.2	Experimental setup .....	48
3.3.3	Results.....	51
3.3.4	Discussion, concluding remarks and perspectives.....	54
<b>4</b>	<b>Spectral interpretation with two-dimensional correlation spectroscopy</b>	<b>57</b>
4.1	Wheat bread aging (staling) .....	57
4.1.1	Aim .....	58
4.1.2	Experimental setup .....	58
4.1.3	Results.....	59
4.1.4	Discussion, concluding remarks and perspectives.....	60
4.2	Barley phenotype characterization .....	62
<b>5</b>	<b>Conclusions and perspectives</b>	<b>67</b>
	<b>References</b>	<b>69</b>
	<b>Appendix: List of spectrometers</b>	<b>79</b>
	<b>Papers I-III</b>	
	<b>Proceeding</b>	
	<b>Poster I-IV</b>	

# Preface

This PhD study was carried out at the Department of Food Science, Faculty of Science, University of Copenhagen. The work was part of the Light & Food project, which was a collaboration between University of Copenhagen, The Technical University of Denmark (DTU), Aarhus University, FOSS and NKT Photonics. The project was financially supported by The Danish National Advanced Technology Foundation (now Innovation Fund Denmark).

## Acknowledgements

I am very grateful for the opportunity to work in a research group where a friendly and humoristic atmosphere is mixed well with top class science. I am especially thankful for all the interesting discussions with my supervisor Professor Søren B. Engelsen who could keep talking about science even on the train ride back to Copenhagen after a long day at Aarhus University. I also highly appreciate all the good discussions on instrumentation and process measurements with Associate Professor Frans van den Berg.

The Light & Food partners from Aarhus University, DTU, FOSS and NKT Photonics have all been very helpful. This project was truly a collaboration and I could not have done all the exciting work with the supercontinuum light without their expertise. I would particularly like to thank Professor Søren Rud Keiding and his group at Aarhus University for their committed work on the spectrometers for barley measurements. I am also very thankful for the big effort at FOSS laid on the dispersive Fourier transformation spectrometer.

I am very happy for the opportunity to visit Professor Heinz W. Siesler at the University of Duisburg-Essen for 1.5 month. Besides the interesting experiments with deuterium, I also very much liked our discussions on near-infrared vs. mid-infrared spectroscopy.

I would like to thank everybody at the Chemometrics and Analytical Technology (CAT) group for fun discussions at lunch, for crazy Christmas lunches, for great summer parties and learning about cultures from all over the world.

Finally, I would like to thank my family and my friends for all their support and for making me laugh and take my mind off the PhD. I would also like to give a special thanks to my boyfriend Matteo for being understanding, supportive and a good chef.

# List of publications

## Peer-reviewed publications

### PAPER I

Ringsted, T., Dupont, S., Ramsay, J., Jespersen, B.M., Sørensen, K.M., Keiding, S.R., Engelsen, S.B., 2016. Near-infrared spectroscopy using a supercontinuum laser: application to long wavelength transmission spectra of barley endosperm and oil. *Applied Spectroscopy* 70, 1176-1185.

### PAPER II

Ringsted, T., Siesler, H.W., Engelsen, S.B., 2017. Monitoring the staling of wheat bread using 2D MIR-NIR correlation spectroscopy. *Journal of Cereal Science* 75, 92-99.

### PAPER III

Ringsted, T., Ramsay, J., Jespersen, B.M., Keiding, S.R., Engelsen, S.B. Long wavelength near-infrared transmission spectroscopy of barley seeds using a supercontinuum laser: prediction of beta-glucan content. *Analytica Chimica Acta*. Manuscript submitted March 2017.

## **Other publications**

### **PROCEEDING**

Ringsted, T., Dupont, S., Ramsay, J., Jespersen, B.M., Sørensen, K.M, Keiding, S.R., Engelsen, S.B. Long wavelength near-infrared transmission spectra of barley endosperm and oil using a supercontinuum laser. Proceedings of the 17th International Conference on Near Infrared Spectroscopy (ICNIRS 2015). Foz do Iguassu, Brazil, 2015.

### **POSTER I**

Ringsted, T., Dupont, S., Ramsay, K.M., Keiding, S.R., Engelsen, S.B. 2D NIR-MIR correlation spectroscopy A useful tool to augment the interpretation of NIR spectra. 8th International Symposium on Two-Dimensional Correlation Spectroscopy (2DCOS-8). Vienna, Austria, 2015.

### **POSTER II**

Ringsted, T., Dupont, S., Ramsay, J., Keiding, S.R., Engelsen, S.B. Near-infrared spectroscopy using a supercontinuum laser. Application to long-wavelength transmission spectra of barley seeds. 8th International Conference on Advanced Vibrational Spectroscopy (ICAVS 8). Vienna, Austria, 2015.

### **POSTER III**

Ringsted, T., S.R., Engelsen, S.B. 2D NIR-MIR correlation spectroscopy - A useful tool to augment the interpretation of NIR spectra. 17th International Conference on Near Infrared Spectroscopy (ICNIRS 2015). Foz do Iguassu, Brazil, 2015.

*Awarded best poster.*

### **POSTER IV**

Ringsted, T., Dupont, S., Ramsay, J., Jespersen, B.M, Keiding, S.R., Engelsen, S.B. Near-infrared spectroscopy using a supercontinuum laser - Application to long-wavelength transmission spectra of barley seeds. International Diffuse Reflectance Conference (IDRC). Chambersburg, USA, 2016.

*Awarded honorable mentioning.*

## **POSTER V**

Ringsted, T., Engelsen, S.B. 2D NIR-MIR covariance spectroscopy - Augmenting the interpretation of NIR spectra of bread staling. International Diffuse Reflectance Conference (IDRC). Chambersburg, USA. 2016.

*Awarded 3<sup>rd</sup> best student poster.*

# List of abbreviations

1OT-NIR	1 <sup>st</sup> Overtone Near-InfraRed
2D	Two-Dimensional
2DCOS	Two-Dimensional Correlation Spectroscopy
AOTF	Acousto-Optic Tunable Filter
ATR	Attenuated Total Reflectance
CV	Cross-Validation
EMSC	Extended Multiplicative Scatter Correction
DCF	Dispersion Compensating Fiber
FT	Fourier Transform
FT-IR	Fourier Transform InfraRed
FT-NIR	Fourier Transform Near-InfraRed
FWHM	Full Width at Half Maximum
LEDs	Light-Emitting Diodes
LW-NIR	Long Wavelength Near-InfraRed
MIR	Mid-InfraRed
MSC	Multiplicative Scatter Correction
NAS	Net Analyte Signal
NIR	Near-InfraRed
NIR/VIS	Near-InfraRed/VISible
PARAFAC	PARAllel FACtor analysis
PCA	Principal Component Analysis
PLS	Partial Least Squares
RMSECV	Root Mean Square Error of Cross-Validation
SNV	Standard Normal Variate
S/N	Signal/Noise
SW-NIR	Short Wavelength Near-InfraRed
VOCSY	Vibrational Overtone Combination SpectroscopY

# Abstract

Mid-infrared and particularly near-infrared spectroscopy is extremely useful for food analysis because they measure chemical and physical properties fast and non-destructively. The advancement of a supercontinuum light source covering the near-infrared and parts of the ultraviolet and mid-infrared regions, gives new possibilities in spectroscopy. The theoretical advantages are: (a) that the supercontinuum light does not illuminate in all directions and therefore do not heat the surrounding spectrometer components, (b) that the beam is collimated and therefore a high spectral brightness ( $W/(m^2 \cdot nm)$ ) can be obtained, (c) that the supercontinuum light is fiber compatible i.e. it can couple directly to fibers, and (d) that the fast repetition rate of the supercontinuum pulses makes it possible to do very fast measurements.

For these reasons, the supercontinuum light stands out from the commonly applied near- and mid-infrared incandescent light bulbs. This thesis aim to explore the utility of using a supercontinuum source in two food applications. (1) The supercontinuum light was applied for the first time to barley seeds in transmission mode in the long wavelength near-infrared region from 2260-2380 nm. From these spectra it was possible to predict the  $\beta$ -glucan content of individual seeds. The measurements of single seeds can be used in plant breeding to sort according to trait or in grain industries to sort according to quality or property. (2) The supercontinuum light has been used with a new wavelength separation method called dispersive Fourier transformation. Different wavelengths travel at different speed through a dispersive element, which in this case is a 10.6 km long silica fiber, and the polychromatic light pulses will therefore be separated by wavelength. The signal will then be transformed from the time-domain to a frequency domain. The spectrometer has no moving parts, which makes it insensitive to mechanical vibrations. A spectrometer with a wavelength separating fiber is therefore an obvious candidate for industrial process measurements. This thesis presents preliminary results on sucrose in water and melamine in milk powder using a supercontinuum light and a dispersive fiber from 1300-1650 nm. The possibility for the new spectrometer to measure  $\beta$ -glucan in barley and bread hardness in aging bread was evaluated by calculating Pearson's correlation coefficients. The spectral correlation to  $\beta$ -glucan and bread hardness showed  $r^2$  values equal to 0.98 and 0.94, respectively.

The interpretation of near- and mid-infrared spectra can be difficult due to, for instance, overlapping absorbance bands, overtones, combination bands, coupling, Fermi resonance and matrix effects. Two-dimensional correlation spectroscopy was

applied to near- and mid-infrared spectra of aging bread to aid interpretation. The well-known information on starch recrystallization in aging bread was followed by mid-infrared spectroscopy and correlated to the near-infrared spectra to increase spectral interpretation. The unwanted physico-chemical changes that happen during bread aging, called staling, was quantified by bread hardness. The analysis revealed that the 1<sup>st</sup> overtone near-infrared region at 1688 nm, the long wavelength near-infrared region at 2288 nm and the mid-infrared at 1047 cm<sup>-1</sup> exhibited the highest correlations to bread hardness. A principal component analysis (PCA) was carried out from 2150-2370 nm and 1100-850 cm<sup>-1</sup>, separately. The high correlation ( $r^2$  equal to 0.98) observed between the two 1<sup>st</sup> principal component scores indicates that near- and mid-infrared spectroscopy measure the same staling phenomena.

In conclusion, this work shows that it is possible to use a supercontinuum source for spectroscopy measurements on intact barley seeds in transmission mode in the long wavelength near-infrared region. The supercontinuum light has advantages in combination with a wavelength separating fiber. However, this application needs further experimental studies to be confirmed in its usefulness. The interpretation of near-infrared spectra can be enhanced by the correlation to other infrared spectra with a more clear interpretation.

# Dansk resumé

Midt-infrarød og især nær-infrarød spektroskopi er meget brugbar til analyse af fødevarer, da de måler kemiske og fysiske egenskaber hurtigt og ikke-destruktivt. Den nyligt lancerede superkontinuum lyskilde dækker det nær-infrarøde og dele af det ultraviolette og midt-infrarøde område, og giver nye muligheder i spektroskopi. De teoretiske fordele er: (a) at superkontinuum lyskilden ikke lyser i alle retninger og derfor ikke opvarmer de omgivende komponenter i et spektrometeret, (b) at lysstrålen er kollimeret og en høj spektral lysstyrke ( $W/(m^2 \cdot nm)$ ) kan opnås, (c) at superkontinuum lyskilden er fiber kompatibel dvs. den kan kobles direkte til fibre, og (d) at den hurtige repetitions-hastighed af superkontinuum pulser, gør det muligt at udføre meget hurtige målinger.

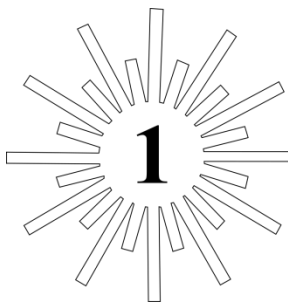
En superkontinuum lyskilde skiller sig ud fra de almindeligt anvendte nær- og midt-infrarøde glødepærer pga. de ovennævnte egenskaber. Denne afhandling satte sig for at undersøge mulighederne for en superkontinuum lyskilde anvendt på fødevarer i to tilfælde. (1) en superkontinuum lyskilde blev anvendt for første gang på bygkorn til at måle transmission af lange nær-infrarøde bølgelængder fra 2260-2380 nm. Fra disse spektre var det muligt at forudsige  $\beta$ -glucan indholdet af individuelle kerner. Målinger på hver enkelt kerne kan bruges i planteforædling til at sortere efter egenskaber eller i korn industrier til at sortere efter kvalitet eller kemiske komponent. (2) en superkontinuum lyskilde har været brugt med en ny bølgelængde separationsmetode som hedder dispersiv Fourier transformation. Forskellige bølgelængder bevæger sig med forskellig hastighed gennem et dispersivt element, i dette tilfælde en 10,6 km lang silica fiber, og de polykromatiske lyspulser vil derfor adskilles efter bølgelængde. Signalet vil dernæst blive transformeret fra tidsdomænet til et frekvens-domæne. Spektrometeret har ingen bevægelige dele, hvilket gør det ufølsomt over for mekaniske vibrationer. Et spektrometer med en bølgelængde adskillende fiber er derfor et fordelagtigt instrument til industrielle procesmålinger. Denne afhandling viser foreløbige resultater på målinger af sucrose i vand og melamin i mælkepulver under anvendelse af en superkontinuum lyskilde og en dispersiv fiber fra 1300-1650 nm. Muligheden for målinger med det nye spektrometer til bestemmelse af  $\beta$ -glucan i byg og brød hårdhed i aldrende brød blev evalueret ved at beregne Pearsons korrelations koefficienter. Den spektrale korrelation til  $\beta$ -glucan og brød hårdhed viste  $r^2$ -værdier på hhv. 0,98 og 0,94.

Fortolkningen af nær- og midt-infrarøde spektre kan være vanskelig på grund af for eksempel overlappende absorptions toppe, overtoner, kombinations bånd, kobling,

Fermi resonans og matrix effekter. To-dimensionel korrelation spektroskopi blev anvendt til at øge fortolkningen af nær- og midt-infrarøde spektre af aldrende brød. Den kendte information af re-krystallisering af stivelse i aldrende brød blev fulgt med midt-infrarød spektroskopi og korreleret til de nær-infrarøde spektre for at øge den spektrale fortolkning. De uønskede fysisk-kemiske ændringer, der sker i løbet af brød aldring, kaldet staling, blev kvantificeret ved brød hårdhed. Analysen viste, at 1. overtone i det nær-infrarøde område ved 1688 nm, de lange bølgelængder i det nær-infrarøde område ved 2288 nm, og det midt-infrarøde ved 1047  $\text{cm}^{-1}$  udviste de højeste korrelationer til brød hårdhed. En principal komponent analyse blev udført separat fra hhv. 2150-2370 nm og 1100-850  $\text{cm}^{-1}$ . Den høje korrelation ( $r^2$  på 0,98) observeret mellem de to første score komponenter angiver, at nær- og midt-infrarød spektroskopi måler samme ældningsfænomen.

Afslutningsvis viser dette arbejde, at det er muligt at anvende en superkontinuum lyskilde til transmission målinger på intakte bygkorn ved de lange bølgelængder i nær-infrarød spektroskopi. En superkontinuum lyskilde i kombination med en bølgelængde separerende fiber har fordelagtige egenskaber. Men denne kombination kræver yderligere eksperimentelle undersøgelser, til at bekræfte dens brugbarhed. Fortolkningen af nær-infrarøde spektre kan forbedres ved korrelationen til andre infrarøde spektre med en mere klar fortolkning.





# Introduction

---

*...since it is ascertained that we have rays of heat which give no light, it can only become a subject of inquiry whether some of these heat-making rays may not have a power of rendering objects visible, superadded to their now already established power of heating bodies.*

— Sir William Herschel, 1880

## 1.1 Scope

The increased industrialization of food production in the last century has led to big production sites with a fast and huge generation of food and beverages for the exploding city populations. At the same time, there has been an increased demand from consumers for safe and high quality products. These requirements can only be fulfilled by controlling the production and doing quality checks on the finished product. Both mid-infrared (MIR) and near-infrared (NIR) spectroscopy have been used to analyse many food products.<sup>1,2</sup> Their advantages are (a) that they measure fast, from milliseconds to minutes, (b) that they can measure several quality traits at the same time, (c) that they are non-destructive and (d) that they are environmentally friendly because they do not use chemicals.<sup>1,3</sup> The detection of minor components present at less than 0.1% can be difficult, but it depends on the quality trait being measured and the food matrix.<sup>1,4</sup> NIR and MIR spectroscopy are therefore obvious candidates in automated and systematic food quality measurements and may even extend to 100 % quality control.

The supercontinuum source is collimated like a laser with a broad spectral range like a bulb. The first commercial supercontinuum light source became available in 2003 (NKT Photonics, Denmark) for the NIR region and is currently being developed to go further into the UV and MIR region.<sup>5,6</sup> The commonly used incandescent light bulbs for NIR and MIR spectroscopy have been developed over many years and they are stable and relatively low cost sources. The supercontinuum source cannot compete on price with incandescent light bulbs. Instead it should be applied

when its ability to not heat its surroundings, the collimated beam, the fiber compatibility and fast pulse repetition rate is an advantage. This is for instance the case in gas spectroscopy, remote sensing and microscopy. So far the supercontinuum light has been limited to special applications within gas-phase spectroscopy and microscopy<sup>5</sup> as well as in a hyperspectral imaging application.<sup>7</sup> This thesis set out to investigate the possible applications of supercontinuum light used in NIR spectroscopy on food products.

The NIR region can be difficult to interpret because of for instance overlapping peaks, coupled vibrations and matrix effects. The fundamental absorbance bands in the MIR are repeated as overtones and combination bands in the NIR. The relation between MIR and NIR can be studied with two-dimensional (2D) correlation spectroscopy for improved spectral interpretation.<sup>8</sup> It was the aim of this thesis to apply 2D correlation spectroscopy on NIR and MIR spectra in order to augment the spectral interpretation and increase our knowledge about which NIR or MIR region to use for the measurement of bread aging and barley  $\beta$ -glucan content.

## 1.2 Outline

- **Chapter 2: Theory**

The chapter will give an introduction to NIR and MIR spectroscopy instrumentation. In addition, the chemical and physical information in NIR and MIR spectroscopy, data analysis and a comparison between NIR and MIR spectroscopy is described. Finally, spectral interpretation with 2D correlation spectroscopy and deuteration is demonstrated.

- **Chapter 3: Advantages of using a supercontinuum laser in food analysis**

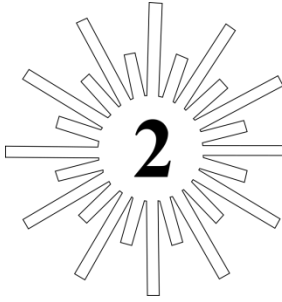
The experimental results of applying a supercontinuum source in NIR spectroscopy to single barley seeds are presented. Then a theoretical evaluation of gas measurements with a supercontinuum source in infrared spectroscopy is given. Lastly, experimental results of a supercontinuum source in combination with a new instrument principle using a fiber as the dispersive element.

- **Chapter 4: Spectral interpretation with two-dimensional correlation spectroscopy**

A discussion is given on the experimental results of bread staling processes interpreted by 2D NIR-MIR spectroscopy and deuterium exchange. In addition, experimental results of NIR and MIR spectra of barley flour and the search for  $\beta$ -glucan information is investigated.

- **Chapter 5: Conclusions and perspectives**

A summary of the results and an outreach of future experiments to be performed and the future of the supercontinuum light.



*By convention sweet is sweet, by convention bitter is bitter, by convention hot is hot, by convention cold is cold, by convention colour is colour. But in reality there are atoms and the void. That is, the objects of sense are supposed to be real and it is customary to regard them as such, but in truth they are not. Only the atoms and the void are real.*

— Democritus of Abdera, 470 B.C. - 380 B.C.

## 2.1 Instrumental design of near- and mid-infrared spectrometers

Spectrometers for the NIR and MIR have three main components, namely a light source, a wavelength separation method and a detector (Figure 2-1).

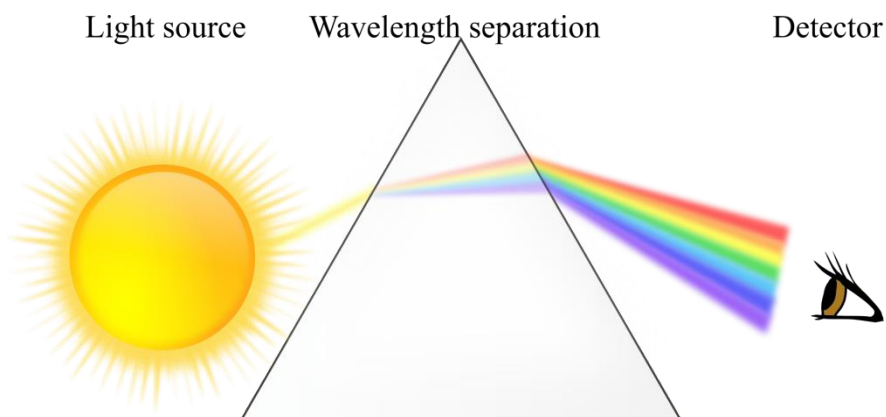


Figure 2-1. The three main components in NIR and MIR spectrometers are a light source, a wavelength separation method and a detector. The sun, a glass prism and the eye were the three components that Sir Isaac Newton used in his famous experiments where he separated the white sun light into colors.

This section will mention some of the most common MIR and NIR spectrometers and their light sources. For a more detailed description on spectrometer hardware the reader is referred to other references.<sup>9-12</sup> NIR and MIR spectrometers are commonly grouped by the technology used to separate wavelengths. Most MIR spectrometers today are Fourier transform infrared (FT-IR) spectrometers which use an interferometer to separate the light into a time-domain followed by a Fourier transformation into a frequency domain (Table 2-1). Another group of instruments are named scanning-grating or dispersive instruments and they use a monochromator which has a moving grating that bit by bit scans several wavelengths. For NIR spectrometers there is a bigger variation in wavelength separation technologies. On top of the scanning-grating and FT instruments, some NIR spectrometers apply a fixed-grating where the non-moving grating spreads out the light source onto a detector array. Another type of NIR spectrometer can be used to measure discrete wavelengths by applying optical filters. Yet another technology for NIR spectrometers uses an acousto-optic tunable filter (AOTF), which is a crystal that works essentially as a bandpass filter that can be electronically tuned very rapidly to scan a large spectral region. NIR spectrometers also apply discrete wavelength light sources named light-emitting diodes (LEDs), which can be an advantage in compact portable instruments. The bandwidths of LEDs are on the order of 100 nm so several light sources are needed to generate a full NIR spectrum.<sup>11</sup>

Table 2-1. Common wavelength separation methods and broad band light sources used in NIR and MIR spectrometers.

Region	Wavelength separation	Source
MIR	Scanning-grating	Nernst glower
	Fourier transform	SiC rod (Globar®, Norton)
		Mercury lamp Synchrotron
NIR	Scanning-grating	Tungsten-halogen lamp
	Fourier transform	Xenon lamp
	Fixed-grating	Arc lamp
	Filter	
	AOTF LEDs	

Optical fibers are another technology that is useful, especially in process applications because it allows several probes to be connected to one instrument. In addition, the instrument can be placed away from the process line. For NIR spectroscopy

py the most common fiber used is the low - hydroxyl silica fiber.<sup>11,13</sup> Optical fibers for the MIR region have limited applications and they are usually not more than a few meters in contrast to the silica fibers which can be hundreds of meters practically without loss.<sup>14</sup>

The Nernst glower shown in Figure 2-2A was the preferred light source for MIR spectroscopy for several decades and it was used in some of the earliest commercial spectrometers developed in the 1920's.<sup>15</sup> A common light source used in today's MIR spectrometers uses a silicon carbide (SiC) rod where the Global<sup>®</sup> or the Norton source are common examples.<sup>12,16</sup> At wavenumbers below  $100\text{ cm}^{-1}$ , the Global has a low intensity and it is common to use a mercury lamp from  $50\text{ cm}^{-1}$  and until the microwave region.<sup>17</sup> The most powerful MIR source is the synchrotron source. However, synchrotron sources are big, very expensive and not available many places. Synchrotron sources are therefore not applicable in mass-produced commercial spectrometers.<sup>17</sup>



Figure 2-2. (A) The Nernst lamp with a ceramic rod by courtesy of Landesmuseum für Technik und Arbeit in Mannheim, Germany. (B) The halogen lamp with tungsten filament and halogen gas inside a glass capsule from a dispersive NIR spectrometer (6500, NIR systems, Inc.). Figure A is from [www.commonswikimedia.org](http://www.commonswikimedia.org).

The far most used broad band light source for NIR spectroscopy is the tungsten-halogen lamp in Figure 2-2B.<sup>10,11,18</sup> However, other light sources such as the xenon and arc lamp are possible alternatives.<sup>19,20</sup> However, the high cost and low stability have made them less favorable compared to the tungsten-halogen lamp.<sup>19</sup>

### 2.1.1 The supercontinuum source

The supercontinuum light combines the broad spectral range of a lamp with the collimated beam of a laser. It is generated from a high power source entering a material which results in non-linear processes that broadens the initial pulses to a spectrum as seen in Figure 2-3 which is seeded with a 1064 nm laser. The first supercontinuum generation was reported in 1970 by Alfano and Shapiro<sup>21</sup>. Today's commercial supercontinuum light is generated with a pump source, which is commonly a pulsed pico- or nano-second laser that is broadened in photonic crystal fibers.<sup>5,22,23</sup> Photonic crystal fibers are fibers with a microstructure that guides the light as shown in Figure 2-4. The most common material for the fibers is silica glass. The high absorbance from silica above 2400 nm makes it necessary to use other fiber materials to generate MIR supercontinuum sources. The world record in research generated MIR supercontinuum sources was generated in an ultra-high numerical-aperture chalcogenide step-index fiber from 1.4 – 13.3  $\mu\text{m}$  (7143 to 752  $\text{cm}^{-1}$ ).<sup>6</sup>

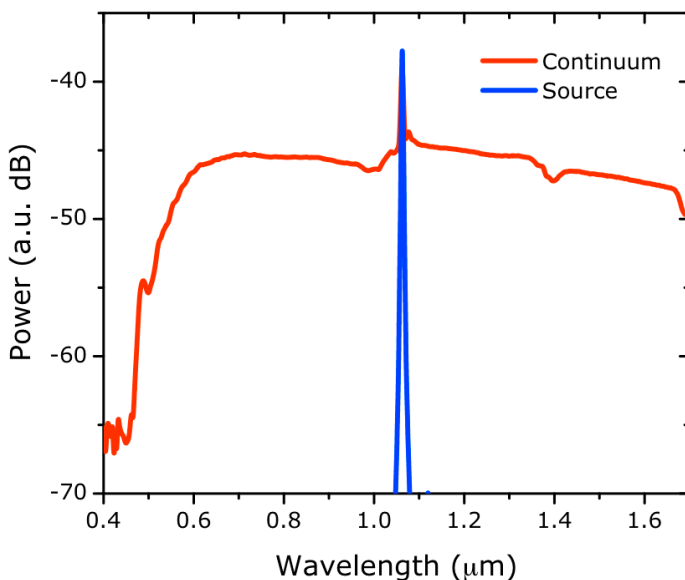


Figure 2-3. A spectrum of the pump source (blue) and the broad supercontinuum spectrum (red) generated in a photonic crystal fiber. The figure is from [www.commonswikimedia.org](http://www.commonswikimedia.org).

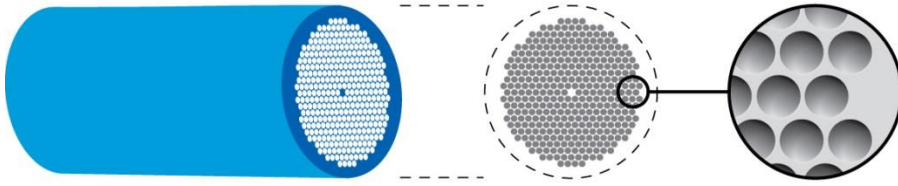


Figure 2-4. Photonic crystal fiber with a blue coating, a cladding with air holes and, in the middle, the core guiding the light. The figure is from [www.commons.wikimedia.org](http://www.commons.wikimedia.org).

A comparison between the spectrum of a light bulb, the sun and a supercontinuum source can be seen in Figure 2-5. Some of the characteristics of the supercontinuum source are: (a) that the supercontinuum light does not radiate in all directions and local overheating is therefore avoided, (b) that the beam is collimated and a high spectral brightness ( $W/(m^2 \cdot nm)$ ) can be obtained, (c) that the supercontinuum light exits from a fiber and it can therefore be coupled directly to fibers, and (d) that the fast repetition rate of pico- or nano-second pulses makes it possible to do very fast measurements.

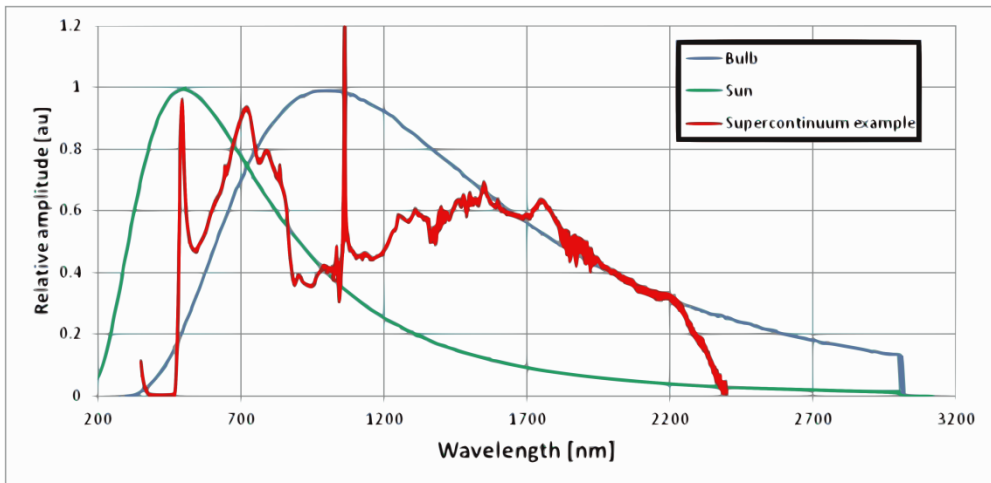


Figure 2-5. Spectra of a light bulb, the sun and a supercontinuum source. Figure by courtesy of NKT Photonics.

## 2.1.2 Dispersive Fourier transformation spectroscopy

Optical fibers can be used to guide light from one point to another. However, optical fibers have also recently been used as the wavelength separating element in dispersive Fourier transformation spectroscopy.<sup>24</sup> The principle behind this method is that a polychromatic pulse is passing a dispersive element such as a very long optical fiber where the wavelengths will move a different speed and hence separate (Figure 2-6). The wavelengths are now separated in time and a Fourier transformation will transform the signal into a frequency domain. This method will be investigated further in Section 3.3.

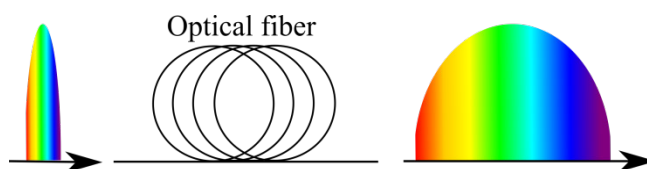


Figure 2-6. In dispersive Fourier transformation a dispersive element such as an optical fiber works as the wavelength separating method, where the fiber separates the different wavelengths in time.

## 2.2 Information in near- and mid-infrared spectroscopy

The infrared region is typically divided into the NIR (800-2500 nm), the MIR (2.5-25  $\mu\text{m}$ ) and the far-infrared (25-500  $\mu\text{m}$ ).<sup>9</sup> This thesis will focus on the NIR and MIR regions because of their utility in food analysis.

### 2.2.1 Chemical information in near- and mid-infrared spectra

Molecular vibrations are the periodic movement of atoms with no overall change in the movement of a molecule. All molecules exhibit molecular vibrations on an atomic level and many of these vibrations absorb NIR and MIR light. The molecular vibrations that absorb light are associated with a change in the polarity of the bonds, also called a *dipole moment*. Water is an example of a molecule with a strong dipole moment where the electronegativity of the oxygen atom is stronger than the electronegativity of the hydrogen atom, thus creating polarized bonds (Figure 2-7). In larger more complex molecules all molecular vibrations will absorb to some degree. However, the level of absorbance is higher for molecular vibrations with a greater dipole moment.<sup>25</sup>

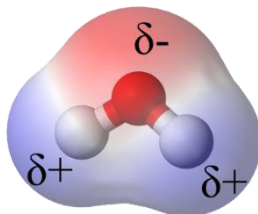


Figure 2-7. The bonds in a water molecule are more negatively charged close to the oxygen atom and more positively charged close to the hydrogen atoms. The polarity of a chemical bond is called the dipole moment. The figure is from [www.commonswiki.org](http://www.commonswiki.org).

The vibrations in a molecule can be described as different basic movements, as for instance a change in bond lengths (stretching), a change in bond angle (bending/deformation) and rotation/libration. The basic vibrations, also named *normal modes*, of water are shown in Figure 2-8.

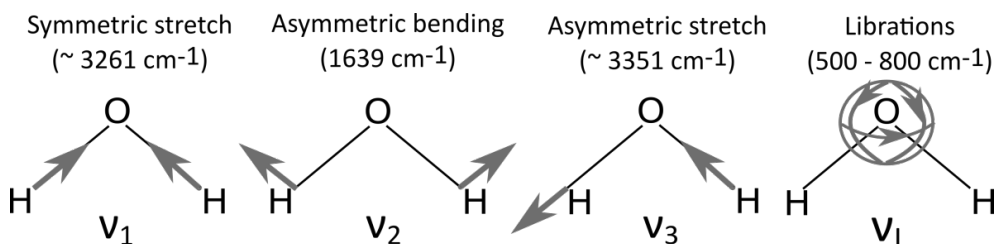


Figure 2-8. The normal modes of water.<sup>26,27</sup>

A vibrating bond absorbs light when the light wave and the vibrating bond have the same resonant frequency. This is detected as *absorbance bands* in NIR and MIR spectroscopy. In addition to the fundamental absorbance bands, absorbance bands due to the *overtone*s of fundamental vibrations appear at approximately the frequencies of a fundamental vibration multiplied by an integer. This means that the absorbance band of the 1<sup>st</sup>, 2<sup>nd</sup> and 3<sup>rd</sup> overtone absorbs at approximately 2, 3 and 4 times the frequency of the fundamental vibration, respectively.

Also absorbance bands from *combination tones* are generated and they absorb at the frequencies which are almost the sum of frequencies of fundamental and/or overtone vibrations. In order for vibrations to be joined in combination bands they have to be of the same functional group and have the same symmetry.<sup>28,29</sup> The intensities of overtones and combination bands are stronger for vibrations with both a high

dipole moment and a high *anharmonicity*. This is the case for vibrations involving hydrogen atoms as for instance C-H, N-H and O-H which have relatively low dissociation energies and thus a more anharmonic potential energy curve. The NIR region consists mainly of overtones and combination bands and C-H, N-H and O-H groups are therefore strong and primary absorbers here. Figure 2-9 shows an example of the MIR and NIR spectrum of water displaying the absorbance bands from fundamental, overtone and combination vibrations. Figure 2-9 depicts both wavelength and wavenumber for the NIR and MIR region but in the following the NIR will generally be plotted with wavelength and MIR with wavenumber because the areas with larger absorbance bands are more spread out. The MIR spectra in this thesis have been measured with the Attenuated Total Reflectance (ATR) element (described in Section 2.2.2) and the spectra will therefore be slightly different from MIR transmission spectra. This is due to that the sample penetration depth of the ATR is wavelength dependent.<sup>30</sup> The linear relationship between penetration depth and wavenumber can be used to calculate the transmission spectra with an *ATR correction*. Since the purpose of this work was not to compare ATR and transmission spectra then the ATR correction was not applied in this work.

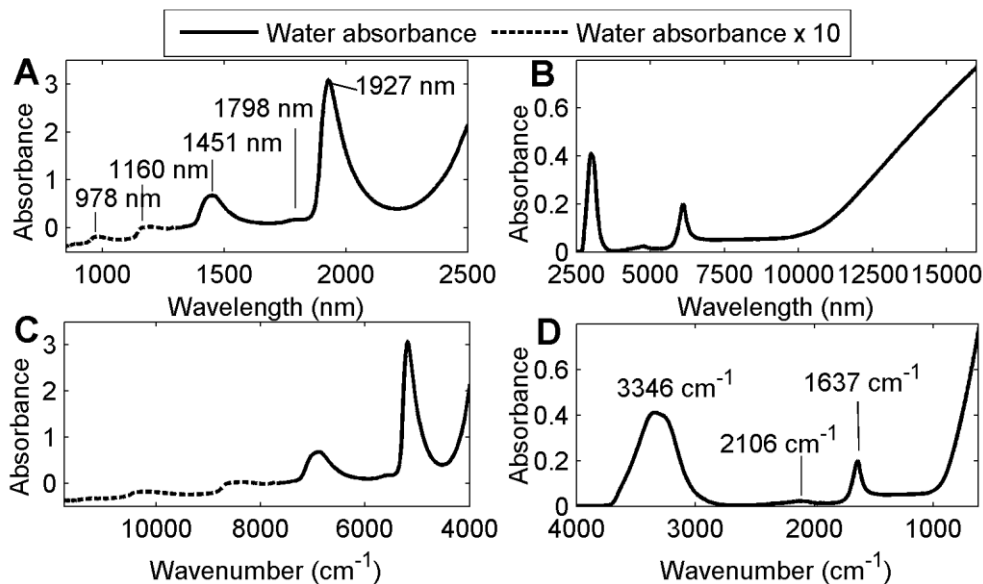


Figure 2-9. Water measured on a FT-NIR spectrometer (FTLA2000-160, ABB Bomem) with 0.5 mm pathlength and on a FT-IR spectrometer (MB100, ABB Bomem) on a 3-bounce diamond ATR. (A) NIR spectra on wavelength axis. (B) MIR spectra on wavelength axis. (C) NIR spectra on wavenumber axis. (D) MIR spectra on wavenumber axis.

The vibrations of bonds in a molecule are not always independent of neighboring atoms and this is known as *coupling*. This is the case for amino acids and proteins where the vibrations of adjacent C=O, C-N and N-H are coupled in the commonly known “amide I” and “amide II” vibrations.<sup>25</sup> Coupling is also common between adjacent bonds of C–C stretching, C–O stretching, C–N stretching and C–H bending.<sup>31</sup>

*Fermi and Darling-Dennison resonance* are effects that complicates spectral interpretation because it changes the frequency position and intensity of two neighboring absorbance bands.<sup>32</sup> This can occur for absorbance bands which have almost the same frequency and are from the same functional group with the same symmetry. If the resonance is between a fundamental vibration and an overtone or combination band then it is called Fermi resonance and if it is between overtones and combination bands then it is called Darling-Dennison resonance.<sup>33</sup>

Another effect observed when going from lower to higher order overtones is that the spectra become simpler. This has been called the *local mode* phenomena and is interpreted as a decoupling between the vibrating bonds in a normal mode.<sup>25</sup> The idea behind the local mode model is to treat a molecule as if it was made up of diatomic vibrations. The switch from normal to local mode phenomena is about  $\geq 3^{\text{rd}}$  overtone.<sup>32</sup>

The frequencies of fundamental vibrations together with their anharmonicity constants can be used to calculate possible frequencies of overtones and combination bands.<sup>34</sup> As an example, Table 2-2 shows the assignment of the water bands in the NIR and MIR region. Notice the increased complexity of band assignments when going from the MIR to the NIR region even for a simple molecule like water. The assignment of NIR and MIR absorbance bands have been done in several reviews,<sup>35,36</sup> but it is advisable to also consult specific litteratur for the sample of interest because of the complex nature of NIR and MIR spectra.

*Neighboring functional groups* can affect NIR and MIR absorption bands of specific functional groups (*group frequencies*). The effect is more pronounced for strong electron withdrawing and electron donating groups because they can change the bond strength and dipole moment of the surrounding atoms.<sup>25</sup> Figure 2-10 shows the spectra of acetic acid and ethanol which both have a CH<sub>3</sub> and an OH group, but the absorbance bands do not have maxima at the exact same frequencies. In Figure 2-11, the spectra of Nujol (a pure mineral oil with long hydrocarbon chains) and olive oil (with esters, unsaturation and glycerol skeleton functionality) shows how some functional groups will not have a large effect on neighboring groups. The olive oil and the Nujol sample both contains CH<sub>2</sub>-CH<sub>2</sub> bonds but the olive oil also

contains esters and CH=CH which the Nujol sample does not have. The peak maxima's in olive oil and Nujol are very similar because the esters and CH=CH groups does not cause a significant change in the frequencies of the CH<sub>2</sub> absorbance bands and more importantly because the esters and double bonds are outnumbered compared to the CH<sub>2</sub> groups.

Table 2-2. MIR and NIR band assignments of water. The normal modes of water ( $\nu_1$ ,  $\nu_2$ ,  $\nu_3$  and  $\nu_L$ ) are explained in Figure 2-8.

Region	Frequency (cm <sup>-1</sup> )	Wavelength (nm)	Assignment	Reference
MIR	500-800	20,000 - 12,500	$\nu_L$	27,37
	1637	6109	$\nu_2$	27,37-39
	2106	4748	$\nu_2 + \nu_L$	27,37,38
	~ 3250	3077	$2\nu_2$	27,38,39
	~ 3261	3067	$\nu_1$	27,38,39
	~ 3351	2984	$\nu_3$	27,38,39
NIR	5189	1927	$\nu_2 + \nu_3$	39-41
	5562	1798	$\nu_2 + \nu_3 + \nu_L$	40
	6892	1451	$\nu_1 + \nu_3$	39,40,42
	8621	1160	$\nu_1 + \nu_2 + \nu_3$	39,43
	10225	978	$2\nu_1 + \nu_3$	39,43

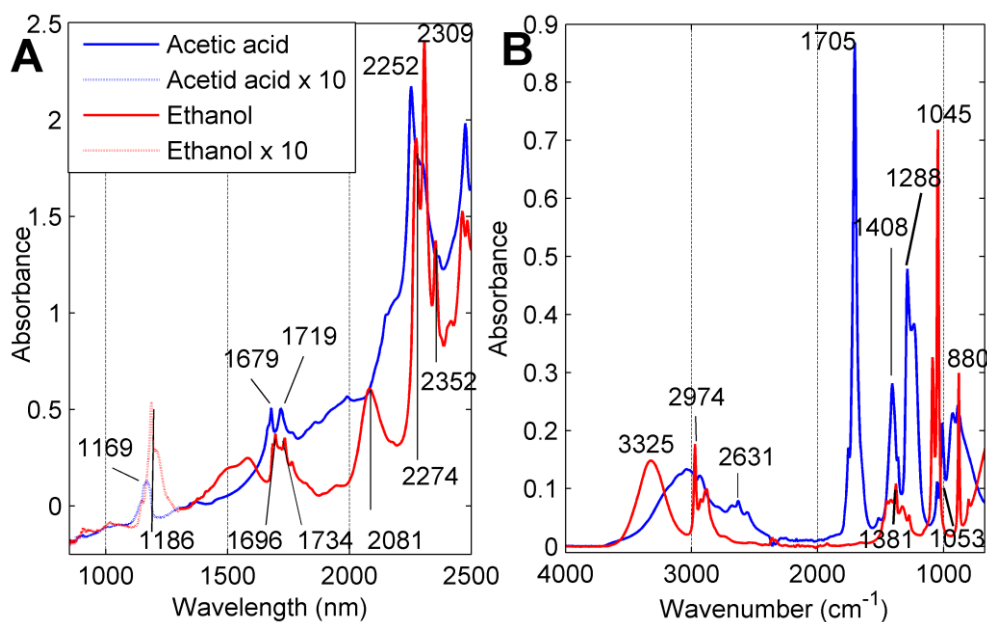


Figure 2-10. Acetic acid and ethanol. (A) Measured on a FT-NIR spectrometer (FTLA2000-160, ABB Bomem) with 1 mm pathlength. (B) Measured on a FT-IR spectrometer (MB100, ABB Bomem) on a 3-bounce diamond ATR.

*Hydrogen bonding* between a hydrogen bond donor (e.g. OH and NH) and a hydrogen bond acceptor (e.g. OH, NH, C-O-C, C=O and  $-N<$ ) will affect the NIR and MIR spectra.<sup>25</sup> Changes in the hydrogen bonding will have two effects: (a) slightly shift the band positions, and (b) broadening of the absorbance band of the hydrogen bond donor. *Temperature* changes will affect the intermolecular interactions including the hydrogen bonding and in that way change the NIR and MIR spectra.<sup>44</sup> Temperature can also have an impact on compounds that can have several conformational states. If the conformational states will influence the dipole moment, the bond strength or the anharmonicity constant then the different conformational states will cause a change in the spectra.

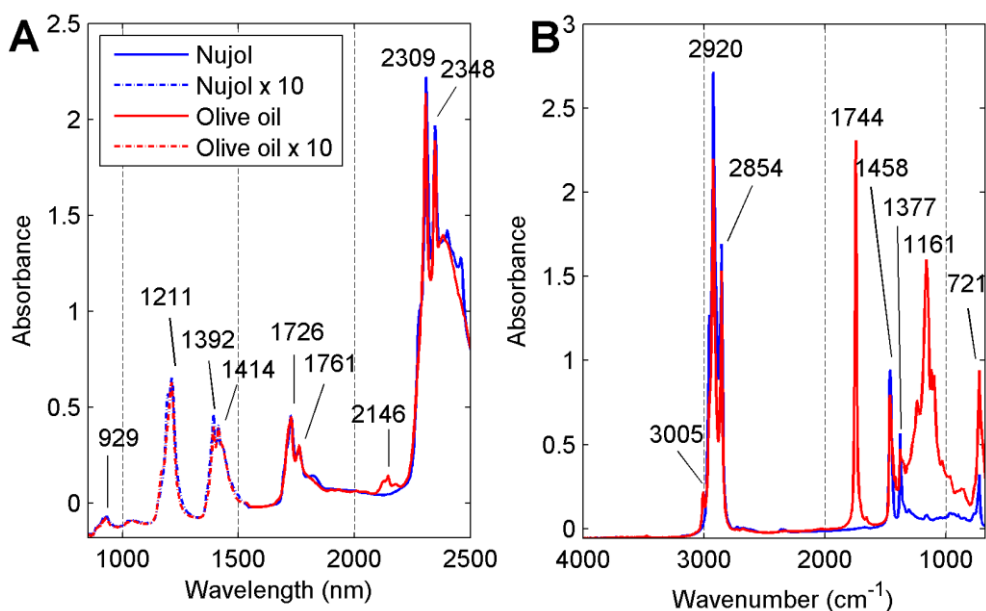


Figure 2-11. Nujol and olive oil. (A) Measured on a FT-NIR spectrometer (FTLA2000-160, ABB Bomem) with 1 mm pathlength. (B) Measured on a FT-IR spectrometer (MB100, ABB Bomem) on a 12-bounce ZnSe ATR.

*Crystalline and amorphous structure* is often seen as narrow and broad absorbance peaks, respectively. The change from an ordered crystalline structure to a random amorphous structure causes changes in the molecular interactions and environment which in turn affects the hydrogen-bonding pattern and therefore result in spectral changes.<sup>25</sup>

### 2.2.2 Physical information in near- and mid-infrared spectra

The physical state of a sample, such as *particle size*, will also affect the NIR and MIR spectra. Particles change the direction of light if there is a difference in the refractive index of the particle and the surrounding medium.<sup>45</sup> When light hits a surface it can either be reflected as *specular reflectance* or enter the particle and give *diffuse reflection* which is a uniform reflection at all angles (Figure 2-12). In the following, reflectance will be used as a term that describes both diffuse and specular reflectance. The light that enters the particle is called *scattered light* and it can be partially absorbed or reflected before it exits the particle.<sup>46</sup> The scattered light has interacted with the sample and therefore has chemical information whereas the specular reflectance has not.

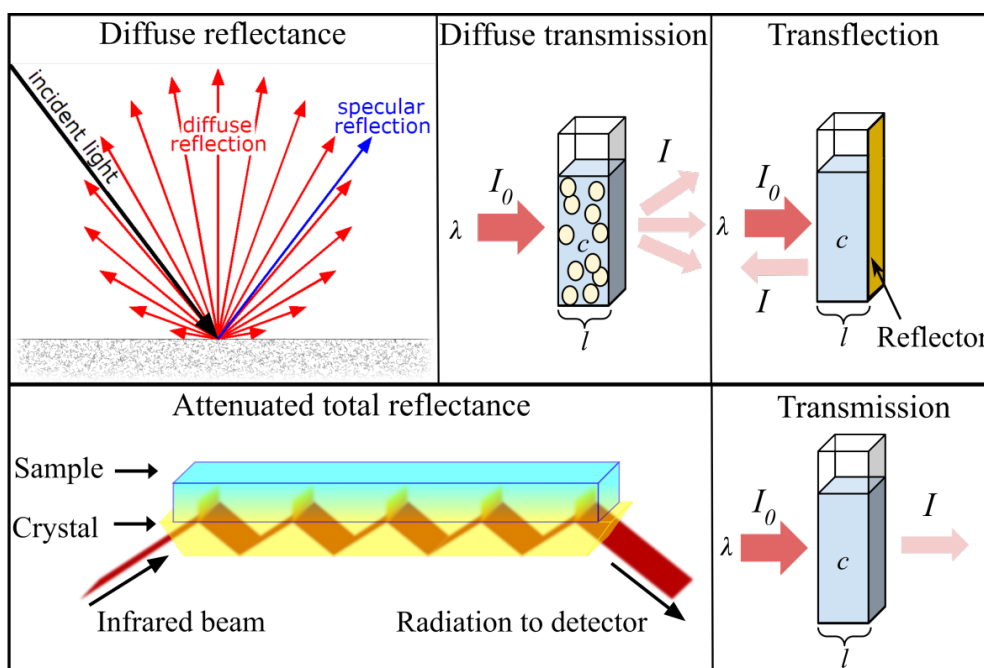


Figure 2-12. Some common sample presentations in NIR and MIR spectroscopy. Abbreviations: the intensity of the incoming light ( $I_0$ ), light wavelengths ( $\lambda$ ), path-length ( $l$ ), concentration ( $c$ ) and the intensity of the non-absorbed light ( $I$ ). Figures are from [www.commonswiki.org](http://www.commonswiki.org).

Samples that reflect the light can be measured by diffuse reflectance and diffuse transmission (Figure 2-12). Liquid samples that do not reflect the light can be measured by transmission or transflection. The use of ATR or transmission meas-

urements in the MIR is normally performed on samples with  $\mu\text{m}$  light path-lengths through the sample because of the extremely high absorbance in this region. NIR spectroscopy uses about 0.5 mm to more than 3 cm path-lengths and is therefore far more sensitive to particle size compared to MIR spectroscopy in transmission or ATR mode.

By decreasing the particle size of a sample, then the surface area is increased. This results in more specular reflection and, as a consequence, a lowering of the absorbance.<sup>46</sup> An example of the higher absorbance from larger particles can be seen from the sugar spectra in Figure 2-13. A second effect of particle size is that particles with a diameter smaller than the incoming wavelength will scatter more at shorter wavelengths compared to longer wavelengths. Very large particles will scatter equally at all NIR and MIR wavelengths. Particles with a diameter about the size of the incoming wavelength will scatter in-between the two extremes.<sup>45</sup>

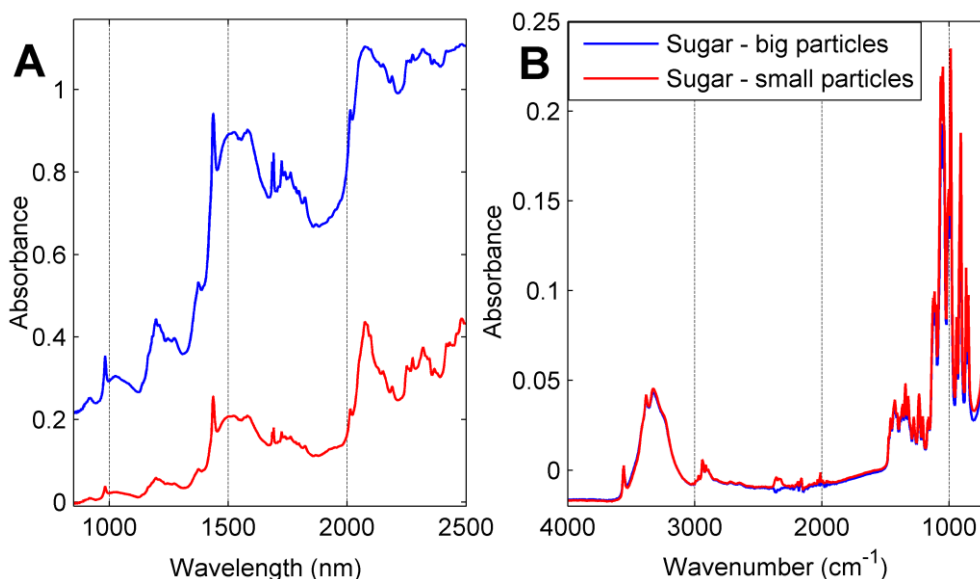


Figure 2-13. Table sugar (big particles) and granulated sugar + 2 % potato starch (small particles). (A) Measured on a FT-NIR spectrometer (FTLA2000-160, ABB Bomem) in reflectance mode. (B) Measured on a FT-IR spectrometer (MB100, ABB Bomem) on a 3-bounce diamond ATR.

The compression of particles has also been studied with NIR spectroscopy on pharmaceutical tablets where a larger compression gives increased absorbance at all wavelengths.<sup>47,48</sup>

The spectral changes from varying particle size and compression can result in an absorbance increase or decrease at all wavelengths (*additive effect*). The additive effect can also be increasing with e.g. longer wavelengths and this effect will here be called additive linear function. In addition, for samples with variations in particle size and packing the light will not travel the same length through the sample because it will be remitted a different number of times inside the sample. The resulting different path-lengths gives rise to a *multiplicative effect*.<sup>46</sup> The ideal behavior of additive, additive linear function and multiplicative effects can be seen in Figure 2-14.

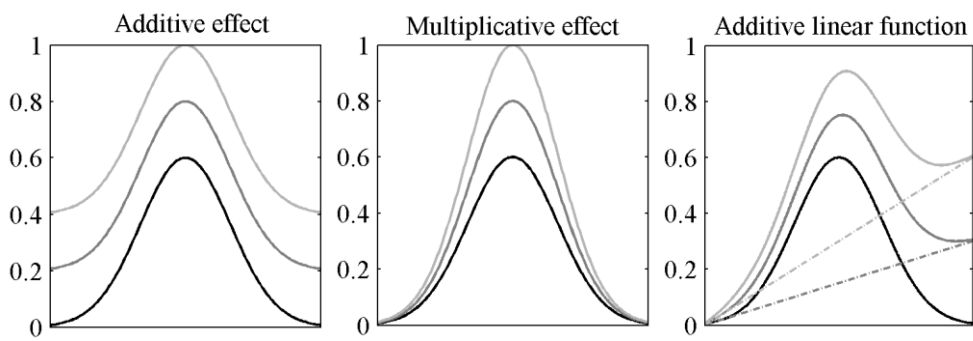


Figure 2-14. Gaussian curves. The additive effect is calculated as the black curve + 0.2 or 0.4 at all wavelengths. The multiplicative effect is calculated as the black curve times 1.33 or 1.67 at all wavelengths. The additive linear function is calculated as the black curve + a linear function from 0 to 0.3 or 0 to 0.6.

In order to remove additive, additive linear function and multiplicative effects it is often necessary to preprocess the spectra (Section 2.4). An example of spectra with a clear additive effect is reported in Figure 2-15, which shows a downward shift of the NIR spectra as the bread ages.

In summary, the number of normal modes from each functional group and the high number of possible overtones and combination bands make it clear that especially NIR spectra can be difficult to interpret. It is obvious that NIR and MIR spectra contain complex chemical and physical information when the effects from coupling, Fermi and Darling-Dennison resonance, hydrogen bonding and scattering is added. The complex information from NIR and MIR spectroscopy is investigated in the bread staling paper (**PAPER II**) with the primary goal of increasing the spectral interpretation of aging bread (Section 4.1).

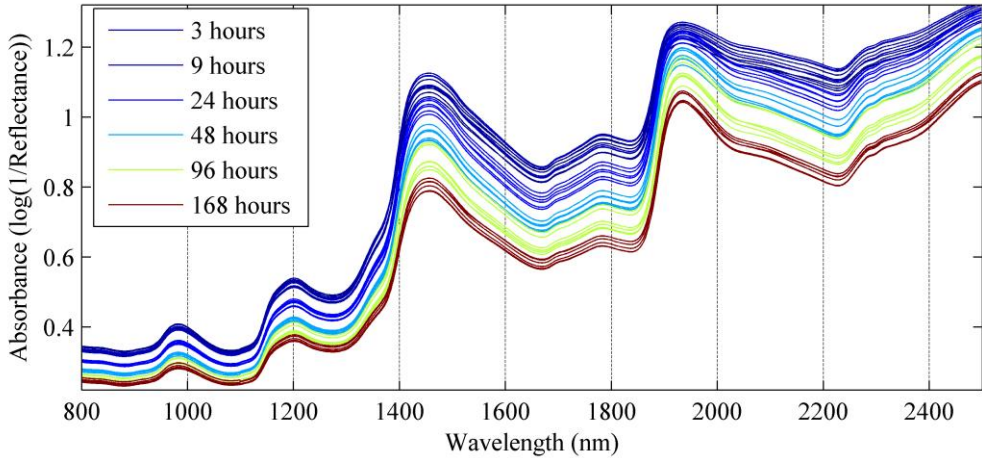


Figure 2-15. NIR spectra in diffuse reflectance mode on wheat bread measured at different hours after baking. Measured on a dispersive NIR spectrometer (6500, NIR systems, Inc.).

## 2.3 Multivariate modelling of near- and mid-infrared spectra

The relationship between absorbance and molar concentration is given by the Beer-Lambert-Bouguer law described in Eq. 1 and 2.<sup>49</sup>

$$T = \frac{I}{I_0} = e^{-\epsilon cl} \quad \text{Eq. 1}$$

$$A = -\log_{10} T = \log_{10} \left( \frac{1}{T} \right) = \epsilon cl \quad \text{Eq. 2}$$

where  $T$  is transmittance,  $I$  is the light intensity after sample interaction,  $I_0$  is the light intensity without sample interaction (also called background or reference),  $A$  is absorbance,  $\epsilon$  is the molar absorptivity,  $c$  is molar concentration and  $l$  is path-length. From Eq. 1 and 2 it can be seen that the  $\log_{10}$  transformation of transmittance produces a linear relationship between absorbance and concentration. These equations are valid for dilute and non-scattering samples. Some food samples will have problems with fulfilling these requirements and this causes deviations from the linear relationship between concentration and absorbance. However, a proper preprocessing of the spectra can in many cases recover the linear relationship between concentration and absorbance. Diffuse reflectance has an inherent nonlinear relationship to concentration. However, in practice  $\log_{10}(1/R)$  shows in many cases a

good linear relationship to concentration where  $R = I_R/I_{R0}$ ,  $I_R$  and  $I_{R0}$  are the reflected light from the sample and the reference, respectively.<sup>46</sup>

Explorative and predictive models have been developed in the barley endosperm paper (**PAPER I**), the bread staling paper (**PAPER II**) and barley whole grain paper (**PAPER III**) to visualize the spectral variations and to relate the concentration and absorbance values. The methods applied are Principal Component Analysis (PCA)<sup>50</sup> and Partial Least Squares (PLS).<sup>51</sup> Both of them are multivariate methods that project the data into a new space defined by linear combinations of the original variables. PCA is an unsupervised method that finds the maximum variance in a data set  $X$ . In PCA the data matrix  $X$  is decomposed into a score matrix  $P$ , a loading matrix  $T$  and a residuals matrix  $E$  as shown in Eq. 3.

$$X = TP' + E \quad \text{Eq. 3}$$

The selected number of principal components is denoted  $R$ , and it determines the size of  $T$  and  $P$  since  $T = [t_1, \dots, t_R]$  and  $P = [p_1, \dots, p_R]$ .<sup>52</sup> PLS is a linear regression method that maximizes the covariance between a data set  $X$  and a response  $Y$ . In PLS, two separate PCA models are built on  $X$  and  $Y$  as shown in Eq. 3 and 4, while at the same time maximizing the linear relation between  $X$  and  $Y$ .

$$Y = UQ' + F \quad \text{Eq. 4}$$

where  $U$  is the loading matrix,  $Q$  is the score matrix and  $F$  is the residual matrix. PCA and PLS are well suited for multivariate data analysis because (a) they are insensitive to correlated variables, (b) they are insensitive to data sets with fewer samples than variables and (c) they allow to reduce the dimensionality of the data, by considering only a limited number of principal components.

## 2.4 Preprocessing of near- and mid-infrared spectra

Preprocessing of NIR or MIR spectra or spectral ensembles is normally used to remove the physical effects described in Section 2.2.2. In short, if you measure on homogeneous liquids by ATR or transmission then you might only need a baseline correction. If you measure on powders or other solids with ATR or when measuring diffuse reflectance and diffuse transmission spectroscopy of food samples, a purely multiplicative or additive effect appears to be an oversimplification. So called scatter-correction or signal-correction methods have therefore been developed to remove both multiplicative and additive effects. For both liquids and solid samples, removing noisy or irrelevant spectral regions will improve the data analysis.

### 2.4.1 Noisy and irrelevant absorbance

Noisy spectral regions are here defined as instrumental artefacts that occur when for instance the detector sensitivity is challenged in regions with high absorbance or at the edge of the spectral working region of the detector. This noise can sometimes be avoided by for instance (a) measuring transmission or transfection with a shorter path-length or (b) by averaging more scans because the S/N ratio will increase proportional to  $\sqrt{n}$  where  $n$  is number of scans. Irrelevant absorbance is here defined as absorbance bands or spectral regions that do not have information on the compound of interest. The potential advantage of excluding regions of noisy or irrelevant interfering absorbance is that their noise or absorbance would not hide the compound of interest in data analysis. An example of this is given in the paper by Rinnan<sup>53</sup>, where it was the goal to predict fat in milk from MIR spectra. The MIR spectra had large spectral variations at the water bands because very little light reached the detector after passing the milk sample or the water background. By removing the noisy water bands and regions with little or no information on fat, then the prediction of fat in milk was improved. Another example of irrelevant absorbance is shown in Figure 2-16, where the bread spectra have absorbance bands from atmospheric water and CO<sub>2</sub> because the spectrometer was not purged with dry air or nitrogen.

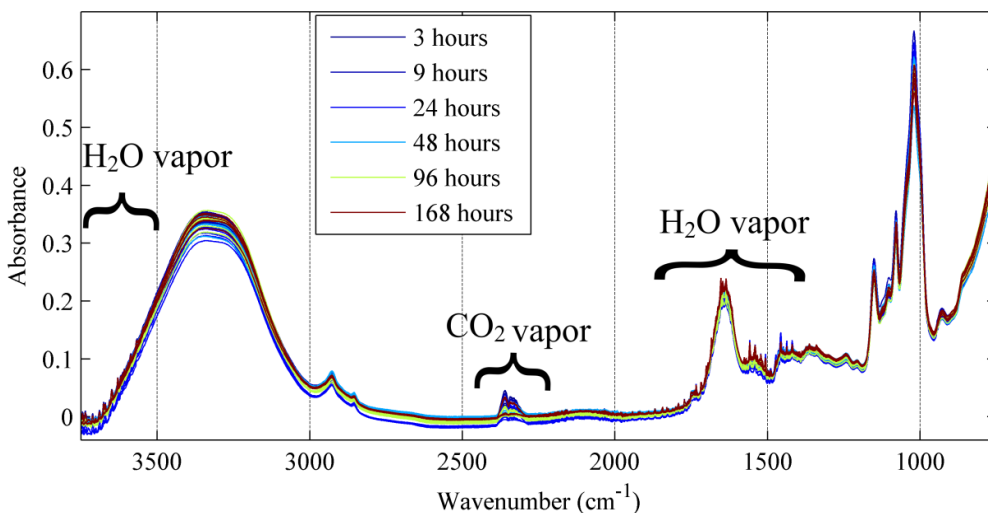


Figure 2-16. MIR spectra of wheat bread measured at different hours after baking. Water vapor bands interfere as ripples around 1,600 and 3,500  $\text{cm}^{-1}$  and CO<sub>2</sub> absorbance bands interfere around 667 and 2,349  $\text{cm}^{-1}$ .<sup>54</sup> Measured on a FT-IR spectrometer (MB100, ABB Bomem) with resolution 4  $\text{cm}^{-1}$  and 128 scans on a 3-bounce diamond ATR.

### 2.4.2 Absolute absorbance variations (multiplicative effect)

Absolute absorbance variations can be caused by variations in optical path lengths, fluctuations in the light source, or variable contact to the ATR crystal, just to mention some of the possible unwanted multiplicative effects.<sup>55</sup> Additive and multiplicative effects are most often observed together and so-called scatter-correction methods are applied to remove both. In the barley endosperm paper (**PAPER I**), the bread staling paper (**PAPER II**) and barley whole grain paper (**PAPER III**), the scatter-correction methods Multiplicative Scatter Correction (MSC)<sup>56</sup>, standard normal variate (SNV)<sup>57</sup> and Extended Multiplicative Scatter Correction (EMSC)<sup>58</sup> have been applied. MSC performs a correction by fitting a polynomial regression between a reference spectrum (commonly the mean spectrum) and the raw spectra. EMSC includes the reference correction from MSC together with a correction for the wavelength dependency. SNV is performed on each spectrum by subtracting its mean value and dividing by the standard deviation of the spectrum. In the papers by Rinnan, et al.<sup>59</sup> and Lasch<sup>55</sup> a more detailed description is given for the scatter-correction methods MSC, EMSC, SNV. Normalization (also known as object-wise standardization) are also scatter-correction methods and some of the common ones are city-block normalization (1-norm) and Euclidean normalization (2-norm). City-block and Euclidean normalization divides each spectrum by its sum of absolute values or the square root of the sum of the squared elements, respectively.<sup>59</sup> Additional ways of normalizing spectra which have been applied to especially MIR spectra, are done by dividing the absorbance at all wavelengths with the absorbance at one wavelength<sup>60</sup> or by setting the area of a certain peak equal for all spectra.<sup>61</sup> By normalizing according to the area of a certain peak, it is assumed that the concentration of the corresponding compound is not changing between samples. It is therefore important to have information on all samples before applying this normalization method.

### 2.4.3 Baseline offsets (additive effect)

NIR and MIR can be influenced by baseline offsets e.g. by scattering or instrument variations. NIR spectroscopy measurements with diffuse reflectance or diffuse transmission might very likely have variations in scattering. Scattering is not as apparent in MIR spectroscopy in transmission or ATR as in NIR diffuse transmission because of the small amount of sample measured by MIR transmission or ATR. As an example, MIR transmission measurements on milk often uses a cuvette with a path-length of about 40-50  $\mu\text{m}$  whereas NIR transmission on milk can use a path-length of between  $\sim 0.5$  mm to more than 3 cm (depending on the wavelength region). For ATR measurements, the penetration depth depends on different instrument settings (e.g. the angle of the incident light, the crystal material, the refractive

index of the sample and the wavelength of the incident light), but approximately 1  $\mu\text{m}$  can be expected.<sup>30</sup> Some authors claim that when measuring on wine or milk with FT-IR then derivatives or scatter correction methods are not necessary, but a simple baseline correction at a single reference wavenumber is enough to obtain robust PLS predictions.<sup>62</sup>

In the bread staling paper (**PAPER II**) the baseline offset has been corrected using Savitzky-Golay derivatives. When applying Savitzky-Golay derivatives, a polynomial fitting is done prior to the calculation of derivatives. This is done to decrease the noise, which would otherwise increase with the number of derivatives. In fact, a derivative calculated by a simple point difference, which is the difference between two adjacent wavelength points, often contains substantially more noise. The number of points used in the polynomial fitting in Savitzky-Golay (called window size) should be chosen not too large to avoid over-smoothing and not too low to avoid noise. As seen in Figure 2-17A the 1<sup>st</sup> and 2<sup>nd</sup> derivative of peaks with a larger width will become smaller compared to a narrow peak. This means that broad baseline changes can be removed with derivatives. At the same time derivatives can be used to enhance the resolution by revealing overlapping peaks as shown in Figure 2-17B and 2-17C. Derivatives can remove the additive effect as seen from Eq. 5 where  $k$  is a constant and  $f$  is a function that defines an absorbance peak.

$$(k \pm f)'(x) = 0 \pm f'(x) \quad \text{Eq. 5}$$

The addition of a linear function can also be removed by derivatives as shown in Eq. 6 where  $g$  is a linear function. However, an additive linear function will result in a baseline offset when preprocessed with a 1<sup>st</sup> derivative and be fully removed with a 2<sup>nd</sup> derivative.

$$(g \pm f)'(x) = g'(x) \pm f'(x) \quad \text{Eq. 6}$$

On the other hand, derivatives cannot remove the multiplicative effect as shown in Eq. 7.

$$(k \cdot f)'(x) = k \cdot f'(x) \quad \text{Eq. 7}$$

It can therefore sometimes be an advantage to combine derivatives with methods that correct for multiplicative effects such as MSC and EMSC. This was the case in the bread staling paper (**PAPER II**).

Further reading on the baseline correction methods called Offset correction, Piecewise baseline correction, Polynomial baseline correction and Savitzky-Golay derivatives is available in Lasch<sup>55</sup>. In addition, Savitzky-Golay and Norris-William/gap-segment derivatives are elaborated in Rinnan, et al.<sup>59</sup>.

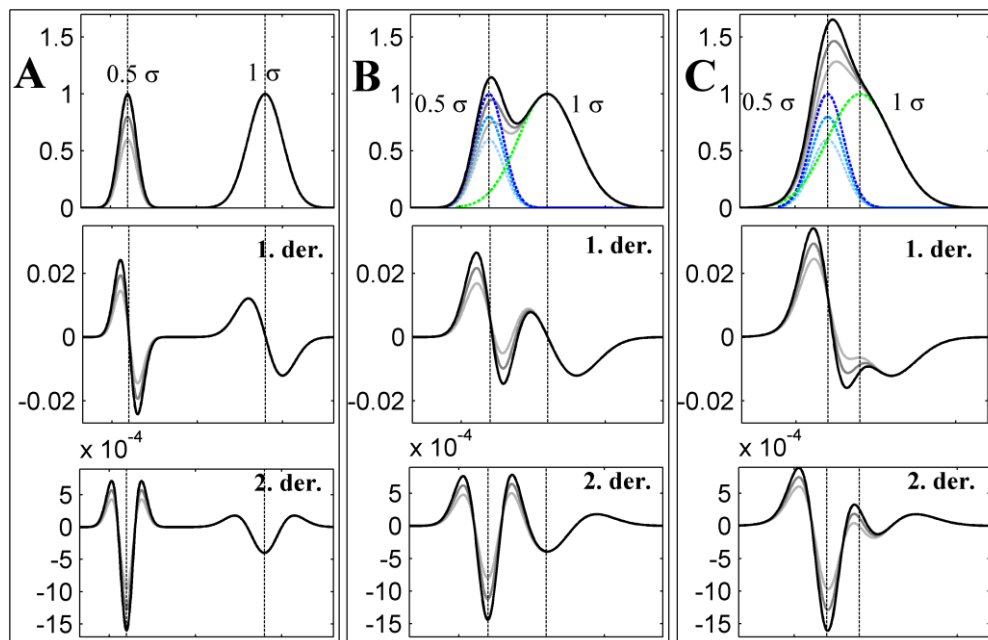


Figure 2-17. Gaussian peaks with a standard deviation of 0.5 and 1. The peak with 0.5 standard deviation is changing intensity (blue spectra) and the other peak is constant (green spectra). The gray spectra are calculated as: light blue spectrum + green spectrum = light gray spectrum, medium blue spectrum + green spectrum = medium gray spectrum, dark blue spectrum + green spectrum = dark gray spectrum.

## 2.5 Near- or mid-infrared spectroscopy?

### That is the question

There are similarities and differences between the chemical information in the NIR and MIR region as described in Section 2.2. NIR and MIR measure basically the same molecular vibrations but with different selection rules. A most relevant question often posed is where in the MIR and NIR region do we find the best possible information about a given compound or application e.g.  $\beta$ -glucan content in barley or bread aging?

### 2.5.1 The influence of path-length

The first thing to be aware of when comparing the ability to measure compounds in different NIR and MIR regions is that the molar absorptivity,  $\epsilon$ , depends on the wavelength. The relationship between molar absorptivity and wavelength is given by the Beer-Lambert-Bouguer law described in Eq.1 and 2 in Section 2.3. The dependence of  $\epsilon$  to wavelength can be seen in the NIR spectra of water in Figure 2-9A where the absorbance decreases when going from longer to shorter wavelengths. In theory, the highest S/N ratio of a spectrum is achieved with an absorbance of about 0.43-0.48 when measuring on a non-scattering liquid on a detector limited spectrometer.<sup>49,63</sup> For liquid samples, the path-length can be adjusted to match this absorbance level. When comparing the information in the MIR with NIR or when comparing different NIR regions then the optimum path-length should be used in the different regions. This is not always the case. As an example, NIR, MIR and Raman were compared in a study on edible oils and fats.<sup>64</sup> The path-length used for the NIR transmission measurements was not mentioned, but the spectra clearly showed that the combination band region from about 2220-2400 nm and the 1<sup>st</sup> overtone region at about 1688 nm had a high absorbance exceeding the detector limit. In addition, butter showed high and noisy absorbance bands in most of the NIR region. The study showed that MIR spectroscopy was superior to NIR in classifying the different fats, but it is unknown if the choice of path-length for the NIR measurements was the cause of this. The comparison of different NIR regions with a different path-length for each region was done in the study by Chen, et al.<sup>65</sup> Here the NIR region from 1538-1818 nm was compared with the region at 2000-2500 nm for aqueous solutions of glucose, lactate, urea, ascorbate, triacetin and alanine. The spectra from 1538-1818 nm were measured with a 7.5 mm path-length and the 2000-2500 nm region was measured with a 1.5 mm path-length. PLS models for the region 2000-2500 nm was superior in comparison to the PLS models for the region 1538-1818 nm for all compounds. The net analyte signal (NAS), which shows the proportion of compound spectra that is orthogonal to all other spectral variations, was also calculated for each compound. The NAS was higher for all compounds in the 2000-2500 nm region compared to the 1538-1818 nm region, and the NAS analysis therefore agreed with the PLS results. The study by Chen, et al.<sup>65</sup> was the only article that was found to compare different NIR regions with different path-lengths. It therefore seems like there is a lack of studies that optimize the path-length when comparing different NIR and MIR regions.

### 2.5.2 The influence of temperature

The second thing to consider is that NIR and MIR spectra are affected by temperature changes, especially samples with high water content. This means that fluctua-

tions in temperature can give unwanted spectral variations in some parts of the spectra whereas other regions will not be affected. In a study by Jensen, et al.<sup>66</sup> NIR and MIR spectroscopy on water with glucose was compared. The best spectral region with information on glucose and low interference from temperature variations from 30-42°C was the MIR region from 1000-1100 cm<sup>-1</sup>. The NIR region from 2222-2381 nm also showed information on glucose and low influence of temperature. However, a matrix effect between water, glucose and temperature in the NIR region made Jensen, et al.<sup>66</sup> favor the MIR region.

### **2.5.3 Comparison of near- and mid-infrared spectroscopy**

Path-length and temperature variations are important factors that will influence the S/N ratio of spectra but other factors such as for instance the S/N ratio of the spectrometer and the sample presentation will also affect. Comparing NIR and MIR spectroscopy is often done on different instruments with different sample presentations and limitations in either of these can therefore influence the performance. If there are one or more NIR and MIR regions that are optimal in terms of chemical information it might therefore be deluded by non-optimal sample presentation or hardware. In spite of these complications, some studies compare the performance of NIR and MIR spectroscopy and a few of them will be presented here. A study on deep frying oils compared NIR and MIR spectroscopy and it was found that both methods could be used to predict the content of free fatty acids, but the peroxide value was less satisfactory predicted by MIR than NIR.<sup>67</sup> The physical and chemical changes during frying oil deterioration were followed in another study that compared near-infrared/visible (NIR/VIS) and MIR spectroscopy. Here it was found that MIR resulted in the most direct and accurate monitoring of the decomposition of triglycerides into free fatty acids, and NIR/VIS spectroscopy performed almost equally well via indirect correlations to the amount of dispersed material and concentration of color pigments.<sup>68</sup> However, the peroxide value was not well correlated with either NIR/VIS or MIR spectra showing R<sup>2</sup> values of 0.2 in PLS models. Another study on oil used NIR and MIR spectroscopy to classify the origin of olive oil and NIR gave superior classification results to MIR.<sup>69</sup> The prediction of oil and moisture content in potato chips has also been compared.<sup>70</sup> In this case, NIR and MIR spectroscopy gave similar predictive results; in addition MIR could easily give information on trans fatty acids at 967 cm<sup>-1</sup>. The fermentation process in red wine or wheat dough has also been measured with NIR and MIR spectroscopy and both methods were able to follow the fermentation process.<sup>71,72</sup> The classification of six different types of Emmental cheese was investigated and NIR spectroscopy was able to correctly classify 100 % of all six different cheeses, whereas MIR performed with a lower correct classification rate.<sup>73</sup> A study on pectin has shown that both NIR

and MIR spectroscopy could be used to predict the degree of esterification and amidation<sup>74</sup>. Another study on pectin also found that both NIR and MIR spectroscopy could be used to predict the degree of esterification, the random de-esterification and block de-esterification.<sup>75</sup> NIR and MIR spectroscopy have also been compared in a study on the ratio of mannuronic and guluronic acid (M/G) in commercial sodium alginate powders. Both NIR and MIR spectroscopy could be used to determine the M/G ratio with similar errors compared to the reference method.<sup>76</sup> From these comparisons between NIR and MIR spectroscopy it does not seem possible to give a general answer to which spectral region is better for what food product and compound of interest. However, both spectral regions have shown to be useful for the analysis of many different products.

## **2.6 Two-dimensional correlation spectroscopy**

The idea of 2D correlation spectroscopy (2DCOS) was first proposed by Noda in 1986 and further developed into *generalized 2D correlation spectroscopy*.<sup>77</sup> The technique can be used to augment the interpretation of overlapping peaks by mapping samples that are modulated systematically (e.g. the samples vary in temperature or the chemical reaction time). The spectra can then be visualized in plots showing how the wavelength variables covary (in the synchronous plot) and change during the systematic modulation (in the asynchronous plot). Barton and co-workers developed a similar technique, where the correlation coefficients between NIR and MIR spectra are mapped in order to show how the fundamental molecular vibrations in the MIR region relates with the overtones and combination bands observed in the NIR.<sup>78</sup> In this thesis 2DCOS was used to connect the information in the NIR and MIR regions and, in that way, increase the spectral interpretation and evaluate which NIR or MIR region has more information about the compound of interest. In theory 2DCOS can be used to facilitate parallel factor analysis (PARAFAC) such as proposed in the vibrational overtone combination spectroscopy (VOCSY) approach.<sup>79</sup> In the VOCSY approach the spectra are rearranged into a new data matrix where each functional group has information from its fundamental and overtone absorbance bands. Ideally this method can be used for quantitative modeling using the second order advantage (i.e. determination of a compound when there are unexpected interferences in the sample).

### **2.6.1 Calculations of two-dimensional correlation spectroscopy**

The synchronous plot is commonly calculated as the covariance as shown in Eq. 8.<sup>8</sup>

$$\Phi(v_1, v_2) = \frac{1}{m-1} \sum_{j=1}^m \tilde{y}_j(v_1) \cdot \tilde{y}_j(v_2) \quad \text{Eq. 8}$$

Where  $m$  is the total number of spectra,  $\tilde{y}_j(v_1)$  and  $\tilde{y}_j(v_2)$  are the  $j^{\text{th}}$  spectrum at two spectral variables  $v_1$  and  $v_2$ .

Barton II, et al.<sup>78</sup> used the Pearson's correlation coefficient instead of the covariance to find the correlation between MIR and NIR spectra. Pearson's correlation coefficient can be calculated as described in Eq. 9.<sup>80</sup>

$$r_{\text{Pearson}} = \frac{\text{cov}(v_1, v_2)}{s_{v_1} s_{v_2}} \quad \text{Eq. 9}$$

Where  $\text{cov}(v_1, v_2)$  is the covariance that is calculated as shown in Eq.8 and  $s_{v_1}$  and  $s_{v_2}$  are the standard deviation at  $v_1$  and  $v_2$ , respectively. The advantage of using Pearson's correlation coefficient is that it gives a value between -1 and +1 that can be compared between peaks. If the covariance between two peaks is 0.03 then that information alone cannot be interpreted as high or low. On the contrary, if Pearson's correlation coefficient is 0.9 then it can be interpreted as a high positive correlation at the two wavenumbers. However, Pearson's correlation coefficient has some shortcomings when it comes to 2DCOS which is mentioned in the bread staling paper (**PAPER II**). These unwanted effects are noise amplification and larger spectral areas of high correlation the so-called neighbor variable covariance which complicates the search for correlation maxima.<sup>81</sup> Another way of calculating the synchronous plot is to use the covariance with Pareto scaling that is calculated as described in Eq. 10.

$$r_{\text{Pareto}} = \frac{\text{cov}(v_1, v_2)}{\sqrt{s_{v_1} s_{v_2}}} \quad \text{Eq. 10}$$

The asynchronous plot is commonly calculated as shown in Eq. 11.<sup>8</sup>

$$\Psi(v_1, v_2) = \frac{1}{m-1} \sum_{j=1}^m \tilde{y}_j(v_1) \cdot \sum_{k=1}^m N_{jk} \cdot \tilde{y}_k(v_2) \quad \text{Eq. 11}$$

Where  $\tilde{y}_j(v_1)$  and  $\tilde{y}_k(v_2)$  are the  $j^{\text{th}}$  and  $k^{\text{th}}$  spectrum at two spectral variables  $v_1$  and  $v_2$ .  $N_{jk}$  is the element in the  $j^{\text{th}}$  row and  $k^{\text{th}}$  column in the discrete Hilbert-Noda transformation matrix defined in Eq. 12.<sup>8</sup>

$$N_{jk} = \begin{cases} 0 & \text{if } j = k \\ 1/\pi(k-j) & \text{otherwise} \end{cases} \quad \text{Eq. 12}$$

The synchronous and asynchronous plots in this thesis were calculated from the following Matlab code modified from Czarnecki<sup>82</sup> and compared with the 2Dshige software<sup>83</sup>:

$$\text{Synchronous / covariance} = (\mathbf{X}_{\text{MIR}}' * \mathbf{X}_{\text{NIR}}) / (n-1) \quad \text{Eq. 13}$$

Where  $n$  is the number of samples,  $\mathbf{X}_{\text{MIR}}$  and  $\mathbf{X}_{\text{NIR}}$  are the mean centered data matrixes with samples as rows and wavenumbers as columns for MIR and NIR, respectively.  $\mathbf{X}_{\text{NIR}}'$  is the transpose of  $\mathbf{X}_{\text{NIR}}$ .

$$\text{Synchronous / } \Gamma_{\text{Pearson}} = \text{corr}(\mathbf{X}_{\text{MIR}}, \mathbf{X}_{\text{NIR}}) \quad \text{Eq. 14}$$

Where corr is a Matlab function that calculates Pearson's correlation coefficient on each matrix element.

$$\text{Synchronous / } \Gamma_{\text{Pareto}} = ((\mathbf{X}_{\text{MIR}}' * \mathbf{X}_{\text{NIR}}) / (n-1)) ./ \text{sqrt}(\text{std}(\mathbf{X}_{\text{MIR}})' * \text{std}(\mathbf{X}_{\text{NIR}})) \quad \text{Eq. 15}$$

Where sqrt and std are Matlab functions that calculate the square root of each array element and the standard deviation for each column, respectively.

$$\text{Asynchronous} = (\mathbf{X}_{\text{MIR}}' * \mathbf{N} * \mathbf{X}_{\text{NIR}}) / (n-1) \quad \text{Eq. 16}$$

Where  $\mathbf{N}$  is the Hilbert-Noda transformation matrix which is calculated as

$$\mathbf{N}_t = \text{ones}(n,1) * [1:n] \quad \text{Eq. 17}$$

$$\mathbf{N}_t = \mathbf{N}_t' - \mathbf{N}_t \quad \text{Eq. 18}$$

$$\mathbf{N}_t = 1 ./ \mathbf{N}_t \quad \text{Eq. 19}$$

$$\mathbf{N}_t(\mathbf{N}_t == \text{inf}) = 0 \quad \text{Eq. 20}$$

$$\mathbf{N} = 1/\pi * \mathbf{N}_t \quad \text{Eq. 21}$$

Where  $\mathbf{N}_t$  is the temporary matrix, ones( $n,1$ ) is a  $n \times n$  matrix of ones, [1: $n$ ] is a vector of successive natural numbers from 1 to  $n$ ,  $\mathbf{N}_t'$  is the transpose of  $\mathbf{N}_t$ . The array division in Eq. 19 results in infinitive values and these are replaced with zero in Eq. 20.

The synchronous and asynchronous plots are contour plots that show the relative peak change compared to the largest peak change. If too few contour lines are chosen then small spectral changes will not be shown. The optimal number of contour lines is therefore found empirically in a trial and error procedure.

### 2.6.2 Examples of two-dimensional correlation spectroscopy

2DCOS consists of a *synchronous*/covariance and an *asynchronous* plot calculated for one spectral region or two different spectral regions. A few examples of 2DCOS will be given below for one spectral region for the sake of simplicity. Figure 2-18A shows two simulated Gaussian absorbance peaks where one is increasing and one is constant. The synchronous plot in Figure 2-18B has a positive covariance (red circle) situated on the diagonal of the plot. This is called an *autopeak* and it indicates that there is one absorbance peak changing intensity.

Figure 2-19A depicts absorbance bands where one band is increasing (blue spectra) and one is decreasing (green spectra). In the synchronous plot in Figure 2-19B there are two autopeaks and two *cross peaks*. The cross peaks lie off the diagonal and represent the covariance between two different absorbance peaks. Therefore, they can have either a positive or negative sign. Hence, from the two autopeaks (along the diagonal) it can be deduced that there are two increasing or decreasing absorbance peaks. In addition, from the negative covariance (blue color) of the cross peaks it can be concluded that the two absorbance peaks move in opposite directions.

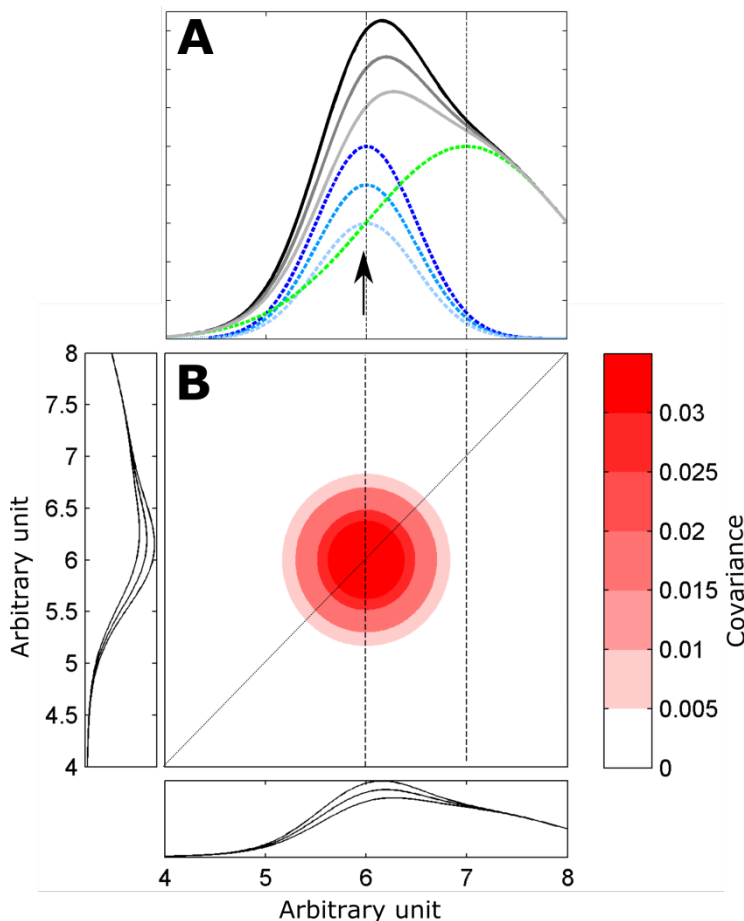


Figure 2-18. (A) Two simulated Gaussian peaks where one peak is increasing in intensity (blue spectra), the other peak is not changing intensity (green spectra) and their resulting summation (gray spectra). The gray spectra are calculated as: light blue spectrum + green spectrum = light gray spectrum, medium blue spectrum + green spectrum = medium gray spectrum, dark blue spectrum + green spectrum = dark gray spectrum. (B) Synchronous/covariance plot of the gray spectra in A.

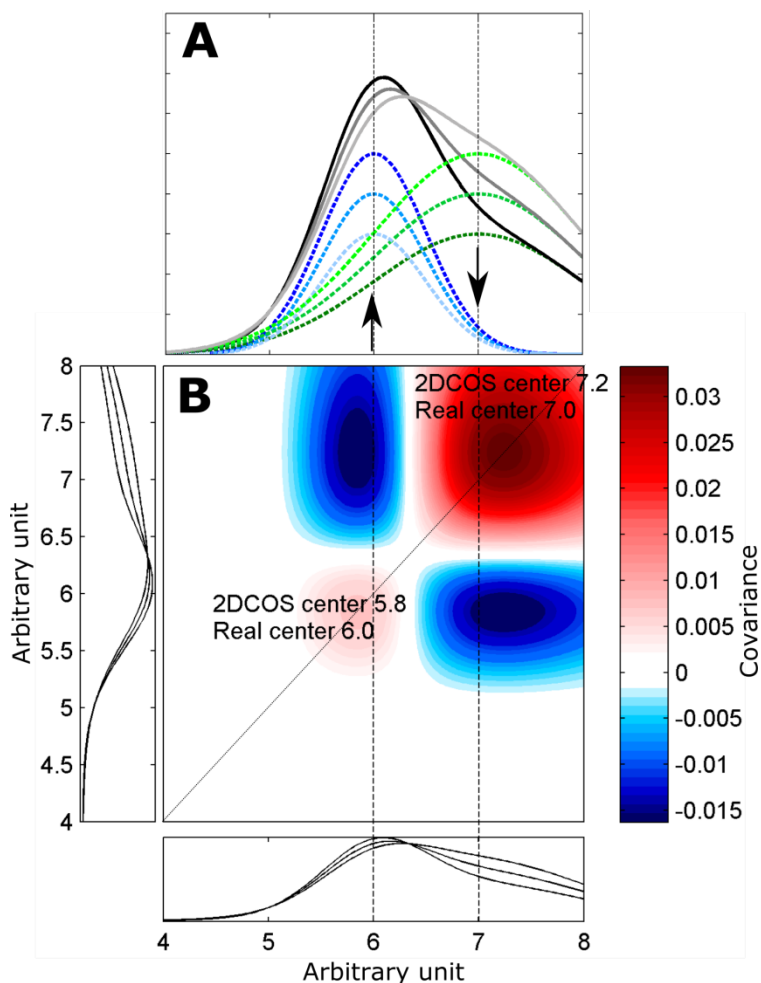


Figure 2-19. (A) Two simulated Gaussian peaks where one peak is increasing in intensity (blue spectra), the other peak is decreasing in intensity (green spectra) and their resulting summation (gray spectra). The gray spectra are calculated as: light blue spectrum + light green spectrum = light gray spectrum, medium blue spectrum + medium green spectrum = medium gray spectrum, dark blue spectrum + dark green spectrum = dark gray spectrum. (B) Synchronous/covariance plot of the gray spectra in A.

It is also possible to use spectra preprocessed as derivatives. Figure 2-20A shows the 2<sup>nd</sup> derivative calculated from the gray spectra in Figure 2-19A. The synchronous plot in Figure 2-20B shows the same two autopeaks and two cross peaks as seen in Figure 2-19B. However, the synchronous plot of derivatives shows more cross peaks because of the unavoidable shoulders of derivatives. It can therefore be very difficult to interpret synchronous plots made on derivatives, because of the difficulty in separating absorbance peaks from shoulders.

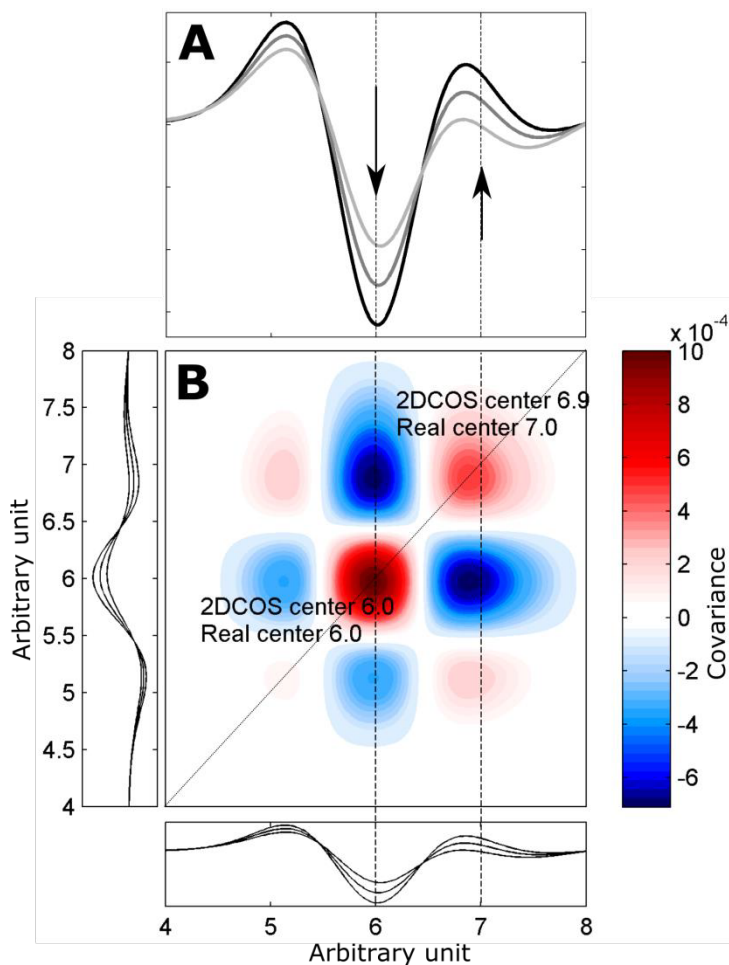


Figure 2-20. (A) The 2<sup>nd</sup> derivative of the gray absorbance spectra in Figure 2-19A. (B) Synchronous/covariance plot of the gray spectra in A.

As is seen from Figure 2-18, 2-19 and 2-20, the synchronous plot shows if peaks are moving in the same or opposite directions. The asynchronous plot shows peaks that are changing at different measurement times. For instance, the asynchronous plot of a chemical reaction will show the order of the generated products, if absorbance bands from intermediate and final products will appear at different measurement times. In Figure 2-19A the blue and the green peak are changing at the same time. The asynchronous plot for these spectra would be blank because no peak is changing before or after the other. An example of the synchronous and asynchronous plots for spectra where the blue peak is increasing first and then the green peak is decreasing is shown in Figure 2-21. The synchronous plot in Figure 2-21A shows that the peaks are moving in opposite directions (negative off-diagonal covariance).

The asynchronous plot in Figure 2-21B shows a positive color at (10,6), which means that the peak at 10  $\text{cm}^{-1}$  changes before the peak at 6  $\text{cm}^{-1}$  unless the synchronous plot shows a negative color at the same wavelength point and in that case the sequence is reversed. The asynchronous plot therefore shows that the peak at 6  $\text{cm}^{-1}$  changes before the peak at 10  $\text{cm}^{-1}$ . This can be a bit confusing; so to simplify the interpretation of the asynchronous plot then the asynchronous matrix can be multiplied with the sign of the synchronous matrix (but this was not done in Figure 2-21B).

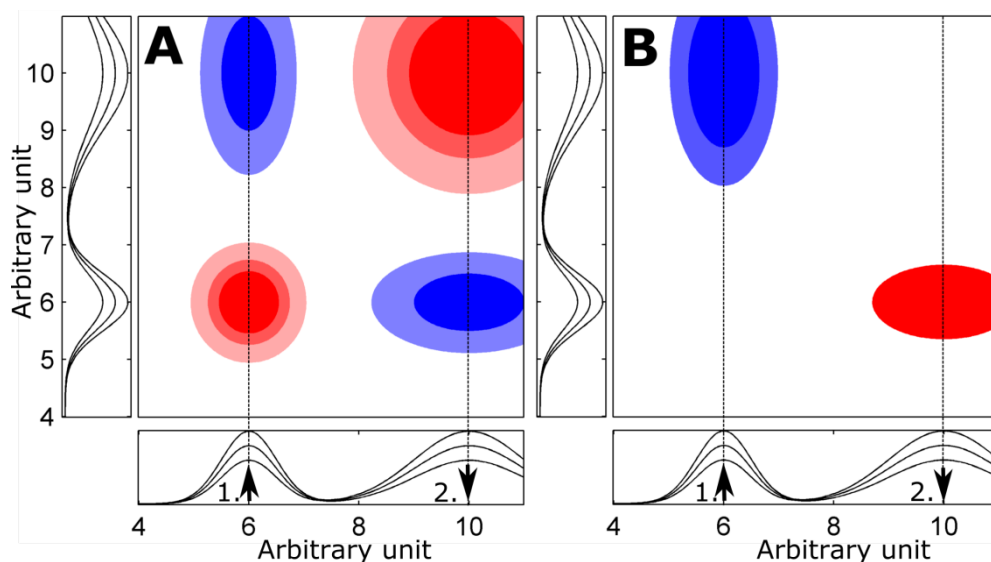


Figure 2-21. Two simulated Gaussian peaks. First the peak at 6  $\text{cm}^{-1}$  increases and next the peak at 10  $\text{cm}^{-1}$  decreases. (A) Synchronous/covariance plot. (B) Asynchronous plot.

Applying 2DCOS to two different spectral regions follows the same principles except that there are no autopeaks when two different spectral regions are used. An example of a synchronous plot with two different spectral regions can be seen in Figure 2-22. This plot is made from NIR and MIR spectra of 51 different vegetable and fish oils. The figure shows high covariance between the fundamental CH absorbance bands from 2800-3000  $\text{cm}^{-1}$  in the MIR and the CH overtones at 1200 and 1700 nm in the NIR. In addition, a high covariance is observed between the fundamental  $>\text{C}=\text{CH}-\text{C}$  absorbance band at 3012  $\text{cm}^{-1}$  in the MIR and a band that has been related to the absorbance of cis unsaturated fatty acids at 2143 nm in the NIR.<sup>84</sup>

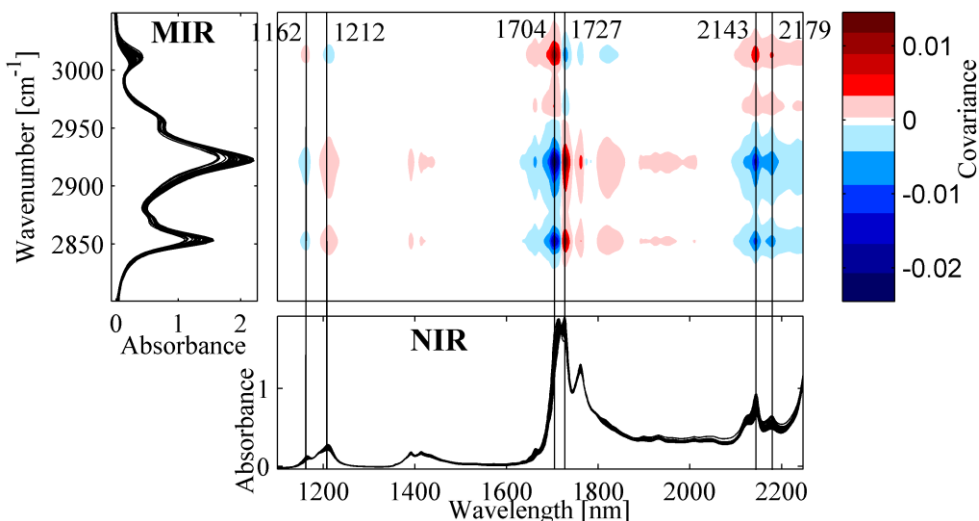


Figure 2-22. The synchronous/covariance plot of 51 different vegetable and fish oils including oil from olive, rapeseed, sunflower seed, sesame, safflower, corn, hemp, grape seed, pumpkin seed, argan, rosehip seed, peanut, apricot kernel, almond, wheat germ, linseed, cumin, macadamia nut, walnut, hazelnut, pecan nut, soybean, pistachio, fish and cod liver. Measured on a FT-NIR spectrometer (FTLA2000-160, ABB Bomem) in a cuvette with 4 mm pathlength and a FT-IR spectrometer (MB100, ABB Bomem) on a 12-bounce ZnSe ATR.

### 2.6.3 Example of covarygram

A covarygram is a plot where spectra are superimposed on for instance the Pearson's correlation coefficient calculated for a property at each wavelength.<sup>85</sup> Figure 2-23 shows an example of a covarygram that contains the spectra of five different barley oils, sunflower seed oil and Nujol oil and the Pearson's correlation coefficient to the iodine number at each wavelength. The iodine number describes the amount of C=C bonds, which fits with the high covariance and high correlation at 2143 nm in Figure 2-22 and 2-23, respectively, since this wavelength has been connected to unsaturated fatty acids.<sup>84</sup> As only seven oils were measured in Figure 2-23 then the correlation coefficient should be interpreted with care because the correlation can be overoptimistic with few samples.

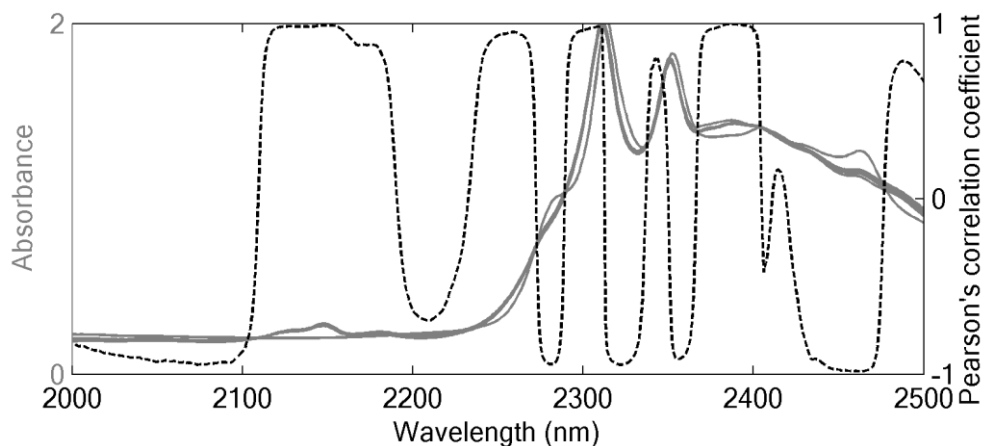


Figure 2-23. Covarygram of the oil spectra (gray color) of five barley genotypes, sunflower seed oil and Nujol oil. The spectra were measured in a 1 mm cuvette on a dispersive NIR spectrometer with a supercontinuum light and monochromator (described in Section 3.1 and the barley endosperm paper, **PAPER I**). Pearson's correlation coefficient (dashed line) was calculated at each wavelength to the iodine number which is a measure of the total amount of C=C bonds.

## 2.7 Spectral interpretation with hydrogen–deuterium exchange

The deuteration of compounds means that  $^1\text{H}$  is exchanged with  $^2\text{H}$  (deuterium). Hydrogen atoms in OH and NH groups can easily be exchanged, up until an equilibrium is reached, by placing the compound in liquid  $\text{D}_2\text{O}$  (deuterium oxide /"heavy water") or placing the compound in an atmosphere saturated with  $\text{D}_2\text{O}$ . On the other hand, CH groups do not exchange their hydrogen atoms with deuterium. The greater weight of deuterium compared to hydrogen means that the NIR and MIR absorbance bands with deuterium occur at lower wavenumbers than the corresponding vibrational bands with hydrogen. Deuteration therefore lowers the absorbance from for instance  $\text{H}_2\text{O}$  and in that way reveal hidden or partially overlapped bands from e.g. CH<sup>86</sup> or amide I.<sup>87</sup> Deuteration is a classical method for assignment of molecular vibrations, but it has also been used to investigate the flexibility of proteins by measuring the exchange rate of  $^1\text{H}/^2\text{H}$  on the amide II band.<sup>87</sup>

On a molecular level, by dissolving a sample in  $\text{D}_2\text{O}$  or a saturated atmosphere of  $\text{D}_2\text{O}$ , the OH groups in for instance carbohydrates and water, and the NH groups in proteins will be exchanged. As an example, the main reactions in the deuteration of wheat bread are shown in Figure 2-24. The practical aspect of creating a saturated

atmosphere of D<sub>2</sub>O in the bread example is shown in Figure 2-25. The spectra of deuterated samples will exhibit new absorbance bands from D<sub>2</sub>O and HDO which has been assigned in Table 2-3. Figure 2-26 is an example of NIR spectra showing the deuteration of wheat bread together with a spectrum of oven dried wheat bread with no deuteration. The decrease and increase of absorbance bands is more easily seen in the Savitzky-Golay 2<sup>nd</sup> derivative spectra in Figure 2-26B. It is observed that the deuteration greatly decreases the 1<sup>st</sup> overtone bands from 1400-1600 nm, while the oven dried bread (black spectrum) still shows absorbance bands in this region. This means that from 1400-1600 nm, the oven dried bread spectrum shows loss of water and the deuterated bread spectra shows a decrease in absorbance bands from OH in water and carbohydrates and a decrease in NH in proteins. In Figure 2-26B it can also be observed that the 1<sup>st</sup> overtone bands of CH from about 1660-1800 nm increases and the water combination band at 1781 nm decreases. As seen from the example on bread, deuteration can be used to assign which absorbance bands are due to OH and NH and which are not. Similarly, oven drying can be used to assign the absorbance bands from water.

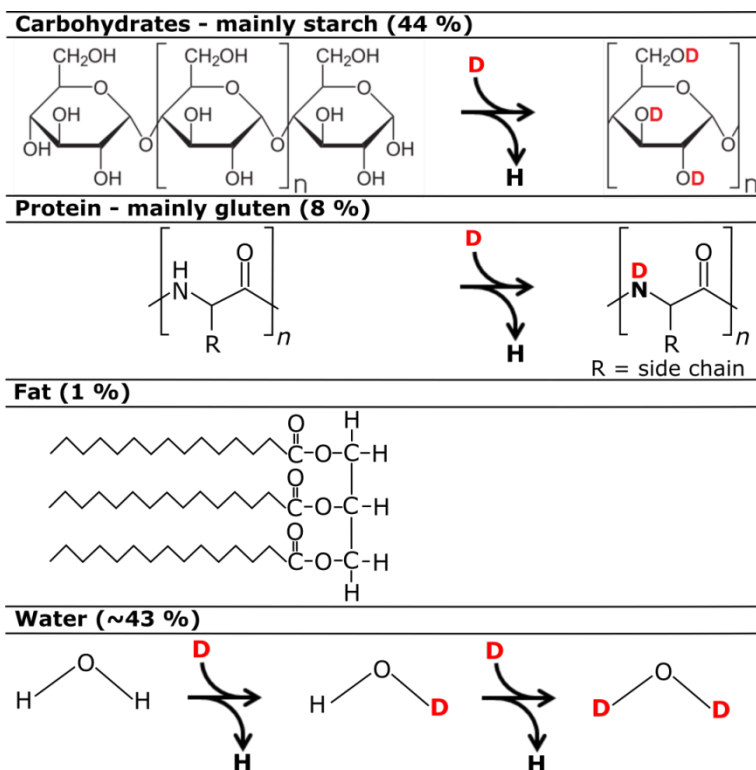


Figure 2-24. The main reactions in the deuteration of wheat bread.

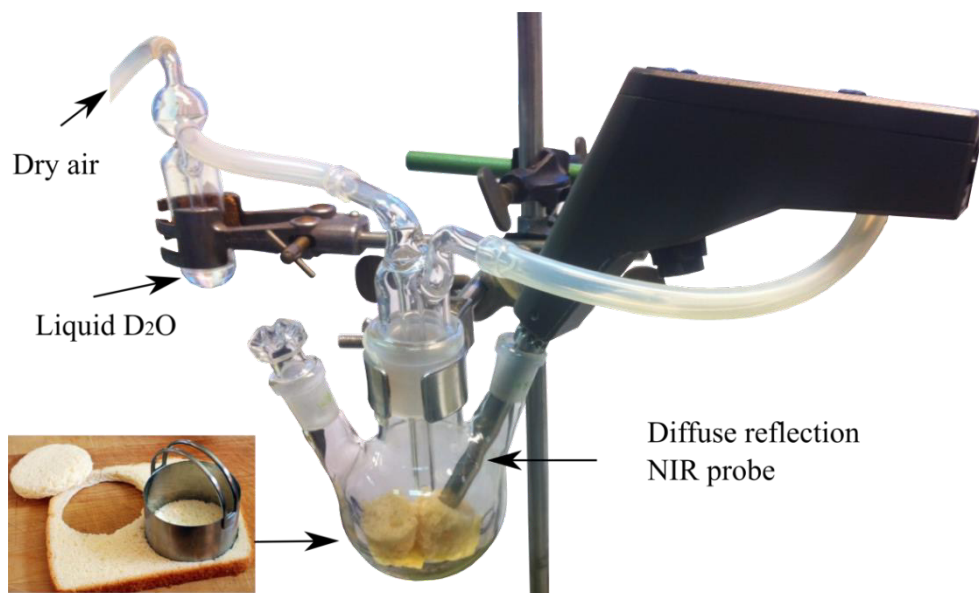


Figure 2-25. The setup for deuteration of wheat bread presented in the bread staling paper (**PAPER II**). A flow of dry air through liquid D<sub>2</sub>O produced a saturated atmosphere with D<sub>2</sub>O. The bread could be measured with a NIR probe in the round bottom flask and with MIR spectroscopy by taking a piece of bread out and quickly measure it on the ATR.

Table 2-3. MIR and NIR band assignments of D<sub>2</sub>O and HDO. The normal modes of D<sub>2</sub>O and HDO ( $\nu_1$ ,  $\nu_2$ ,  $\nu_3$  and  $\nu_L$ ) are the same as for H<sub>2</sub>O in Figure 2-8.

Region	Frequency (cm <sup>-1</sup> )	Wavelength (nm)	Assignment	Reference
MIR	< 600	< 16667	D <sub>2</sub> O $\nu_L$	37
	1207	8285	D <sub>2</sub> O $\nu_2$	27,38
	1458	6859	HDO $\nu_2$	27,37,38,88
	1555	6431	D <sub>2</sub> O $\nu_2 + \nu_L$	27
	2400	4167	D <sub>2</sub> O $2\nu_2$	27,38
	2407-2500	4155-4000	D <sub>2</sub> O $\nu_1$	27,38
	2476-2600	4039-3846	D <sub>2</sub> O $\nu_3$	27,38
	2900	3448	HDO $2\nu_2$	38
	3845	2600	D <sub>2</sub> O $\nu_1 + \nu_2$	27,37
	NIR	4945	2022	HDO $\nu_1 + \nu_2$
5080		1969	D <sub>2</sub> O $\nu_1 + \nu_3$	89,90
5975		1674	HDO $\nu_1 + \nu_3$	89
6165		1622	D <sub>2</sub> O $\nu_1 + \nu_2 + \nu_3$	89
6765		1478	HDO $2\nu_3$	89
7470		1339	D <sub>2</sub> O $2\nu_1 + \nu_3$	89
8065		1240	HDO $2\nu_1 + \nu_3$	89
8550		1170	D <sub>2</sub> O $2\nu_1 + \nu_2 + \nu_3$	89
10000		1000	HDO $2\nu_1 + \nu_2 + \nu_3$	89

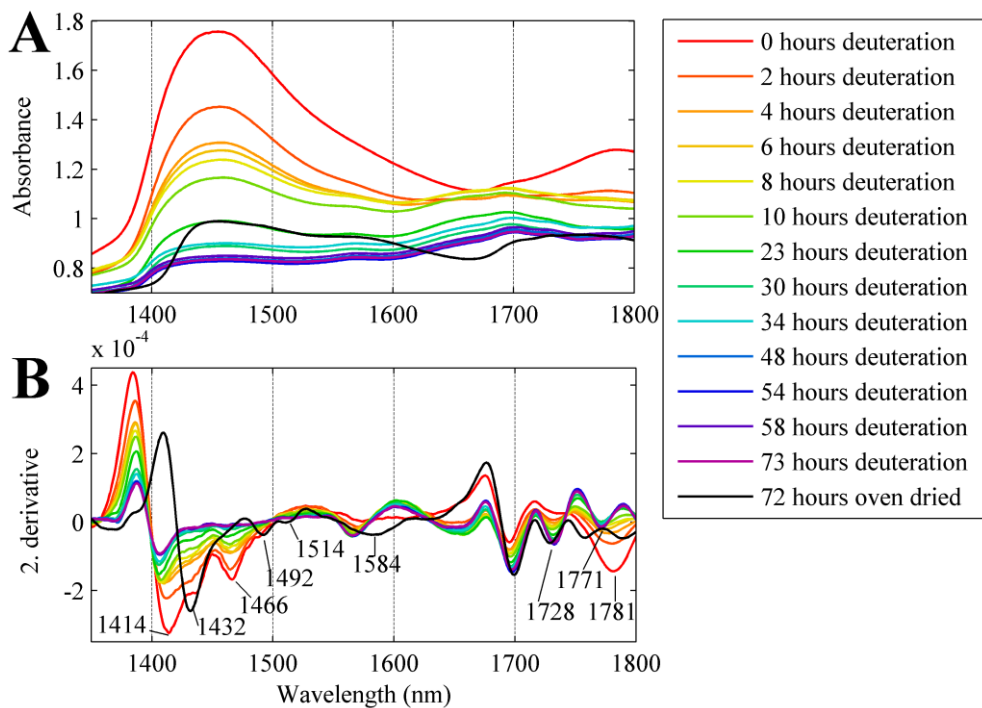
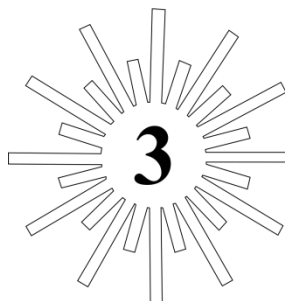


Figure 2-26. NIR spectroscopy of bread deuteration for 0-73 hours and one oven dried bread for 72 hours. A FT-NIR spectrometer (VECTOR 22N, Bruker Optik GmbH) was used and the 2<sup>nd</sup> derivative was calculated with a window size of 29 and 2<sup>nd</sup> degree polynomial.



# Advantages of using a supercontinuum laser in food analysis

---



*From what has been said it is also evident, that the Whiteness of the Sun's Light is compounded all the Colours wherewith the several sorts of Rays whereof that Light consists...*

— Sir Isaac Newton, 1704

## 3.1 Long-wavelength near-infrared spectroscopy of barley seeds

$\beta$ -glucan is a fiber that has shown health promoting properties such as lowering of serum cholesterol levels, stabilization of the blood glucose and insulin rises after food consumption and an increased feeling of fullness.<sup>91</sup> On the other hand, high amounts of  $\beta$ -glucan in barley can cause problems in beer production by clogging of filters and causing an unwanted haze in the final product.<sup>91</sup> Previous studies have shown that the long wavelength (LW) NIR region from 2200–2500 nm in reflectance mode could differentiate barley flour with different  $\beta$ -glucan content<sup>92</sup> and predict the  $\beta$ -glucan content.<sup>93</sup> A non-destructive method that could do the same on whole seeds would be useful in food production to sort seeds according to quality or in plant breeding to sort according to trait. Since the  $\beta$ -glucan is situated in the barley endosperm, it would be advantageous to be able to measure intact seeds in transmission mode (Figure 3-1).<sup>94</sup> Previously, transmission measurements of intact seeds have primarily been done in the short wavelength (SW) region below 1100 nm because of the larger molar absorptivity coefficients at longer wavelengths. In the work presented in the barley endosperm paper (**PAPER I**) and the barley whole grain paper (**PAPER III**), supercontinuum light was used to do the first transmission measurements with LW-NIR spectroscopy on whole barley seeds.

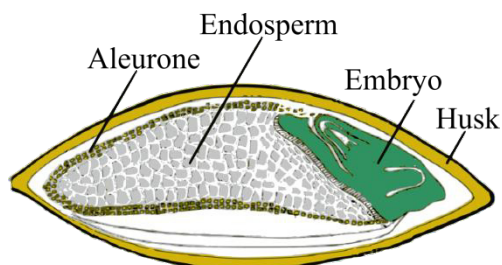


Figure 3-1. Barley structure.<sup>94</sup>

### 3.1.1 Aim

The initial aim of the barley endosperm paper (**PAPER I**) was to investigate the chemical information in LW-NIR spectra of intact barley seeds measured with a supercontinuum source. However, since it was not possible to measure on whole seeds with the available intensity of the supercontinuum light, then 1 mm slices of barley endosperm were measured. Thanks to the development of a more powerful supercontinuum light, the barley whole grain paper (**PAPER III**) had the goal of measuring on intact barley seeds in the LW-NIR region and to develop predictive models for  $\beta$ -glucan and protein content.

### 3.1.2 Experimental setup

The experimental setup consisted in a supercontinuum light source (NKT Photonics) with a spectral range from 1500-4200 nm in the barley endosperm paper (**PAPER I**) and from 2100-2600 nm in the barley whole grain paper (**PAPER III**). A monochromator was applied to separate the wavelengths and two PbSe detectors were used for pulse-normalization. The pulse-normalization was necessary because the supercontinuum pulses vary in intensity and polarization.<sup>95</sup> The spectral region selected for measurement was 2260-2380 nm and each measurement took 1 minute. Five different barley genotypes were used to make a sample set with a relatively big variation in chemical composition. The barley endosperm paper (**PAPER I**) measured on 350 barley seed slices of 1mm and the barley whole grain paper (**PAPER III**) measured on 105 intact barley seeds (~2.5 mm thick) with LW-NIR spectroscopy. The bulk flour content of moisture,  $\beta$ -glucan, starch, protein and lipid was measured in the barley endosperm paper (**PAPER I**) whereas only fiber was measured in the barley whole grain paper (**PAPER III**) by wet chemical analysis for each of the five barley genotypes. The single seed content of  $\beta$ -glucan and protein was measured by wet chemical analysis for each of the 105 seeds in the barley whole grain paper (**PAPER III**).

### 3.1.3 Results

The barley endosperm paper (**PAPER I**) assigned the LW-NIR absorbance bands at 2287, 2323 and 2349 nm to be mainly from starch, starch and  $\beta$ -glucan, respectively. In addition, it was possible to separate the five barley genotypes in a PCA score plot and the best separation was reached by spectral preprocessing with EMSC. In the barley whole grain paper (**PAPER III**) the  $\beta$ -glucan and protein content was measured on the individual barley seeds with variations from 3.0-16.8 % and 8.9-20.2 %, respectively. The spectral preprocessing methods SNV, MSC, EMSC and Savitzky-Golay 2<sup>nd</sup> derivative were applied, but the best predictive result from a PLS model was achieved from using the raw data. It was possible to make PLS models to predict  $\beta$ -glucan in intact barley seeds with  $R^2_{CV}$  equal to 0.83 and root mean square error of cross-validation (RMSECV) equal to 1.67 %. The PLS model for protein gave a  $R^2_{CV}$  equal to 0.45 and a RMSECV of 1.73 %. The PLS model for protein did not perform well, and the focus will therefore be on  $\beta$ -glucan

### 3.1.4 Discussion, concluding remarks and perspectives

The chemical information in the LW-NIR region showed information on  $\beta$ -glucan content and, to a smaller degree, protein content as seen from the predictive result in the barley whole grain paper (**PAPER III**). A covarygram of the whole barley seed spectra in Figure 3-2 shows that starch, lipid, protein,  $\beta$ -glucan and total fiber content all contribute to the absorbance of the CH combination bands in this region. However, the strongest correlation was observed between  $\beta$ -glucan content and the wavelength at about 2350 nm.

The PLS model for  $\beta$ -glucan showed better  $R^2_{CV}$  compared to previous NIR spectroscopy models on  $\beta$ -glucan in intact barley seeds.<sup>96-98</sup> The model could be slightly improved by averaging 2 or 3 repeated measurements. A bit surprisingly, the model could also be improved by regression of the individual spectra towards the average  $\beta$ -glucan value of each of the five barley genotypes. This suggests that the PLS model works more as a classification rather than a regression model. In the barley whole grain paper (**PAPER III**) it was speculated that the small beam size could be the reason why  $\beta$ -glucan was better predicted when the average genotype value was used. It was then hypothesized that a bigger beam size might improve the representative sampling and thus the predictive results. The spectral variations caused by different sizes and shapes of the seeds may be an additional explanation why the predictive results improved when using average  $\beta$ -glucan values as the dependent values. A way to improve the predictive results could be to increase the S/N ratio by using a more sensitive detector. This could, for instance, be a PbS detector which is about 100 times more sensitive at 300 K compared to the PbSe detector used.<sup>10</sup> A

bigger beam size and a more sensitive detector might improve the predictive results and in addition it could possibly decrease the number of bad spectra which was 29 % (91/315 spectra). The high number of spectral outliers is not acceptable in plant breeding or industrial sorting, and it is therefore important to decrease this number in future developments of an instrument.

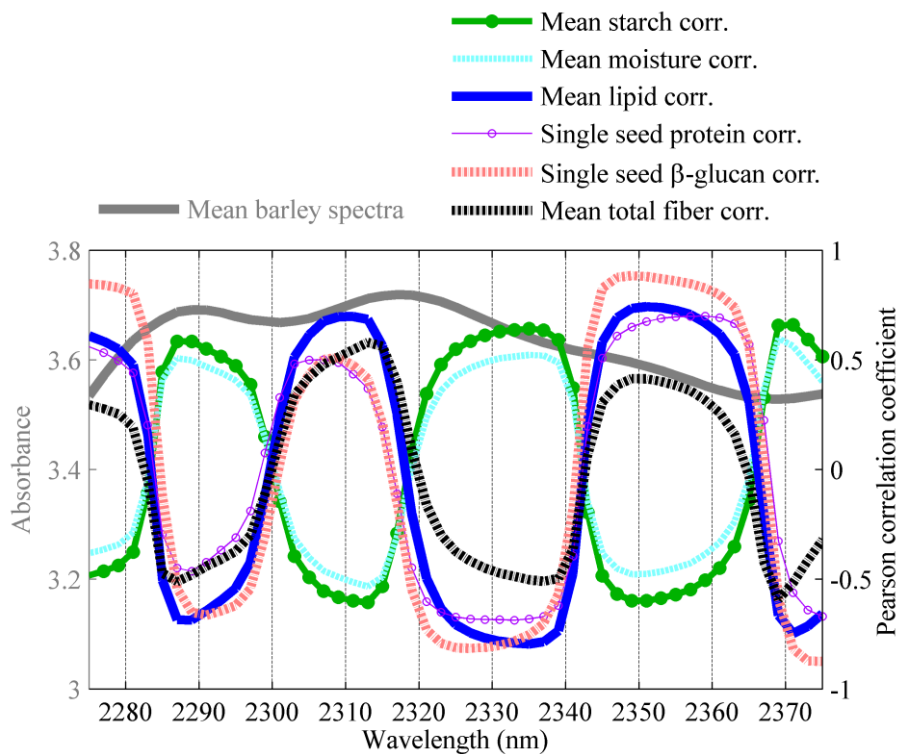


Figure 3-2. Covarygram of the spectra presented in the barley whole grain paper (**PAPER III**) preprocessed with EMSC and showing the correlation to the wet chemical measurements. Starch, moisture, lipid and total fiber was the mean value for each of the five barley genotypes. Protein and  $\beta$ -glucan was measured on each single seed.

For plant breeding a measurement time of 1 minute is acceptable. However, for industrial sorting of seeds, the measurement time needs to be substantially faster. The supercontinuum light contains pulses repeated every  $2.9 \cdot 10^{-5}$  s and it is therefore not the light source that is limiting the measurement speed. The current setup used a monochromator, which needs to move the grating to scan several wavelengths. In order to decrease the measurement time then several options need to be considered. A simple way could be to decrease the number of measured wavelength points

or/and the measurement time/point, which was 105 ms measurement time every 2 nm in the current setup. Another option could be to change the wavelength selection method to, for instance, a diode array spectrometer.<sup>11,99</sup> However, then all 120 mW of supercontinuum light would reach the seed which is more than the average 6 mW that reached the seed in the monochromator setup. A lot more energy will therefore reach the seed and this can potentially damage it. In the study by Museux, et al.<sup>100</sup> it was found that a 1940 nm laser beam on skin caused damage after 10 s of 1.4 W/cm<sup>2</sup>. Chen, et al.<sup>101</sup> found that a 2000 nm laser on skin caused persistent redness after 2.5 s with 2.85 W/cm<sup>2</sup> or 1 s at 4.74 W/cm<sup>2</sup>. In the barley endosperm paper (**PAPER I**) and the barley whole grain paper (**PAPER III**) the beam size was 0.1 mm x 0.5 mm which for the 6 mW would give 3.8 W/cm<sup>2</sup> and for the 120 mW it would give 76.4 W/cm<sup>2</sup>. The power per area might therefore be too high if a diode array spectrometer is used with the beam size applied in the barley endosperm paper (**PAPER I**) and the barley whole grain paper (**PAPER III**). One way of lowering the power/area could be to increase the beam size which as a side effect might also improve the representative measurement of the seed. Another point that should be considered for a diode array spectrometer is that the light, after going through the seed, will be highly scattered, thus complicating the detector array setup. It therefore seems possible to do faster LW-NIR transmission measurements on intact seeds by decreasing the resolution of the setup used in the barley endosperm paper (**PAPER I**) and the barley whole grain paper (**PAPER III**). It might also be that a faster wavelength selection method such as diode array spectrometer can be used, but possible damage of the seeds and detector setup needs to be examined. The sample presentation method can also make a big difference to the number of seeds analyzed in a time interval and this will be discussed in the following.

If the spectrometer applied in the barley endosperm paper (**PAPER I**) and the barley whole grain paper (**PAPER III**) is commercialized then it will compete with other NIR spectrometers for single seed analysis. The speed, spectral region and sample presentation of commercial single seed NIR spectrometers are therefore investigated as a comparison. Commercial single seed NIR spectrometers have received an increasing amount of attention during the last decade. One of the earlier single seed instruments, which are no longer manufactured today, is the Infratec 1255 Food and Feed Analyzer (FossTecator, Höganäs, Sweden). This instrument measured single seeds in transmission mode from 850-1050 nm at a speed of ~ 1.5 minute per seed (Figure 3-3).<sup>102</sup> Another NIR spectrometer for single seed sorting is the single-kernel near-infrared (SKNIR) system (Perten Instruments, Stockholm, Sweden).<sup>103</sup> The instrument uses NIR reflectance from 950-1650 nm to measure e.g. protein and hardness at a speed of about 2 seconds per seed. In 2010 the EyeFoss (FOSS, Hillerød, Denmark) was launched; it uses five wavelengths from

the visible region and one NIR wavelength in image analysis (Figure 3-4).<sup>104</sup> The instrument can do quality assessment on, for instance, the content of small foreign seeds, stained seeds, spotted mould or sprouted seeds with a speed of about 2500 seeds / minute. A newly founded company from 2010 has developed the QSorter (QualySense AG, Glattbrugg, Switzerland), which uses NIR spectroscopy in reflectance mode from 900-1700 nm together with image analysis in the visible region (Figure 3-5). The instrument can sort single seeds according to, for instance, moisture, protein, oil, sugar content, size, color and shape with a speed of ~ 3000 kernels / minute, which corresponds to 10 kg / hour. Another young company developing NIR single seed instruments is BoMill AB (Lund, Sweden), which was founded in 2001. They have developed the IQ and TriQ which use NIR spectroscopy in transmission mode from 1100-1700 nm (Figure 3-6).<sup>105</sup> The instruments can, for example, sort by falling number, vitreousness, fusarium and protein content with a speed of ~ 3 tons / hour for TriQ and ~ 1000 kernels of barley and wheat / minute for IQ. By comparing the different instruments, it can be seen that the highest rate of single seed analysis is achieved with the TriQ. The reasons for this are that TriQ makes fast and many measurements at the same time in the rotating drum. The IQ measures one seed at a time and here the measurement time is approximately 60 ms per seed. It seems clear that the measurement speed of single seed NIR spectroscopy depends on both spectrometer performance, but also on the sample presentation technology. The setup used in the barley endosperm paper (**PAPER I**) and the barley whole grain paper (**PAPER III**) can therefore be improved by decreasing the measurement time and/or the sample presentation.

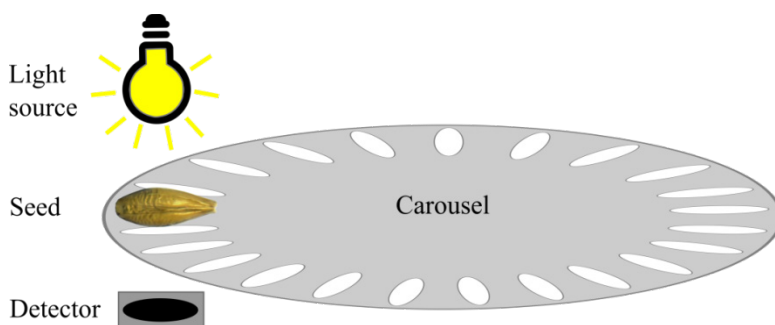


Figure 3-3. Sample presentation of the Infracore 1255 Food and Feed Analyzer from Foss-Tecator. Single seeds are manually placed in a rotating carousel with holes for 23 seeds and they are measured in transmission mode.



Figure 3-4. The EyeFoss from FOSS ([www.foss.dk](http://www.foss.dk)). Seeds are spread out on a conveyer belt to facilitate the image analysis on each single seed. Figure by courtesy of FOSS.

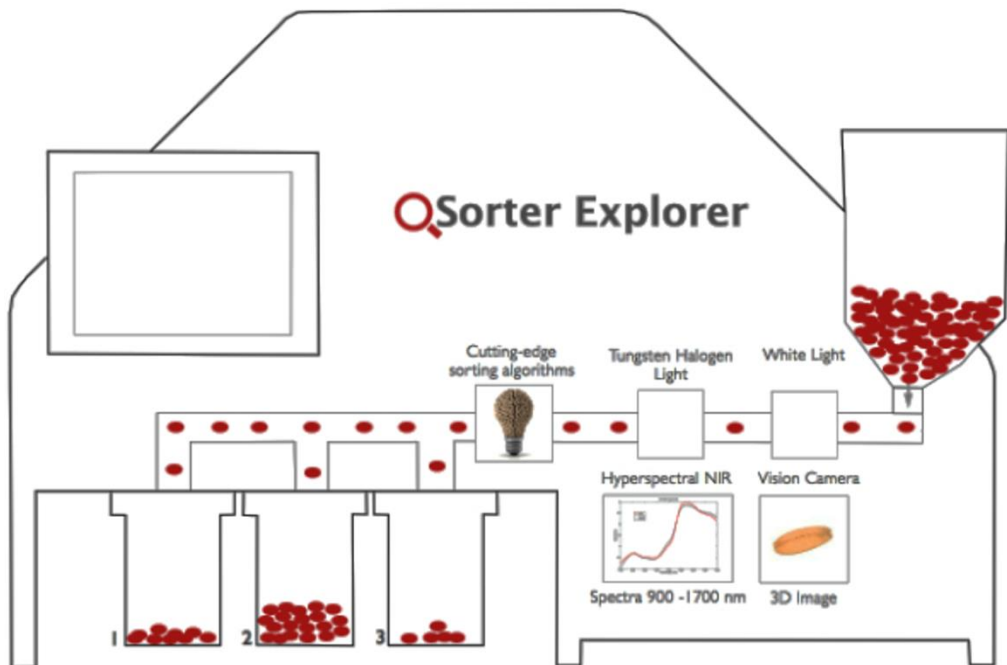


Figure 3-5. Single seed sorter from QualySense ([www.qualysense.com](http://www.qualysense.com)). Figure by courtesy of QualySense.

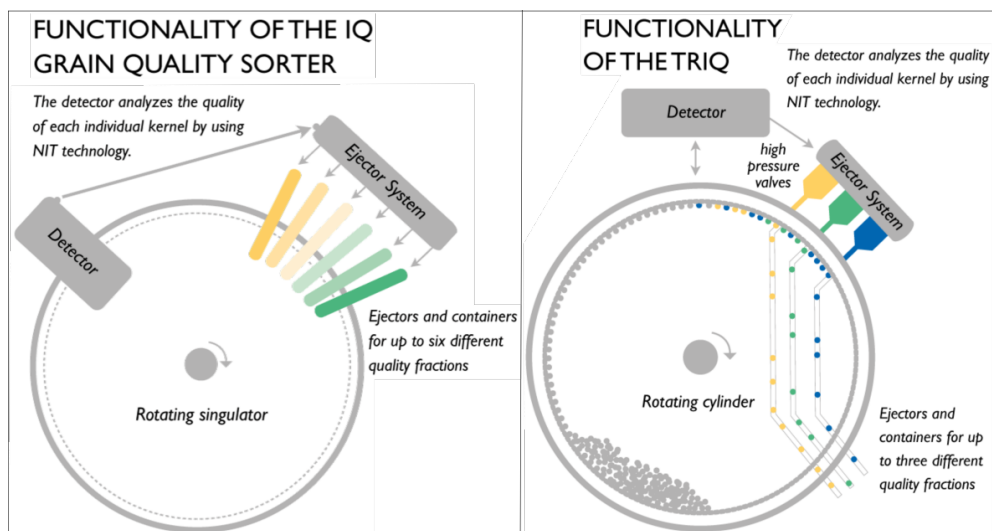


Figure 3-6. The single seed sorter from BoMill ([www.bomill.com](http://www.bomill.com)). The IQ has a carousel with holes for the seeds along the edge which is similar to the Infratec in Figure 3-3. The carousel is tilted so the seeds automatically fall into the holes when it rotates. The TriQ has a cylinder with many holes on the inside. The seeds automatically fall into the holes when the cylinder rotates. Figure by courtesy of BoMill.

### 3.2 Potential for supercontinuum gas measurements

Molecules in gas phase are often measured with gas chromatography (GC), gas sensors or electronic-noses (e-noses).<sup>106</sup> GC can give high precision information on the chemical composition of gases, but the equipment is expensive, requires expert knowledge and is in general not applicable as an *in-situ* measurement technique. Gas sensors come at a lower price and can have a high sensitivity for specific gases, but suffer from cross-responses to other gasses and a high sensitivity to humidity. E-noses comprise a matrix of sensors that can work as a fingerprint for different gases. However, each e-nose is application specific, might not work on all samples and the chemical interpretation of the result may not be possible.<sup>107</sup> In contrast, vibrational spectroscopy can be directly applied to gas mixtures as an *in-situ* measurement and provide useful chemical information. Only a few examples of direct gas analysis with infrared spectroscopy on food samples exist in the literature. In all cases MIR spectroscopy was chosen, but some few studies also measured the LW-NIR region to  $4400\text{ cm}^{-1}$  (2273 nm) (Table 3-1). The reason that gas measurements have been performed with MIR and not with NIR spectroscopy might be due to the lower absorbance of the overtones in the NIR region compared to the MIR as explained in Section 2.5.1 and 2.4.3. Measurements with NIR spectroscopy therefore

need much longer path-lengths to get a good S/N ratio. The spatial coherence of the supercontinuum light makes it possible to use gas cells with extremely long path-lengths without losing a lot of light as would be the case for the traditional NIR and MIR lamps. The supercontinuum light is therefore a very promising new technology for NIR gas measurements.<sup>22</sup>

Table 3-1. Infrared spectroscopy studies on the head space of food. Res. = resolution.

<b>Product</b>	<b>Application</b>	<b>Sampling</b>	<b>Frequency (cm<sup>-1</sup>)</b>	<b>Path- length</b>	<b>Res. (cm<sup>-1</sup>)</b>
Beef <sup>108</sup>	Spoilage	Head space	4400-800	0.5-2.5 m	0.5
Beef <sup>109</sup>	Infection with <i>S. typhimurium</i>	Head space (at 100°C)	4000-500	2 m	0.5
Sausage <sup>110</sup>	Nitrite	Head space of boiled and blended meat	1876	10 cm	2
Seafood <sup>111</sup>	Trimethylamine	Head space of sea- food with trichloro- acetic acid and NaOH (85°C)	3023-2688	10 cm	2
Cheese <sup>112</sup>	Authenticity	Dried samples	4000-650	10 cm	4
Oil <sup>113</sup>	Oxidation	Head space (at 180°C)	3196-2494, 1992-896	9.8 m	16
Grapes <sup>114</sup>	Spoilage	Head space (at 22°C)	4000-600	2 m	0.5
Strawber- ries <sup>115</sup>	Spoilage	Head space (at 20°C)	4000-600	2 m	0.5
Strawber- ries <sup>116</sup>	Determination of volatiles	Head space of mashed fruit in vac- uum (at 50 °C)	4000-950	9 m	low
Apple <sup>117</sup>	Pesticide	Head space (at 22°C)	2990-2830, 1259-1227	2 m	0.5
Vinegar <sup>118</sup>	Differentiate vinegars	Head space (at 40°C)	4400-400	2 m	0.5
Beer, wine and spirits <sup>119</sup>	Ethanol	Head space (at 80°C or 90°C)	1150-950	3.2m	8
Spirit <sup>120</sup>	Differentiate spirits	Head space of spirit in water (at 22°C)	4000-600	2 m	0.5
Must and wine <sup>121</sup>	SO <sub>2</sub>	Head space (at 30°C)	1600-1000	39 mm	16

In addition to the applications mentioned in Table 3-1, the following three examples could also be applications for NIR and MIR spectroscopy gas measurements. The first possibility is to measure diacetyl, which is an important flavor of cheese, butter and yoghurt where it gives a buttery aroma. At low levels, it also gives complexity

to wine, but in beer it is highly undesirable.<sup>122</sup> Diacetyl has also been found in vacuum packed meat where it caused off-odors.<sup>123</sup> A second possibility is the measurement of ethylene, which is a chemical that regulates the ripening of many fruits such as banana, apple, pear, most stone fruits, melons, squash, and tomato.<sup>124</sup> A third possibility is to measure on head space of process water. Atmospheric trace gas analysis has been able to detect gasses at ppt and this approach could be used in a similar way on the head space of process water.<sup>125</sup>

### **3.3 Supercontinuum light and a wavelength separating fiber**

The fact that the supercontinuum light exits from a fiber makes it theoretically possible to direct the light into a fiber with no loss. This advantage was used in a new wavelength separation method called dispersive Fourier transformation spectroscopy (described in Section 2.1.2) where the supercontinuum pulses went through several km of dispersive fiber in order to separate the wavelengths. The principle is similar to chromatography where different molecules travel with different speed through a medium and hence separate. In this case, it is the different wavelengths that travel with varying speed through the fiber and therefore exit the fiber at different time-points.

#### **3.3.1 Aim**

The aim was (a) to perform the first measurements with dispersive Fourier transformation spectroscopy and a supercontinuum laser on food samples and (b) to evaluate possible future applications.

#### **3.3.2 Experimental setup**

The 2 ns pulsed supercontinuum light covers the region from 450-2500 nm as seen in Figure 3-7 and has a total output power of 110 mW (SuperK Compact G4, NKT Photonics). The spectrometer setup is presented in Figure 3-8. The supercontinuum light was set to a repetition rate of 20 kHz and aligned into 10.6 km of silica fiber. The silica fiber was a dispersion compensating fiber (DCF) (LL micro, OFS Fitel). A fiber switch was used to direct the light to a transmission probe or a reflectance and transmittance probe. The light beam was divided in two with a beamsplitter so that the majority of the light would interact with the sample and a smaller part would not. The signals were Fourier transformed from the time domain into a frequency domain. The Fourier transform function was calculated as seen in Figure 3-9 from a 3<sup>rd</sup> degree polynomial fitted to measurements with five optical filters with a high transmission in a narrow wavelength region and blockage of light on either

side of that region. The optical filters had a center wavelength  $\pm 2$ -2.4 nm and a full width at half maximum (FWHM) of  $\pm 10$ -12 nm. Two 150 MHz InGasAs detectors measured the two signals and these signals were divided at each wavelength to normalize for the variations in pulse intensity and polarity as explained in Section 3.1.2. The detector that measured the signal without sample interaction was set at a small angle from the light beam in order to be independent from polarity (Figure 3-10 and 3-11).<sup>95</sup> The sample cups for reflectance and transflection measurements are the large cup and slurry cup from a dispersive NIR spectrometer (NIRS<sup>TM</sup> DS2500 F, FOSS), respectively. The slurry cup has a 1mm path-length and a gold reflector. The beam size reaching the sample in transmission, transflection or diffuse reflectance mode was about 2 mm in diameter. The wavelength region from about 1300-1650 nm could be used due to the increasing Rayleigh scattering at shorter wavelengths and a higher absorbance from silica at longer wavelengths.<sup>126</sup> The signal from 25,000 pulses was averaged into a spectrum in order to improve the S/N ratio. A measurement took  $\sim 14$  s. The resolution (i.e. interval between wavelengths) is 2.2 nm at 1650 nm, 2.9 nm at 1500 nm, 4.4 nm at 1400 nm and 5.8 nm at 1300 nm. Spectra were preprocessed with Savitzky-Golay 2<sup>nd</sup> derivative (window size 11, 2<sup>nd</sup> degree polynomial) (described in Section 2.4).

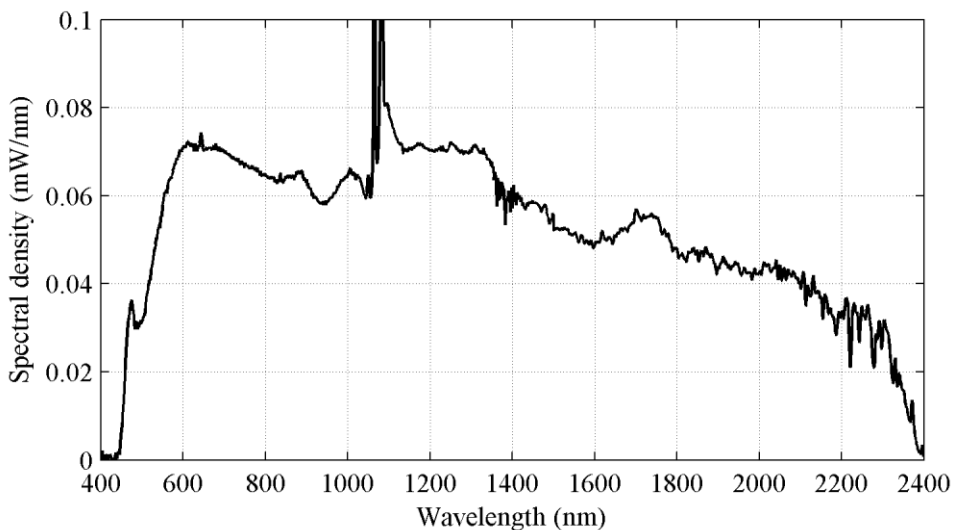


Figure 3-7. Typical spectrum of the SuperK Compact supercontinuum source. Figure by courtesy of NKT Photonics.

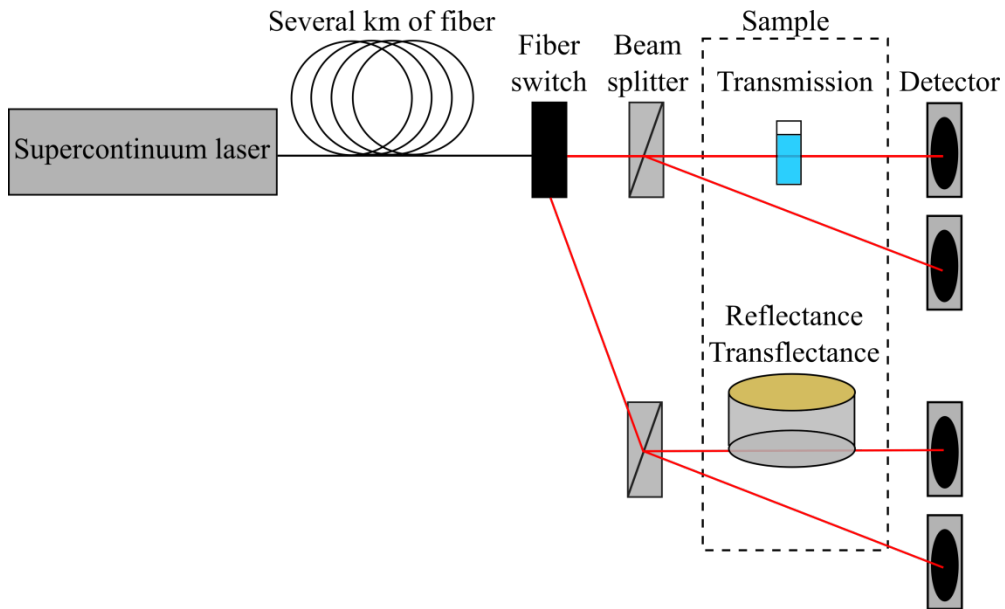


Figure 3-8. An all solid state spectrometer consisting of a supercontinuum laser and a 10.6 km dispersive fiber. The new type of wavelength separation method is called dispersive Fourier transformation. The supercontinuum light passes through the fiber and the different wavelengths separate as they pass through the fiber. A Fourier transformation calculates the signal from a time domain into frequency domain. Afterwards, a fiber switch can be set for transmission or reflectance and transfectance mode. A beamsplitter divides the light in two in order to perform a pulse-to-pulse normalization of the detector signal with and without sample interaction.

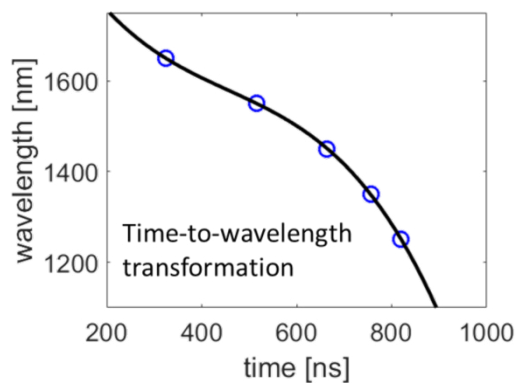


Figure 3-9. Transformation of the spectrometer signal from a time domain to a frequency domain. Figure by courtesy of FOSS.

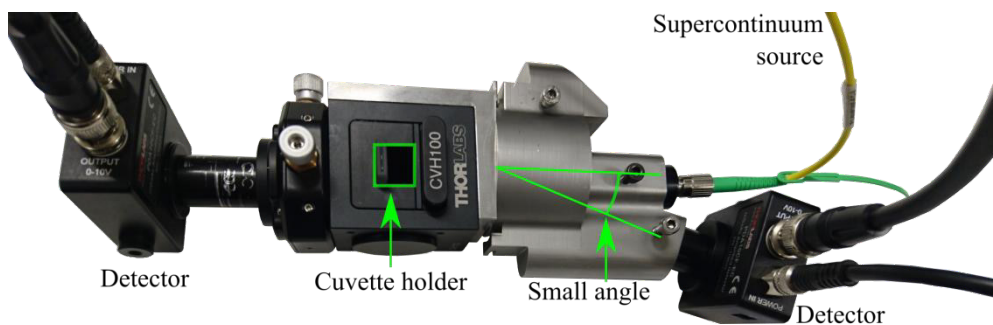
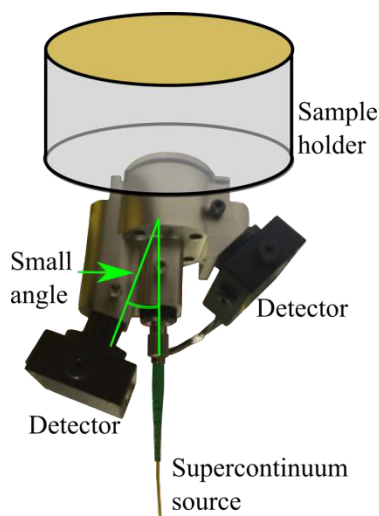


Figure 3-10. The sample holder for transmission measurements.



3-11. The sample holder for reflectance and transreflectance measurements.

### 3.3.3 Results

NIR spectroscopy measurements in transmission mode were performed on 25-31 % (w/w) sucrose in water with water as background (Figure 3-12). The spectral changes followed the sucrose concentration. However, some unknown periodic noise was present on the absorbance band at 1410-1470 nm. A different sample presentation was applied in order to better understand the unknown fluctuations. The sucrose in water samples were therefore also measured in transreflectance mode. Figure 3-13A shows the raw spectra measured in transreflectance mode and the unknown fluctuations in Figure 3-12 are no longer present. Another difference between the transmission and transreflectance spectra is that the transreflectance spectra have base-

line differences (Figure 3-13A). The transfection spectra were preprocessed with 2<sup>nd</sup> derivative, to remove the baseline variations. However, preprocessing could not fully solve the baseline differences. The spectra from the supercontinuum light and a wavelength separating fiber were compared with the spectra from a commercial FT-NIR spectrometer (Figure 3-14). The water and sucrose spectra exhibited absorbance bands at the same wavelengths when measured on the two different spectrometers, which confirm that the wavelength separating fiber is working as intended.

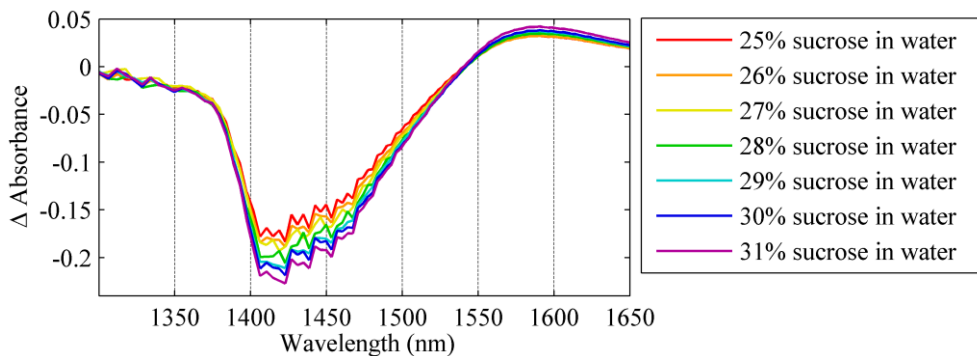


Figure 3-12. Sucrose in water measured on the NIR spectrometer with a supercontinuum light and a wavelength separating fiber in transmission mode. The path-length was 1mm in a cuvette and water was used as background.

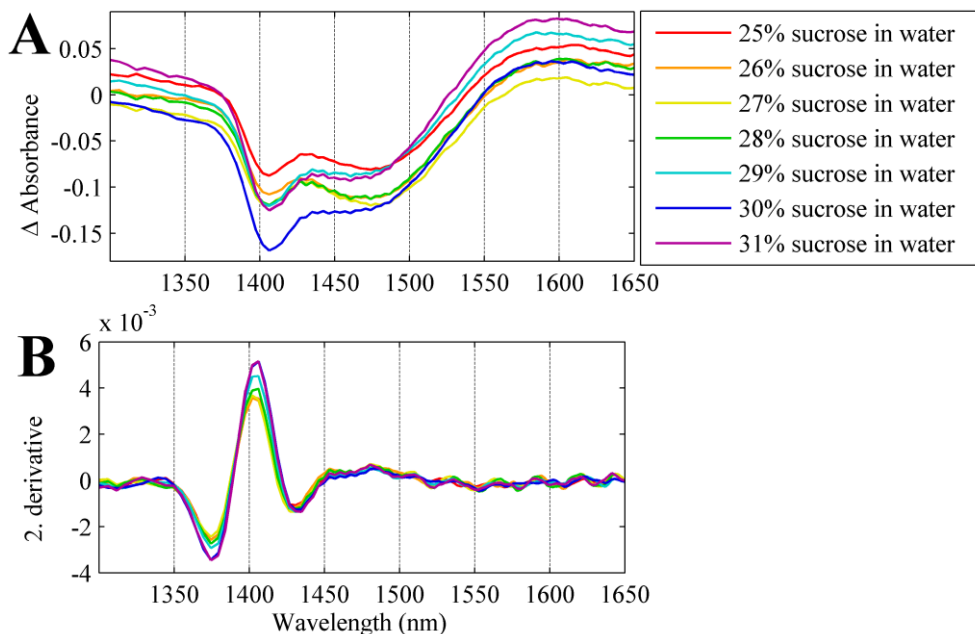


Figure 3-13. Sucrose in water measured on the NIR spectrometer with a supercontinuum light and a wavelength separating fiber in transflection mode. The path-length was 1mm in a NIRS™ DS2500 slurry cup and water was used as background.

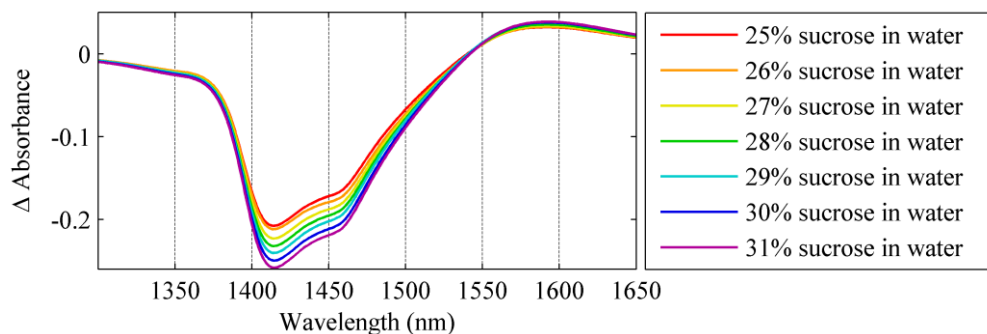


Figure 3-14. Sucrose in water measured on a FT-NIR spectrometer (FTLA2000-160, ABB Bomem) in transmission mode. The path-length was 1 mm in a cuvette and water was used as background.

In a second experiment the supercontinuum fiber spectrometer was used to perform measurements in reflectance mode on skim milk powder with melamine from 5-30 % (w/w). The spectra in Figure 3-15A shows peaks that have been assigned to  $\text{NH}_2$  symmetric stretching (1520-1541 nm) and  $\text{NH}_2$  antisymmetric stretching (1499-1520 nm).<sup>127</sup> As shown in Figure 3-15B, it was possible to remove the baseline dif-

ferences by preprocessing with the 2<sup>nd</sup> derivative. The spectra of skim milk powder with melamine showed the same baseline differences as was seen for the transfection spectra in Figure 3-13. The reflectance and transfection measurements used the same sample presentation except for the sample cup. This indicates that the noise fluctuations in Figure 3-12 and the baseline variations in Figure 3-13 and 3-15 are due to the sample presentation.

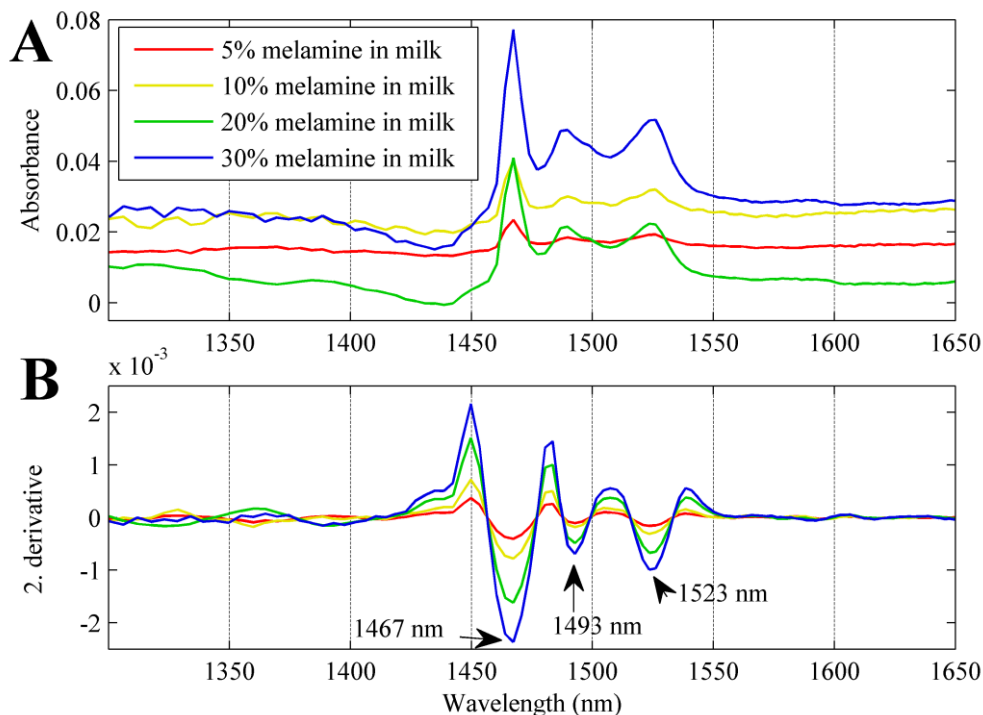


Figure 3-15. Melamine in skim milk powder measured on the NIR spectrometer with a supercontinuum light and a wavelength separating fiber in reflectance mode. Skim milk powder was used as the reference.

### 3.3.4 Discussion, concluding remarks and perspectives

The advantage of a supercontinuum light together with a wavelength separating fiber is that the spectrometer has no moving parts, which means that the vibrations in a production environment will not affect the wavelength separation. Another useful aspect is that the supercontinuum light can easily be transported by fibers to different sites in a production, which makes it possible to have one light source for many measurement points. Another benefit of the supercontinuum source is that the pow-

er consumption is  $< 40$  W which means that it will not cause excessive heating of the instrument. These advantages suggest that the spectrometer can be used in a production environment. The possible applications are many since all the four main food components absorb from 1300-1650 nm, namely carbohydrates, fats, protein and water. An example of this is shown in Figure 3-16 where the spectra of water, wheat germ oil, wheat starch, wheat gluten and cellulose are shown. Some of the possible applications could be fast image analysis on flour with mycotoxin or milk powder with melamine. In these two cases the small beam size would mean that it would be possible to detect small concentrations of toxic compounds and/or adulterations which would not be detected with a bigger beam size because a larger illuminated area will show the average of this area.

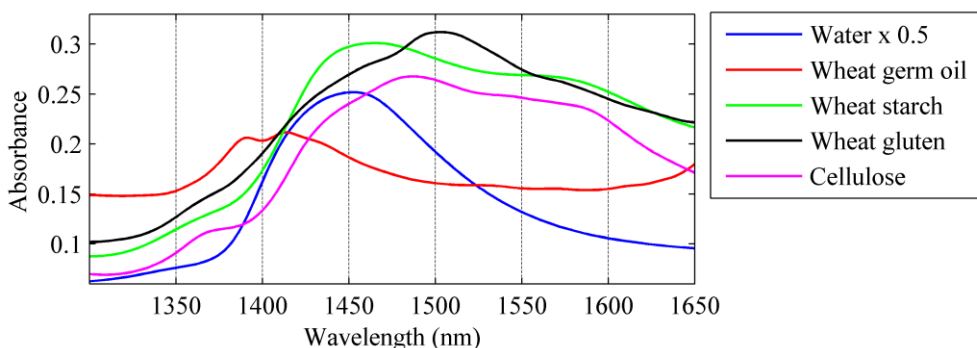


Figure 3-16. NIR spectroscopy measurements in transreflectance mode of water with a 0.2 mm path-length and wheat germ oil with a 1 mm path-length. NIR spectroscopy measurements in reflectance mode of wheat starch, wheat gluten and cellulose with a dispersive NIR spectrometer (NIRS™ DS2500 F, FOSS).

One of the challenges with the supercontinuum source is that it has more signal fluctuations compared to a traditional NIR lamp, which cause more noise in the spectra.<sup>95</sup> An additional aspect to consider is the higher price of the supercontinuum light ( $\sim 5000$  Euro) compared to a NIR lamp ( $\geq 140$  Euro depending on lifetime and power).<sup>128,129</sup> The last and maybe biggest challenge is that the wavelength separating fiber has not previously been applied in commercial spectrometers, hence information of possibilities and limitations are scarce.

The current setup has proved that it is possible to use a wavelength separating fiber in spectroscopy. The resolution seems sufficient for measuring sucrose in water and melamine in milk powder. If a higher resolution is desired then this can be done by (1) changing to a fiber with an increased chromatic dispersion (which affects the

difference in speed of the different wavelengths) or (2) increase the speed of the analog-to-digital conversion in the readout electronics. The presented work used the highest resolution that was possible with the available hardware, but it might be possible to increase the resolution with new hardware. The spectral region seems satisfactory for many applications. If a wider spectral region is wanted then this depends on the fiber. A fiber with a greater dispersion coefficient,  $D$ , need a shorter length to achieve a certain separation in time compared to a fiber with a smaller  $D$ , because the separation is given by length times  $D$ . A shorter fiber will result in less absorption, which gives more signal at shorter wavelengths. The extension to longer wavelengths is more difficult because of the high absorbance from silica, so for this to happen a non-silica fiber is needed. A fiber with a higher dispersion is therefore needed to increase both the resolution and the wavelength region. However, the fiber needs to be long to increase the resolution and it needs to be short to increase the wavelength region. This means that a compromise has to be made between resolution and wavelength region.

In future setups, it could be interesting to improve the sample presentation and thereby remove spectral artefacts. In addition, more experimentation is needed to build an understanding of the performance of this technology on different compounds of interest. Especially the generation of calibration models would be beneficial for determining its possibilities for the future.



# Spectral interpretation with two-dimensional correlation spectroscopy

---

*If someone separated the art of counting and measuring and weighing from all the other arts, what was left of each (of the others) would be, so to speak, insignificant.*

— Plato, 427 B.C. - 347 B.C.

## 4.1 Wheat bread aging (staling)

Bread staling is a term used to describe changes in bakery products, which cause a decreasing consumer acceptance because of non-microbial processes. Bread staling is responsible for food waste with a significant global environmental footprint. Several chemical and physical changes occur in bread during storage. One of the processes is the change from an amorphous starch structure in fresh bread to a more crystalline starch structure (i.e. retrogradation) in stale bread. The starch components, amylose and amylopectin, both change from a more amorphous structure to a more ordered structure during bread aging as shown in Figure 4-1. Bread staling and crystallization of starch gels have been studied with infrared spectroscopy at wavenumbers that were associated with recrystallization of amylopectin ( $1047\text{ cm}^{-1}$ ) and amorphous starch ( $1022\text{ cm}^{-1}$ ).<sup>130,131</sup> A few studies have investigated bread staling with NIR spectroscopy and most of them used raw spectra, which contain both chemical and physical information.<sup>130,132-134</sup>

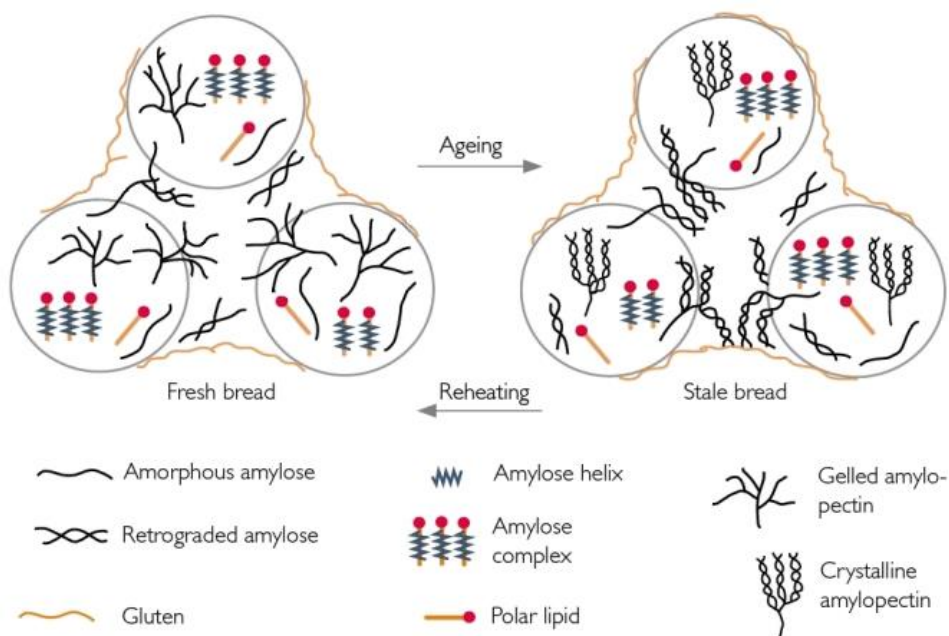


Figure 4-1. Bread staling processes.<sup>135</sup> Starch consists of amylose and amylopectin which both undergo conformational changes from a more amorphous structure in fresh bread to a more ordered and crystalline structure in stale bread.

#### 4.1.1 Aim

The study presented in the bread staling paper (**PAPER II**) aimed at using 2D NIR-MIR correlation spectroscopy on the bread crumb staling process in wheat bread. This consisted in using *a priori* knowledge from the MIR spectra to increase the chemical interpretation of the changes in the NIR spectra with a primary aim at replacing the sampling inefficient MIR measurement with the more sample efficient NIR. For additional interpretation, the hydrogen atoms of OH and NH groups in bread were deuterated in a second experiment.

#### 4.1.2 Experimental setup

NIR and MIR spectroscopy was applied to wheat bread crumb at 3 hours, 9 hours, 1, 2, 4, and 7 days after baking. Three slices from two breads were measured at each time point. The NIR spectra were collected in the range between 400-2500 nm using a dispersive NIR spectrometer (6500, NIR systems, Inc.) in reflectance mode and the MIR spectra were collected in the range 4000-400  $\text{cm}^{-1}$  using a FT-IR spectrometer (MB100, ABB Bomem) equipped with a triple-bounce diamond ATR. The

bread hardness was measured with texture profile analysis (TPA) at 3 hours, 1, 2, 4, and 7 days after baking.

For the deuterium experiment, wheat bread crumb pieces were exposed to a saturated air of D<sub>2</sub>O and MIR spectra were measured after 4, 24, 29, 47, 51, 72 hours on a FT-IR spectrometer (IFS 28, Bruker Optik GmbH). A picture of the setup is shown in Figure 2-25.

Preprocessing was performed on smaller spectral regions because this resulted in similar spectra with different preprocessing methods. The SW-NIR region was preprocessed from 850-1086 nm, the 1<sup>st</sup> overtone (1OT) region from 1270-1840 nm and the long wavelength (LW) NIR region from 2100-2400 nm. The highest correlation to bread hardness was achieved by preprocessing with Savitzky-Golay 2<sup>nd</sup> derivative (window size 7 and 2<sup>nd</sup> degree polynomial) + EMSC (described in Section 2.4).

#### 4.1.3 Results

The assignment of the MIR spectra was in line with previous MIR studies on bread aging and recrystallization of water-starch gels. The absorbance increased with storage time at the wavelengths 862, 1000, 1047 and 1078 cm<sup>-1</sup>. From these, 862 and 1047 cm<sup>-1</sup> were associated with stale bread, 1000 cm<sup>-1</sup> was related with stale bread and water loss, and 1078 cm<sup>-1</sup> was linked to water loss. The absorbance at 1022 cm<sup>-1</sup> decreased with storage time and this wavelength was associated with fresh bread.

The increasing NIR absorbance bands with the highest correlation to bread hardness were found at 910, 1688 and 2288 nm and assigned to CH changes during amylopectin retrogradation. Amongst these, the highest correlation was found in the 1OT-NIR region at 1688 nm and in the LW-NIR region at 2288 nm. The decreasing NIR absorbance bands with the highest correlation to bread hardness were at 974, 1412 and 2258 nm and assigned to the OH changes in starch and water. Amongst these, the highest correlation to bread hardness was found to be in the SW-NIR region at 974 nm.

A PCA on the MIR spectra from 1100-850 cm<sup>-1</sup> and a PCA on the LW-NIR spectra from 2150-2370 nm both had a  $r^2$  of 0.97 between PC1 scores and the bread hardness. The  $r^2$  was 0.98 between PC1 scores of the MIR and PC1 scores of the LW-NIR, which indicate that they both measure the same staling effect.

#### 4.1.4 Discussion, concluding remarks and perspectives

One of the challenges in the analysis of NIR spectra of bread presented in the bread staling paper (**PAPER II**) was the preprocessing because different preprocessing methods showed inconsistent results when applied to larger NIR regions. The reason for this is hypothesized to be due to the complex effects from physical and chemical changes during bread storage. This was further investigated by the difference spectrum between the fresh bread and the stale bread measured at 3 and 168 hours after baking, respectively. In Figure 4-2, the fresh (red spectrum) and stale bread (green spectrum) are shown together with their difference (blue line). This shows that at 1000 nm and 1200 nm the absorbance bands decreased with staling. However, from 1400-2400 nm the difference is more or less a linear offset with small valleys at the absorbance bands (shown with black squares). It therefore seems as if there are different effects below and above 1300 nm, which explains the difficulty of preprocessing the whole NIR region together.

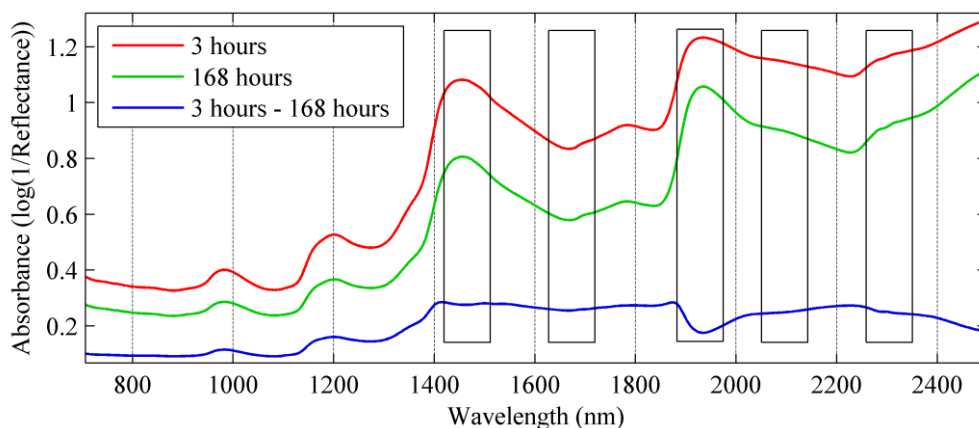


Figure 4-2. Fresh and stale bread measured 3 and 168 hours after baking, respectively. The blue line is the difference between the fresh and the stale bread spectra.

The effect from both physical and chemical changes was also investigated by calculating Pearson's correlation coefficient at all wavelengths on the raw data and pre-processed with Savitzky-Golay 2<sup>nd</sup> derivative + EMSC (Figure 4-3). The correlation coefficients between bread hardness and raw spectra were on average higher than the correlation coefficients between time and raw spectra. This supports the finding in the bread staling paper (**PAPER II**) that bread hardness has a linear and time a nonlinear relationship to aging bread spectra. Pearson's correlation coefficient

measures the linear correlation and it therefore makes sense that bread hardness has a higher correlation.

In Figure 4-3, the preprocessed spectra have higher correlation coefficients to bread hardness compared to the raw spectra in the SW-NIR region at 910 nm, in the 1OT-NIR region at 1688 nm and in the LW-NIR at 2288 nm. The preprocessing of smaller wavelength areas therefore seems to be a good approach for removing the physical effects.

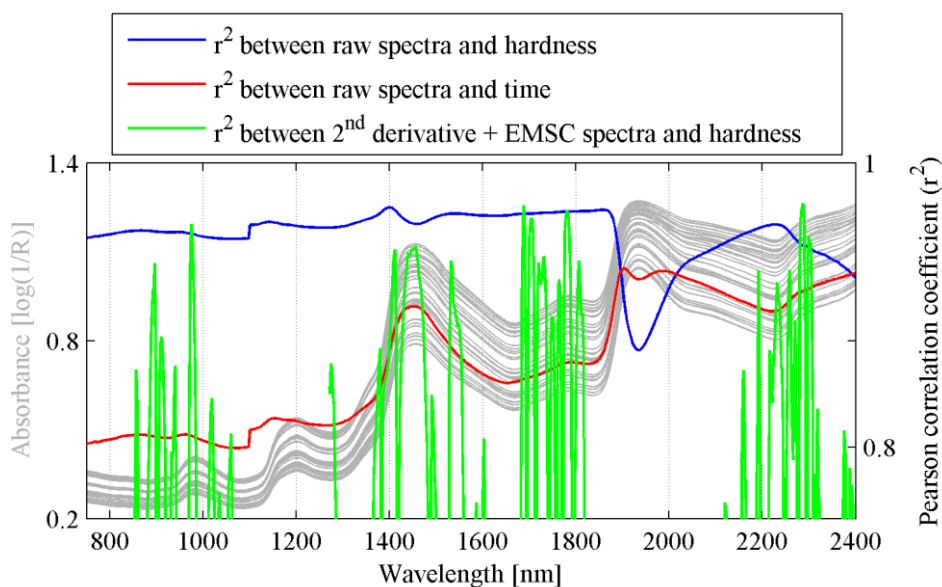


Figure 4-3. Covarygram of the raw NIR spectra (gray color) of wheat bread from 3-168 hours after baking and the Pearson's correlation coefficients at each wavelength.

The covariance was used in the 2D correlation synchronous plots and this was used to resolve overlapping absorbance bands and to interpret if the bands increased or decreased. As explained in the bread staling paper (**PAPER II**), the Pearson's correlation coefficient was also applied in the synchronous plot, but noise amplification and larger areas of high correlation made it more difficult to interpret the plots, and this made covariance more favorable than Pearson's correlation coefficient. However, when absorbance bands have different variance then the covariance cannot be compared whereas the Pearson's correlation coefficient can. The covariance did therefore not give quantitative information while the covarygrams that showed the Pearson's correlation coefficients to bread hardness did. The asynchronous plot did

not show any peaks unless a very high number of contour lines were used (>500). This was interpreted as the chemical changes during bread aging happen simultaneously. To sum up, the 2D correlation synchronous plots with covariance could be used to find peak maxima and the covarygrams with Pearson's correlation coefficients gave qualitative results in the analysis of bread staling.

The analysis presented in the bread staling paper (**PAPER II**) showed promising results for the measurement of staling by NIR and MIR spectroscopy. Especially the MIR region from 850-1100  $\text{cm}^{-1}$ , the 1OT-NIR region from 1350-1800 nm and the LW-NIR region from 2150-2370 nm showed promising results. In future studies, it could be interesting to investigate if these regions are also suited for different bread types with and without anti-staling ingredients. In addition, it could be interesting to include the 2<sup>nd</sup> overtone region of CH at about 1200 nm in order to see if it correlates equally well with staling as the 1OT-NIR region of CH.

## 4.2 Barley phenotype characterization

The possibility to use LW-NIR spectroscopy in transmission mode on seeds gives new opportunities for non-destructive and fast measurements. Suddenly, not only the SW-NIR region, but the whole NIR region can be used for transmission measurements on seeds. This gives the option to choose the wavelength region that is best suited for the type of seed and the chemical component of interest.  $\beta$ -glucan is an example of a component that seems to be better predicted in the LW-NIR region compared to the SW-NIR region in transmission mode as shown in the literature comparison in the barley whole grain paper (**PAPER III**). A literature search is one way of searching for the optimal wavelength region. Another way is to calculate the correlation coefficient to for instance  $\beta$ -glucan at each wavelength. Since the supercontinuum spectrometer was customized for the LW-NIR region, then it was not possible to compare the different infrared regions from the single seed measurements. Because no spectrometer was available to measure transmission on single barley seeds in the entire NIR region then barley flour was used instead to find absorbance bands with high correlation to  $\beta$ -glucan. Measurements were therefore performed on flour from the same five barley genotypes as was used in the barley endosperm paper (**PAPER I**) and the barley whole grain paper (**PAPER III**). The covarygrams for the spectra of barley flour are shown in Figure 4-4 where the spectra have been preprocessed with either EMSC or Savitzky-Golay 2<sup>nd</sup> derivative + EMSC. The  $\beta$ -glucan content used in the covarygrams was measured on the flour of the five barley genotypes in the barley endosperm paper (**PAPER I**). Here it is observed that the LW-NIR spectral region from 2150-2370 nm and the 1OT-NIR region from 1350-1800 nm have slightly higher correlations to  $\beta$ -glucan % compared

to the MIR region from 850-1100  $\text{cm}^{-1}$  and the SW-NIR region from 900-1050 nm. This analysis therefore confirms the result from the barley whole grain paper (**PAPER III**), i.e. that the LW-NIR region has more information on  $\beta$ -glucan compared to the SW-NIR region. Since a covarygram only investigates the correlation of one wavelength at a time and only five flour samples were measured, then these results should be interpreted with care and regarded more as a suggestion of the best NIR region for predicting  $\beta$ -glucan.

Another way to compare different infrared regions is to calculate the covariance as was done in the 2D correlation spectroscopy plot in Figure 4-5. The red and blue areas in Figure 4-5 correspond to positive and negative covariance, respectively. Here it can be observed that the absorbance band at 2350 nm move together (positive covariance) with the absorbance band at about 1700 nm. In contrast, the absorbance band at around 2290 nm that has been associated with starch (Section 3.1.1) moves together with the band at 962 nm. The absorbance at 2350 nm has been assigned to CH antisymmetric stretching + CH deformation and the absorbance at 1700 nm has been assigned to the 1<sup>st</sup> overtone of  $\text{CH}_3$  stretching.<sup>136</sup> The high positive covariance between the LW-NIR region and the 1OT-NIR region together with the high correlation to  $\beta$ -glucan indicates that the absorbance bands originate from the same functional group.

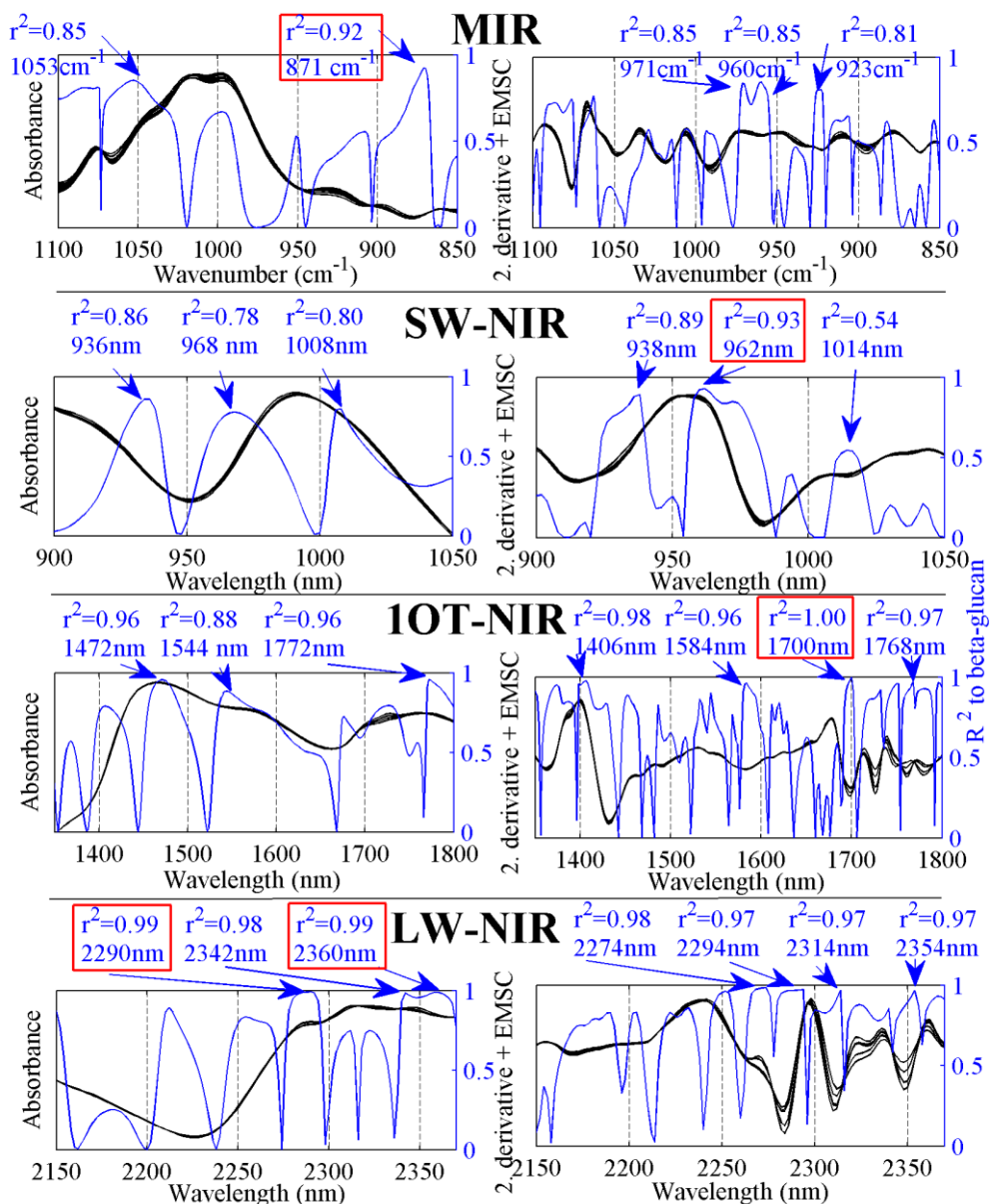


Figure 4-4. Barley flour from five barley genotypes measured in duplicate on a dispersive NIR spectrometer (NIRS<sup>TM</sup> DS2500 F, FOSS) and a FT-IR spectrometer (Vertex 70, Bruker Optik GmbH). Black spectra to the left and right have been preprocessed with EMSC and Savitzky-Golay 2<sup>nd</sup> derivative + EMSC, respectively. Blue lines are the Pearson's correlation coefficient ( $r^2$ ) to  $\beta$ -glucan %.

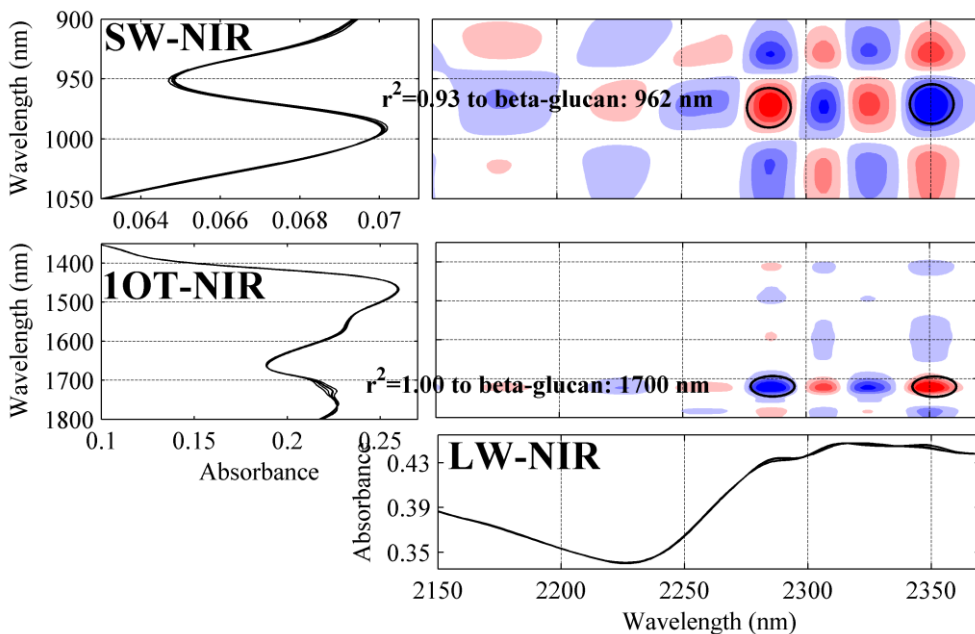


Figure 4-5. Two-dimensional correlation spectroscopy on NIR spectra of flour from five barley genotypes. The horizontal axis is the LW-NIR region from 2150-2370 nm and the vertical axis is the NIR regions from 900-1050 nm and 1350-1800 nm. The spectra were all preprocessed with EMSC. The colors represent the level of covariance where red is positive and blue is negative. The Pearson's correlation coefficients ( $r^2$ ) were taken from Figure 4-4.





## Conclusions and perspectives

---

*If I have seen further it is by standing on the  
shoulders of Giants.*

— Sir Isaac Newton, 1676

This thesis work have demonstrated that a supercontinuum laser can be used to measure transmission spectra of barley seeds in the LW-NIR region from 2260-2380 nm and measure the content of  $\beta$ -glucan, which had never been done before. An obvious extension of this study would be to measure on oats because, together with barley, they are the most important sources of  $\beta$ -glucan. The measurement speed used in LW-NIR spectroscopy on barley was one minute per seed, which could be appropriate in plant breeding, but not in industrial seed sorting. Some possibilities for measurement improvements are suggested: (a) improving the S/N ratio with a better detector, (b) using faster measurement speed by lowering the resolution of the monochromator spectrometer or using a different wavelength selection method and (c) performing better representative sampling with a larger beam.

The use of supercontinuum light in gas measurements is proposed as a whole new branch in spectroscopy because of the big advantage of the collimated beam of the light source. Especially NIR spectroscopy could benefit from the focused beam of the supercontinuum light because a much larger path-length is needed in NIR compared to MIR spectroscopy. The next step would be to determine the actual potential in experimental studies of food systems.

The use of a supercontinuum light together with a wavelength separating fiber produces a robust and easily fiber connected spectrometer. The experimental instrument is operational in the 1300-1650 nm region, which contains information on all major food components, namely carbohydrates, fats, proteins and water. Preliminary measurements show that the new dispersive Fourier transformation spectrometer works well, but a more precise quantification of how well it works still needs to be investigated in selected food systems.

In order to better understand the selection of a spectral region for a given food application, 2D correlation spectroscopy on aging bread was conducted. This method was used to relate the information on amylopectin retrogradation in the MIR at  $1047\text{ cm}^{-1}$  with the CH absorbance bands in the NIR at 910, 1688 and 2288 nm. In addition, the absorbance band associated with fresh bread in the MIR at  $1022\text{ cm}^{-1}$  was related with the OH absorbance bands in the NIR at 974, 1412 and 2258 nm. This study was performed on normal wheat bread and an obvious extinction to this study would be to investigate if the results from this work would also apply to breads with anti-staling agents or different types of bread. The present study determined the peak maxima from the synchronous/covariance plot and the quantitative relationship to bread hardness from the Pearson's correlation coefficient. Future studies should investigate if the enhanced resolution of the covariance and the quantitative value of the Pearson's correlation coefficient could be combined into one information-rich plot.

One of the trends in NIR spectroscopy is miniaturization of instrumentation with the focus of making instruments more portable and for some instruments also more affordable. Especially lowering of the instrument price will have a huge impact on the group of potential buyers of NIR spectrometers. Small or medium sized companies that previously would have disregarded NIR spectroscopy because of the high acquisition price might reconsider buying if the price is lowered. Another potential group of buyers are consumers who would like to analyse the food that they buy. As an example, the company Telspec sells a hand-held NIR spectrometer that consumers can use to detect potential allergens, energy content or the content of fats, proteins and carbohydrates in food. The fact that NIR spectroscopy can easily measure transmission and diffuse reflectance due to the low  $\epsilon$ 's makes it an ideal (and maybe only choice) for hand-held consumer devices. One way to make smaller and cheaper NIR spectrometers is to use LEDs by finding the LEDs that best covers the NIR regions with the most information on the compounds of interest.

The commercial supercontinuum sources are at the moment compact and with the size of a shoebox. The future of the supercontinuum source might also be miniaturized by using smaller pump sources such as e.g. microchip lasers. New photonic crystal fibers will also allow for supercontinuum sources to be broadened even more into the UV and MIR regions.

# References

1. R. Karoui, G. Downey, C. Blecker. "Mid-Infrared Spectroscopy Coupled with Chemometrics: A Tool for the Analysis of Intact Food Systems and the Exploration of Their Molecular Structure-Quality Relationships - A Review". *Chem. Rev.* 2010. 110(10): 6144-6168.
2. J.U. Porep, D.R. Kammerer, R. Carle. "On-line application of near infrared (NIR) spectroscopy in food production". *Trends Food Sci. Technol.* 2015. 46(2): 211-230.
3. S.B. Engelsen. "Near infrared spectroscopy - a unique window of opportunities". *NIR news.* 2016. 27(5): 14-17.
4. T. Woodcock, G. Downey, C.P. O'Donnell. "Better quality food and beverages: the role of near infrared spectroscopy". *J. Near Infrared Spectrosc.* 2008. 16(1): 1-29.
5. C.F. Kaminski, R.S. Watt, A.D. Elder, J.H. Frank, J. Hult. "Supercontinuum radiation for applications in chemical sensing and microscopy". *Appl. Phys. B.* 2008. 92(3): 367-378.
6. C.R. Petersen, U. Møller, I. Kubat, B.B. Zhou, S. Dupont, J. Ramsay, T. Benson, S. Sujecki, N. Abdel-Moneim, Z.Q. Tang, D. Furniss, A. Seddon, O. Bang. "Mid-infrared supercontinuum covering the 1.4-13.3  $\mu\text{m}$  molecular fingerprint region using ultra-high NA chalcogenide step-index fibre". *Nat. Photonics.* 2014. 8(11): 830-834.
7. S. Dupont, C. Petersen, J. Thøgersen, C. Agger, O. Bang, S.R. Keiding. "IR microscopy utilizing intense supercontinuum light source". *Opt. Express.* 2012. 20(5): 4887-4892.
8. I. Noda, A.E. Dowrey, C. Marcott, G.M. Story, Y. Ozaki. "Generalized two-dimensional correlation spectroscopy". *Appl. Spectrosc.* 2000. 54(7): 236A-248A.
9. R.A. Spragg. "IR Spectrometers". In: J.C. Lindon, G.E. Tranter, D.W. Koppenaal, editors. *Encyclopedia of Spectroscopy and Spectrometry.* Oxford, UK: Academic Press, 2017. 3rd ed., Pp. 419-427.
10. R.A. Shaw, H.H. Mantsch. "Near-IR spectrometers". In: J.C. Lindon, G.E. Tranter, D.W. Koppenaal, editors. *Encyclopedia of Spectroscopy and Spectrometry.* Oxford, UK: Academic Press, 2017. 3rd ed., Pp. 50-58.
11. M.B. Simpson. "Near-infrared spectroscopy for process analytical technology: theory, technology and implementation". In: K.A. Bakeev. *Process Analytical Technology: Spectroscopic Tools and Implementation Strategies for the Chemical and Pharmaceutical Industries.* Chichester, UK: John Wiley & Sons, Ltd, 2010. 2nd ed., Pp. 107-155.

12. J.P. Coates. "Infrared spectroscopy for process analytical applications". In: K.A. Bakeev. *Process Analytical Technology: Spectroscopic Tools and Implementation Strategies for the Chemical and Pharmaceutical Industries*. Chichester, UK: John Wiley & Sons, Ltd, 2010. 2nd ed., Pp. 157-194.
13. I.R. Lewis, S.S. Rosenblum. "General introduction to fiber optics". In: J.M. Chalmers, P.R. Griffiths, editors. *Handbook of Vibrational Spectroscopy*. Chichester, England: John Wiley & Sons, Ltd, 2002. Vol. 2, Pp. 1533-1540.
14. B. Lendl, B. Mizaikoff. "Optical fibers for mid-infrared spectrometry". In: J.M. Chalmers, P.R. Griffiths, editors. *Handbook of Vibrational Spectroscopy*. Chichester, England: John Wiley & Sons, Ltd, 2002. Vol. 2, Pp. 1541-1550.
15. N. Sheppard. "The historical development of experimental techniques in vibrational spectroscopy". In: J.M. Chalmers, P.R. Griffiths, editors. *Handbook of vibrational spectroscopy*. Chichester, England: John Wiley & Sons Ltd., 2002. Vol. 1, Pp. 1-32.
16. H. Buijs. "Incandescent sources for mid- and far-infrared spectrometry". In: J.M. Chalmers, P.R. Griffiths, editors. *Handbook of vibrational spectroscopy*. Chichester, England: John Wiley & Sons Ltd., 2002. Vol. 1, Pp. 337-340.
17. P.R. Griffiths, C.C. Homes. "Instrumentation for far-infrared spectroscopy". In: J.M. Chalmers, P.R. Griffiths, editors. *Handbook of Vibrational Spectroscopy*. Chichester, England: John Wiley & Sons, Ltd, 2002. Vol. 1, Pp. 326-336.
18. F.A. DeThomas, P.J. Brimmer. "Monochromators for Near-infrared Spectroscopy". In: J.M. Chalmers, P.R. Griffiths, editors. *Handbook of Vibrational Spectroscopy*. Chichester, England: John Wiley & Sons Ltd., 2002. Vol. 1, Pp. 383-392.
19. E.W. Stark. "Near-infrared array spectrometers". In: J.M. Chalmers, P.R. Griffiths, editors. *Handbook of Vibrational Spectroscopy*. Chichester, England: John Wiley & Sons, Ltd, 2002. Vol. 1, Pp. 393-422.
20. J. Workman. "Near infrared instrumentation". *The concise handbook of analytical spectroscopy: theory, applications, and reference materials*. World scientific, 2016. Vol. 3, Pp. 85-129.
21. R.R. Alfano, S.L. Shapiro. "Emission in the region 4000 to 7000 Å via 4-photon coupling in glass". *Phys. Rev. Lett.* 1970. 24(11): 584-587.
22. K.C. Cossel, E.M. Waxman, I.A. Finneran, G.A. Blake, J. Ye, N.R. Newbury. "Gas-phase broadband spectroscopy using active sources: progress, status, and applications". *J. Opt. Soc. Am. B.* 2017. 34(1): 104-129.
23. J.M. Dudley, G. Genty, S. Coen. "Supercontinuum generation in photonic crystal fiber". *Rev. Mod. Phys.* 2006. 78(4): 1135-1184.
24. K. Goda, B. Jalali. "Dispersive Fourier transformation for fast continuous single-shot measurements". *Nat. Photonics.* 2013. 7(2): 102-112.
25. C.E. Miller. "Chemical Principles of Near-Infrared Technology". In: P. Williams, K. Norris, editors. *Near-infrared technology, in the agricultural and food industries*. St. Paul, MN, USA: American Association of Cereal Chemists, 2001. 2nd ed., Pp. 19-37.

26. G. Herzberg. "Determination of normal vibrations". Molecular spectra and molecular structure. Malabar, FL, USA: Krieger Publishing company, 1991. 2nd ed., Vol. 2, Pp. 171.
27. S.Y. Venyaminov, F.G. Prendergast. "Water (H<sub>2</sub>O and D<sub>2</sub>O) molar absorptivity in the 1000-4000 cm<sup>-1</sup> range and quantitative infrared spectroscopy of aqueous solutions". Anal. Biochem. 1997. 248(2): 234-245.
28. A.S. Bonanno, J.M. Olinger, P.R. Griffiths. "The origin of band positions and widths in near infrared spectra". In: K.I. Hildrum, T. Isaksson, T. Naes, A. Tandberg, editors. Near infra-red spectroscopy. Chichester, England: Ellis Horwood Limited, 1992. Pp. 19-28.
29. W. Kaye. "Near-infrared spectroscopy". Spectrochim. Acta. 1954. 6(4): 257-287.
30. P.R. Griffiths, J.A. de Haseth. "Attenuated Total Reflection". Fourier transform infrared spectrometry. Hoboken, NJ, USA: John Wiley & Sons, Inc., 2006. Pp. 321-348.
31. B.H. Stuart. "Coupling". Infrared spectroscopy: fundamentals and applications. John Wiley & Sons, Ltd, 2004. Pp. 12.
32. L. Bokobza. "Origin of Near-Infrared Absorption Bands". In: H.W. Siesler, Y. Ozaki, S. Kawata, H.M. Heise, editors. Near-Infrared Spectroscopy: Principles, Instruments, Applications. Weinheim, Germany: Wiley-VCH Verlag GmbH, 2002. Pp. 11-41.
33. J.E. Bertie. "Glossary of Terms used in Vibrational Spectroscopy". In: J.M. Chalmers, P.R. Griffiths, editors. Handbook of Vibrational Spectroscopy. Chichester, England: John Wiley & Sons, Ltd, 2002. Vol. 5, Pp. 3745-3794.
34. H.W. Siesler. "Near-Infrared spectra, interpretation ". In: J.C. Lindon, G.E. Tranter, D.W. Koppenaal, editors. Encyclopedia of Spectroscopy and Spectrometry. Oxford, UK: Academic Press, 2017. 3rd ed., Pp. 30-39.
35. L.G. Weyer, S.C. Lo. "Spectra– structure correlations in the near-infrared". In: J.M. Chalmers, P.R. Griffiths, editors. Handbook of Vibrational Spectroscopy. Chichester, England: John Wiley & Sons, Ltd, 2002. Vol. 3, Pp. 1817-1837.
36. H.F. Shurvell. "Spectra– structure correlations in the mid- and far-infrared". In: J.M. Chalmers, P.R. Griffiths, editors. Handbook of Vibrational Spectroscopy. Chichester, England: John Wiley & Sons, Ltd, 2002. Vol. 3, Pp. 1783-1816.
37. P. Larouche, J.J. Max, C. Chapados. "Isotope effects in liquid water by infrared spectroscopy. II. Factor analysis of the temperature effect on H<sub>2</sub>O and D<sub>2</sub>O". J. Chem. Phys. 2008. 129(6): 064503.
38. S.E. Lappi, B. Smith, S. Franzen. "Infrared spectra of H<sub>2</sub><sup>16</sup>O, H<sub>2</sub><sup>18</sup>O and D<sub>2</sub>O in the liquid phase by single-pass attenuated total internal reflection spectroscopy". Spectrochim. Acta, Part A. 2004. 60(11): 2611-2619.
39. G. Herzberg. "Infrared and raman bands of H<sub>2</sub>O vapor". Molecular spectra and molecular structure. Malabar, FL, USA: Krieger Publishing company, 1991. 2nd ed., Vol. 2, Pp. 281.

40. J.W. Ellis, J. Bath. "Modifications in the near infra-red absorption spectra of protein and of light and heavy water molecules when water is bound to gelatin". *J. Chem. Phys.* 1938. 6(11): 723-729.
41. V. Fornés, J. Chaussidon. "Interpretation of evolution with temperature of  $\nu_2+\nu_3$  combination band in water". *J. Chem. Phys.* 1978. 68(10): 4667-4671.
42. G.R. Choppin, M.R. Violante. "Near-infrared studies of structure of water. III. Mixed solvent systems". *J. Chem. Phys.* 1972. 56(12): 5890-5898.
43. O.D. Bonner, G.B. Woolsey. "The effect of solutes and temperature on structure of water". *J. Chem. Phys.* 1968. 72(3): 899-905.
44. B. Czarnik-Matusiewicz, S. Pilorz, J.P. Hawranek. "Temperature-dependent water structural transitions examined by near-IR and mid-IR spectra analyzed by multivariate curve resolution and two-dimensional correlation spectroscopy". *Anal. Chim. Acta.* 2005. 544(1-2): 15-25.
45. D.J. Dahm. "Explaining some light scattering properties of milk using representative layer theory". *J. Near Infrared Spectrosc.* 2013. 21(5): 323-339.
46. D.J. Dahm, K.D. Dahm. "The physics of near-infrared scattering". In: P. Williams, K. Norris, editors. *Near-infrared technology, in the agricultural and food industries*. St. Paul, MN, USA: American Association of Cereal Chemists, 2001. 2nd ed.
47. K.M. Morisseau, C.T. Rhodes. "Near-infrared spectroscopy as a nondestructive alternative to conventional tablet hardness testing". *Pharm. Res.* 1997. 14(1): 108-111.
48. J.D. Kirsch, J.K. Drennen. "Nondestructive tablet hardness testing by near-infrared spectroscopy: a new and robust spectral best-fit algorithm". *J. Pharm. Biomed. Anal.* 1999. 19(3-4): 351-362.
49. P.R. Griffiths. "Beer's Law". In: J.M. Chalmers, P.R. Griffiths, editors. *Handbook of Vibrational Spectroscopy*. Chichester, England: John Wiley & Sons, Ltd, 2002. Vol. 3, Pp. 2225-2234.
50. S. Wold, K. Esbensen, P. Geladi. "Principal component analysis". *Chemom. Intell. Lab. Syst.* 1987. 2(1-3): 37-52.
51. S. Wold, H. Martens, H. Wold. "The multivariate calibration-problem in chemistry solved by the PLS method". *Lect. Notes Math.* 1983. 973: 286-293.
52. R. Bro, A.K. Smilde. "Principal component analysis". *Anal. Methods.* 2014. 6(9): 2812-2831.
53. Å. Rinnan. "Pre-processing in vibrational spectroscopy - when, why and how". *Anal. Methods.* 2014. 6(18): 7124-7129.
54. G. Herzberg. "Infrared and raman bands of gaseous CO<sub>2</sub>". *Molecular spectra and molecular structure*. Malabar, FL, USA: Krieger Publishing company, 1991. 2nd ed., Vol. 2, Pp. 274.
55. P. Lasch. "Spectral pre-processing for biomedical vibrational spectroscopy and microspectroscopic imaging". *Chemom. Intell. Lab. Syst.* 2012. 117: 100-114.

56. P. Geladi, D. MacDougall, H. Martens. "Linearization and scatter-correction for near-infrared reflectance spectra of meat". *Appl. Spectrosc.* 1985. 39(3): 491-500.
57. R.J. Barnes, M.S. Dhanoa, S.J. Lister. "Standard normal variate transformation and de-trending of near-infrared diffuse reflectance spectra". *Appl. Spectrosc.* 1989. 43(5): 772-777.
58. H. Martens, J.P. Nielsen, S.B. Engelsen. "Light scattering and light absorbance separated by extended multiplicative signal correction. Application to near-infrared transmission analysis of powder mixtures". 2003. 75(3): 394-404.
59. Å. Rinnan, F. van den Berg, S.B. Engelsen. "Review of the most common pre-processing techniques for near-infrared spectra". *TrAC, Trends Anal. Chem.* 2009. 28(10): 1201-1222.
60. E. Goormaghtigh, J.M. Ruyschaert, V. Raussens. "Evaluation of the information content in infrared spectra for protein secondary structure determination". *Biophys. J.* 2006. 90(8): 2946-2957.
61. A. Gagneaux, J.M. Ruyschaert, E. Goormaghtigh. "Cell discrimination by attenuated total reflection-Fourier transform infrared spectroscopy: The impact of preprocessing of spectra". *Appl. Spectrosc.* 2006. 60(9): 1022-1028.
62. S.K. Andersen, P.W. Hansen, H.V. Andersen. "Vibrational spectroscopy in the analysis of dairy products and wine". In: J.M. Chalmers, P.R. Griffiths, editors. *Handbook of vibrational spectroscopy*. Chichester, England: John Wiley & Sons, Ltd, 2002. Vol. 5, Pp. 3672-3682.
63. P.S. Jensen, J. Bak. "Near-infrared transmission spectroscopy of aqueous solutions: Influence of optical pathlength on signal-to-noise ratio". *Appl. Spectrosc.* 2002. 56(12): 1600-1606.
64. H. Yang, J. Irudayaraj, M.M. Paradkar. "Discriminant analysis of edible oils and fats by FTIR, FT-NIR and FT-Raman spectroscopy". *Food Chem.* 2005. 93(1): 25-32.
65. J. Chen, M.A. Arnold, G.W. Small. "Comparison of combination and first overtone spectral regions for near-infrared calibration models for glucose and other biomolecules in aqueous solutions". *Anal. Chem.* 2004. 76(18): 5405-5413.
66. P.S. Jensen, J. Bak, S. Andersson-Engels. "Influence of temperature on water and aqueous glucose absorption spectra in the near- and mid-infrared regions at physiologically relevant temperatures". *Appl. Spectrosc.* 2003. 57(1): 28-36.
67. R. Du, K.Q. Lai, Z.Q. Xiao, Y.G. Shen, X.C. Wang, Y.Q. Huang. "Evaluation of the quality of deep frying oils with fourier transform near-infrared and mid-infrared spectroscopy". *J. Food Sci.* 2012. 77(2): C261-C266.
68. S.B. Engelsen. "Explorative spectrometric evaluations of frying oil deterioration". *J. Am. Oil Chem. Soc.* 1997. 74(12): 1495-1508.

69. M. Bevilacqua, R. Bucci, A.D. Magrì, A.L. Magrì, F. Marini. "Tracing the origin of extra virgin olive oils by infrared spectroscopy and chemometrics: A case study". *Anal. Chim. Acta.* 2012. 717: 39-51.
70. C. Shiroma, L. Rodriguez-Solona. "Application of NIR and MIR spectroscopy in quality control of potato chips". *J. Food Compos. Anal.* 2009. 22(6): 596-605.
71. N. Sinelli, E. Casiraghi, G. Downey. "Studies on proofing of yeasted bread dough using near- and mid-infrared spectroscopy". *J. Agric. Food Chem.* 2008. 56(3): 922-931.
72. V. Di Egidio, N. Sinelli, G. Giovanelli, A. Moles, E. Casiraghi. "NIR and MIR spectroscopy as rapid methods to monitor red wine fermentation". *Eur. Food Res. Technol.* 2010. 230(6): 947-955.
73. L. Pillonel, W. Luginbühl, D. Picque, E. Schaller, R. Tabacchi, J.O. Bosset. "Analytical methods for the determination of the geographic origin of Emmental cheese: mid- and near-infrared spectroscopy". *Eur. Food Res. Technol.* 2003. 216(2): 174-178.
74. S.B. Engelsen, L. Nørgaard. "Comparative vibrational spectroscopy for determination of quality parameters in amidated pectins as evaluated by chemometrics". *Carbohydr. Polym.* 1996. 30(1): 9-24.
75. H. Winning, N. Viereck, T. Salomonsen, J. Larsen, S.B. Engelsen. "Quantification of blockiness in pectins-A comparative study using vibrational spectroscopy and chemometrics". *Carbohydr. Res.* 2009. 344(14): 1833-1841.
76. T. Salomonsen, H.M. Jensen, D. Stenbæk, S.B. Engelsen. "Chemometric prediction of alginate monomer composition: A comparative spectroscopic study using IR, Raman, NIR and NMR". *Carbohydr. Polym.* 2008. 72(4): 730-739.
77. I. Noda. "Generalized two-dimensional correlation method applicable to infrared, raman, and other types of spectroscopy". *Appl. Spectrosc.* 1993. 47(9): 1329-1336.
78. F.E. Barton II, D.S. Himmelsbach, J.H. Duckworth, M.J. Smith. "Two-dimensional vibration spectroscopy: correlation of mid- and near-infrared regions". *Appl. Spectrosc.* 1992. 46(3): 420-429.
79. E. Alm, R. Bro, S.B. Engelsen, B. Karlberg, R.J.O. Torgrip. "Vibrational overtone combination spectroscopy (VOCSY) - a new way of using IR and NIR data". *Anal. Bioanal. Chem.* 2007. 388(1): 179-188.
80. A.G. Asuero, A. Sayago, A.G. González. "The correlation coefficient: An overview". *Crit. Rev. Anal. Chem.* 2006. 36(1): 41-59.
81. I. Noda. "Techniques useful in two-dimensional correlation and codistribution spectroscopy (2DCOS and 2DCDS) analyses". *J. Mol. Struct.* 2016. 1124: 29-41.
82. M.A. Czarnecki. "Two-dimensional correlation analysis of hydrogen-bonded systems: basic molecules". *Appl. Spectrosc. Rev.* 2011. 46(1): 67-103.
83. S. Morita. "2Dshige (c)". Kwansai-Gakuin University, 2004-2005.

84. D. Cozzolino, I. Murray, A. Chree, J.R. Scaife. "Multivariate determination of free fatty acids and moisture in fish oils by partial least-squares regression and near-infrared spectroscopy". *LWT*. 2005. 38(8): 821-828.
85. T. Skov, A.H. Honoré, H.M. Jensen, T. Næs, S.B. Engelsen. "Chemometrics in foodomics: Handling data structures from multiple analytical platforms". *TrAC, Trends Anal. Chem.* 2014. 60: 71-79.
86. M. Golic, K. Walsh, P. Lawson. "Short-wavelength near-infrared spectra of sucrose, glucose, and fructose with respect to sugar concentration and temperature". *Appl. Spectrosc.* 2003. 57(2): 139-145.
87. A. Barth. "Infrared spectroscopy of proteins". *Biochim. Biophys. Acta, Bioenerg.* 2007. 1767(9): 1073-1101.
88. K.L.A. Chan, S. Gulati, J.B. Edel, A.J. de Mello, S.G. Kazarian. "Chemical imaging of microfluidic flows using ATR-FTIR spectroscopy". *Lab Chip*. 2009. 9(20): 2909-2913.
89. J.G. Bayly, V.B. Kartha, W.H. Stevens. "The absorption spectra of liquid phase H<sub>2</sub>O, HDO and D<sub>2</sub>O from 0.7  $\mu$ m to 10  $\mu$ m". *Infrared Phys.* 1963. 3(4): 211-222.
90. J.J. Max, C. Chapados. "Isotope effects in liquid water by infrared spectroscopy. III. H<sub>2</sub>O and D<sub>2</sub>O spectra from 6000 to 0 cm<sup>-1</sup>". *J. Chem. Phys.* 2009. 131(18): 184505.
91. M. Gupta, N. Abu-Ghannam, E. Gallagher. "Barley for brewing: characteristic changes during malting, brewing and applications of its by-products". *Compr. Rev. Food Sci. Food Saf.* 2010. 9(3): 318-328.
92. L. Munck, J.P. Nielsen, B. Møller, S. Jacobsen, I. Søndergaard, S.B. Engelsen, L. Nørgaard, R. Bro. "Exploring the phenotypic expression of a regulatory proteome-altering gene by spectroscopy and chemometrics". *Anal. Chim. Acta.* 2001. 446(1-2): 171-186.
93. H.F. Seefeldt, A. Blennow, B.M. Jespersen, B. Wollenweber, S.B. Engelsen. "Accumulation of mixed linkage (1  $\rightarrow$  3) (1  $\rightarrow$  4)- $\beta$ -D-glucan during grain filling in barley: A vibrational spectroscopy study". *J. Cereal Sci.* 2009. 49(1): 24-31.
94. G.P. Fox. "Chemical Composition in Barley Grains and Malt Quality". In: G. Zhang, C. Li, editors. *Genetics and Improvement of Barley Malt Quality*. Berlin Heidelberg: Springer, 2010. Chap. 3, Pp. 63-98.
95. J. Ramsay, S. Dupont, S.R. Keiding. "Pulse-to-pulse noise reduction in infrared supercontinuum spectroscopy: polarization and amplitude fluctuations". *Laser Phys. Lett.* 2014. 11(9): 095702.
96. R.M. de Sá, G.H. Palmer. "Analysis of  $\beta$ -glucan in single grains of barley and malt using NIR-spectroscopy". *J. Inst. Brew.* 2006. 112(1): 9-16.
97. M. Sohn, D.S. Himmelsbach, F.E. Barton II, C.A. Griffey, W. Brooks, K.B. Hicks. "Near-infrared analysis of whole kernel barley: Comparison of three spectrometers". *Appl. Spectrosc.* 2008. 62(4): 427-432.

98. J. Schmidt, S. Gergely, R. Schönlechner, H. Grausgruber, S. Tömösközi, A. Salgó, E. Berghofer. "Comparison of different types of NIR Instruments in ability to measure  $\beta$ -glucan content in naked barley". *Cereal Chem.* 2009. 86(4): 398-404.
99. L.E. Agelet, C.R. Hurburgh. "Limitations and current applications of Near Infrared Spectroscopy for single seed analysis". *Talanta.* 2014. 121: 288-299.
100. N. Museux, L. Perez, L. Autrique, D. Agay. "Skin burns after laser exposure: Histological analysis and predictive simulation". *Burns.* 2012. 38(5): 658-667.
101. B. Chen, S.L. Thomsen, R.J. Thomas, J. Oliver, A.J. Welch. "Histological and modeling study of skin thermal injury to 2.0  $\mu$ m laser irradiation". *Lasers Surg. Med.* 2008. 40(5): 358-370.
102. E. Tønning, L. Nørgaard, S.B. Engelsen, L. Pedersen, K.H. Esbensen. "Protein heterogeneity in wheat lots using single-seed NIT - A Theory of Sampling (TOS) breakdown of all sampling and analytical errors". *Chemom. Intell. Lab. Syst.* 2006. 84(1-2): 142-152.
103. F.E. Dowell, E.B. Maghirang, R.A. Graybosch, P.S. Baenziger, D.D. Baltensperger, L.E. Hansen. "An automated near-infrared system for selecting individual kernels based on specific quality characteristics". *Cereal Chem.* 2006. 83(5): 537-543.
104. L.S. McDonald, J.F. Panozzo, P.A. Salisbury, R. Ford. "Discriminant analysis of defective and non-defective field pea (*Pisum sativum* L.) into broad market grades based on digital image features". *Plos One.* 2016. 11(5): 0155523.
105. M.E. Kautzman, M.L. Wickstrom, T.A. Scott. "The use of near infrared transmittance kernel sorting technology to salvage high quality grain from grain downgraded due to *Fusarium* damage". *Animal Nutrition.* 2015. 1(1): 41-46.
106. M. Biniecka, S. Caroli. "Analytical methods for the quantification of volatile aromatic compounds". *TrAC, Trends Anal. Chem.* 2011. 30(11): 1756-1770.
107. A.K. Deisingh, D.C. Stone, M. Thompson. "Applications of electronic noses and tongues in food analysis". *Int. J. Food Sci. Technol.* 2004. 39(6): 587-604.
108. B. Zhang, S. Ye, G. Xiao, D. Dong. "Identification of beef spoilage via the analysis of volatiles using long optical-path Fourier transform infrared spectroscopy". *Anal. Methods.* 2015. 7(14): 5891-5897.
109. J.K. Amamcharla, S. Panigrahi, C.M. Logue, M. Marchello, J.S. Sherwood. "Application of vapour-phase Fourier transform infrared spectroscopy (FTIR) and statistical feature selection methods for identifying *Salmonella enterica typhimurium* contamination in beef". *Biosyst. Eng.* 2010. 107(1): 1-9.
110. M. Gallignani, M. Valero, C. Ayala, M.D. Brunetto, A. Sánchez, J.L. Burguera, M. Burguera. "Flow analysis-vapor phase generation-Fourier transform infrared (FA-VPG-FTIR) spectrometric determination of nitrite". *Talanta.* 2004. 64(5): 1290-1298.

111. S. Armenta, N.M.M. Coelho, R. Roda, S. Garrigues, A. de la Guardia. "Seafood freshness determination through vapour phase Fourier transform infrared spectroscopy". *Anal. Chim. Acta.* 2006. 580(2): 216-222.
112. J. Hruzikova, D. Milde, P. Krajancova, V. Ranc. "Discrimination of cheese products for authenticity control by infrared spectroscopy". *J. Agric. Food Chem.* 2012. 60(7): 1845-1849.
113. M. Ahro, M. Hakala, J. Kauppinen, H. Kallio. "Headspace FT-IR analysis of rapeseed oil oxidation". *Appl. Spectrosc.* 2002. 56(2): 217-222.
114. D. Dong, W. Zheng, W. Wang, X. Zhao, L. Jiao, C. Zhao. "Analysis and discrimination of grape spoilage via volatiles: a comparison between long optical path Fourier-transform-infrared spectroscopy and sensor arrays". *Analyst.* 2014. 139(19): 5028-5034.
115. D.M. Dong, C.J. Zhao, W.G. Zheng, W.Z. Wang, X.D. Zhao, L.Z. Jiao. "Analyzing strawberry spoilage via its volatile compounds using longpath Fourier transform infrared spectroscopy". *Sci. Rep.* 2013. 3: 2585.
116. M. Hakala, M. Ahro, J. Kauppinen, H. Kallio. "Determination of strawberry volatiles with low resolution gas phase FT-IR analyser". *Eur. Food Res. Technol.* 2001. 212(4): 505-510.
117. G.D. Xiao, D.M. Dong, T.Q. Liao, Y. Li, L. Zheng, D.Y. Zhang, C.J. Zhao. "Detection of pesticide (Chlorpyrifos) residues on fruit peels through spectra of volatiles by FTIR". *Food Anal. Methods.* 2015. 8(5): 1341-1346.
118. D. Dong, W. Zheng, L. Jiao, Y. Lang, X. Zhao. "Chinese vinegar classification via volatiles using long-optical-path infrared spectroscopy and chemometrics". *Food Chem.* 2016. 194: 95-100.
119. A. Pérez-Ponce, S. Garrigues, M. de la Guardia. "Vapour generation Fourier transform infrared direct determination of ethanol in alcoholic beverages". *Analyst.* 1996. 121(7): 923-928.
120. D. Dong, W. Zheng, W. Wang, X. Zhao, L. Jiao, C. Zhao. "A new volatiles-based differentiation method of Chinese spirits using longpath gas-phase infrared spectroscopy". *Food Chem.* 2014. 155: 45-49.
121. A. Pérez-Ponce, S. Garrigues, M. de la Guardia. "Direct determination of total SO<sub>2</sub> in musts and wines by vapour phase Fourier transform infrared spectrometry". *Quim. Anal.* 2000. 19(3): 151-158.
122. S.Q. Liu. "Flavors and Food Fermentation". In: Y.H. Hui. *Handbook of Plant-Based Fermented Food and Beverage Technology*. Boca Raton, FL, USA: CRC Press, 2012. 2nd ed., Pp. 23-34.
123. L. Gram. "Microbial Food Spoilage". In: Y.H. Hui. *Handbook of Food Science, Technology, and Engineering*. Boca Raton, FL, USA: CRC Press, 2005. Vol. 1, Chap. 51.
124. C.S. Barry, J.J. Giovannoni. "Ethylene and fruit ripening". *J. Plant Growth Regul.* 2007. 26(2): 143-159.
125. J.B. McManus, M.S. Zahniser, D.D. Nelson, J.H. Shorter, S.C. Herndon, D. Jervis, M. Agnese, R. McGovern, T.I. Yacovitch, J.R. Roscioli. "Recent progress in laser-based trace gas instruments: performance and noise analysis". *Appl. Phys. B: Lasers Opt.* 2015. 119(1): 203-218.

126. T. Nakahara, S. Tanaka, M. Nishimura. "Fiber Optics". Ullmann's Encyclopedia of Industrial Chemistry. Wiley-VCH Verlag GmbH & Co. KGaA, 2000.
127. L.J. Mauer, A.A. Chernyshova, A. Hiatt, A. Deering, R. Davis. "Melamine detection in infant formula powder using near- and mid-infrared spectroscopy". J. Agric. Food Chem. 2009. 57(10): 3974-3980.
128. [www.unityscientific.com.au/catlist.asp?id=50](http://www.unityscientific.com.au/catlist.asp?id=50). Blaxland, NSW, Australia: Unity Scientific Asia Pacific, accessed: March 2017.
129. [www.shop.spectrecology.com/Light-Sources-UV-VIS-NIR\\_c37.htm](http://www.shop.spectrecology.com/Light-Sources-UV-VIS-NIR_c37.htm). SpectrEcology, accessed: March 2017.
130. R.H. Wilson, B.J. Goodfellow, P.S. Belton, B.G. Osborne, G. Oliver, P.L. Russell. "Comparison of Fourier transform mid infrared spectroscopy and near infrared reflectance spectroscopy with differential scanning calorimetry for the study of the staling of bread". J. Sci. Food Agric. 1991. 54(3): 471-483.
131. J.J.G. van Soest, H. Tournois, D. de Wit, J.F.G. Vliegthart. "Short-range structure in (partially) crystalline potato starch determined with attenuated total reflectance Fourier-transform IR spectroscopy". Carbohydr. Res. 1995. 279: 201-214.
132. M. Abu-Ghoush, T.J. Herald, F. Dowell, F. Xie, F.M. Aramouni, R. Madl. "Effect of preservatives addition on the shelf-life extensions and quality of flat bread as determined by near-infrared spectroscopy and texture analysis". Int. J. Food Sci. Technol. 2008. 43(2): 357-364.
133. C. Cevoli, A. Gianotti, R. Troncoso, A. Fabbri. "Quality evaluation by physical tests of a traditional Italian flat bread *Piadina* during storage and shelf-life improvement with sourdough and enzymes". Eur. Food Res. Technol. 2015. 240(6): 1081-1089.
134. F. Xie, F.E. Dowell, X.Z.S. Sun. "Using visible and near-infrared reflectance spectroscopy and differential scanning calorimetry to study starch, protein, and temperature effects on bread staling". Cereal Chem. 2004. 81(2): 249-254.
135. H.F. Zobel, K. Kulp. "The staling mechanism". In: R.E. Hebeda, H.F. Zobel, editors. Baked goods: freshness, technology, evaluation and inhibition of staling. New York, N.Y: Marcel Dekker, 1996. Pp. 1-64.
136. B.G. Osborne, T. Fearn, P.H. Hindle. Practical NIR spectroscopy, with applications in food and beverage analysis. Harlow, UK: Longman Scientific and Technical, 1993. 2nd ed.

# Appendix: List of spectrometers

## **FT-IR spectrometer: MB100**

(ABB Bomem, Quebec, Canada). Resolution of  $8\text{ cm}^{-1}$  and 64 scans.

## **FT-IR spectrometer: Vertex 70**

(Bruker Optik GmbH, Ettlingen, Germany). Resolution of  $4\text{ cm}^{-1}$  and 256 scans.

## **FT-IR spectrometer: IFS 28**

(Bruker Optik GmbH, Ettlingen, Germany). Resolution of  $4\text{ cm}^{-1}$  and 64 scans.

---

## **Diamond ATR with 1-bounce: Durascope Dicomp**

(SensIR technologies, Danbury, CT, USA).

## **Diamond ATR with 3-bounces: Durascope Dicomp**

(SensIR technologies, Danbury, CT, USA).

## **ZnSe ATR with 12-bounces: Spectra-Tech**

(Spectra-Tech, Inc., Shelton, CT, USA).

---

## **FT-NIR spectrometer: FTLA2000 – 160**

(ABB Bomem, Quebec, Canada). Resolution of  $8\text{ cm}^{-1}$  and 64 scans.

## **FT-NIR spectrometer : VECTOR 22N FT-NIR spectrometer**

(Bruker Optik GmbH, Ettlingen, Germany). Resolution of  $8\text{ cm}^{-1}$  and 64 scans.

## **Dispersive NIR spectrometer: 6500**

(NIR systems, Inc., Silver Springs, MD, USA). Scans: 32.

## **Dispersive NIR spectrometer: NIRS<sup>TM</sup> DS2500 F**

(FOSS, Hillerød, Denmark). Scans: 256.

## **Dispersive NIR spectrometer: Supercontinuum light and monochromator**

(Described in Section 3.1, PAPER I and III).

## **Fiber NIR spectrometer: Supercontinuum light and a wavelength separating fiber**

(Described in Section 3.3).



---

# Paper I

---

## **Near-Infrared Spectroscopy Using a Supercontinuum Laser: Application to Long Wavelength Transmission Spectra of Barley Endosperm and Oil**

Tine Ringsted, Sune Dupont, Jacob Ramsay, Birthe Møller Jespersen, Klavs Martin Sørensen, Søren Rud Keiding, and Søren Balling Engelsen

*Applied Spectroscopy* 70 (2016) 1176–1185





# Near-Infrared Spectroscopy Using a Supercontinuum Laser: Application to Long Wavelength Transmission Spectra of Barley Endosperm and Oil

Tine Ringsted<sup>1</sup>, Sune Dupont<sup>2</sup>, Jacob Ramsay<sup>2</sup>,  
Birthe Møller Jespersen<sup>1</sup>, Klavs Martin Sørensen<sup>1</sup>,  
Søren Rud Keiding<sup>2</sup>, and Søren Balling Engelsen<sup>1</sup>

## Abstract

The supercontinuum laser is a new type of light source, which combines the collimation and intensity of a laser with the broad spectral region of a lamp. Using such a source therefore makes it possible to focus the light onto small sample areas without losing intensity and thus facilitate either rapid or high-intensity measurements. Single seed transmission analysis in the long wavelength (LW) near-infrared (NIR) region is one area that might benefit from a brighter light source such as the supercontinuum laser. This study is aimed at building an experimental spectrometer consisting of a supercontinuum laser source and a dispersive monochromator in order to investigate its capability to measure the barley endosperm using transmission experiments in the LW NIR region. So far, barley and wheat seeds have only been studied using NIR transmission in the short wavelength region up to 1100 nm. However, the region in the range of 2260–2380 nm has previously shown to be particularly useful in differentiating barley phenotypes using NIR spectroscopy in reflectance mode. In the present study, 350 seeds (consisting of 70 seeds from each of five barley genotypes) in 1 mm slices were measured by NIR transmission in the range of 2235–2381 nm and oils from the same five barley genotypes were measured in a cuvette with a 1 mm path length in the range of 2003–2497 nm. The spectra of the barley seeds could be classified according to genotypes by principal component analysis; and spectral covariances with reference analysis of moisture,  $\beta$ -glucan, starch, protein and lipid were established. The spectral variations of the barley oils were compared to the fatty acid compositions as measured using gas chromatography–mass spectrometry (GC-MS).

## Keywords

Barley seed, beta-glucan, food, near-infrared spectroscopy, NIR, near-infrared transmission spectroscopy, NIT, single seed, supercontinuum laser

Date received: 2 September 2015; accepted: 26 November 2015

## Introduction

The light source which is most frequently used in near-infrared (NIR) spectrometers is a filament light source, namely the quartz tungsten halogen lamp.<sup>1,2</sup> This source provides broadband light covering both the visible and NIR region; however, its brightness is much lower compared to the almost monochromatic light offered by a laser. A supercontinuum laser combines the spectral bandwidth of a lamp with the collimated beam of a laser. The supercontinuum source is generated from laser light entering a material with high optical non-linear properties, such as an optical fiber.<sup>3,4</sup> The main advantage of the supercontinuum source for broadband transmission spectroscopy is

that the beam exits from an optical fiber and therefore has a high spatial coherence. Therefore, the beam can be focused tightly onto a sample and thus be able to achieve high spectral brightness compared to traditional filament-based light sources. So far, the supercontinuum light source

<sup>1</sup>Spectroscopy & Chemometrics, Department of Food Science, University of Copenhagen, Frederiksberg, Denmark

<sup>2</sup>Department of Chemistry, Aarhus University, Aarhus, Denmark

## Corresponding author:

Tine Ringsted, Spectroscopy & Chemometrics, Department of Food Science, University of Copenhagen, Rolighedsvej 26, 1958 Frederiksberg, Denmark.

Email: tine.ringsted@food.ku.dk

has been limited to special applications within gas-phase spectroscopy and microscopy<sup>5</sup> as well as in a hyperspectral imaging application.<sup>6</sup>

The highly coherent and bright light from the supercontinuum laser has a potential advantage when the light needs to travel a long distance (e.g., gas-phase spectroscopy or remote sensing) or when a small area needs to be analyzed (e.g., microscopy or imaging) or when fast measurements are required. The possibility of focusing all the light from the supercontinuum laser onto a small area makes it possible to measure the transmission of light through cereal seeds at longer NIR wavelengths, which so far has only been performed in reflectance mode. The analysis of seeds by light transmission in the NIR region has primarily been made in the short wavelength region from 700 to 1100 nm.<sup>7</sup> This is due to the lower extinction coefficients at shorter wavelengths compared to the longer wavelengths in the NIR region. The short wavelengths in the NIR contain primarily strongly overlapped information from the second and third overtones of the O–H, C–H, and N–H stretching vibrations and thus are very useful for bulk composition analysis of water, carbohydrates, fat, and protein. It is, for example, well-known that short wave (850–1050 nm) NIR transmission spectra can predict protein content in single wheat seeds with an accuracy of 0.5%.<sup>8</sup> This principle is used today for breeding and sorting of cereals. However, other more complex quality parameters such as the important  $\beta$ -glucan content have not been accurately predicted from this spectral range.  $\beta$ -glucans are mixed linkage (1 $\rightarrow$ 3, 1 $\rightarrow$ 4)- $\beta$ -D-glucan polysaccharides consisting of a molecular blockstructure of cellotriosyl/cellobiotetraosyl units connected through beta-(1 $\rightarrow$ 3) linkages.<sup>9</sup>  $\beta$ -glucan content in barley remains an important issue for the brewing industry in order to prevent clogging of filters and ultimately to form “grandma’s cough” precipitation in beer. In parallel, there is an opposite trend in breeding barley seeds with high  $\beta$ -glucan content because of health benefits. Both barley and oat  $\beta$ -glucans in food give rise to health promoting effects and nutritional benefits such as the flattening of the blood glucose and insulin rises after food consumption as well as the reduction of serum cholesterol levels.<sup>10</sup> It is therefore desirable to be able to use NIR transmission at wavelengths much longer than 1100 nm as for instant the first overtone region (approximately 1400–1800 nm) or the combination tone region (approximately 1900–2500 nm) that provides a more detailed and selective picture of the chemical composition. Near-infrared spectroscopy on barley flour in reflectance mode using the LWV region of 2200–2500 nm has previously shown to be particularly useful in differentiating barley phenotypes<sup>11</sup> and for the prediction of mixed linkage  $\beta$ -glucan content.<sup>12</sup> A fast transmission setup using LWV NIR will therefore allow new possibilities in the analysis of intact seeds for breeding or even sorting purposes.<sup>13</sup>

While long wave NIR radiation through intact single seeds is the ultimate goal, this study demonstrates the transmission of LW NIR through a 1 mm disk of barley endosperm and for reference purposes through 1 mm of barley oil in a liquid cell. The light that passes through a seed will be scattered in all directions because of the endosperm cell structure. Liquids, including oils, scatter light to a far less extent and are therefore included in order to investigate how the supercontinuum source will perform on high- and low-scattering samples, respectively. The present study investigated the ability to differentiate between five different barley mutants by the application of LW NIR transmission spectroscopy using a supercontinuum light source. The barley mutants were analyzed from single seed slices and bulk extracted oil. The differences in their level of moisture,  $\beta$ -glucan, starch, protein, lipids, and unsaturated fatty acids were used for spectral interpretation.

## Experimental

### The Instrument

The instrument setup is shown in Figure 1a. The supercontinuum light source (NKT Photonics) used for the instrument is based on a 1550 nm laser pumping a thulium doped fiber at a repetition rate of 35 kHz, followed by a few-meter step-index ZBLAN fiber. The supercontinuum spectrum is in the range of 1500–4200 nm with an average output power of 60 mw (Figure 1b).

In the experimental setup, an off-axis parabolic mirror was used to collimate the supercontinuum source output in order to reduce chromatic aberration. Another parabolic mirror was used to focus the light into a scanning grating monochromator for wavelength selection. After re-collimation, the beam was focused onto the sample by a plano-convex CaF<sub>2</sub> lens. The laser beam had a spot size of 0.1  $\times$  0.5 mm at the sample. The sample can be presented in a cuvette holder for liquid measurements or in a rotating seed sample holder. A PbSe detector was placed directly behind the sample holder to detect the transmitted light. The reflection from the backside of the focusing lens was collected by another CaF<sub>2</sub> lens, and was used as a reference measurement. Since the repetition rate of the laser is 35 kHz, the detectors were chosen such that they were fast enough to separate each pulse individually. This proved to be essential, as each supercontinuum pulse fluctuates from pulse to pulse in both amplitude and polarization.<sup>14</sup> In order to avoid the polarization noise, the beam-splitting lens was set at a small angle relative to the incident light in order to decrease polarization dependence of the reflectance. Two lock-in amplifiers were used to amplify the signals and the resulting sample and reference signals were divided to obtain a normalized intensity value

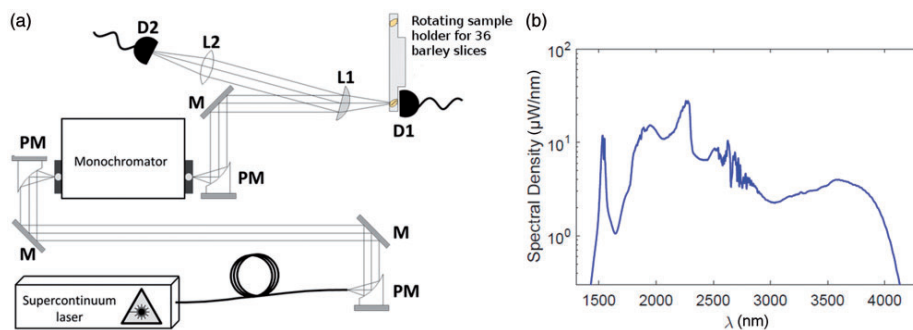


**Figure 1.** (a) The barley transmission setup. The mid-infrared supercontinuum source is launched from a fiber onto an off-axis parabolic mirror (PM) for collimation. The light is then guided by silver mirrors (M) and focused by another PM into a grating monochromator for wavelength selection. The narrow-band light is subsequently collimated with a PM before it is focused by a plano-convex CaF<sub>2</sub> lens (L1) onto the barley grain of interest. A PbSe detector (D1) is used for detection of the transmitted light. The plano-convex lens (L1) is tilted at a small angle, and the back-reflection is used as a reference, which is focused by the CaF<sub>2</sub> lens (L2) onto another PbSe detector (D2). (b) Spectrum of the mid-infrared supercontinuum source.

for each wavelength step. This pulse-to-pulse normalization was crucial in order to eliminate the variation between the pulses and thus to obtain a high signal-to-noise (S/N) ratio of the spectra. The seeds were scanned in the region of 2235–2381 nm but only the region of 2261–2381 nm was used in the data analysis. The oils were scanned in a slightly broader range, namely 2003–2497 nm. In both cases, the wavelength resolution was set to 10 nm by the output slit of the monochromator and the NIR intensity recorded in 2 nm intervals. In order to obtain a useful S/N ratio for the seed measurements, each wavelength point was an average of 105 ms of laser. To further enhance the S/N ratio, five consecutive spectral scans were collected and averaged, giving a total measurement time of 60 s. For the oil measurements, each wavelength point was measured as a 35 ms average of laser pulses, which also resulted in a total measurement time of 60 s for the six spectral scans collected per oil sample.

### Sample Presentation

Using the bright supercontinuum, it is possible to record transmission spectra of whole barley seeds (see Supplemental Material Figure S1). However, the S/N ratio is significantly improved when measuring on 1 mm slices and this sample preparation was therefore chosen. For this purpose, a barley slicer with a fixed distance between two blades was developed in order to ensure a consistent thickness of the 1 mm slices (Figure 2). In addition, a rotatable sample holder was produced, which could automatically hold and measure 36 seed samples in one run. Slices of 1 mm were cut from barley seeds and measured within 1.5 h by NIR transmission. Furthermore, barley oils extracted from

the five genotypes as well as sunflower and mineral oil were measured in a quartz cuvette with a 1 mm path length.

### Barley Samples

Five barley genotypes were included in this study. Four structural carbohydrate mutants with depleted starch and high  $\beta$ -glucan content were included (*lys5.f*, *lys5.g*, *lys16*, and *lys95*) and a reference genotype (*Bomi*) which has normal levels of lipids, starch,  $\beta$ -glucan, etc.<sup>15,16</sup> *Bomi* is the mother line for *lys5.f* and *lys16*, and *lys95* is a mutant in the barley variety Perga. The barley samples were grown in field trials in collaboration with Lantmännen SW Seeds (Sweden) in 2004 and have been stored in a refrigerator. Slices from 70 seeds of each barley genotype were measured, giving a total of 350 seeds which were measured for LW NIR transmission using the supercontinuum instrument.

### Barley Oil Extraction

Lipid extraction was performed using a Pressurised Solvent Extractor (PSE), ASE200 from Dionex (Sunnyvale, CA, USA). Extraction cells with 10 g of milled barley were used. Extraction was performed using 100% hexane according to the following conditions: Preheat: 0 min; heat: 6 min; static extraction: 5 min, flush volume: 50% of extraction cell; purge: 2 min; cycles: 3, pressure: 1500 psi, temperature: 105 °C. The extracts were evaporated to dryness.

In total, five barley oil samples were produced and measured with the supercontinuum instrument. For comparison, one sample of sunflower oil and one mineral oil (nujol) was included in the analysis as samples with high and low content of C=C double bonds, respectively.

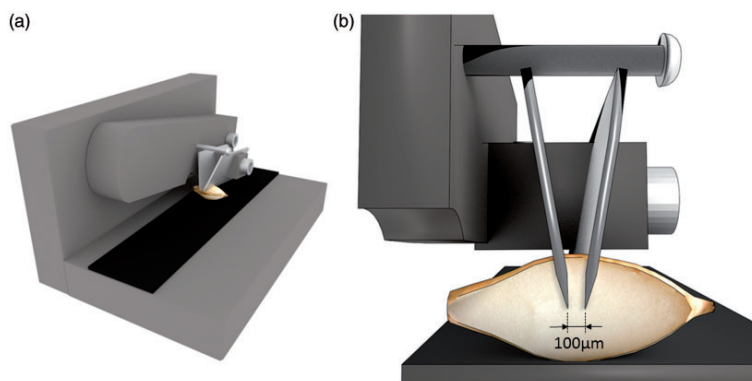


**Figure 2.** (a) The grain cutter with a barley kernel positioned under the cutting blades. A slice of the kernel is produced by gently pressing on the cutting arm, forcing the knife blades through the kernel. The black rubber under the kernel keeps the kernel steady and prevents knife wear out. (b) Cross-section of the cutting blades pressed half through the kernel. The blades are angled so that the inner edges are parallel and perpendicular to the base plate and are spaced 1 mm apart. The angling produces a kernel slice of uniform thickness.

### Reference Measurements

Bulk samples of each of the five barley genotypes were milled on a hammermill (sieve 0.5 mm) and moisture,  $\beta$ -glucan, starch, protein, and lipid content were determined in duplicates. Total  $\beta$ -glucan content was measured using an enzyme kit (Megazyme, Wicklow, Ireland).<sup>17</sup> Protein content was analyzed using the Kjeldahl method ( $N \times 6.25$ ) using a Tecator 2020 Digester and 1026 Distilling unit (FOSS, Hillerød, Denmark).<sup>18</sup> The total starch content was determined from an enzymatic kit (Megazyme, Wicklow, Ireland) following the AOAC Method 996.11 adapted to cereal and food products not containing resistant starch, D-glucose, and/or maltodextrin.<sup>19</sup> The moisture content was measured by the 44-15.02 AACC method.<sup>20</sup> The lipid content was extracted with petroleum ether and a Soxtec System HT and 1043 extraction unit (Tecator AB, Höganäs, Sweden).<sup>21</sup>

The fatty acid composition of the barley oils and the sunflower oil was determined by gas chromatography-mass spectrometry (GC-MS) (Agilent Technologies 6890A GC system) using a capillary column (Phenomenex ZebroM ZB-WAX 30 m/0.25 mm ID/250  $\mu$ m FT) and a mass spectrometer (Agilent 7890B). Approximately 100 mg of barley oil was methylated as described by Sørensen et al.<sup>22</sup> A total of 1  $\mu$ L of the methylated sample was injected with a 50:1 split ratio with a run-time of 20 min in an injector set at 250 °C, with oven isothermal at 210 °C and a hydrogen carrier flow constant at 1.2 mL/min. The EI MS was run in scan mode (50–350 m/z range), with a 1 min solvent delay. Fatty acid esters C8:0, C10:0, C12:0, C14:0, C16:0, C18:0, C18:1 (cis-9), C18:2 (cis,cis-9,12), C18:3 (cis,cis,cis-9,12,15),

C20:0, C20:1 (cis-11), C22:0, and C 24:0 were identified using a GC-MS RTL FAME database.<sup>23</sup> Individual fatty acid concentration was determined by relative peak area in percentage of the total peak area. As an example of a total fatty acid quality parameter, the iodine value of the oils was calculated from the GC-MS data using the AOCS recommended practice.<sup>24</sup> The iodine value is a measure of the total amount of C=C double bonds in the unsaturated fatty acids of the oils. For comparative purposes a sunflower oil (iodine value = 133) and a mineral oil (iodine value = 0) was included in the analysis.

### Multivariate Data Analysis

The absorbance was calculated as the  $\log_{10}(I_0/I_s)$  where  $I_0$  is the light intensity with no sample in the sample holder and  $I_s$  is the light intensity with a sample inserted in the sample holder. Spectra were preprocessed with different methods including MSC (multiplicative scatter correction), SNV (standard normal variate), EMSC (extended multiplicative scatter correction), and first and second derivative (Savitzky–Golay, two-degree polynomial, window size between 5 and 15).<sup>25</sup> Preprocessed spectra were mean centered before modeling.

Principal component analysis (PCA)<sup>26</sup> was used to visualize the similarities and differences between the spectra, including outlier detection.

The Pearson correlation coefficient was calculated to see how each wavelength covaried with the reference measurements. These covarygrams were therefore used to increase spectral interpretation.<sup>27</sup> The spectra were analyzed in Matlab (version R2013b) (The Mathworks, Inc.,

Natick, MA, USA) and PLS toolbox 7.5 (Eigenvector Research, Inc., Manson, WA, USA).

## Results and Discussion

As mentioned in the introduction, it would be highly desirable to obtain a fast method for  $\beta$ -glucan screening of intact seeds. Initial supercontinuum LW NIR measurements were conducted on whole barley seeds, but the measured absorbance levels were on the limit of the dynamic range of the instrument which resulted in noisy spectra (see Supplemental Material Figure S1). The potential of LW NIR transmission spectroscopy was therefore investigated on barley slices instead of whole seeds. The slices were cut from the center of the seed and measured through the endosperm only.<sup>28</sup> By comparison with measurements through the entire seed the endosperm will contain marginally more  $\beta$ -glucan and starch whereas lipids and proteins will be found in higher concentrations in the embryo and in the aleurone.<sup>28–30</sup> The comparison between the spectra of the barley seed slices and the reference methods will thus be biased due to the chemical heterogeneity of the barley seed.

Due to cracks, some of the 350 barley seeds allowed light to pass directly to the detector. This causes a flattening of the absorbance spectrum since the stray light creates a large background offset. On the basis of histograms and PCA it was decided that samples with an absorbance<sub>max</sub> – absorbance<sub>min</sub>  $\leq 0.67$  were outliers, and 58 samples were therefore removed. The raw spectra are shown in Figure 3a and reveal significant variations in the levels of light scattering as seen from the varying levels of the apparent absorbance. Figure 3 also clearly shows the high S/N ratio which was obtained due to the effective pulse-to-

pulse normalization which eliminates the inherent intensity fluctuations between pulses from the supercontinuum source.

In order to eliminate the light scattering effects from the spectra, different preprocessing methods were applied. It was found that the preprocessing methods SNV, MSC, and EMSC yielded practically the same level of scatter elimination with the latter being slightly more efficient. Figure 3b presents the average spectra of each genotype after scatter correction with EMSC. The spectra contains three peaks, at 2287 nm, 2323 nm, and 2349 nm, which is in agreement with previous LW NIR reflectance studies on the flour of the same barley genotypes.<sup>12,15,31</sup>

The spectral differences and similarities were investigated by PCA in order to study the genotype diversification. The resulting PCA score plot is shown in Figure 4 and overall this plot confirms that LW NIR measurements are very useful for phenotyping of the barley genotypes.<sup>31</sup> In the score plot the *Bomi* motherline (red diamonds) displays a more uniform variance structure than the four mutants. While the *Bomi* samples are clearly separated from the four mutants, there exists some overlap in the variance structure among mutants. Nevertheless, their centers of “gravity” are clearly separated in the scores plot with the *lys95* as the most extreme and with the highest intra-phenotype variance. In fact, several samples were found to be extreme within their own genotype (three *lys5.f*, one *lys5.g*, one *lys16*, and eight *lys95*). These genotype outliers were in 12 out of 13 cases placed closer to the normal barley genotype (*Bomi*) in a PCA containing all genotypes, indicating that the outliers were much more similar to the *Bomi* genotype compared to their own genotype. An example of this can be seen in Figure 4 where eight samples of *lys95* are situated closer to the *Bomi* samples compared to the

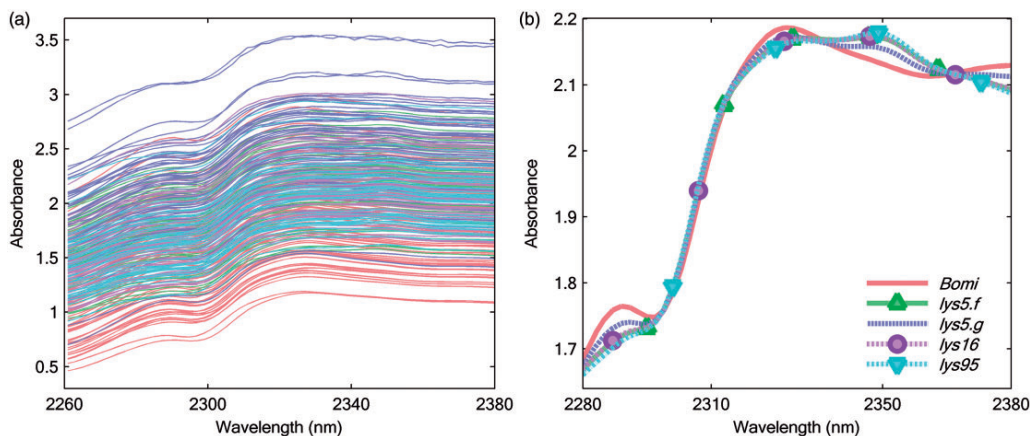


**Figure 3.** (a) Raw long wavelength (LW) NIR spectra of barley slices from 287 seeds from five different genotypes and (b) average LW NIR spectra of the five genotypes spectra in the range of 2280–2380 nm preprocessed with EMSC.

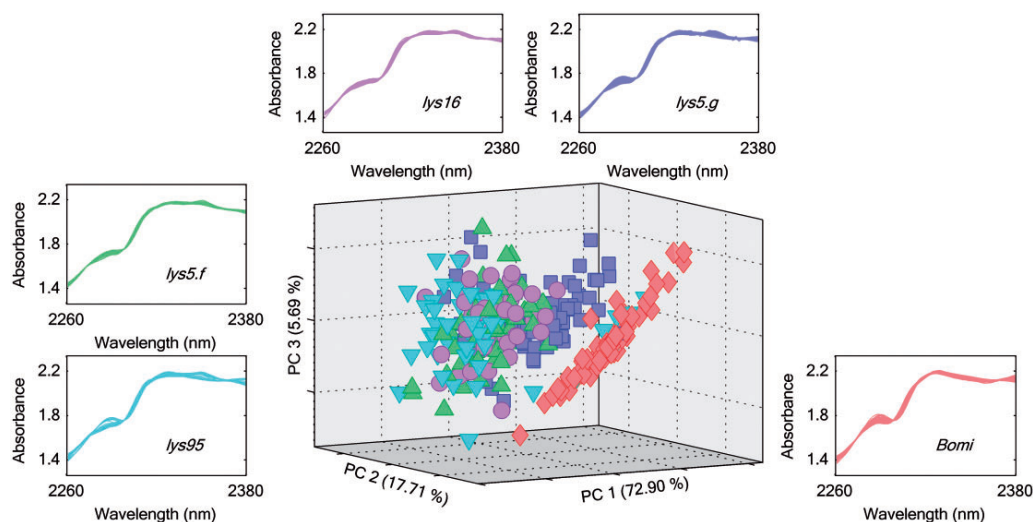


**Figure 4.** Spectra of 287 seeds from five different genotypes were preprocessed with EMSC and a PCA was calculated. The spectra of the individual genotypes are presented in the small plots. Genotype *lys95* had eight spectra which were more similar to the *Bomi* phenotype and these were removed as adulterations.

**Table 1.** The average reference measures for the five barley genotypes: moisture,  $\beta$ -glucan, starch, protein, and lipid content. The average iodine values for the oil extracted from each barley genotype are given.<sup>a</sup> The standard deviation of duplicates is given.

	Moisture (%)	$\beta$ -glucan (%)	Starch (%)	Protein (%)	Lipids (%)	Iodine value for oil
<i>Bomi</i>	9.5 $\pm$ 0.2	5.5 $\pm$ 0.1	49.5 $\pm$ 0.02	11.8 $\pm$ 0	2.05 $\pm$ 0.02	105.6 $\pm$ 1.6
<i>lys5.f</i>	8.1 $\pm$ 0.4	13.2 $\pm$ 0.1	30.7 $\pm$ 4.8	13.3 $\pm$ 0.1	3.96 $\pm$ 0.11	102.5 $\pm$ 0.2
<i>lys5.g</i>	9.1 $\pm$ 0.04	8.0 $\pm$ 0.1	39.9 $\pm$ 1.0	12.3 $\pm$ 0.1	2.91 $\pm$ 0.19	104.0 $\pm$ 1.7
<i>lys16</i>	7.9 $\pm$ 0.001	14.2 $\pm$ 0.1	27.4 $\pm$ 0.8	12.8 $\pm$ 0.003	3.71 $\pm$ 0.08	103.4 $\pm$ 1.1
<i>lys95</i>	8.1 $\pm$ 0.09	13.1 $\pm$ 0.1	27.3 $\pm$ 1.0	14.5 $\pm$ 0.2	4.44 $\pm$ 0.01	104.4 $\pm$ 1.4

<sup>a</sup>The iodine value for sunflower oil was measured to be 133.3  $\pm$  0.7. Mineral oil does not have C=C bonds and the iodine value is therefore 0.

majority of the *lys95* samples. It is difficult to know why most of the genotype outliers resembled *Bomi*. One possibility is that the field experiments had accidental mixing of seeds. Another possibility is that the sampling technique could be biased towards seed with a smaller weight, larger volume, or other properties. In fact, the presented study used grab/spoon sampling which was found in another study, which measured protein in wheat by NIR transmittance spectroscopy, to have a variance of the global estimation error which was 70% higher for grab sampling compared to riffle split sampling.<sup>32</sup> In other words, grab sampling can result in non-random sample selection which could influence the diversity of the selected samples. Nevertheless, it was decided that this phenomenon was likely due to an occasional mixing of seeds in the field experiments and the samples were accordingly treated as outliers. After outlier removal, 279 sample spectra were

left in the data set (67 *Bomi*, 54 *lys5.f*, 61 *lys5.g*, 54 *lys16*, and 43 *lys95*).

The average content of moisture,  $\beta$ -glucan, starch, protein, and lipid was determined for each barley phenotype in order to support the chemical interpretation of the super-continuum spectral data (Table 1). The chemical analysis is in good agreement with previous determinations considering the fact that the concentrations in this study are made on wet weight.<sup>15</sup> The  $\beta$ -glucan content range from 5.5 g/100 g in *Bomi* to 14.2 g/100 g in *lys16*. The starch content range from 27.3 g/100 g in *lys95* to 49.5 g/100 g in *Bomi*. Starch and  $\beta$ -glucan content are correlated with a Pearson correlation coefficient of  $r = -0.91$  which underlines the close relationship between the biochemical pathways of these two metabolites and the fact that the barley seed is a closed system. The chemical information of the spectra was studied by correlating each wavelength with the

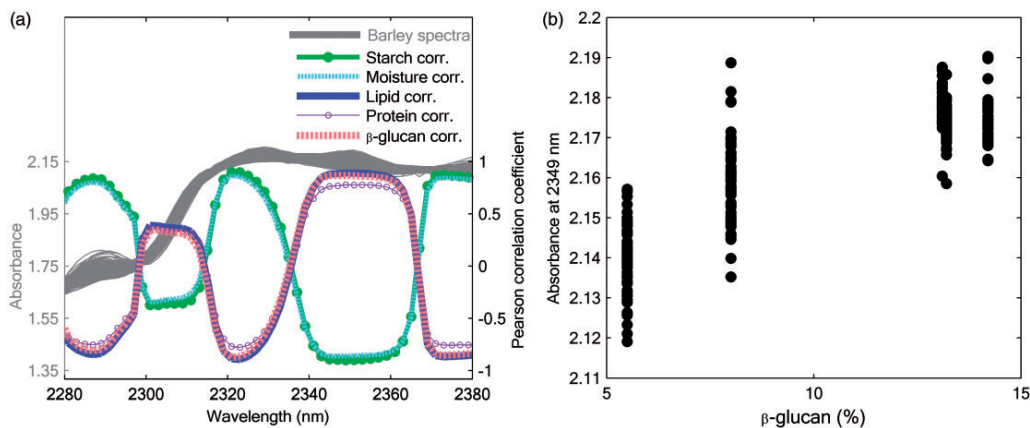


**Figure 5.** (a) Near-infrared spectra of barley slices from 279 seeds from five different genotypes preprocessed with EMSC. The correlation between spectral variables and the moisture, starch, protein, lipid, and  $\beta$ -glucan content is presented to increase spectral interpretation. (b) The content of  $\beta$ -glucan versus the absorbance at 2349 nm.

content of moisture,  $\beta$ -glucan, starch, protein, and lipid (Figure 5). From the figure it is clear that moisture,  $\beta$ -glucan, starch, lipid, and protein are all correlated because they are either overlapping or mirror images. It is also clear that the three peaks at 2287, 2323, and 2349 nm covary strongly with starch, starch, and  $\beta$ -glucan, respectively.

The absorbance at 2287 nm has a correlation coefficient of  $r = 0.86$  with starch (Figure 5) which is in good agreement with literature that assigns this to the O–H + C–C stretch (or O–H stretching + C–O stretch) combination tone.<sup>15,33–35</sup> The precise position of this peak has furthermore been related to the ratio between the amylose and amylopectin components of starch<sup>36</sup> which makes good sense because the C–O vibrations in starch will depend on the packing of the granule and the crystallinity of the amylopectin. The peak at 2287 nm might also have a contribution from the combination band of the CH<sub>2</sub> groups (C–H asymmetric stretching ( $2924\text{ cm}^{-1}$ ) + C–H def ( $1460\text{ cm}^{-1}$ )) which may come from all three major families of food molecules: carbohydrates, fats, and proteins.

The absorbance at 2323 nm has a correlation coefficient of  $r = 0.91$  with starch which again is in good agreement with the literature.<sup>35,37</sup> This peak seems to move or shift slightly towards higher wavenumbers with higher starch/water content, a phenomenon that was particular pronounced in NIR measurements on flours of the developing barley endosperm.<sup>12</sup> The peak has been assigned to the overtone (C–H stretching + C–H deformation) in starch primary hydroxyl groups that depend on the crystallinity of the amylopectin packing.

The literature has assigned peaks at slightly higher wavelengths to cellulose at 2335 nm and  $\beta$ -glucan at 2349 nm.<sup>33–35</sup> The 2335 nm peak is not visible on our spectra as cellulose is

only a minor component of the barley endosperm. The peak at around 2349 nm has been targeted as the primary point in the NIR calibration for dietary fiber in wheat bran<sup>38</sup> and indeed the correlation between the absorbance level at 2349 nm and  $\beta$ -glucan was found to be  $r = 0.87$ . One reason why this correlation is not even higher might be due to the fact that this region also contains the combination tone of unsaturated fatty acids (CH<sub>2</sub> symmetrical stretching = CH<sub>2</sub> deformation) around 2347 nm, and the second overtone of cellulose and proteins (second C–H deformation) around 2352 nm. The absorbance variations at 2349 nm within each genotype as seen from Figure 5b is caused by different seed compositions (lot heterogeneity). In fact, a study found a variation from 0.4–1.4 or 0.6–1.6 mg  $\beta$ -glucan per seed within two barley cultivars.<sup>39</sup>

In addition to the assignments mentioned above, all three peaks may have contributions from the barley lipids. However, it does not seem likely that lipids contribute significantly to the spectra since the total content of lipids in barley is rather low (2.1 to 4.4 g/100 g; see Table 1) and the content of lipids in the endosperm is very low.<sup>30</sup>

In order to investigate which peak in the LW NIR spectra of the barley endosperm that originates primarily from the lipid component and simultaneously how the supercontinuum instrument performs on liquid samples, oils from the five barley genotypes were extracted and measured by LW NIR. The resulting LW NIR spectra together with a nujol mineral oil and sunflower oil are shown in Figure 6. The spectra show a peak at 2148 nm which has been assigned to a combination band of unsaturated fat vibrations (=C–H stretching + C=C stretching)<sup>33,40</sup> which matches with the results in this study since the mineral oil has no double bonds and no absorbance in that wavelength range. The shoulder at 2280 nm and the peaks at 2310 and 2353 nm resemble the absorbance pattern

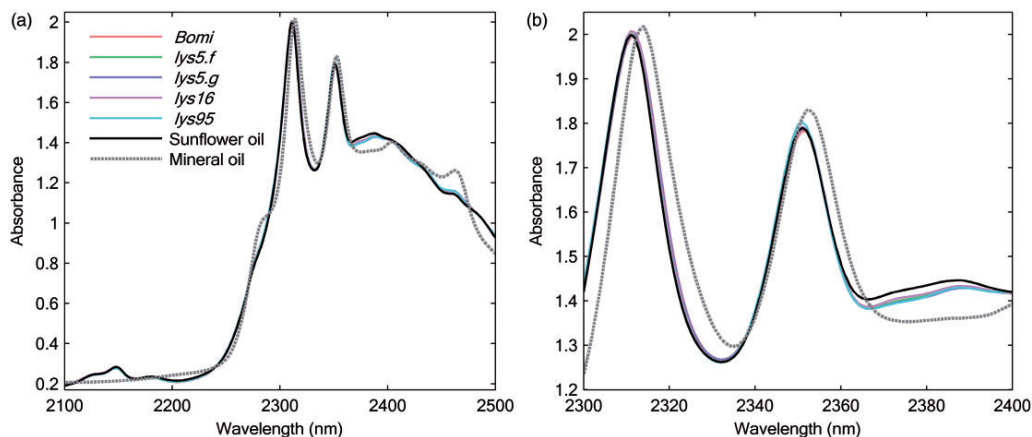


**Figure 6.** Oil extracted from five barley genotypes and a sunflower oil and a mineral oil shown as (a) spectra in the range of 2100–2500 nm preprocessed with EMSC and (b) spectra in the range of 2300–2400 nm preprocessed with EMSC.

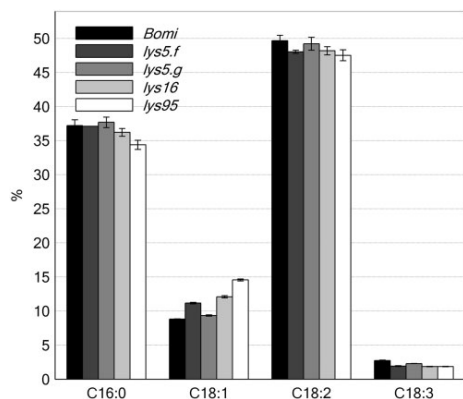


**Figure 7.** The percentage of the main fatty acids from oil extracted from the five barley genotypes.

seen for barley slices in Figure 3b. As mentioned above, for the barley endosperm analysis it is clearly possible that barley oils may absorb at nearly the same wavelengths as for the endosperm. For a pure fat matrix, however, the assignments are simpler. The peak at 2280 nm is due to the combination band of CH<sub>2</sub> groups (C–H asymmetric stretching (2924 cm<sup>-1</sup>) + C–H deformation (1460 cm<sup>-1</sup>)). The peak at 2310 nm is due to an overtone (second C–H deformation) and/or a combination tone (C–H asymmetric stretching + C–H deformation) of the dominating methylene groups in the oil. The peak at 2351 nm is due to the combination band of CH<sub>2</sub> groups (C–H symmetric stretching (2874 cm<sup>-1</sup>) + C–H def. (1460 cm<sup>-1</sup>)) of the fats.

The small spectral differences between barley oils seen in Figure 6a and 6b were investigated by comparing the fatty

acid compositions (Figure 7). We have previously observed the pleiotropy concerted by these barley mutants, with significant changes in metabolites cascading through the different omics levels and giving rise to subtle changes in the metabolome pattern of vitamin E.<sup>31</sup> This phenomenon is also present at the lipidomics level as evidenced by Figure 7. While the major oil C18:2 is relatively constant near 50%, the C18:1 vary from 8.8% in *Bomi* to 14.6% in *lys95*. Interestingly, the total fatty acid parameter the iodine value of the different barley oils remains relatively constant since the upregulation of the C18:1 is counteracted by a downregulation of the C18:3. The variation in iodine value between the genotypes ranged from 102.5 to 105.6 (see Table 1). As expected, a strong positive correlation between the absorbance level at 2148 nm and the iodine value ( $r = 0.98$ ) was found.

## Conclusions

A novel NIR spectrometer using a supercontinuum laser as a light source was developed and for the first time tested for LW NIR transmission analysis of barley endosperm and extracted barley oil from different barley genotypes. This research has demonstrated that supercontinuum light sources have the potential to facilitate NIR transmission spectra of single seeds on the fly.

A major obstacle in the construction of a competitive supercontinuum instrument for seed analysis was to develop an efficient pulse-to-pulse normalization, which was necessary for producing good quality spectra. However, this feature might be a huge advantage for future real applications as it will facilitate time-resolved spectroscopy and it will create adaptive measurements that will be independent on drift.

On the sample side, the major obstacle in obtaining transmission LW NIR spectra is the light scattering that occurs in the amorphous seed. As this obstacle is inherent to the light matter interaction the only route to improve the situation is to increase the intensity of the incident light, which can be done by using supercontinuum lasers.

From this research it seems likely that supercontinuum spectrometers might be even more competitive at even longer wavelengths extended into the deep mid-infrared<sup>41</sup> where the normal light sources are weak and the photon energy is only slightly above *kT* giving rise to substantial thermal noise.

It would appear that instruments using supercontinuum lasers have the advantage of providing ultrarapid measurements with a very high brightness. This can, for example, be utilized for fast scanning purposes, for gas phase measurements, and for fast seed analysis as demonstrated here in a feasibility study.

### Acknowledgments

The authors wish to acknowledge the generous financial support from The Danish National Advanced Technology Foundation (now Innovation Fund Denmark) to the project entitled "Light & Food." Gratitude is also expressed to Sebastian Nielsen (Precision Engineering Workshop, Department of Plant and Environmental Sciences, University of Copenhagen) who helped to manufacture and develop the barley slicer. In addition, the authors would like to thank Heidi Blok Frandsen (Biochemistry and Bioprocessing, Department of Food Science, University of Copenhagen) who facilitated the extraction of barley oils. The authors are also thankful for the laboratory assistance from Abdelrhani Mourhrib and Lisbeth Tina Dahl (Spectroscopy and Chemometrics, Department of Food Science, University of Copenhagen).

### Conflict of Interest

The authors report there are no conflicts of interest.

### Supplemental Material

All supplemental material mentioned in the text, consisting of near-infrared transmission spectra of whole barley seeds and a table of the GC-MS measurements of the fatty acid composition of barley and sunflower oils, is available in the online version of the journal, at <http://asp.sagepub.com/supplemental>.

### References

- L.E. Agelet, C.R. Hurburgh. "A Tutorial on Near Infrared Spectroscopy and Its Calibration". *Crit. Rev. Anal. Chem.* 2010. 40(4): 246–260.
- F.A. DeThomas, P.J. Brimmer. "Monochromators for Near-infrared Spectroscopy". In: J.M. Chalmers, P.R. Griffiths (eds) *Handbook of Vibrational Spectroscopy*. Vol. 1, Chichester, UK: John Wiley & Sons Ltd, 2002, pp.383–392.
- R.R. Alfano, S.L. Shapiro. "Emission in the Region 4000 to 7000 Å via 4-Photon Coupling in Glass". *Phys. Rev. Lett.* 1970. 24(11): 584–587.
- J.M. Dudley, G. Genty, S. Coen. "Supercontinuum Generation in Photonic Crystal Fiber". *Rev. Mod. Phys.* 2006. 78(4): 1135–1184.
- C.F. Kaminski, R.S. Watt, A.D. Elder, J.H. Frank, J. Hult. "Supercontinuum Radiation for Applications in Chemical Sensing and Microscopy". *Appl. Phys. B-Lasers Opt.* 2008. 92(3): 367–378.
- S. Dupont, C. Petersen, J. Thøgersen, C. Agger, O. Bang, S.R. Keiding. "IR Microscopy Utilizing Intense Supercontinuum Light Source". *Opt. Express*. 2012. 20(5): 4887–4892.
- L.E. Agelet, C.R. Hurburgh. "Limitations and Current Applications of Near Infrared Spectroscopy for Single Seed Analysis". *Talanta*. 2014. 121: 288–299.
- D.K. Pedersen, H. Martens, J.P. Nielsen, S.B. Engelsen. "Near-Infrared Absorption and Scattering Separated by Extended Inverted Signal Correction (EISC): Analysis of Near-Infrared Transmittance Spectra of Single Wheat Seeds". *Appl. Spectrosc.* 2002. 56(9): 1206–1214.
- M.S. Mikkelsen, B.M. Jespersen, F.H. Larsen, A. Blennow, S.B. Engelsen. "Molecular Structure of Large-Scale Extracted Beta-Glucan from Barley and Oat: Identification of a Significantly Changed Block Structure in a High Beta-Glucan Barley Mutant". *Food Chem.* 2013. 136(1): 130–138.
- P.J. Wood. "Cereal Beta-Glucans in Diet and Health". *J. Cereal Sci.* 2007. 46(3): 230–238.
- L. Munck, J.P. Nielsen, B. Møller, S. Jacobsen, I. Søndergaard, S.B. Engelsen, L. Nørgaard, R. Bro. "Exploring the Phenotypic Expression of a Regulatory Proteome-Altering Gene by Spectroscopy and Chemometrics". *Anal. Chim. Acta.* 2001. 446(1–2): 171–186.
- H.F. Seefeldt, A. Blennow, B.M. Jespersen, B. Wollenweber, S.B. Engelsen. "Accumulation of Mixed Linkage (1 → 3) (1 → 4)-Beta-D-Glucan During Grain Filling in Barley: A Vibrational Spectroscopy Study". *J. Cereal Sci.* 2009. 49(1): 24–31.
- E. Tønning, A.K. Thybo, L. Pedersen, L. Munck, Å. Hansen, F.A. Tøgersen, S.B. Engelsen, L. Nørgaard. "Bulk Functionality Diversification by Unsupervised Single-Kernel Near-Infrared (SKNIR) Sorting of Wheat". *Cereal Chem.* 2009. 86(6): 706–713.
- J. Ramsay, S. Dupont, S.R. Keiding. "Pulse-to-Pulse Noise Reduction in Infrared Supercontinuum Spectroscopy: Polarization and Amplitude Fluctuations". *Laser Phys. Lett.* 2014. 11(9): 4.
- L. Munck, B. Møller, S. Jacobsen, I. Søndergaard. "Near Infrared Spectra Indicate Specific Mutant Endosperm Genes and Reveal a New Mechanism for Substituting Starch with (1 → 3,1 → 4)-Beta-Glucan in Barley". *J. Cereal Sci.* 2004. 40(3): 213–222.
- S. Jacobsen, I. Søndergaard, B. Møller, T. Desler, L. Munck. "A Chemometric Evaluation of the Underlying Physical and Chemical Patterns that Support Near Infrared Spectroscopy of Barley Seeds as a Tool for Exploratory Classification of Endosperm, Genes and Gene Combinations". *J. Cereal Sci.* 2005. 42(3): 281–299.
- AACC. "β-Glucan Content of Barley and Oats-Rapid Enzymatic Procedure". In: *Approved Methods of Analysis*. St. Paul, MN: AACC International, 1999, Method 32-23.01.
- AOAC. "Protein (Crude) in Animal Feed, Forage (Plant Tissue), Grain and Oilseeds". In: *Official Methods of Analysis of AOAC International*. Gaithersburg, MD: AOAC International, 2005, Official Method 2001.11.
- AOAC. "Starch (Total) in Cereal Products". In: *Official Methods of Analysis of AOAC International*. Gaithersburg, MD: AOAC International, 2005, Official Method 996.11.
- AACC. "Moisture-Air-Oven Methods". In: *Approved Methods of Analysis*. St. Paul, MN: AACC International, 1999, Method 44-15.02.
- AOAC. "Crude Fat in Feeds, Cereal Grains, and Forages". In: *Official Methods of Analysis of AOAC International*. Gaithersburg, MD: AOAC International, 2006, Official Method 2003.06.
- K.M. Sørensen, H. Petersen, S.B. Engelsen. "An On-Line Near-Infrared (NIR) Transmission Method for Determining Depth Profiles of Fatty Acid Composition and Iodine Value in Porcine Adipose Fat Tissue". *Appl. Spectrosc.* 2012. 66(2): 218–226.
- Agilent. "Application note 5988-5871EN". Santa Clara, CA: Agilent Technologies, 2012.

24. AOCS. "Calculated Iodine Value". In: *Official Methods and Recommended Practices of the AOCS*. Champaign, IL: American Oil Chemists Society, 2009, Recommended Practice Cd 1c-85.
25. Å. Rinnan, F. van den Berg, S.B. Engelsen. "Review of the Most Common Pre-Processing Techniques for Near-Infrared Spectra". *Trends Anal. Chem.* 2009. 28(10): 1201–1222.
26. R. Bro, A.K. Smilde. "Principal Component Analysis". *Anal. Methods*. 2014. 6(9): 2812–2831.
27. T. Skov, A.H. Honoré, H.M. Jensen, T. Næs, S.B. Engelsen. "Chemometrics in Foodomics: Handling Data Structures from Multiple Analytical Platforms". *Trends Anal. Chem.* 2014. 60: 71–79.
28. G.P. Fox. "Chemical Composition in Barley Grains and Malt Quality". In: G. Zhang, C. Li, editors. *Genetics and Improvement of Barley Malt Quality*. Berlin Heidelberg: Springer, 2010. Chap. 3, Pp. 63–98.
29. G.S. Chandra, M.O. Proudlove, E.D. Baxter. "The Structure of Barley Endosperm - An Important Determinant of Malt Modification". *J. Sci. Food Agric.* 1999. 79(1): 37–46.
30. T. Neuberger, N. Sreenivasulu, M. Rokitta, H. Rolletschek, C. Göbel, T. Rutten, V. Radchuk, I. Feussner, U. Wobus, P. Jakob, A. Webb, L. Borisjuk. "Quantitative Imaging of Oil Storage in Developing Crop Seeds". *Plant Biotechnol. J.* 2008. 6(1): 31–45.
31. L. Munck, B.M. Jespersen, Å. Rinnan, H.F. Seefeldt, M.M. Engelsen, L. Nørgaard, S.B. Engelsen. "A Physicochemical Theory on the Applicability of Soft Mathematical Models-Experimentally Interpreted". *J. Chemom.* 2010. 24(7–8): 481–495.
32. E. Tønning, L. Nørgaard, S.B. Engelsen, L. Pedersen, K.H. Esbensen. "Protein Heterogeneity in Wheat Lots Using Single-Seed NIT-A Theory of Sampling (TOS) Breakdown of All Sampling and Analytical Errors". *Chemom. Intell. Lab. Syst.* 2006. 84(1–2): 142–152.
33. B.G. Osborne, T. Fearn, P.H. Hindle. *Practical NIR Spectroscopy, with Applications in Food and Beverage Analysis*, 2nd ed. Harlow, UK: Longman Scientific and Technical, 1993.
34. Z. Czuchajowska, J. Szczodrak, Y. Pomeranz. "Characterization and Estimation of Barley Polysaccharides by Near-Infrared Spectroscopy. I. Barley, Starches, and Beta-Deuterium-Glucans". *Cereal Chem.* 1992. 69(4): 413–418.
35. P. Williams. "Implementation of Near-Infrared Technology". In: P. Williams, K. Norris (eds) *Near-Infrared Technology in the Agriculture and Food Industries*, 2nd ed. St. Paul, MN: American Association of Cereal Chemists, 2001, p.168.
36. M. Hódsági, S. Gergely, T. Gelencsér, A. Salgó. "Investigations of Native and Resistant Starches and Their Mixtures Using Near-Infrared Spectroscopy". *Food Bioprocess Technol.* 2012. 5(1): 401–407.
37. B.G. Osborne, T. Fearn. "Applications of Near Infrared Spectroscopy in Food Analysis". In: B.G. Osborne (ed) *Near Infrared Spectroscopy in Food Analysis*. Harlow, UK: Longman Scientific & Technical, 1986. Chap. 7, Pp. 133.
38. L. Horvath, K.H. Norris, M. Horvathmosonyi, J. Rigo, E. Hegedusvolgyesi. "Study into Determining Dietary Fiber of Wheat Bran by NIR-Technique". *Acta Aliment.* 1984. 13(4): 355–382.
39. R.M. de Sá, G.H. Palmer. "Assessment of Enzymatic Endosperm Modification of Malting Barley Using Individual Grain Analyses". *J. Inst. Brew.* 2004. 110(1): 43–50.
40. D. Cozzolino, I. Murray, A. Chree, J.R. Scaife. "Multivariate Determination of Free Fatty Acids and Moisture in Fish Oils by Partial Least-Squares Regression and Near-Infrared Spectroscopy". *LWT.* 2005. 38(8): 821–828.
41. C.R. Petersen, U. Møller, I. Kubat, B.B. Zhou, S. Dupont, J. Ramsay, T. Benson, S. Sujecki, N. Abdel-Moneim, Z.Q. Tang, D. Furniss, A. Seddon, O. Bang. "Mid-Infrared Supercontinuum Covering The 1.4-13.3  $\mu$ m Molecular Fingerprint Region Using Ultra-High NA Chalcogenide Step-Index Fibre". *Nat. Photonics.* 2014. 8(11): 830–834.

---

# Paper II

---

## **Monitoring the staling of wheat bread using 2D MIR-NIR correlation spectroscopy**

Tine Ringsted, Heinz Wilhelm Siesler, Søren Balling Engelsen

*Journal of Cereal Science 75 (2017) 92-99*





## Monitoring the staling of wheat bread using 2D MIR-NIR correlation spectroscopy



Tine Ringsted<sup>a,\*</sup>, Heinz Wilhelm Siesler<sup>b</sup>, Søren Balling Engelsen<sup>a</sup>

<sup>a</sup> Chemometrics and Analytical Technology, Department of Food Science, University of Copenhagen, Rolighedsvej 26, 1958 Frederiksberg, Denmark

<sup>b</sup> Department of Physical Chemistry, University of Duisburg-Essen, Schützenbahn 70, D 45117 Essen, Germany

### ARTICLE INFO

#### Article history:

Received 25 October 2016

Received in revised form

15 February 2017

Accepted 12 March 2017

Available online 16 March 2017

#### Keywords:

Near-infrared spectroscopy

Mid-infrared spectroscopy

2DCOS

Bread staling

### ABSTRACT

Staling of bread is a major source of food waste and efficient monitoring of it can help the food industry in the development of anti-staling recipes. While the staling fingerprint in the mid-infrared region is fairly well established this paper set out to find the most informative parts of the near-infrared spectra with respect to staling. For this purpose, two-dimensional correlation spectroscopy on near- and mid-infrared spectra of wheat bread crumb during aging was employed for the first time. The important mid-infrared absorption band at  $1047\text{ cm}^{-1}$  related to amylopectin retrogradation was found to correlate positively with increased bread hardness and to co-vary with the near-infrared band at  $910\text{ nm}$  in the short wavelength region ( $r^2 = 0.88$  to hardness), the near-infrared band at  $1688\text{ nm}$  in the 1. overtone region ( $r^2 = 0.97$  to hardness) and to the near-infrared band in the long wavelength region at  $2288\text{ nm}$  ( $r^2 = 0.97$  to hardness). The spectral information from the first principal component on near-infrared and the first principal component on mid-infrared was found to be highly correlated by a  $r^2 = 0.98$ . It is demonstrated that the major bread staling processes such as amylopectin retrogradation and water loss can be followed with both near- and mid-infrared spectroscopy.

© 2017 Elsevier Ltd. All rights reserved.

### 1. Introduction

The non-microbial changes in bread during storage which lead to consumer disapproval are called staling. Some of the staling processes are loss of flavor, increased hardness of the crumb and a decreased freshness (Fadda et al., 2014). Stale bread contributes significantly to the amount of food waste and many studies have therefore investigated staling by varying bread constituents such as maltogenic enzymes and production parameters. The physical-chemical processes that contribute to the staling effect are complex and still today not fully understood. However, some of the most important mechanisms are starch transformations, starch-gluten interactions and moisture redistribution (Fadda et al., 2014; Gray and Bemiller, 2003).

The industrial reference measurement to bread staling and the most direct correlation to sensory evaluation is texture profile analysis (TPA) (Amigo et al., 2016; Bourne, 1978). Several other methods are available for measuring staling/starch retrogradation,

including X-ray diffraction, differential scanning calorimetry (DSC), mid-infrared spectroscopy (MIR) and proton nuclear magnetic resonance (NMR) relaxation (Gray and Bemiller, 2003). Of these methods, the most convenient is probably the vibrational spectroscopic method because of its fast measurement speed, little or no sample preparation and it can measure several quality parameters simultaneously. MIR spectroscopy on bread has been used to measure the change from a more amorphous starch structure in fresh bread to a more structured and crystalline starch in stale bread by an intensity increase at  $1047\text{ cm}^{-1}$  and an intensity decrease at  $1022\text{ cm}^{-1}$  (Sevenou et al., 2002; van Soest et al., 1995; Wilson et al., 1991). The changes in starch structure which can be studied by MIR spectroscopy have been related to the double helix content and alignment in starch, the so-called short-range order (Sevenou et al., 2002; Wilson et al., 1987). However, MIR spectroscopy typically uses the attenuated total reflection (ATR) set-up that provides a rather small sampling area and thus potentially non-representative sampling. ATR crystals with multiple reflections are available but the voids in the bread structure make it difficult to obtain a good and reproducible contact with the reflection element. The sampling area can be effectively increased if near-infrared (NIR) spectroscopy can be used instead (Engelsen,

\* Corresponding author.

E-mail addresses: [tine.ringsted@food.ku.dk](mailto:tine.ringsted@food.ku.dk) (T. Ringsted), [hw.siesler@uni-due.de](mailto:hw.siesler@uni-due.de) (H.W. Siesler), [se@food.ku.dk](mailto:se@food.ku.dk) (S.B. Engelsen).

2016). Some studies have used NIR spectroscopy on staling bread, but most studies used raw absorbance spectra which contain both physical and chemical information (Abu-Ghoush et al., 2008; Cevoli et al., 2015; Wilson et al., 1991; Xie et al., 2004). If the physical information in the spectra is removed, then NIR and MIR contain similar chemical information based on molecular vibrations, although they may be influenced in slightly different ways by intermolecular interactions (Engelsen, 2016). This work aims at investigating if the NIR region can provide the same information about bread staling as is found in the MIR region. This will be investigated by studying the assignment of MIR spectra of bread by using deuterium exchange experiments and by applying for the first time two-dimensional (2D) correlation spectroscopy to the bread staling process with the aim of improving the assignments of the vibrational modes that change during the staling process. The 2D correlation spectroscopy on MIR and NIR spectra relates the fundamental vibrations in the MIR region with the overtones and combination bands in the NIR region (Barton et al., 1992; Noda, 1993). This technique can be used to augment the interpretation of peaks which are well known in one dimension (e.g. MIR spectra), but elusive in the other dimension (e.g. NIR spectra).

## 2. Experimental

### 2.1. Preparation of breads

#### 2.1.1. Breads for staling experiment

The flour applied in this project was kindly donated by Danisco (Brabrand, Denmark). The flour was Reform Wheat Flour from Denmark of medium quality. The water content in the flour was ~14%, protein content ~10% and ~0.5% ashes. Small amounts of  $\alpha$ -amylase and ascorbic acid had been added to the flour in order to improve the dough quality, especially the dough strength. The flour was also added 1.5% salt and 1.5% sugar. A buffer (50 mM Sodium acetate, 2 mM  $\text{CaCl}_2$ , pH 5.9) was added instead of water to assimilate the effect of yeast.

The breads were prepared as follows. First all dry ingredients were mixed for 1 min at slow speed in a Diosna mixer. Then buffer was added and the dough was mixed 2 min at low speed and 4 min at high speed (temperature of the dough was 24–25 °C). Afterwards the dough was set to rest for 10 min at 30 °C. Next the dough was put to rest for 5 min at room temperature. Following this, the dough pieces were molded before they were put into tins to proof for 60 min at 33 °C at 85% relative humidity in a proofing cabinet. The loaves were baked for 30 min at 220 °C with 12 s initial steam in a Bago rotation oven with MIWE stone decks. The loaves were cooled for 3 h to make sure that the center temperature of the breads reached room temperature. The finished loaves were packed in vacuum bags and stored at ambient temperature. Right before the measurements, the bread was sliced into 10 mm slices using an industrial slicing machine and a 50 mm cylinder was used to stick out a sample from the center of each bread slice. Two breads were measured at each time point. NIR and MIR spectroscopic measurements on bread crumb were performed after 3 h, 9 h, 1, 2, 4, and 7 days. Two bread slices from each end and one center slice was measured. TPA was measured after 3 h, 1, 2, 4, and 7 days and ten bread slices were measured from each bread and the average result was used.

#### 2.1.2. Breads for deuterium experiment

Bread prepared from wheat flour, water, salt and yeast were purchased from a local bakery few hours before measurements. From one bread, 14 crumb pieces of  $2 \times 2$  cm were placed in a three-neck angled round bottom flask. The first MIR spectrum (which was referred to as 0 h) was taken from bread that had not been exposed

to  $\text{D}_2\text{O}$ . The bread crumb pieces were then exposed to air saturated with  $\text{D}_2\text{O}$  and MIR spectra was measured after 4, 24, 29, 47, 51 and 72 h. Two bread pieces were measured at each time point and the spectra were averaged.

### 2.2. Texture profile analysis

TPA was performed with a TA.XT2 Texture Analyser (Stable Micro Systems Ltd., Surrey, UK). The applied probe was a 50 mm aluminum cylinder probe (P/50, Stable Micro Systems Ltd., Surrey, UK). The TPA measurement was set to: pre-test speed 2 mm/s, test speed 2 mm/s, post-test speed 10 mm/s. Prior to the measurement, the probe was calibrated to the height of the bread sample and set to compress the sample 40% with a 5 kg load cell. The time interval between measurement of the first and second peak was set to 5 s. The force was measured in Newton (N). Hardness was calculated as the height of the first compression peak.

### 2.3. Spectroscopy measurements

#### 2.3.1. Mid-infrared spectroscopy

MIR spectra on bread were collected on a MB100 FT-IR spectrometer (Bomem, Quebec, Canada). Spectra were acquired in the ATR mode with a triple-bounce diamond crystal (Durascope, SensIR Technologies, Danbury, CT, USA). The pressure applied to squeeze the bread sample towards the diamond was 5 N/cm<sup>2</sup>. A total of 128 scans were averaged for each sample and the spectral resolution was 4 cm<sup>-1</sup>. A clean ATR crystal was used as a background. Wheat starch, wheat gluten, granular/native amylose from barley (Carcioli et al., 2012), granular/native amylopectin from maize and D-glucose were measured with the same settings of the MIR spectrometer as the bread. The deuterated bread was measured on an IFS 28 FT-IR spectrometer (Bruker Optik GmbH, Ettlingen, Germany) with a resolution of 4 cm<sup>-1</sup> and averaging of 64 scans. Spectra were acquired using an ATR module with a single-bounce diamond crystal (Durascope, SensIR Technologies, Danbury, CT, USA).

#### 2.3.2. Near-infrared spectroscopy

A 6500 NIR spectrometer (NIR systems, Inc., Silver Springs, MD, USA) was used to measure the bread in reflectance mode. The instrument contained a monochromator and a split detector system where a Si detector was used between 400 and 1100 nm and a PbS detector was used between 1100 and 2498 nm. The measurement interval was every 2 nm. Angle of incident light was 180° and reflectance was measured at a 45° angle. A rotating sample cup with a quartz window was used. A white ceramic plate was used as a reference. The spectrum was an average of 32 scans. Wheat starch, wheat gluten, granular/native amylose from barley (Carcioli et al., 2012), granular/native amylopectin from maize and D-glucose were measured on a NIRS™ DS2500 F (Foss, Hillerød, Denmark) equipped with a monochromator and Si and PbS detectors. The spectrum from DS2500 was an average of 256 scans measured from 400 to 2500 nm with an interval of 0.5 nm.

### 2.4. Data treatment

The spectra were analyzed in Matlab (version R2013b) (The Mathworks, Inc., Natick, MA, USA) and PLS toolbox 7.5 (Eigenvector Research, Inc., Manson, WA, USA). Principal component analysis (PCA) was used to visualize how samples were varying with respect to each other (Bro and Smilde, 2014).

#### 2.4.1. Mid-infrared data treatment

The MIR spectra were calculated as  $\log_{10}(I_0/I_s)$  where  $I_0$  is the

light intensity with no sample on the ATR and  $I_s$  is the light intensity with a sample on the ATR. The data analysis was focused only on the MIR region from 850 to 1100  $\text{cm}^{-1}$  because of the residing intense pyranosidic (ether) vibrations (van Soest et al., 1995; Wilson et al., 1991). The effect of preprocessing with SNV (standard normal variate), MSC (multiplicative scatter correction), EMSC (extended multiplicative scatter correction) (Martens et al., 2003) and Savitzky–Golay 2nd derivative spectra (2nd degree polynomial, window size 7) was investigated (Rinnan et al., 2009).

#### 2.4.2. Near-infrared data treatment

The NIR spectra were calculated as  $\log_{10}(1/\text{reflectance})$  where reflectance =  $I_R/I_{R0}$  and  $I_R$  and  $I_{R0}$  are the reflected light from the sample and the reference, respectively. The focus in the NIR region was chosen as the short wavelength (SW) region from 900 to 1050 nm, the first overtone (1OT) region from 1350 to 1800 nm and the long wavelength (LW) region from 2150 to 2370 nm. These three NIR regions were chosen because of their information on OH and CH vibrations. The effect of preprocessing with SNV, MSC, EMSC (Martens et al., 2003) and Savitzky–Golay 2nd derivative spectra (2nd degree polynomial, window size 11) was investigated (Rinnan et al., 2009). The different preprocessing methods resulted in dissimilar peak movements when applied to the full spectrum. On the other hand, similar peak movements were achieved when the preprocessing methods were used on smaller spectral regions. It was therefore considered a more robust approach to proceed with the preprocessing of smaller regions because of the higher agreement between the different preprocessing methods. The SW region was therefore preprocessed from 850 to 1086 nm, the 1OT region from 1270 to 1840 nm and the LW region from 2100 to 2400 nm.

#### 2.4.3. Two-dimensional correlation spectroscopy

The idea of 2D correlation spectroscopy was proposed by Noda in 1986 and further developed into generalized 2D correlation spectroscopy (Noda, 1993). Barton and co-workers developed a similar technique (Barton et al., 1992). The technique can be used to augment the interpretation of peaks which are well known in one dimension, but elusive in the other dimension. It can also be used to separate overlapping peaks by mapping samples that are influenced by external perturbation (e.g. the samples vary in temperature or in the chemical reaction time). The spectra can then be visualized in plots showing how the wavelength variables co-vary (in the synchronous plot) and change during the external perturbation (in the asynchronous plot).

In this study, the 2D correlation spectroscopy plots were calculated as the covariance (also called the synchronous plot) between NIR and MIR spectra. The covariance was calculated by the Matlab code  $(\mathbf{X}_{\text{NIR}} * \mathbf{X}_{\text{MIR}}) / (n-1)$  where  $n$  is the number of samples,  $\mathbf{X}_{\text{MIR}}$  and  $\mathbf{X}_{\text{NIR}}$  are the data matrixes with samples as rows and wavenumbers as columns for MIR and NIR, respectively (Czarnecki, 2011).  $\mathbf{X}_{\text{NIR}}'$  is the transpose of  $\mathbf{X}_{\text{NIR}}$ .

The MIR spectra used for the 2D correlation spectroscopy were preprocessed with EMSC from 850 to 1100  $\text{cm}^{-1}$ . The NIR spectra used for the 2D correlation spectroscopy were preprocessed with EMSC from 850 to 1086 nm, 1270–1840 nm and 2100–2400 nm (see Section 2.4.2 for an explanation of the small preprocessing regions). The 2D correlation spectroscopy plots were very similar when the MIR and NIR spectra were preprocessed with EMSC or with 2nd derivative spectra followed by EMSC (2DEV + EMSC). It was therefore decided to preprocess with only EMSC because the 2D correlation spectroscopy plots using EMSC were simpler. Preprocessed spectra were mean centered before modeling.

### 3. Results and discussion

#### 3.1. Assignment of the mid-infrared data

From the raw MIR spectra in Fig. 1A, the small pyranosidic ether region from 850 to 1100  $\text{cm}^{-1}$  was selected (in Fig. 1B) because of its established correlation to bread staling and amorphous/crystalline structure of carbohydrates (van Soest et al., 1995; Wilson et al., 1991). The region involves highly coupled vibrational modes that cannot be assigned to specific functional groups. Table 1 shows an overview of the suggested assignments of this region. The absorbance from amylopectin, amylose, starch, gluten and D-glucose was also measured in order to see which of these components could be responsible for the different absorbance peaks (Supplementary Information Fig. S5). Fig. S5 shows that amylopectin and starch absorb in the same spectral areas which makes sense because starch contains around 75% of amylopectin. It could also be observed that amylopectin, amylose and starch were the only species that absorb at 862  $\text{cm}^{-1}$  which fits with the peak assignment to the alpha-anomeric carbon (C1) in the glycosidic bond. It was surprising that amylose seemed to absorb at slightly higher wavenumbers than starch and amylopectin at 1022 and 1047  $\text{cm}^{-1}$ . Amylose and amylopectin are both polymers of  $\alpha$ -D-glucose units with mainly  $\alpha(1 \rightarrow 4)$  glycosidic bonds but amylopectin also contains ~5%  $\alpha(1 \rightarrow 6)$  bonds (Pérez and Bertoft, 2010). The difference between amylose and amylopectin at about 1047 and 1022  $\text{cm}^{-1}$  can be that the hydroxyl groups (COH) are involved in different levels of intra- and inter-molecular hydrogen-bonding in amylose and amylopectin because of their single helical and double helical nature, respectively (Damager et al., 2010). Another interesting observation is that amylose seemed to have a smaller absorbance at 1047  $\text{cm}^{-1}$  in comparison to (crystalline) amylopectin which supports the assignment to amylopectin retrogradation. From the raw spectra in Fig. S5 it was observed that gluten had a relatively low absorbance in this region compared to amylose, amylopectin and starch. Furthermore, the protein content was around 8% in the bread and the effect from gluten is therefore not significant in the region from 850 to 1100  $\text{cm}^{-1}$ . Deuteration of fresh bread during approx. 3 days of storage showed that all the peaks at 1000, 1022, 1047 and 1078  $\text{cm}^{-1}$  changed with deuteration (Fig. 2). This was expected since  $\text{D}_2\text{O}$  will exchange the hydrogen atoms of water and hydroxyl groups (COH), but not with the skeletal vibrations of CCH or OCH. The deuteration experiment therefore supports the strong involvement of hydroxyl groups (COH) to the peaks at 1000, 1022, 1047 and 1078  $\text{cm}^{-1}$ . In contrast, the peaks at 861 and 1011  $\text{cm}^{-1}$  did not show an intensity decrease in absorbance during the deuteration which supports their assignments to COC, CCH, CC, OCH and CCO groups.

The most efficient preprocessing method for separating storage time or bread crumb hardness in a PCA on MIR spectra was found to be 2DEV + EMSC. Fig. 3A shows how the first principal component (PC1) displays an exponential decay with storage time and a linear decay with hardness (Fig. 3C). In the remainder of this study the bread crumb hardness is used because of its linear relationship with the MIR spectra. Since the PCA input was 2nd derivative spectra then the interpretation of the loading plots in Fig. 3B and D must be inverted when compared to the raw spectra. From the loading plot it can therefore be observed that raw spectra of the new bread have higher values at 1084, 1065, 1024 and 995  $\text{cm}^{-1}$  whereas the old “stale” bread have higher absorbance values at 1074, 1049, 1007 and 862  $\text{cm}^{-1}$ . The peaks at 1084 and 1074  $\text{cm}^{-1}$  identified by the loading plot, have not received much attention in previous studies on bread or starch. However, one study found that the absorbance in this region did not show significant changes with varying degree of crystallinity in starch-water solutions (van Soest

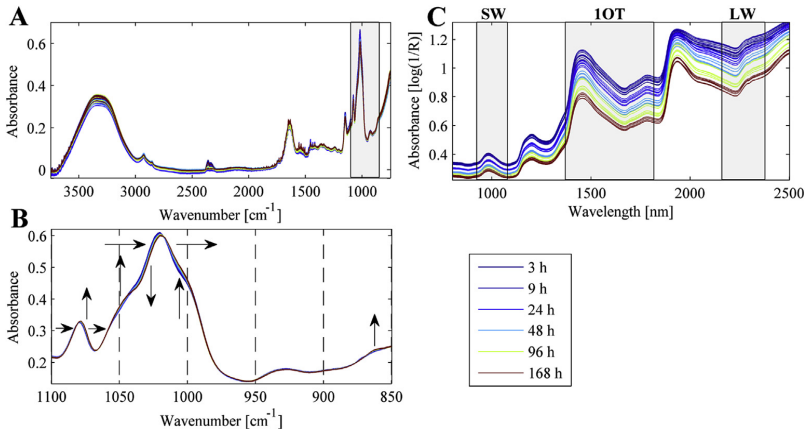


**Fig. 1.** (A) Raw MIR spectra of aging bread crumb highlighting the area shown in Fig. 1B. (B) Spectra of selected MIR region preprocessed with EMSC. (C) Raw NIR spectra of aging bread crumb highlighting the SW (900–1050 nm), the IOT (1350–1800 nm) and the LW (2150–2370 nm) NIR region. The arrows indicate the spectral movement from 3 to 168 h.

**Table 1**  
MIR peak assignments.

Wavenumbers [cm <sup>-1</sup> ]	Functional groups	Sensitive to deuteration (Fig. 2)	Reference
861	C(1)-O(5)-C(5) str., CCH	No	(Cael et al., 1975)
1000	CO, CC, CCO, CCH, COH	Yes	(Cael et al., 1975) (Vasko et al., 1972)
1011	CC, OCH, CCH, CCO	No	(Vasko et al., 1972)
1025–1026	COH def.	Yes	(Cael et al., 1975) (Vasko et al., 1972)
1045–1047	CO, CC, CCO, COH	Yes	(Cael et al., 1975) (Vasko et al., 1972)
1076–1079	CO, CC, COH	Yes	(Cael et al., 1975) (Vasko et al., 1972)

1049 cm<sup>-1</sup> and oppositely more amorphous starch and fresh bread with a high absorbance at 1024 cm<sup>-1</sup>, which fits perfectly with previous studies (van Soest et al., 1995; Wilson et al., 1991). The absorption band at around 1007 cm<sup>-1</sup> has also been observed to increase in previous studies on aging amylose and amylopectin gels (Goodfellow and Wilson, 1990) as well as on aging wheat-starch gels under drying conditions (Wilson and Belton, 1988). This matches with the assignment to CC, OCH, CCH and CCO since the migration of water from crumb to crust will result in a percentage increase of carbohydrates. However in another study, starch in 0–25% water exhibited an increase in absorbance at around 1000 cm<sup>-1</sup> with both higher water content and higher amounts of crystallinity (Capron et al., 2007). It is therefore a possibility that the band at about 1007 cm<sup>-1</sup> can be influenced by both crystallinity and water migration. The peak at 862 cm<sup>-1</sup> found in the loading plot has also previously been observed to change with crystallinity (van Soest et al., 1995).

et al., 1995). The loading plot also reveal an association between more crystalline starch and stale bread with a high absorbance at

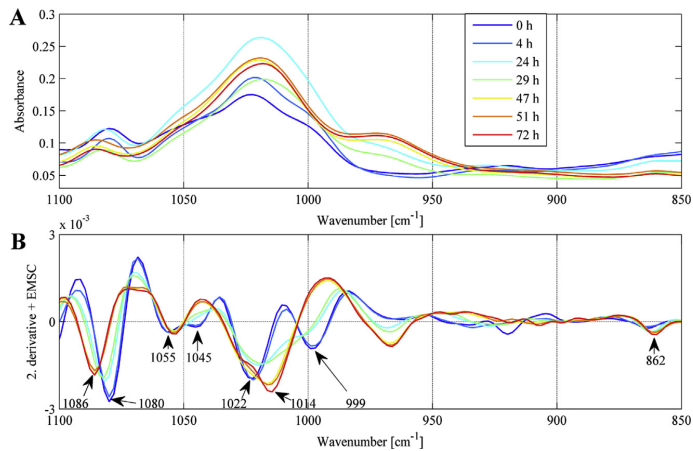


**Fig. 2.** MIR spectra of wheat bread crumb stored in an atmosphere saturated with D<sub>2</sub>O for 0–72 h. (A) Raw MIR spectra. (B) MIR spectra preprocessed with 2DEV + EMSC. Black arrows indicate the peak minimum.

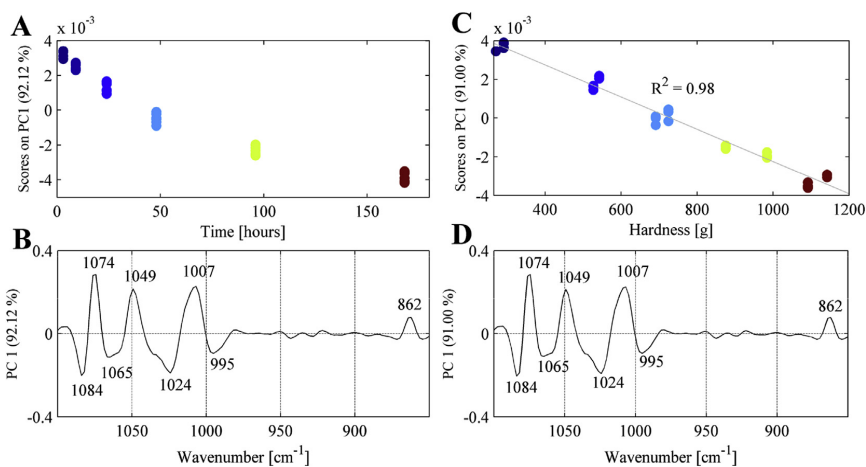


**Fig. 3.** Principal component 1 (PC1) from a principal component analysis (PCA) on MIR spectra of aging bread crumb preprocessed with 2DEV + EMSC. (A) PC 1 scores versus time and (B) the corresponding loading plot to Fig. 3A. (C) PC 1 scores versus bread crumb hardness and (D) the corresponding loading plot to Fig. 3C. Points are colored according to hours after baking. (For interpretation of the references to colour in this figure legend, the reader is referred to the web version of this article.)

In summary, this study supports the assignments of the peaks at 1047 and 1022  $\text{cm}^{-1}$  to stale and fresh bread, respectively. The peaks at about 1000 and 1078  $\text{cm}^{-1}$  both increased with storage time and the absorbance at 1000  $\text{cm}^{-1}$  might be related with water content and staling and the peak at 1078  $\text{cm}^{-1}$  could be related to the water content. The peak at 862  $\text{cm}^{-1}$  increased with storage time and was associated with stale bread.

### 3.2. Two-dimensional correlation spectroscopy on near- and mid-infrared spectra

The raw NIR spectra are shown in Fig. 1C and display a decreasing absorbance from 3 to 168 h at all wavelengths. Three regions (indicated with gray areas) were selected from the NIR spectra in order to investigate how the SW, 1OT and LW region correlate to bread staling and the MIR spectra. NIR and MIR spectra were used in 2D correlation spectroscopy and Fig. 4 shows the resulting covariance/synchronous plot. The absorbance bands which are moving in the same direction have a positive covariance (shown with red color) and absorbance bands moving in opposite directions have a negative covariance (shown with a blue color). It was also investigated if Pearson's correlation coefficient could be used instead of the covariance in the 2D plots, but this resulted in less well defined peaks. Pearson's correlation coefficient sometimes results in square-looking correlation peaks as for instance the correlation peak at 1502 nm in the Supplementary Information Fig. S3C. Pearson's correlation coefficient can also amplify the baseline as for example the area at 1600 nm in the Supplementary Information Fig. S3D and it was therefore decided to use the covariance in the 2D correlation plots. Since the covariance itself does not tell us how much the NIR and MIR spectra correlate, then the Pearson's correlation coefficient ( $R^2$ ) was calculated between selected wavelengths and the bread hardness. The NIR and MIR preprocessing method which resulted in the highest  $R^2$  values was 2DEV + EMSC and this preprocessing method was therefore used in the calculations of  $R^2$  (Supplementary Information Figs. S1–4).

The highest  $R^2$  to bread hardness are shown in Fig. 4 and it can

be observed that the peak at 1047  $\text{cm}^{-1}$  increase together with the NIR wavelengths at 910, 1688 and 2288 nm. The SW-NIR band at 910 nm is the 3rd overtone of CH stretching presumably of protein (gluten). The 1OT-NIR absorbance at 1688 nm is the aromatic CH vibrations probably from gluten (Osborne et al., 1993; Williams, 2001). This is supported by the absorbance spectrum of gluten (Supplementary Information Figs. S6–8) which shows that the absorbance at 910 and 1688 nm are superimposed by the CH vibrations in gluten. The LW-NIR band at 2288 nm is closest to the absorbance peak from amylose, but also starch, amylopectin and gluten could contribute. The interpretation of the combination band region is complex and the absorbance at 2288 nm could potentially be the combination band of the CH antisymmetric stretching + CH deformation (Ringsted et al., 2016). The assignment of the 910, 1688 and 2288 nm bands was confirmed by a deuteration experiment on aging bread which showed almost no spectral change or an increasing band intensity at the three wavelengths (Supplementary Information Figs. S9–11). These findings support that OH or NH is not absorbing at these wavelengths.

Fig. 4 also shows that the important MIR peak at 1022  $\text{cm}^{-1}$  decrease together with the NIR wavelengths at 974, 1412 and 2258 nm. The absorbance at the SW-NIR band at 974 nm is the 2nd overtone of OH stretching due to water, but it may be influenced by OH stretching in starch, amylopectin and amylose (Supplementary Information Fig. S6). The 1OT band at 1412 nm is primarily related to the 1OT OH stretching from secondary hydroxyl groups which primarily have absorbance from water, starch, amylopectin and amylose (Supplementary Information Fig. S7). It is therefore hypothesized that this decrease in absorbance (or rather shift towards longer wavelengths) is caused mainly by a decrease in the average number (and/or strength) of polymer hydrogen bonding to water due to the lowering of moisture. The LW band at 2258 nm could be caused by absorption from gluten, starch, amylopectin and amylose (Supplementary Information Fig. S8) and it has been assigned to OH stretching + OH deformation (Osborne et al., 1993). It is also likely that water is contributing to the changes at 2258 nm since water starts to absorb from about 2230 nm and continues into the MIR spectrum (Law and Tkachuk, 1977).

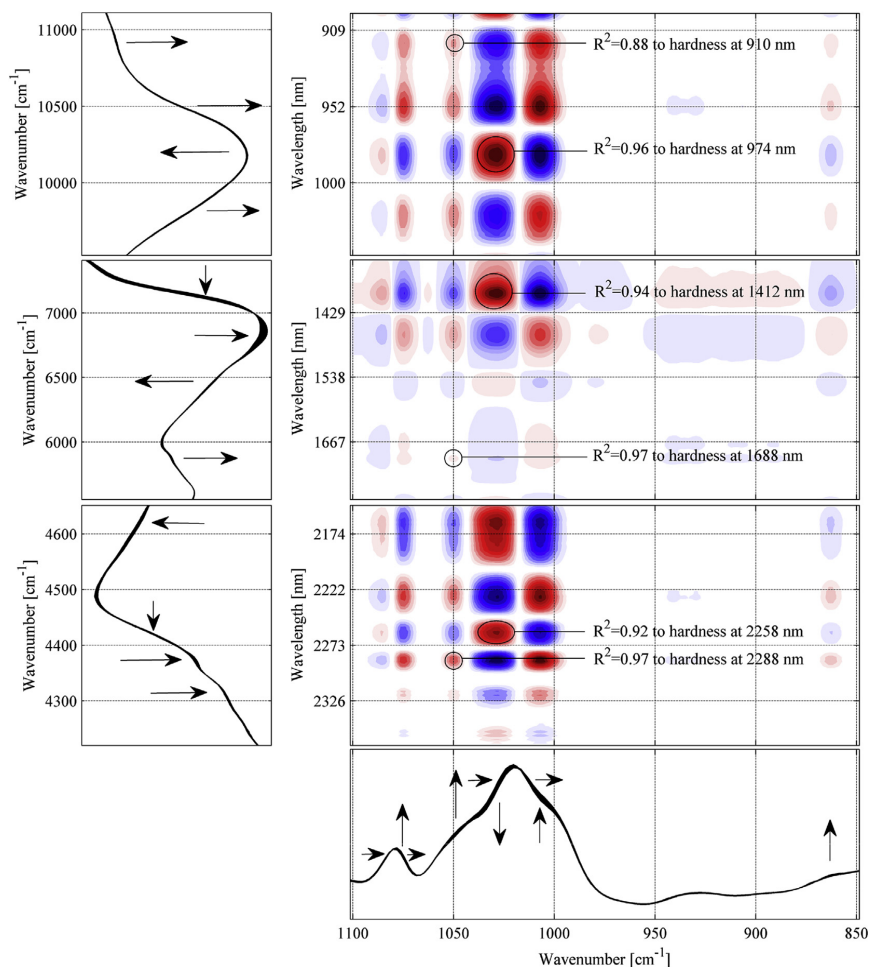


**Fig. 4.** MIR and NIR spectra of aging wheat bread crumb used in 2D correlation spectroscopy. The horizontal axis is the MIR region from 850 to 1100  $\text{cm}^{-1}$  and the vertical axis is the NIR regions from 900 to 1050 nm, 1350–1800 nm and 2150–2370 nm. The spectra were all preprocessed with EMSC. The colors represent the level of covariance where red is positive and blue is negative. The Pearson's correlation coefficient ( $R^2$ ) was calculated between the spectra preprocessed with 2DEV + EMSC (shown in [Supplementary information Fig. S2D, S3D and S4D](#)) and bread crumb hardness. Arrows indicate spectral movement from 3 to 168 h. (For interpretation of the references to colour in this figure legend, the reader is referred to the web version of this article.)

### 3.3. Assignment of the long wavelength near-infrared (2150–2370 nm) data

From Section 3.2 it was found that the highest  $R^2$  value between hardness and a NIR wavelength was in the LW region at 2288 nm. The correlations to the 10T region from 1670 to 1800 nm were only marginally lower, but the covariation around the LW band at 2288 nm is stronger than around the 10T band at 1688 nm (Fig. 4). It was then decided to examine the LW region from 2150 to 2370 nm in more details. A PCA built on the NIR region from 2150 to 2370 nm is shown in Fig. 5A. The score of PC1 show a linear decrease to bread crumb hardness as was also the case for the PCA on the MIR spectra shown previously in Fig. 3C.

Finally, the PC1 scores of the MIR and NIR spectra in Figs. 3C and 5A was correlated in order to see how much they were associated

during the staling process. The result is shown in Fig. 5B and has a Pearson's correlation coefficient of 0.98 which indicate that both LW NIR and MIR spectroscopy basically measure the same staling process and that they both can be used to describe changes in aging bread crumb.

## 4. Conclusions

Bread staling is a major source of food waste and we are in demand for more efficient methods to monitor staling. This work represents the first application of 2D MIR-NIR correlation spectroscopy to the bread staling process. The aim of the work was primarily to investigate if NIR spectroscopy can be as informative about the staling process as the MIR and to determine which region of the NIR is the most appropriate for monitoring staling. The work

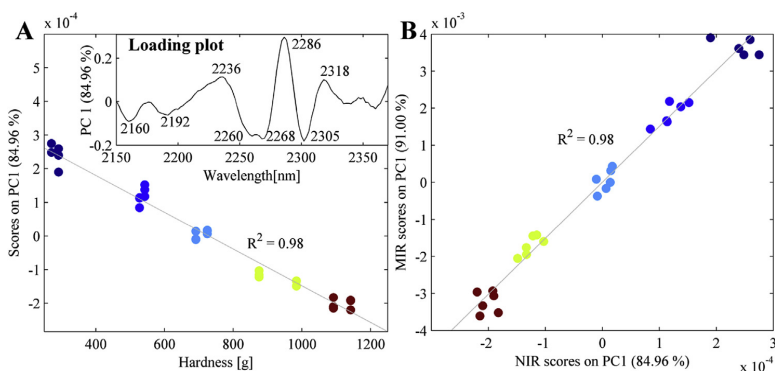


**Fig. 5.** (A) Scatter plot of Principal component 1 (PC1) from a principal component analysis (PCA) on NIR spectra of aging wheat bread crumb preprocessed with 2DEV + EMSC and bread crumb hardness. (B) Scatter plot of NIR PC1 scores vs MIR PC1 scores. Points are colored according to hours after baking. (For interpretation of the references to colour in this figure legend, the reader is referred to the web version of this article.)

starts by confirming the well-established correlation between the MIR absorbance at  $1047\text{ cm}^{-1}$  and bread crumb hardness which is interpreted as the retrogradation of amylopectin in aging bread.

The 2D correlation spectroscopy shows that the MIR band at  $1047\text{ cm}^{-1}$  moves together with three characteristic NIR bands identified at  $910\text{ nm}$  (SW-NIR),  $1688\text{ nm}$  (1OT-NIR) and  $2288\text{ nm}$  (LW-NIR). Of these bands the strongest covariation to the  $1047\text{ cm}^{-1}$  band and highest correlation to the bread hardness was found at the LW-NIR band at  $2288\text{ nm}$ . Both the 1OT and the LW-NIR regions exhibit  $R^2$  values of 0.97 to bread crumb hardness. The 1OT and LW region was therefore superior compared to the SW region in monitoring the CH changes during bread retrogradation. In contrast, the other important MIR band at  $1022\text{ cm}^{-1}$  displayed a high negative correlation to bread crumb hardness and was interpreted as COH def. possibly affected by different levels of hydrogen-bonding. The 2D correlation spectroscopy shows that the MIR absorbance at  $1022\text{ cm}^{-1}$  co-varied with NIR absorbance bands from OH at  $974\text{ nm}$  in the SW-NIR region, at  $1412\text{ nm}$  in the 1OT-NIR region and at  $2258\text{ nm}$  in the LW-NIR region. In this case, the SW-NIR region ( $900\text{--}1050\text{ nm}$ ) was found to be marginally better than the 1OT and LW regions at describing the OH changes in starch and water. In conclusion, this paper clearly demonstrates that the NIR region equals the information content found in the MIR region when it comes to staling of wheat bread. This is most clearly and convincingly shown by examining the high  $R^2$  value of 0.98 between the first principal components from the staling sensitive regions in the MIR and NIR in Fig. 5B.

## Acknowledgements

The authors wish to acknowledge the generous financial support from The Danish National Advanced Technology Foundation (now Innovation Fund Denmark) to the project entitled "Light & Food". Thanks also go to DuPont (5184-00012B) for supporting the research with breads and reference analysis and to Andreas Blennow for providing the granular amylose and amylopectin samples.

## Appendix A. Supplementary data

Supplementary data related to this article can be found at <http://dx.doi.org/10.1016/j.jcs.2017.03.006>.

## References

- Abu-Ghoush, M., Herald, T.J., Dowell, F., Xie, F., Aramouni, F.M., Madl, R., 2008. Effect of preservatives addition on the shelf-life extensions and quality of flat bread as determined by near-infrared spectroscopy and texture analysis. *Int. J. Food Sci. Technol.* 43, 357–364.
- Amigo, J.M., Alvarez, A.D., Engelsen, M.M., Lundkvist, H., Engelsen, S.B., 2016. Staling of white wheat bread crumb and effect of maltogenic alpha-amylases. Part 1: spatial distribution and kinetic modeling of hardness and resilience. *Food Chem.* 208, 318–325.
- Barton II, F.E., Himmelsbach, D.S., Duckworth, J.H., Smith, M.J., 1992. Two-Dimensional vibration spectroscopy: correlation of mid- and near-infrared regions. *Appl. Spectrosc.* 46, 420–429.
- Bourne, M.C., 1978. Texture profile analysis. *Food Technol.* 32, 62–66.
- Bro, R., Smilde, A.K., 2014. Principal component analysis. *Anal. Methods* 6, 2812–2831.
- Cael, J.J., Koenig, J.L., Blackwell, J., 1975. Infrared and raman spectroscopy of carbohydrates. Part VI: normal coordinate analysis of V-amylose. *Biopolymers* 14, 1885–1903.
- Capron, I., Robert, P., Colonna, P., Brogly, M., Planchot, V., 2007. Starch in rubbery and glassy states by FTIR spectroscopy. *Carbohydr. Polym.* 68, 249–259.
- Carciofi, M., Blennow, A., Jensen, S.L., Shaik, S.S., Henriksen, A., Buléon, A., Holm, P.B., Hebelstrup, K.H., 2012. Concerted suppression of all starch branching enzyme genes in barley produces amylose-only starch granules. *Bmc Plant Biol.* 12, 223.
- Cevoli, C., Gianotti, A., Troncoso, R., Fabbri, A., 2015. Quality evaluation by physical tests of a traditional Italian flat bread Piadina during storage and shelf-life improvement with sourdough and enzymes. *Eur. Food Res. Technol.* 240, 1081–1089.
- Czarnecki, M.A., 2011. Two-dimensional correlation analysis of hydrogen-bonded systems: basic molecules. *Appl. Spectrosc. Rev.* 46, 67–103.
- Damager, I., Engelsen, S.B., Blennow, A., Møller, B.L., Motawia, M.S., 2010. First principles insight into the alpha-glucan structures of starch: their synthesis, conformation, and hydration. *Chem. Rev.* 110, 2049–2080.
- Engelsen, S.B., 2016. Near infrared spectroscopy - a unique window of opportunities. *NIR news* 27, 14–17.
- Fadda, C., Sanguinetti, A.M., Del Caro, A., Collar, C., Piga, A., 2014. Bread staling: updating the view. *Compr. Rev. Food Sci. Food Saf.* 13, 473–492.
- Goodfellow, B.J., Wilson, R.H., 1990. A Fourier transform IR study of the gelation of amylose and amylopectin. *Biopolymers* 30, 1183–1189.
- Gray, J.A., Bemiller, J.N., 2003. Bread staling: molecular basis and control. *Compr. Rev. Food Sci. Food Saf.* 2, 1–21.
- Law, D.P., Tkachuk, R., 1977. Near-infrared diffuse reflectance spectra of wheat and wheat components. *Cereal Chem.* 54, 256–265.
- Martens, H., Nielsen, J.P., Engelsen, S.B., 2003. Light scattering and light absorbance separated by extended multiplicative signal correction. Application to near-infrared transmission analysis of powder mixtures. *Anal. Chem.* 75, 394–404.
- Noda, I., 1993. Generalized two-dimensional correlation method applicable to infrared, raman, and other types of spectroscopy. *Appl. Spectrosc.* 47, 1329–1336.
- Osborne, B.G., Fearn, T., Hindle, P.H., 1993. *Practical NIR Spectroscopy, with Applications in Food and Beverage Analysis*, second ed. Longman Scientific and Technical, Harlow, UK.
- Pérez, S., Bertoft, E., 2010. The molecular structures of starch components and their contribution to the architecture of starch granules: a comprehensive review. *Starch - Stärke* 62, 389–420.
- Rinnan, A., van den Berg, F., Engelsen, S.B., 2009. Review of the most common pre-

- processing techniques for near-infrared spectra. *Trac-Trends Anal. Chem.* 28, 1201–1222.
- Ringsted, T., Dupont, S., Ramsay, J., Jespersen, B.M., Sørensen, K.M., Keiding, S.R., Engelsen, S.B., 2016. Near-infrared spectroscopy using a supercontinuum laser: application to long wavelength transmission spectra of barley endosperm and oil. *Appl. Spectrosc.* 70, 1176–1185.
- Sevenou, O., Hill, S.E., Farhat, I.A., Mitchell, J.R., 2002. Organisation of the external region of the starch granule as determined by infrared spectroscopy. *Int. J. Biol. Macromol.* 31, 79–85.
- van Soest, J.J.G., Tournois, H., de Wit, D., Vliegenthart, J.F.G., 1995. Short-range structure in (partially) crystalline potato starch determined with attenuated total reflectance Fourier-transform IR spectroscopy. *Carbohydr. Res.* 279, 201–214.
- Vasko, P.D., Blackwell, J., Koenig, J.L., 1972. Infrared and raman spectroscopy of carbohydrates. Part II: normal coordinate analysis of alpha-D-glucose. *Carbohydr. Res.* 23, 407–416.
- Williams, P., 2001. Implementation of near-infrared technology. In: Williams, P., Norris, K. (Eds.), *Near-infrared Technology, in the Agricultural and Food Industries*, second ed. American Association of Cereal Chemists, St. Paul, MN, USA, p. 168.
- Wilson, R.H., Belton, P.S., 1988. A Fourier-transform infrared study of wheat starch gels. *Carbohydr. Res.* 180, 339–344.
- Wilson, R.H., Kalichevsky, M.T., Ring, S.G., Belton, P.S., 1987. A Fourier-transform infrared study of the gelation and retrogradation of waxy-maize starch. *Carbohydr. Res.* 166, 162–165.
- Wilson, R.H., Goodfellow, B.J., Belton, P.S., Osborne, B.G., Oliver, G., Russell, P.L., 1991. Comparison of Fourier transform mid infrared spectroscopy and near infrared reflectance spectroscopy with differential scanning calorimetry for the study of the staling of bread. *J. Sci. Food Agric.* 54, 471–483.
- Xie, F., Dowell, F.E., Sun, X.Z.S., 2004. Using visible and near-infrared reflectance spectroscopy and differential scanning calorimetry to study starch, protein, and temperature effects on bread staling. *Cereal Chem.* 81, 249–254.

---

# Paper III

---

## **Long Wavelength Near-Infrared Transmission Spectroscopy of Barley Seeds Using a Supercontinuum Laser: Prediction of Beta-Glucan Content**

Tine Ringsted, Jacob Ramsay, Birthe M. Jespersen, Søren R. Keiding,  
Søren B. Engelsen

*Manuscript submitted to Analytica Chimica Acta*



# Long Wavelength Near-Infrared Transmission Spectroscopy of Barley Seeds Using a Supercontinuum Laser: Prediction of Beta-Glucan Content

Tine Ringsted\*<sup>a</sup>, Jacob Ramsay<sup>b</sup>, Birthe M. Jespersen<sup>a</sup>, Søren R. Keiding<sup>b</sup>, Søren B. Engelsen\*<sup>a</sup>

<sup>a</sup>Chemometrics and Analytical Technology, Department of Food Science, University of Copenhagen, Frederiksberg, Denmark.

<sup>b</sup>Department of Chemistry, Aarhus University, Aarhus, Denmark.

---

**ABSTRACT:** A supercontinuum laser was used to perform the first transmission measurements on intact seeds with long wavelength near-infrared spectroscopy. A total of 105 barley seeds from five different barley genotypes (*Bomi*, *lys5.f*, *lys5.g*, *lys16* and *lys95*) were measured from 2275-2375 nm. The  $\beta$ -glucan and protein content was measured with wet chemical analysis for each single seed. A partial least squares model correlated the  $\beta$ -glucan % (w/w) with the spectral measurements with a  $R^2_{\text{cross-validation}}$  and  $R^2_{\text{prediction}}$  of 0.83 and 0.90, respectively. The predictive model for  $\beta$ -glucan could be improved by averaging spectra from the same seed and by replacing the individual seed  $\beta$ -glucan content with the average  $\beta$ -glucan of each barley genotype.

---

Near-infrared (NIR) spectroscopy has been used since the 1970s as a fast and quantitative analysis in various production areas such as the food, pharma and chemical industry. The first generation of instruments used the quartz-tungsten-halogen lamp which is still the main light source applied today.<sup>1</sup> More recently, a supercontinuum source was developed which has a laser-like collimated beam and a broad spectral coverage.<sup>2</sup> Supercontinuum sources radiate in the NIR region and are being developed to go further into the UV and mid-infrared region.<sup>3,4</sup> The traditional lamp which is being used in NIR spectroscopy has been developed over many years and it is a robust and relatively low cost light source. The supercontinuum source cannot compete on price with a traditional filament lamp. Instead the supercontinuum source will have an advantage in situations where a spatially coherent beam (high brightness) is needed. A coherent beam can be an advantage when the source needs to pass a long distance (e.g. remote sensing and gas measurements) or when measuring very small areas (e.g. microscopy).<sup>3,5</sup> A possible industrial application is the non-invasive analysis of individual seeds for plant breeding or seed-sorting. The possibility to non-destructively sort single seeds gives the possibility to remove for example fusarium damaged kernels or insect infected seeds which would not be detected in bulk analysis because bulk analysis measures the average of many seeds and thus desensitize the detection limit. Single seed measurements can also be used to sort more precisely according to e.g. baking, health or feed quality parameters which are not possible in bulk analysis because it does not take into account the seed to seed variation.

One potential application for single seed analysis is sorting of barley seeds by their  $\beta$ -glucan content.  $\beta$ -glucans are generally linear glucose polymers in the plant cell wall and are also called mixed linkage  $\beta$ -glucans to be distinguished from cellulose which contain only  $\beta$ -(1-4) linkages as mixed linkage  $\beta$ -

glucan contain occasional  $\beta$ -(1-3) linkages. Barley breeders have generally selected against mixed linkage  $\beta$ -glucan because they can precipitate from the beer and because they can increase viscosity of the beer and in turn slow down filtration rates and result in unwanted haze formation in the final beer.<sup>6</sup> On the other hand,  $\beta$ -glucan in barley and particular oat are known to have beneficial health effects including lowering of the serum cholesterol level, increased satiety, and stabilization of the blood glucose and insulin rises after food consumption.<sup>6</sup> As a result, food products with high  $\beta$ -glucan content can have a positive influence against heart diseases and type-2 diabetes.

The analysis of single seeds compared to the traditional bulk seed analysis requires adjustments of the NIR spectrometer but also the wet chemical analysis.<sup>7</sup> This is the reason why the majority of studies with NIR spectroscopy predicting  $\beta$ -glucan in barley have been conducted on bulk samples.<sup>8-13</sup> In fact, only one study used NIR spectroscopy to measure  $\beta$ -glucan on single barley seeds in reflectance mode, and the main conclusion was that further development was needed.<sup>14</sup> The reason for this could be the low content of  $\beta$ -glucan (0-1.2 mg/seed) in the barley seeds. Other studies on barley flour or barley slices have found that long-wavelength (LW) NIR spectroscopy from 2200-2500 nm has the potential to differentiate barley seeds with different  $\beta$ -glucan content.<sup>9,13,15-16</sup> NIR transmission spectroscopy of seeds is routinely performed at wavelengths below 1100 nm because of the low extinction coefficients at shorter wavelengths. However, the LW-NIR region has not yet been investigated in the transmission mode on whole seeds despite the fact that  $\beta$ -glucan in barley is located in the endosperm cell walls.<sup>17</sup> The primary reason is the higher extinction coefficients in the LW-NIR region together with the lower intensity of the light sources in this region. However, with the high brightness of the new supercontinuum sources new possibilities for transmission measurements at longer wavelengths have emerged.

The aim of this study was to measure on whole single barley seeds with a NIR spectrometer equipped with a supercontinuum laser from 2275–2375 nm in transmission mode. The protein and  $\beta$ -glucan content was measured on the exact same barley seeds in order to relate the spectral results to classical reference analysis. The target was thus to examine if the LW NIR measurements could be used to predict the  $\beta$ -glucan and protein content. Secondly the effect of re-sampling was studied in order to obtain lower prediction errors.

## MATERIALS AND METHODS

**Barley samples.** In order to create a large  $\beta$ -glucan variation five barley genotypes were included in this study. Four structural carbohydrate mutants with depleted starch and high  $\beta$ -glucan content were included (*lys5.f*, *lys5.g*, *lys16*, and *lys95*) and a reference genotype (*Bomi*) which has normal levels of lipids, starch,  $\beta$ -glucan, etc.<sup>18–19</sup> *Bomi* is the mother line for *lys5.f* and *lys16*. The mutant *lys95* is from the barley variety Perga. The barley samples were grown in field trials in collaboration with Lantmännen SW Seeds (Sweden) in 2004 and have been stored in a refrigerator. From each barley genotype, 21 seeds were randomly selected, giving a total of 105 seeds. Bulk flour samples were generated from each of the five barley genotypes by milling each genotype on a hammermill (sieve 0.5 mm). A purified  $\beta$ -glucan sample (B1) was produced by extraction of the  $\beta$ -glucan from the *Bomi* genotype using hot water, enzyme assisted hydrolysis and ethanol precipitation.<sup>20</sup>

**Spectroscopic instruments.** The supercontinuum light source (NKT Photonics) used in this study was based on a 1550 nm laser launched into a red-shift fiber, subsequently pumping a thulium doped fiber at a repetition rate of 35 kHz (Figure 1A). In another study on barley slices, a step-index ZBLAN fiber was also used to further widen the spectrum.<sup>16</sup> However, in order to concentrate as much power as possible in the wavelength region from 2260–2380 nm the ZBLAN fiber was removed and replaced with different lengths of a red-shifting single-mode optical fiber (SMF). As a result the supercontinuum spectrum covers approximately 150 nm in full width at half maximum (FWHM), and can be tuned in the range of 2100–2600 nm by varying the SMF length. It has an average output power of  $\sim$ 120mW (Figure 1B).

In the experimental setup shown in Figure 2, an off-axis parabolic mirror was used instead of a lens to collimate the supercontinuum source output in order to reduce chromatic aberration. Another parabolic mirror was used to focus the light into a scanning grating monochromator with 300 groves/mm and 2  $\mu$ m blazed grating (Princeton instruments). After re-collimation, the beam was focused onto the sample by a plano-convex CaF<sub>2</sub> lens. The laser beam had a spot size of 0.1 x 0.5 mm at the sample. The sample was presented in a rotating seed sample holder which could contain 36 seeds (Figure 3). A PbSe detector was placed directly behind the sample holder to detect the transmitted light. The reflection from the backside of the focusing lens was collected by another CaF<sub>2</sub> lens, and was used as a reference measurement. The detectors were chosen such that they were fast enough to separate each pulse individually by measuring faster than the repetition rate of the laser which is 35 kHz. Separating the pulses proved to be essential, as each supercontinuum pulse fluctuates from pulse to pulse in both amplitude and polarization, as described in a previous study of the source.<sup>21</sup> In order to avoid the polarization noise, the beam-splitting lens was set at a small angle relative to the incident light in order to de-

crease polarization dependence of the reflectance. Two lock-in amplifiers were used to amplify the signals and the resulting sample and reference signals were divided to obtain a normalized intensity value for each wavelength step. This pulse-to-pulse normalization was crucial in order to eliminate the variation between the pulses and thus to obtain a high signal-to-noise (S/N) ratio of the spectra.<sup>21</sup>

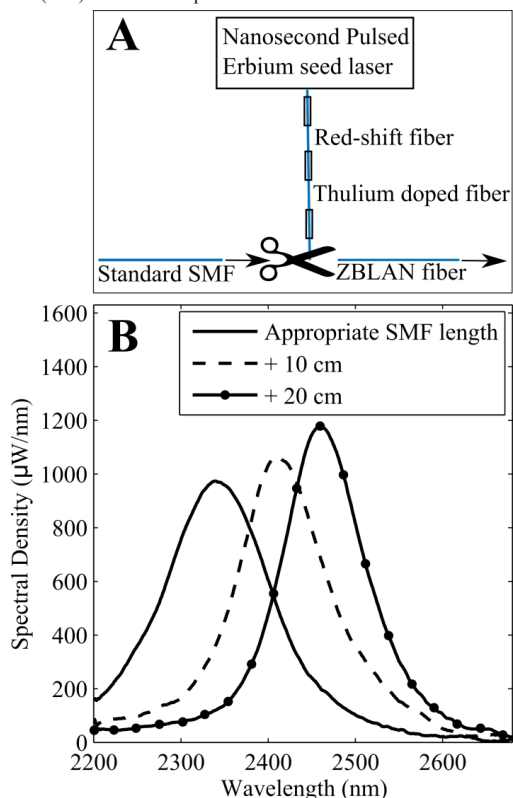


Figure 1. The supercontinuum source. (A) The light from the source was generated by a nanosecond pulsed laser entering a red-shift fiber and a thulium doped fiber. A ZBLAN fiber which had been used in a previous study on barley slices<sup>16</sup> was removed and different lengths of a single-mode optical fiber (SMF) inserted instead. (B) The center wavelength of the supercontinuum source could be tuned by changing the length of the SMF.

The seeds were scanned in the region of 2255–2381 nm, but only the region of 2275–2375 nm was used in the data analysis. The wavelength resolution was set to 10 nm by the output slit of the monochromator and the NIR spectral intensity recorded in 2 nm intervals. In order to obtain a useful S/N ratio for the seed measurements, each wavelength point was an average of 105 ms of laser illumination. To further enhance the S/N ratio, five consecutive spectral scans were collected and averaged, giving a total measurement time of 60 s. In the current setup, the speed is limited by the scanning grating monochromator. The acquisition time may in principle be lowered significantly by using for instance a fixed grating spectrometer and balanced detector arrays. All 105 seeds were measured three times (re-sampled) with LW NIR transmission spectroscopy. This resulted in a total of 315 spectra.

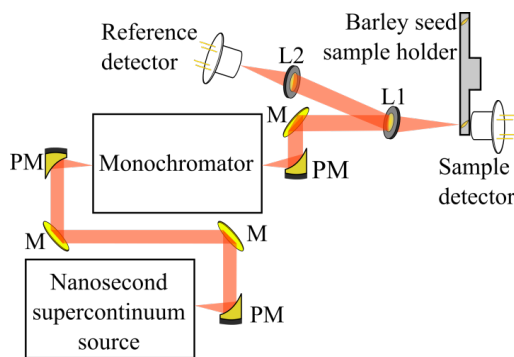


Figure 2. The barley seed transmission setup. The supercontinuum source is launched from a fiber onto an off-axis parabolic mirror (PM) for collimation. The light is then guided by silver mirrors (M) and focused by another PM into a grating monochromator for wavelength selection. The narrow-band light is subsequently collimated with a PM before it is focused by a plano-convex CaF<sub>2</sub> lens (L1) onto the barley grain of interest. A PbSe detector (D1) is used for detection of the transmitted light. The plano-convex lens (L1) is tilted at a small angle, and the back-reflection is used as a reference, which is focused by the CaF<sub>2</sub> lens (L2) onto another PbSe detector (D2).

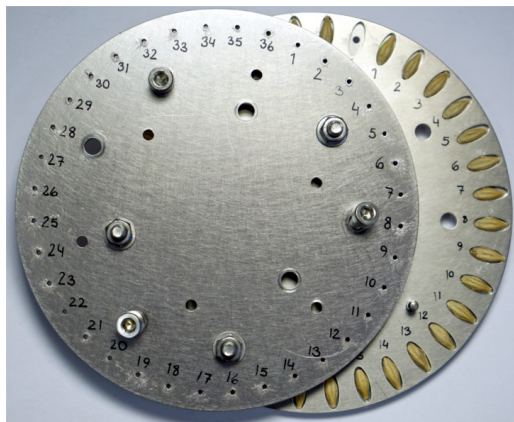


Figure 3. The sample holder is made of three stainless steel plates. The front- and back-plate have small holes with 2mm and 1mm in diameter, respectively. The middle plate has big holes that fit a single barley seed (1 cm long and 4 mm wide). The plates are kept together with bolts and nuts.

Bulk flours from *lys5.f*, *lys5.g*, *lys16*, *lys95* and *Bomi* and the high  $\beta$ -glucan sample B1 were measured on a NIRS<sup>TM</sup> DS2500 F (Foss, Hillerød, Denmark) equipped with a monochromator and a dual Si and PbS detector. The spectrum from DS2500 was an average of 128 scans measured from 400-2500 nm recorded with an interval of 0.5 nm.

**Chemical analysis.** After spectroscopic measurements the single seeds were freeze-dried for two days to ease the milling process. Then they were milled individually using a ball mill with stainless steel containers (5 ml volume) with two stainless steel balls (7 mm  $\phi$ ) (Retsch GmbH, Germany). The milled single seeds were subsequently divided in two, so that

half of the seed was used for  $\beta$ -glucan determination and the other half for protein analysis. Single seed  $\beta$ -glucan content was measured with an enzyme kit (Megazyme, Wicklow, Ireland).<sup>22</sup> The half seeds used for  $\beta$ -glucan analysis had sample weights of 11-21 mg instead of the normal 80-120 mg required for this analysis. It was not possible to make replicates because of the low sample weights. Instead the standard deviation was estimated from five *Bomi* seeds that were tested in duplicate. The *Bomi* duplicates had 18-22 mg/sample and an average standard deviation of 0.12 % (ranging between 0.04-0.22 %)  $\beta$ -glucan (w/w). The single seed protein analysis was done using a vario MACRO cube (Elementar Analysensysteme GmbH, Germany) and the Nitrogen result was multiplied with 6.25. A standard of sulfanilamide was run with each sequence in order to verify the accuracy of the instrument. The half seeds used for protein analysis had sample weights of 18-28 mg. It was not possible to make replicates because of the low sample weights. Instead the standard deviation was estimated from five *Bomi* seeds that were tested in duplicate. The *Bomi* duplicates had 20-26 mg/sample and an average standard deviation of 0.27 % (ranging between 0.13-0.53 %) protein (w/w).

Bulk total dietary fiber, soluble dietary fiber and insoluble dietary fiber content were determined in duplicates using an enzymatic kit (Megazyme, Wicklow, Ireland).<sup>23</sup> Bulk lipid content in the extracted  $\beta$ -glucan B1 sample was measured by extraction with petroleum ether and a Soxtec System HT and 1043 extraction unit (Tecator AB, Höganäs, Sweden).<sup>24</sup>

**Data analysis.** The absorbance was calculated as the  $\log_{10}(I_0/I_s)$  where  $I_0$  is the light intensity with no sample in the sample holder and  $I_s$  is the light intensity with a sample inserted in the sample holder.

Principal component analysis (PCA) was used to visualize the similarities and differences between the spectra, including outlier detection.<sup>25</sup> Partial least squares (PLS) was used to predict the  $\beta$ -glucan and protein content from the spectral measurements.<sup>26</sup> No preprocessing was applied to the spectra since the raw absorbance spectra were found to give the best PLS model. Spectra were mean centered before modeling. The PLS model was validated by leave-one-seed-out cross-validation and test set validation. The test set was selected by ordering the seeds according to  $\beta$ -glucan or protein content and selecting every third seed. The number of latent variables was chosen as the number when the root mean square error of calibration (RMSE), root mean square error of cross-validation (RMSECV) and the root mean square error of prediction (RMSEP) stopped decreasing. Another criterion for choosing the number of latent variables was that the loading vectors should not include noise.

The spectra were analyzed in Matlab (version R2013b) (The Mathworks, Inc., Natick, MA, USA) and PLS toolbox 7.5 (Eigenvector Research, Inc., Manson, WA, USA).

## RESULTS AND DISCUSSION

**The chemical composition of the barley genotypes.** The chemical analysis of individual barley seeds showed that the  $\beta$ -glucan and protein content vary from 3.0-16.8 % and 8.9-20.2 %, respectively. The relatively broad range and the distribution of samples across the entire range is a good starting point for a robust calibration (Table 1).

Table 1. Barley single seed mean values for seed weight,  $\beta$ -glucan and protein content. The standard deviation of the 19-21 seeds is given.

	Weight (mg)	$\beta$ -glucan (%)	Protein (%)
<i>Bomi</i>	50.5 $\pm$ 5.0	4.9 $\pm$ 0.8	12.6 $\pm$ 1.4
<i>lys5.f</i>	40.6 $\pm$ 3.9	14.2 $\pm$ 1.6	14.1 $\pm$ 2.1
<i>lys5.g</i>	46.2 $\pm$ 4.5	8.4 $\pm$ 1.0	11.4 $\pm$ 1.2
<i>lys16</i>	42.2 $\pm$ 4.3	13.2 $\pm$ 1.6	13.6 $\pm$ 1.6
<i>lys95</i>	41.4 $\pm$ 2.9	14.1 $\pm$ 1.5	16.6 $\pm$ 0.9

Within the five barley genotypes a considerable variation was observed from the distribution of  $\beta$ -glucan values in Figure 4. The smallest  $\beta$ -glucan variation was among the seeds from the *Bomi* variety (3.0-6.3 %), then *lys5.g* (6.5-10.9 %) and the biggest  $\beta$ -glucan variation was observed between the seeds from the varieties *lys5.f* (10.4-16.8 %), *lys16* (10.1-16.2 %) and *lys95* (10.4-16.3 %). The protein content also showed substantial variation within each barley genotype (supporting information Figure S-1). The smallest protein variation between seeds was observed in the variety *lys95* (14.9-18.0 %), then *Bomi* (10.6-15.7 %) and *lys5.g* (8.9-14.1 %), and the biggest protein variation between seeds was in *lys16* (11.3-19.1 %) and *lys5.f* (11.3-20.2 %). The variation in  $\beta$ -glucan and protein concentration within each genotype shows the within batch variation.

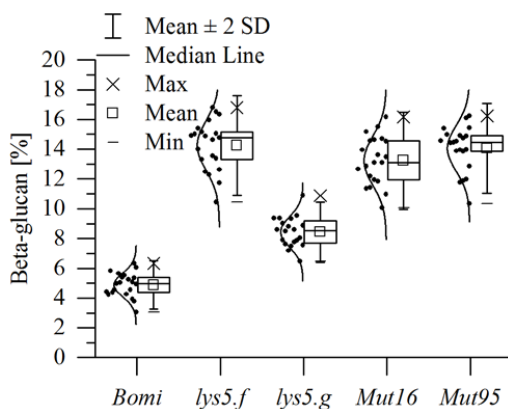


Figure 4.  $\beta$ -glucan distribution of 104 seeds from the barley genotypes *Bomi*, *lys5.f*, *lys5.g*, *lys16* and *lys95*. Standard deviation (SD).

The bulk chemical analysis of  $\beta$ -glucan, fiber, starch and lipids showed a variation between the barley genotypes (supporting information Table S-1). It was observed that the genotypes order in a similar way by the different chemical constituents which shows the close relation between genetic up- and down-regulation.

**Predictive models.** The 315 spectra of the 105 barley seeds were examined for outliers by PCA and by comparisons of the three spectra of each individual seed. It was found that some spectra had a decreasing or increasing absorbance from 2300-2380 nm (which possibly stems from chromatic aberration), some spectra had minor peak shifts (maybe from instrumental drift) and some spectra exhibited an absorbance above 4.4 which were considered too high/noisy. After this relative

strong sample outlier and data cleaning, 224 spectra from 92 seeds remained (Figure 5). Furthermore, errors during the chemical analysis of  $\beta$ -glucan and protein measurements occurred in one and four samples, respectively and removal of these samples resulted in a total of 222 spectra with corresponding  $\beta$ -glucan values from 91 seeds. With respect to protein determinations 212 spectra remained with corresponding protein values from 88 seeds. Figure 5 shows the raw spectra after outlier removal and reveals three peaks at about 2289, 2317 and 2349 nm which is in good accordance with previous studies.<sup>13, 16, 18</sup> The main contributors of the peaks at about 2289, 2317 and 2349 nm has been assigned to starch, starch and  $\beta$ -glucan, respectively.<sup>16</sup> However, the spectral region covers combination bands and overtones of O-H, C-C, C-O, C-H,  $\text{CH}_2$ ,  $=\text{CH}_2$ , and therefore also fat, protein and other fibers than  $\beta$ -glucan will absorb in this region.

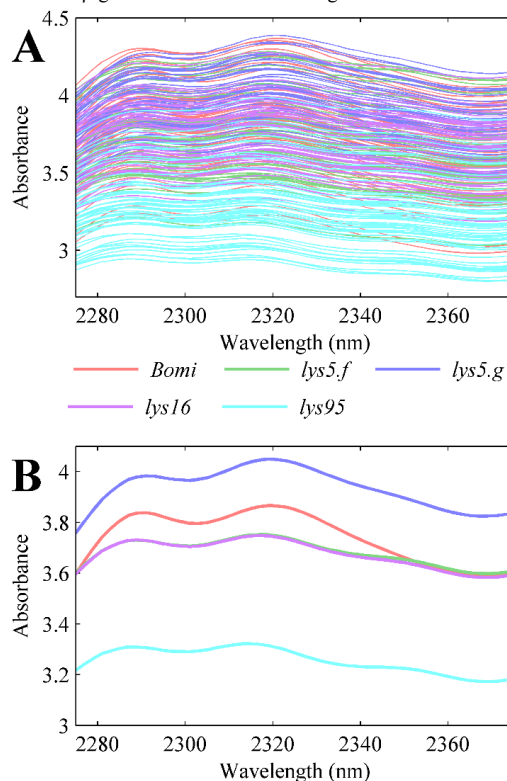


Figure 5. Raw transmission spectra of single barley seeds from 2275-2375 nm. (A) All 224 spectra after outlier removal, (B) mean spectra of the five barley genotypes.

Table 2. Literature models on the prediction of  $\beta$ -glucan in barley from NIR spectroscopy

Samples	Training/test set (#)	Y range	Instrument wl (nm)	Selected wl (nm)	LV (#)	Correlation ( $R^2$ )	Error <sup>e</sup>
Flour <sup>8</sup>	50/25	3-5 <sup>a</sup>	1100-2500 <sup>c</sup>	1656, 1676, 1752	-	0.48	C = 0.40 P = 0.40
Flour <sup>9</sup>	78/34,21	2.99-9.51 <sup>a</sup>	1100-2500 <sup>c</sup>	2234, 2374, 2500	-	0.85	C = 0.68 P = 1.13, 0.79
Single seed <sup>14</sup>	319/-	0-1.2 <sup>b</sup>	900-1700 <sup>c</sup>		?	0.58	
Flour <sup>10</sup>	138/68	2.33-5.76 <sup>a</sup>	1000-2500 <sup>c</sup>		3	0.68	CV = 0.44 P = 1.47
Flour <sup>10</sup>	138/68	2.33-5.76 <sup>a</sup>	400-2500 <sup>c</sup>	1100-2500	8	0.67	CV = 0.42 P = 0.41
Bulk seeds <sup>11</sup>	138/68	2.33-5.76 <sup>a</sup>	1000-2500 <sup>c</sup>		5	0.80	CV = 0.52 P = 0.43
Bulk seeds <sup>11</sup>	138/68	2.33-5.76 <sup>a</sup>	400-2500 <sup>c</sup>	1100-2500	6	0.47	CV = 0.50 P = 0.48
Bulk seeds <sup>11</sup>	138/68	2.33-5.76 <sup>a</sup>	400-2500 <sup>c</sup>	1100-2500	4	0.51	P = 0.44
Flour <sup>13</sup>	90/-	0-23 <sup>a</sup>	400-2500 <sup>c</sup>	1194-1240	4	0.94	CV = 1.57
Flour <sup>13</sup>	90/-	0-23 <sup>a</sup>	400-2500 <sup>c</sup>	1100-2500	2	0.84	CV = 2.60
Bulk seeds <sup>12</sup>	194/-	3.33-5.85 <sup>a</sup>	400-2500 <sup>c</sup>	1100-2200	13	0.78	CV = 0.36
Flour <sup>12</sup>	203/-	3.33-7.24 <sup>a</sup>	400-2500 <sup>c</sup>	1100-2500	8	0.96	CV = 0.30
Bulk seeds <sup>12</sup>	93/-	3.33-7.24 <sup>a</sup>	850-1050 <sup>d</sup>		9	0.77	CV = 0.44
Flour <sup>12</sup>	190/-	3.33-7.24 <sup>a</sup>	850-1050 <sup>d</sup>		11	0.76	CV = 0.43

Wavelength (wl) and latent variables (LV)

a: mg/100 mg

b: mg/seed

c: Reflectance measurement

d: Transmission measurement

e: Calibration error given by RMSE/standard error of estimate (C), cross-validation error given by RMSECV/standard error of cross-validation (CV) and prediction error given by RMSEP/standard error of prediction (P).

Starch, cellulose and  $\beta$ -glucan are all polymers of glucose. The difference between these carbohydrates is the linkages between the glucose molecules and on their intermolecular associations. Starch is an  $\alpha$ -glucan consisting of  $\alpha(1-4)$ -linkages with occasional branches of  $\alpha(1-6)$ -linkages while cellulose is exclusively  $\beta(1-4)$ -linkages and  $\beta$ -glucan is made of  $\beta(1-4)$ -linkages with regular inserts of  $\beta(1-3)$ -linkages. Measuring  $\beta$ -glucan in cereals with spectroscopy is thus performed by scrutinizing spectra for small differences that can be related to connectivity and intermolecular arrangements between carbohydrates. Literature models on  $\beta$ -glucan in barley predicted with NIR spectroscopy is presented in Table 2. The table shows that the range in  $\beta$ -glucan values seems to have some effect on the model performance as the two models with the smallest  $\beta$ -glucan range and smallest  $\beta$ -glucan values only have  $R^2$  values of 0.48 and 0.58. On the other hand, the three models with the biggest  $\beta$ -glucan range have  $R^2$  values of 0.84, 0.85 and 0.94. Two of the models with the highest  $\beta$ -glucan range were also some of the few models that had selected a smaller number of wavelengths. Most of the  $\beta$ -glucan models used the SW-NIR region from 850-1050 nm or a more broadband NIR region from 1100-2500 nm. Models have been built for both bulk barley seeds and bulk barley flour, but it is consistent that bulk seed models reach a maximum of  $R^2$  0.80 whereas several flour models get  $R^2$  from 0.85-0.96. It thus seems as if there is an advantage from measuring on flour in comparison to bulk seeds when it comes to  $\beta$ -glucan predic-

tions. However, measuring on bulk seeds with NIR spectroscopy is non-destructive whereas measurements on flour samples is destructive and cannot be used for plant breeding.

In this work a PLS model for  $\beta$ -glucan was built on a training set of 147 spectra from 61 seeds. The test set had 75 spectra from 30 seeds. Different preprocessing methods were tried in order to improve the predictions, but no method significantly improved the  $R^2$ , the RMSECV or the RMSEP. The results from the preprocessing trials are presented in the supporting information Table S-2. The best PLS model for predicting  $\beta$ -glucan used raw spectra which were mean centered. The resulting  $R^2$  in cross-validation and test set validation was 0.83 and 0.90, respectively (Figure 6).

The reason why non-preprocessed spectra resulted in the best predictions compared to preprocessed spectra remain elusive, but it is hypothesized that the small spectral range which only covers 100 nm contain very little wavelength dependent issues to correct for. The spectra will still contain variations from the different light path-length through the seeds due to the natural variation in seed size. The seeds may also scatter the light slightly different according to local variations in e.g. hardness. However, the regression vector of the PLS model indicates that the model extracts chemical information from the three peak-like minima and maxima (Figure 7). It therefore appears that the PLS model focuses on the

chemical information and disregards irrelevant spectral variations.

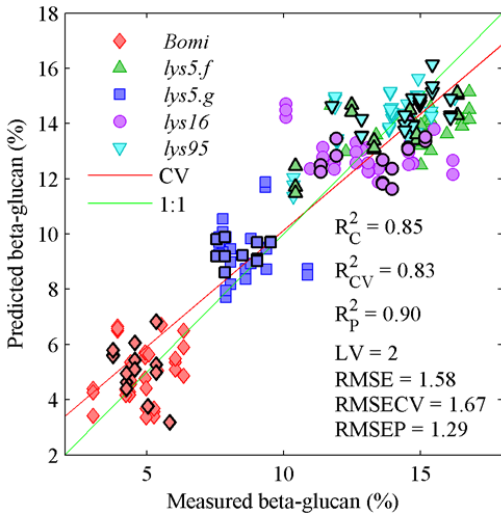


Figure 6. Measured  $\beta$ -glucan versus predicted  $\beta$ -glucan in cross-validation and test set validation of a PLS model on intact barley seed spectra. Test set samples are marked with a black line. Root mean square error (RMSE), calibration (C), cross-validation (CV), test set prediction (P) and latent variables (LV).

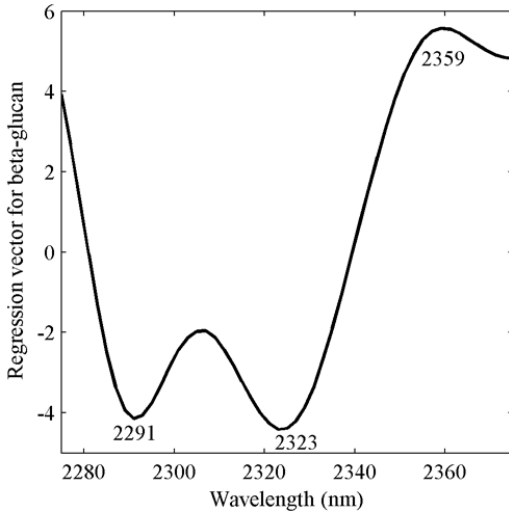


Figure 7. The regression vector of a PLS model on whole barley seed spectra from 2275-2375 nm with  $\beta$ -glucan as the response variable.

The peaks at 2291, 2323 and 2359 nm in the regression vector shown in Figure 7 resembles the peak maxima in the raw data, but they are positioned at slightly higher wavelengths. The interpretation of which chemical components that absorb in this spectral region is not easy since all the three major groups of food, namely carbohydrates, fat and protein absorb in this complex combination tone area. In order to augment the interpretation of the 2349 nm peak, bulk flour from all five

barley genotypes and one high concentration  $\beta$ -glucan (B1) were measured on a commercial NIR spectrometer. Figure 8A shows that the flour spectra resemble the raw spectra of barley seeds. Since (barley) fat absorbs at 2310 nm and 2353 nm<sup>16</sup> it was investigated if the information from fat could be removed by dividing the absorbance at 2350 nm with the absorbance at 2310 nm. The result is shown in Figure 8B which reveals a very high correlation of  $R^2 = 1.00$  between  $\beta$ -glucan content and the absorbance ratio 2350 nm/2310 nm. It is thus concluded that the absorbance at 2349 nm include a significant signal contribution from  $\beta$ -glucan.

The PLS model for protein % (w/w) was built on a training set with 139 spectra from 59 seeds and test set validated with 73 spectra from 29 seeds. It had a  $R^2$  in cross-validation and test set validation of 0.45 and 0.49, respectively. It was therefore concluded that the spectral region from 2275-2375 nm does not contain sufficient information for protein predictions and accordingly these models were not investigated any further.

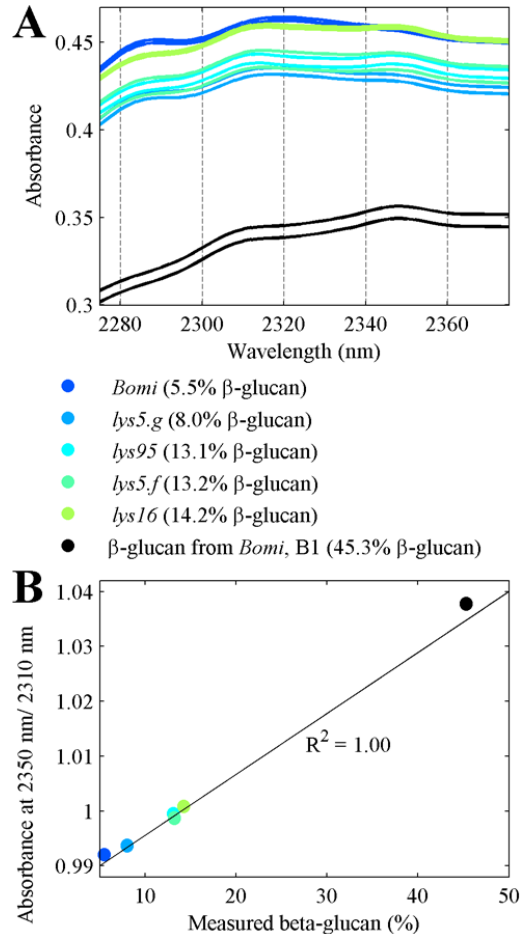


Figure 8. (A) Spectra of bulk flour from five barley genotypes (*Bomi*, *lys5.g*, *lys95*, *lys5.f* and *lys16*) with  $\beta$ -glucan values from Ringsted et al.<sup>16</sup> and  $\beta$ -glucan extracted from *Bomi* (B1) with  $\beta$ -glucan value from Mikkelsen et al.<sup>20</sup> (B) Measured  $\beta$ -glucan versus the absorbance ratio 2350 nm / 2310 nm. Each sample was measured with and without a paper lid.

Plant scientists have used the unit mg/seed in order to follow the different stages in kernel development which in certain cases can be hidden when using the % of dry weight.<sup>27</sup> The Lambert-Beer law used in NIR spectroscopy has a linear relationship between absorbance and concentration %. Studies on single seeds do not agree on whether mg/seed or % (w/w) gives the best predictive models.<sup>28-29</sup> In the study by Spielbauer et al.,<sup>30</sup> oil and protein in maize were predicted with similar performance from mg/seed and % (w/w), but starch had better predictions with mg/seed. Spielbauer et al. hypothesized that mg/seed gave better results for starch because starch had a high correlation with seed weight ( $R^2$  of 0.94). In the present study, PLS models on mg protein/seed or mg  $\beta$ -glucan/seed were generated, but per seed values they gave worse prediction results compared to the predictive models using % (w/w). This is not surprising because in this study only a small area of the seed was measured. In addition, the correlation between seed weight and  $\beta$ -glucan or protein was  $R^2$  0.35 and 0.14, respectively. So even if the spectrometer had illuminated the entire seed it is possible that % (w/w) would perform better. More details about the mg/seed models can be viewed in the supporting information (Figure S-2, S-3 and S-4).

**Re-sampling of barley seeds.** In order to investigate the influence of the reference analysis and of the reproducibility of the spectral measurements a sampling study was performed. This was done on the 53 seeds which had all three spectra after outlier removal and removal of the seed with missing  $\beta$ -glucan value. For this purpose PLS models were built on (1) one randomly selected spectrum from each of the 53 seeds, (2) the average of two randomly selected spectra from each of the 53 seeds and (3) the average of all three spectra from each of the 53 seeds. The random selection of one or two spectra was repeated 100 times. Figure 9 shows the result of the PLS models built on the individual  $\beta$ -glucan values and the average  $\beta$ -glucan values.

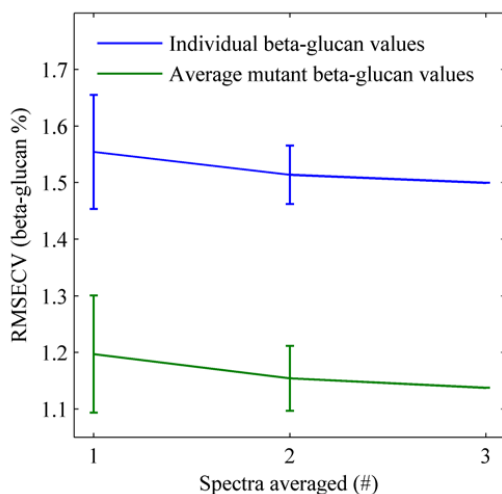


Figure 9. The number of averaged spectra from the same barley seed versus the RMSECV error from a PLS model. The selection of one or two spectra was randomly repeated 100 times. The error bars show  $\pm$  two standard deviations.

From Figure 9 it is shown that both the individual and average  $\beta$ -glucan models exhibit a lower RMSECV with increasing number of averaged spectra. This is not surprising since the S/N ratio is proportional to the  $\sqrt{\text{measurement time}}$  and accordingly averaging more spectra provides a better S/N. However it is a bit surprising that the models built on the average  $\beta$ -glucan values have lower RMSECV values. Perhaps the wet chemical measured  $\beta$ -glucan values are not accurate enough, but on the other hand the *Bomi* replicates showed a standard deviation of 0.12 %. Another possible explanation could be that too much sample is lost in the milling process. On average 13 % of each seed was lost with a range from 7 to 27 %. However, the *Bomi* replicates also contained the uncertainty from the milling process so it is not expected that this should influence the result strongly. A third possibility is that the spectral measurements have a variation so that the  $\beta$ -glucan values cannot be determined with a higher precision. This is quite likely since the seeds have different sizes and shapes which will cause spectral variations. A fourth option is that there are compositional variations in the part of the seed that are not illuminated by the light source. This is also a potential case that will worsen predictive results. If the light source spot (0.1 x 0.5 mm) and a barley seed (10 x 4 mm) were assumed to have a shape of an ellipse then it would mean that 0.1 % of the surface area was measured. There might therefore be some variation between doing a measurement of for instance the barley crease or other areas of the seed.<sup>31</sup> It could be that by increasing the illuminated area of the seed then a more representative measurement could be done which would result in more precise predictions of  $\beta$ -glucan.

## CONCLUSIONS

Single seed sorting has the potential of improving the precision in sorting and grading of seeds. Bulk analysis has problems with detecting the sporadic high concentrations of infected seeds because the overall concentration is much lower. Bulk analysis is also not a solution to the plant breeding problem or to investigations that are focused on measuring the variation within a batch of seeds such as for example seeds on the same straw. The development of fast and non-destructive measurements can therefore have a huge impact on the plant breeding, food and feed industries. This study shows that a new supercontinuum light source applied in a NIR spectrometer was able to predict  $\beta$ -glucan in whole barley seeds with high accuracy and potentially with extremely high speed.

## ASSOCIATED CONTENT

### Supporting Information

The content of the supporting information file: Figure of the protein distribution, Table with bulk barley seed reference values, Table with PLS results from trials with different preprocessing methods, PLS model for protein % (w/w), PLS model for mg protein/seed and PLS model for mg  $\beta$ -glucan/seed. (PDF)

## AUTHOR INFORMATION

### Corresponding Authors

\* Tine Ringsted: [tine.ringsted@food.ku.dk](mailto:tine.ringsted@food.ku.dk), Soren Balling Engelsen: [se@food.ku.dk](mailto:se@food.ku.dk)

### Author Contributions

The manuscript was written through contributions of all authors. / All authors have given approval to the final version of the manuscript.

## ACKNOWLEDGMENT

The authors wish to acknowledge the generous financial support from The Danish National Advanced Technology Foundation (now Innovation Fund Denmark) to the project entitled "Light & Food." In addition, the authors would like to thank Jens Christian Sørensen (Biochemistry and Bioprocessing, Department of Food Science, University of Copenhagen) who facilitated the protein analysis. The authors are also grateful for the laboratory assistance from Lisbeth Tina Dahl (Spectroscopy and Chemometrics, Department of Food Science, University of Copenhagen).

## REFERENCES

- Rosenthal, T. C. In *Handbook of vibrational spectroscopy*; Chalmers, J. M.; Griffiths, P. R., Eds.; John Wiley & Sons Ltd.: Chichester, England, 2002; Vol. 1, pp 461-465.
- Dudley, J. M.; Genty, G.; Coen, S. *Rev. Mod. Phys.* **2006**, *78*, 1135-1184.
- Kaminski, C. F.; Watt, R. S.; Elder, A. D.; Frank, J. H.; Hult, J. *Appl. Phys. B* **2008**, *92*, 367-378.
- Petersen, C. R.; Møller, U.; Kubat, I.; Zhou, B. B.; Dupont, S.; Ramsay, J.; Benson, T.; Sujecki, S.; Abdel-Moneim, N.; Tang, Z. Q.; Furniss, D.; Seddon, A.; Bang, O. *Nat. Photonics* **2014**, *8*, 830-834.
- Dupont, S.; Petersen, C.; Thøgersen, J.; Agger, C.; Bang, O.; Keiding, S. R. *Opt. Express* **2012**, *20*, 4887-4892.
- Gupta, M.; Abu-Ghannam, N.; Gallagher, E. *Compr. Rev. Food Sci. Food Saf.* **2010**, *9*, 318-328.
- Agelet, L. E.; Hurburgh, C. R. *Talanta* **2014**, *121*, 288-299.
- Henry, R. J. *Carbohydr. Res.* **1985**, *141*, 13-19.
- Szczodrak, J.; Czuchajowska, Z.; Pomeranz, Y. *Cereal Chem.* **1992**, *69*, 419-423.
- Sohn, M.; Himmelsbach, D. S.; Barton II, F. E.; Griffey, C. A.; Brooks, W.; Hicks, K. B. *Appl. Spectrosc.* **2007**, *61*, 1178-1183.
- Sohn, M.; Himmelsbach, D. S.; Barton II, F. E.; Griffey, C. A.; Brooks, W.; Hicks, K. B. *Appl. Spectrosc.* **2008**, *62*, 427-432.
- Schmidt, J.; Gergely, S.; Schönlechner, R.; Grausgruber, H.; Tömösközi, S.; Salgó, A.; Berghofer, E. *Cereal Chem.* **2009**, *86*, 398-404.
- Seefeldt, H. F.; Blennow, A.; Jespersen, B. M.; Wollenweber, B.; Engelsen, S. B. *J. Cereal Sci.* **2009**, *49*, 24-31.
- de Sá, R. M.; Palmer, G. H. *J. Inst. Brew.* **2006**, *112*, 9-16.
- Munck, L.; Nielsen, J. P.; Møller, B.; Jacobsen, S.; Søndergaard, I.; Engelsen, S. B.; Nørgaard, L.; Bro, R. *Anal. Chim. Acta* **2001**, *446*, 171-186.
- Ringsted, T.; Dupont, S.; Ramsay, J.; Jespersen, B. M.; Sørensen, K. M.; Keiding, S. R.; Engelsen, S. B. *Appl. Spectrosc.* **2016**, *70*, 1176-1185.
- Fox, G. P. In *Genetics and Improvement of Barley Malt Quality*; Zhang, G.; Li, C., Eds.; Springer: Berlin Heidelberg, 2010; pp 63-98.
- Munck, L.; Møller, B.; Jacobsen, S.; Søndergaard, I. *J. Cereal Sci.* **2004**, *40*, 213-222.
- Jacobsen, S.; Søndergaard, I.; Møller, B.; Desler, T.; Munck, L. *J. Cereal Sci.* **2005**, *42*, 281-299.
- Mikkelsen, M. S.; Jespersen, B. M.; Larsen, F. H.; Blennow, A.; Engelsen, S. B. *Food Chem.* **2013**, *136*, 130-138.
- Ramsay, J.; Dupont, S.; Keiding, S. R. *Laser Phys. Lett.* **2014**, *11*, 095702.
- AACC,  $\beta$ -Glucan Content of Barley and Oats-Rapid Enzymatic Procedure. In *Approved Methods of Analysis*, 11th ed.; AACC International: St. Paul, MN, USA, 1999.
- AACC, Soluble, Insoluble, and Total Dietary Fiber in Foods and Food Products. In *Approved Methods of Analysis*, 11th ed.; AACC International: St. Paul, MN, USA, 1999.
- AOAC, Crude Fat in Feeds, Cereal Grains, and Forages. In *Official Methods of Analysis of AOAC International*, 18th ed.; AOAC International: Gaithersburg, MD, USA, 2006.
- Wold, S.; Esbensen, K.; Geladi, P. *Chemom. Intell. Lab. Syst.* **1987**, *2*, 37-52.
- Wold, S.; Martens, H.; Wold, H. *Lect. Notes Math.* **1983**, *973*, 286-293.
- Gergely, S.; Salgó, A. *J. Near Infrared Spectrosc.* **2005**, *13*, 9-17.
- Peiris, K. H. S.; Dowell, F. E. *Cereal Chem.* **2011**, *88*, 45-50.
- Dowell, F. E.; Ram, M. S.; Seitz, L. M. *Cereal Chem.* **1999**, *76*, 573-576.
- Spielbauer, G.; Armstrong, P.; Baier, J. W.; Allen, W. B.; Richardson, K.; Shen, B.; Settles, A. M. *Cereal Chem.* **2009**, *86*, 556-564.
- Andersson, A. A. M.; Andersson, R.; Autio, K.; Åman, P. *J. Cereal Sci.* **1999**, *30*, 183-191.

# Long Wavelength Near-Infrared Transmission Spectroscopy of Barley Seeds Using a Supercontinuum Laser: Prediction of Beta-Glucan Content

---

Tine Ringsted<sup>a</sup>, Jacob Ramsay<sup>b</sup>, Birthe M. Jespersen<sup>a</sup>, Søren R. Keiding<sup>b</sup>, Søren B. Engelsen<sup>a</sup>

<sup>a</sup>*Department of Food Science, University of Copenhagen, Frederiksberg, Denmark.*

<sup>b</sup>*Department of Chemistry, Aarhus University, Aarhus, Denmark.*

## Contents

Figure S-1. The protein distribution in single barley seeds.....	S-2
Table S-1. Bulk barley seed reference values.....	S-3
Table S-2. PLS results from trials with different preprocessing methods.....	S-4
Figure S-2. PLS model for protein % (w/w) .....	S-5
Figure S-3. PLS model for mg protein/seed.....	S-6
Figure S-4. PLS model for mg $\beta$ -glucan/seed.....	S-7

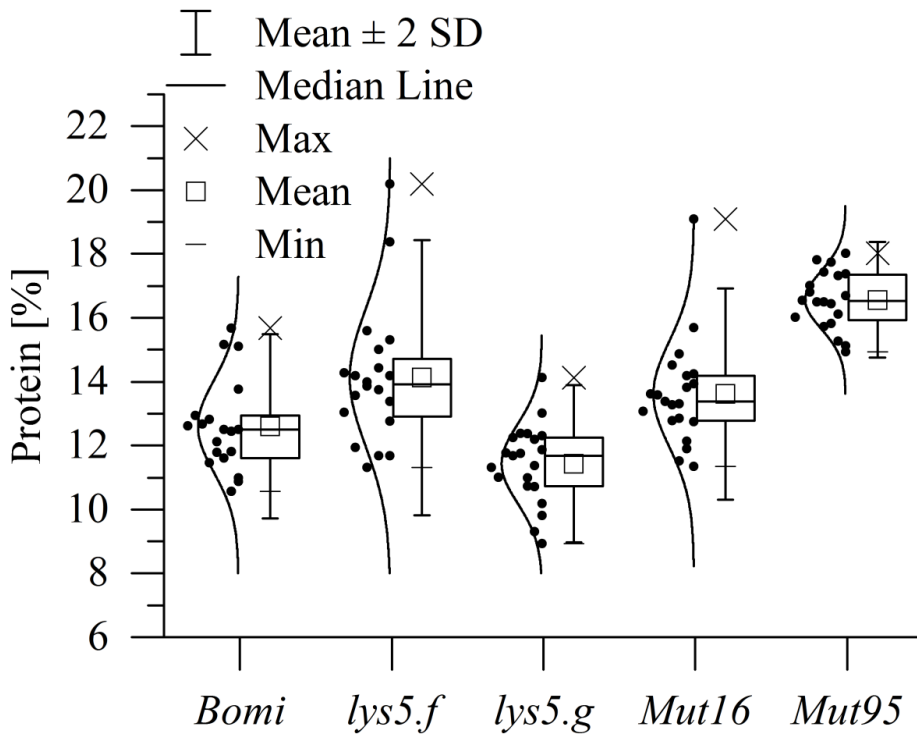


Figure S-1. Protein distribution of 101 seeds from the barley genotypes *Bomi*, *lys5.f*, *lys5.g*, *lys16* and *lys95*.

## Supporting material

Table S-1. Barley bulk mean values for the content of  $\beta$ -glucan, fiber, starch and lipids. The standard deviation of duplicates is given.

	$\beta$ -glucan (%)	TDF (%)	SDF (%)	IDF (%)	Starch (%)	Lipids (%)
<i>Bomi</i>	5.5 $\pm$ 0.1 <sup>a</sup>	22.5 $\pm$ 0.1	5.2 $\pm$ 0.8	17.3 $\pm$ 0.6	49.5 $\pm$ 0.02 <sup>a</sup>	2.05 $\pm$ 0.02 <sup>a</sup>
<i>lys5.f</i>	13.2 $\pm$ 0.1 <sup>a</sup>	37.5 $\pm$ 1.3	12.5 $\pm$ 1.5	25.0 $\pm$ 0.2	30.7 $\pm$ 4.8 <sup>a</sup>	3.96 $\pm$ 0.11 <sup>a</sup>
<i>lys5.g</i>	8.0 $\pm$ 0.1 <sup>a</sup>	28.2 $\pm$ 0.4	7.8 $\pm$ 1.0	20.4 $\pm$ 0.6	39.9 $\pm$ 1.0 <sup>a</sup>	2.91 $\pm$ 0.19 <sup>a</sup>
<i>lys16</i>	14.2 $\pm$ 0.1 <sup>a</sup>	46.7 $\pm$ 2.7	13.3 $\pm$ 1.0	33.4 $\pm$ 3.7	27.4 $\pm$ 0.8 <sup>a</sup>	3.71 $\pm$ 0.08 <sup>a</sup>
<i>lys95</i>	13.1 $\pm$ 0.1 <sup>a</sup>	43.0 $\pm$ 0.8	12.4 $\pm$ 0.4	30.5 $\pm$ 0.4	27.3 $\pm$ 1.0 <sup>a</sup>	4.44 $\pm$ 0.01 <sup>a</sup>
B1	45.3 $\pm$ 2.0 <sup>b</sup>	39.9 $\pm$ 4.2 <sup>b</sup>	18.5 $\pm$ 1.1 <sup>b</sup>	23.8 $\pm$ 1.0 <sup>b</sup>	18.3 $\pm$ 1.5 <sup>b</sup>	3.33 $\pm$ 0.11

Total dietary fiber (TDF), soluble dietary fiber (SDF) and insoluble dietary fiber (IDF)

<sup>a</sup>: from Ringsted et al. (2016) and expressed as % "as is".

<sup>b</sup>: from Mikkelsen et al. (2013) and expressed as % of dry matter.

Table S-2. Results of PLS models for  $\beta$ -glucan with different preprocessing methods.

	Leave-one-seed-out CV			Test set validation		Leave-one-genotype-out CV		
	# LV	R <sup>2</sup>	RMSECV	R <sup>2</sup>	RMSEP	# LV	R <sup>2</sup>	RMSECV
Raw	2	0.83	1.67	0.90	1.29	2	0.81	1.87
MSC	2	0.77	1.98	0.90	1.31	2	0.68	2.42
EMSC	2	0.74	2.10	0.86	1.58	1	0.45	3.19
2. der. GS (3,3)	3	0.80	1.83	0.88	1.40	4	0.72	2.27
2. der. GS (3,3) + MSC	3	0.75	2.05	0.85	1.58	4	0.54	3.11
2. der. SG (win. 3, 2 pol.)	1	0.70	2.25	0.78	1.96	1	0.50	3.01
2. der. SG (win 3, 2. pol) +MSC	1	0.63	2.50	0.76	2.10	1	0.35	3.58
2. der. SG (win 7, 2. pol)	3	0.78	1.92	0.84	1.61	3	0.64	2.63
2. der. SG (win 7, 2. pol) +MSC	2	0.71	2.22	0.76	1.99	2	0.41	3.64
2. der. SG (win 11, 2. pol)	4	0.80	1.84	0.88	1.39	4	0.73	2.22
2. der. SG (win 11, 2. pol) +MSC	4	0.77	1.99	0.89	1.38	4	0.57	3.01
1. der. SG (win 11, 2. pol)	3	0.83	1.72	0.90	1.32	3	0.80	1.88
1. der. SG (win 11, 2. pol) + MSC	3	0.73	2.16	0.89	1.38	3	0.44	3.84

Latent variables (LV), cross-validation (CV), derivative (der.), gap-segment (GS), Savitzky–Golay (SG), window size (win), degree polynomial (pol).

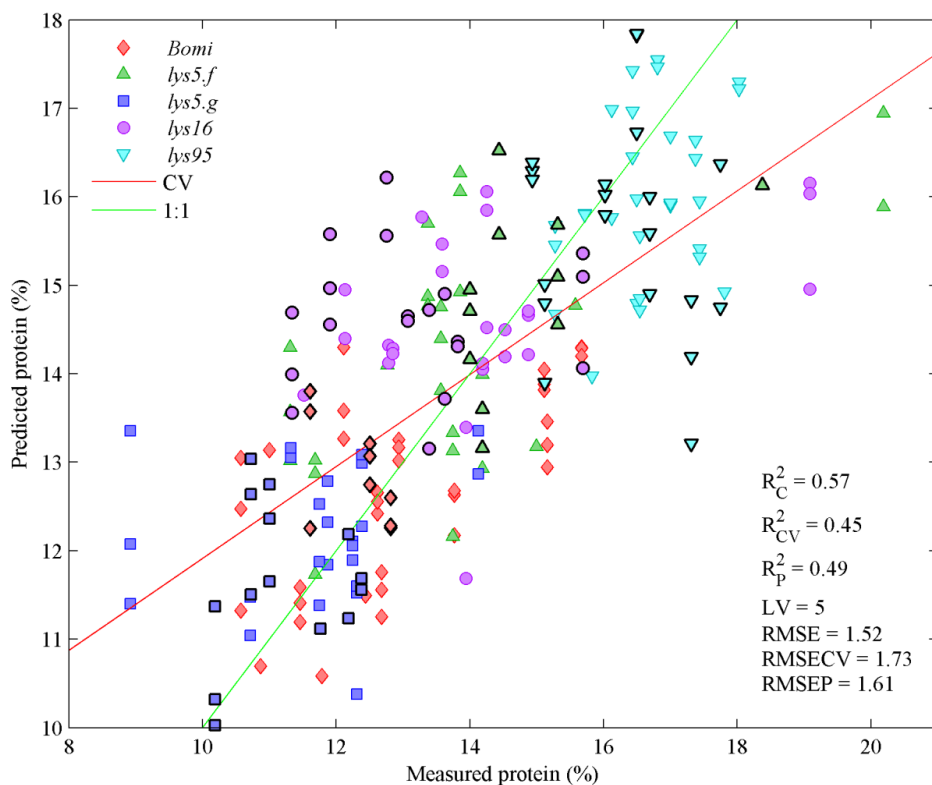


Figure S-2. Measured protein versus predicted protein in cross-validation and test set validation of a PLS model on whole barley seed spectra. Test set samples are marked with a black line. Root mean square error (RMSE), calibration (C), cross-validation (CV), test set prediction (P) and latent variables (LV).

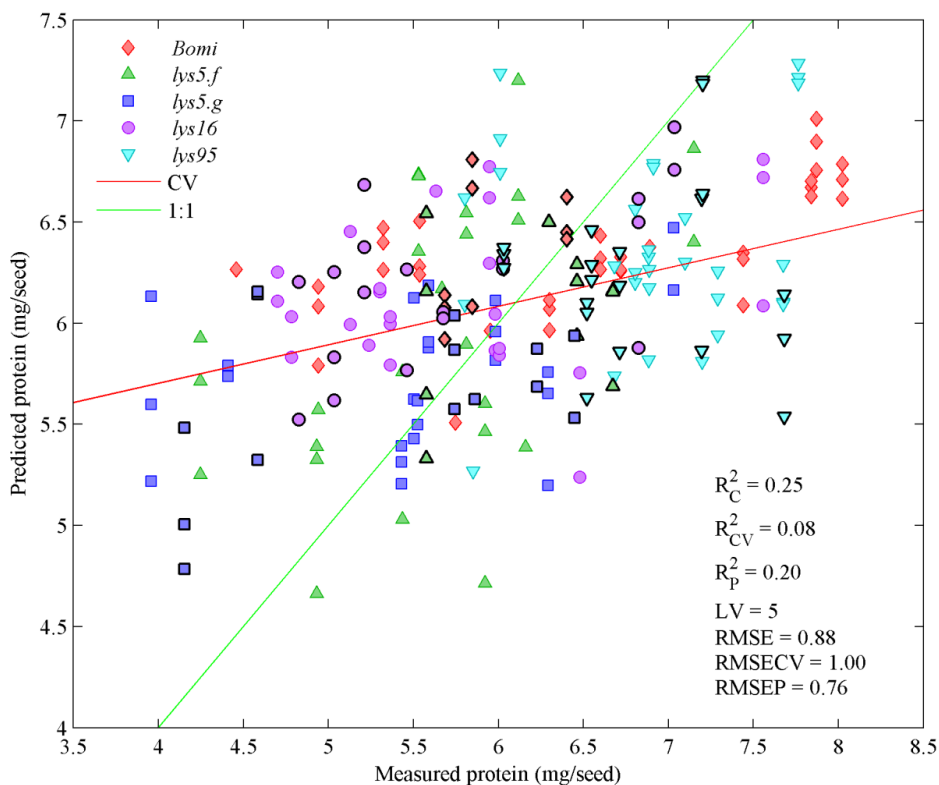


Figure S-3. Measured protein versus predicted protein in cross-validation and test set validation of a PLS model on whole barley seed spectra. Test set samples are marked with a black line. Root mean square error (RMSE), calibration (C), cross-validation (CV), test set prediction (P) and latent variables (LV).

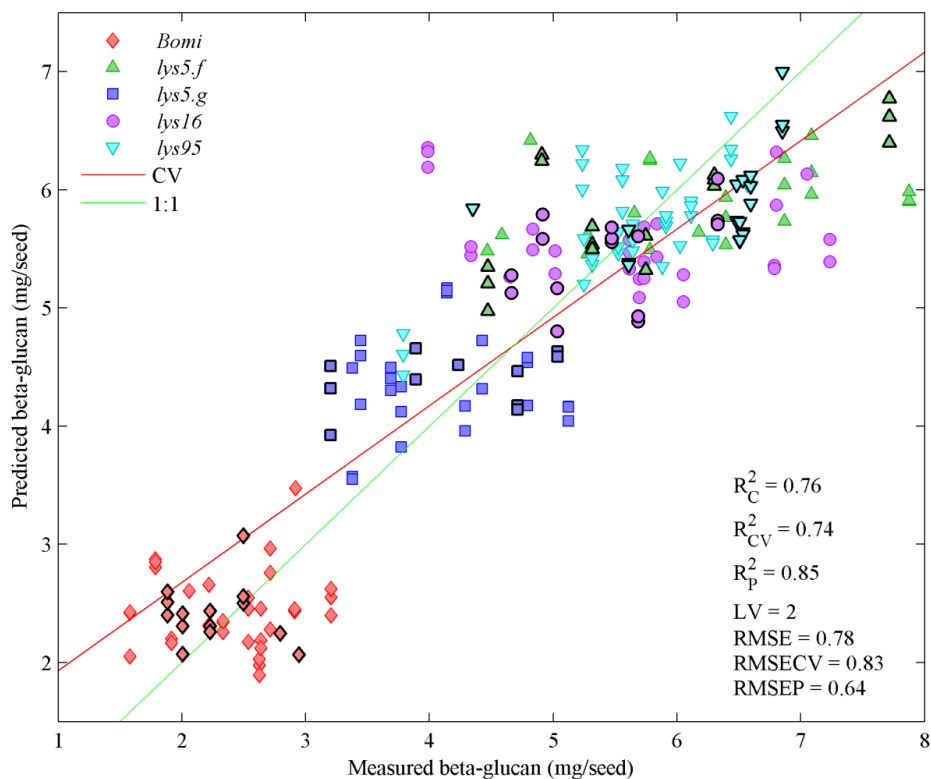


Figure S-4. Measured  $\beta$ -glucan versus predicted  $\beta$ -glucan in cross-validation and test set validation of a PLS model on whole barley seed spectra. Test set samples are marked with a black line. Root mean square error (RMSE), calibration (C), cross-validation (CV), test set prediction (P) and latent variables (LV).



---

# Proceeding

---

## **Long wavelength near-infrared transmission spectra of barley endosperm and oil using a supercontinuum laser**

Tine Ringsted, Sune Dupont, Jacob Ramsay, Birthe Møller Jespersen, Klavs Martin Sørensen, Søren Rud Keiding, and Søren Balling Engelsen

*Proceedings of the 17th International Conference on Near Infrared Spectroscopy (ICNIRS 2015). Foz do Iguassu, Brazil, 2015*



## Long wavelength near-infrared transmission spectra of barley endosperm and oil using a supercontinuum laser

T. Ringsted<sup>1,\*</sup>, S. Dupont<sup>2</sup>, J. Ramsay<sup>2</sup>, B.M. Jespersen<sup>1</sup>, K.M. Sørensen<sup>1</sup>, S.R. Keiding<sup>2</sup>, S.B. Engelsen<sup>1</sup>

<sup>1</sup> University of Copenhagen, Department of Food Science, Rolighedsvej 26, 1958 Frederiksberg, Denmark.

<sup>2</sup> Aarhus University, Department of Chemistry, Langelandsgade 140, 8000 Aarhus, Denmark.

\* Corresponding author: [tine.ringsted@food.ku.dk](mailto:tine.ringsted@food.ku.dk)

### Abstract

The supercontinuum laser is a new type of laser which has the spatially coherent beam as seen in traditional lasers, but unlike these lasers, the supercontinuum laser has a broad, continuous spectrum. It is therefore possible to measure a broad spectrum from very small samples. An experimental spectrometer was built, containing a scanning-grating monochromator, a PbSe detector and the supercontinuum light source. Previous studies on barley seeds by near-infrared spectroscopy in reflection mode revealed an information rich area from 2260-2380 nm. In the present study, it was the goal to investigate the potential of the supercontinuum laser applied to barley seeds in transmission mode in the region 2260-2380 nm and to explore the chemical information obtained. One mm slices from 350 barley seeds from five barley genotypes were measured through the endosperm. To add chemical interpretation, oils from the same five barley genotypes were measured from 2003-2497 nm. The quality of the obtained spectra showed a good signal-to-noise ratio after applying a pulse-to-pulse normalization of the supercontinuum light. The spectra showed information on C-H vibrations from starch and  $\beta$ -glucan.

**Keywords:** Near-infrared transmission spectroscopy; NIT; Supercontinuum laser; Food; Barley.

### Introduction

The supercontinuum laser combines the broad spectral range of a lamp with the collimated beam of a laser. These properties might prove to be an advantage when measuring on small samples, gases or remote sensing. Single seed analysis, is one area that could benefit from the high brightness of the laser. So far, single seed transmission measurements have mainly been performed in the wavelength region below 1100 nm because of the increased absorbance at longer wavelengths. In some situations it could be beneficial to use longer wavelengths because of the possibility to get information from the first overtone region (1400-1800 nm) or the combination tone region (1900-2500 nm). One example is the measurement of  $\beta$ -glucan in barley which is not well predicted from the wavelength region below 1100 nm,<sup>1</sup> whereas long-wavelength near-infrared (NIR) measurements from 2260-2380 nm in reflectance mode have shown information on the level of  $\beta$ -glucan.<sup>2</sup> The content of  $\beta$ -glucan is important in beer production because a high content can result in clogging of filters and the generation of "grandma's cough" precipitation in the final beer.  $\beta$ -glucans have also received attention because of their health promoting properties such as their stabilizing effect on the blood glucose level and the lowering of serum cholesterol.<sup>3</sup>

The aim of the present study was to investigate the potential of a supercontinuum laser as the light source in a long-wavelength NIR spectrometer applied to the barley endosperm in the transmission mode. The spectral region from 2260-2380 nm was used and it was the goal to interpret which chemical constituents contributed to the absorbance in this region.<sup>4</sup>

### Materials and methods

The NIR instrumental setup is depicted in Figure 1. It consisted in the supercontinuum source (NKT Photonics), a scanning-grating monochromator and a PbSe detector. The supercontinuum source is a pulsed source, and these pulses have intensity variations across the spectrum. It was therefore necessary to perform a pulse-to-pulse normalization with the signal from a second detector which only measured pulse variations without the sample. The size of the laser beam reaching the sample was 0.1 mm x 0.5 mm. A rotating sample holder was produced which could automatically present 36 barley slices in one run. The five barley oils together with a nujol mineral oil and a sunflower oil was measured in a quartz cuvette with a 1 mm path-length. Each spectrum for a barley slice or oil measurement took 60 seconds.

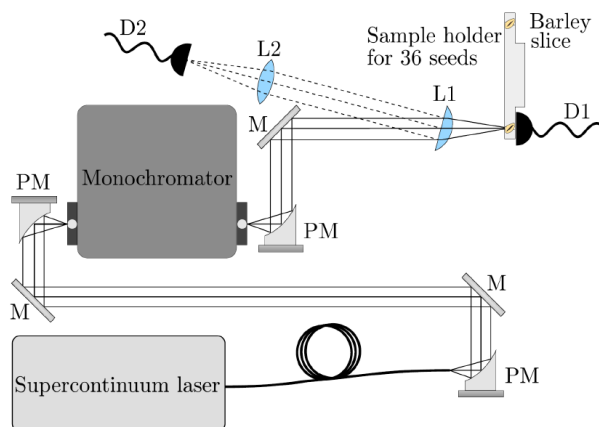


Figure 1. The supercontinuum light exits a fiber and is guided by off-axis parabolic mirrors (PM) and silver mirrors (M) into the scanning-grating monochromator. The light that exits the monochromator is then focused by a plano-convex CaF<sub>2</sub> lens (L1) onto the sample. PbSe detectors are placed behind the sample (D1) and the back-reflection of the L1 lens (D2). The second detector was used for pulse-to-pulse normalization.

A custom-made barley slicer shown in Figure 2a was produced in order to make precise and fast one mm slices from 350 grains (70 of each of five barley genotypes). As seen from Figure 2b the cut was made from the center of the grain which contains the endosperm. Four out of the five barley genotypes were mutants with low starch and high  $\beta$ -glucan content (*lys5.f*, *lys5.g*, *lys16* and *lys95*) and the last genotype was a normal barley (*Bomi*).

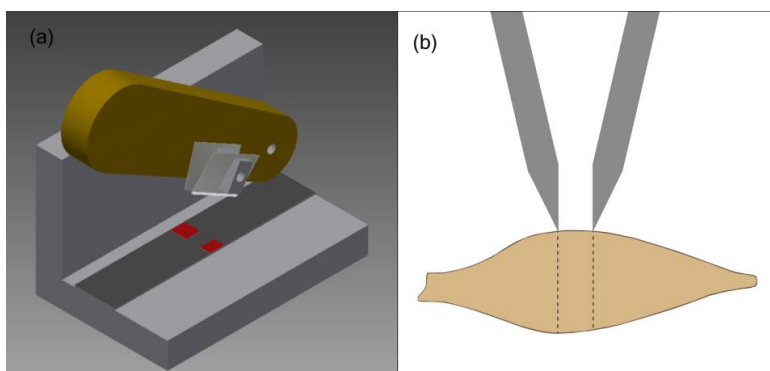


Figure 2. (a) The barley slicer. (b) The knives of the barley slicer were tilted to position the angle of the bevel perpendicular on the seed. This was done to increase the precision of the slice thickness and ease the collection of the slices.

The barley oils were extracted with 100 % hexane by Pressurized Solvent Extractor (PSE), ASE200® from Dionex (Sunnyvale, CA).

Reference measurements on moisture,  $\beta$ -glucan, starch, protein and lipid content were performed for each barley genotype by measuring on flour prepared from bulk samples.

The absorbance was calculated with air as the background for the barley slices and an empty cuvette for the oil measurements. The absorbance spectra were preprocessed as second derivative spectra (Savitzky Golay, 2. degree polynomial, window size 7).

### Results and Discussion

Figure 3 shows the content of moisture,  $\beta$ -glucan, starch, protein and lipid for each barley genotype. The highest variation was found in the content of starch and  $\beta$ -glucan which corresponded to findings in previous studies.<sup>5</sup>

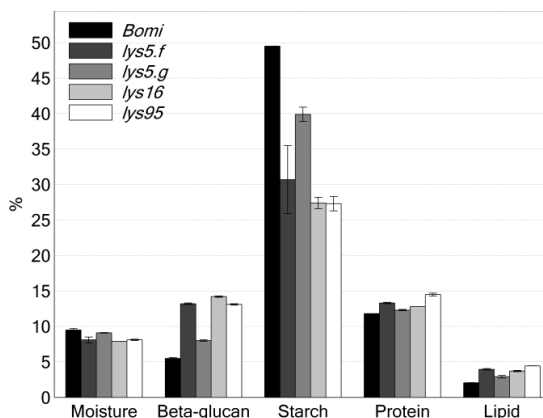


Figure 3. The content of moisture,  $\beta$ -glucan, starch, protein and lipid in the five barley genotypes.

The second derivative of the spectra of barley endosperm in Figure 4a showed absorbance bands (depicted as valleys) at 2287 nm, 2311 nm, 2325 nm and 2349 nm. The covarygram shown in Figure 4b shows the correlation between the absorbance at each wavelength and the content of moisture,  $\beta$ -glucan, starch, protein and lipid. Since an increased absorbance is shown as a valley in the second derivative spectrum then a Pearson correlation coefficient of -1 will in this case mean that the absorbance and reference measure are positively correlated. It can therefore be seen that the starch and moisture content has a positive correlation with the wavelengths at 2287 nm and 2325 nm. Whereas the content of lipid, protein and  $\beta$ -glucan is positively correlated with the absorbance bands at 2311 nm and 2349 nm.

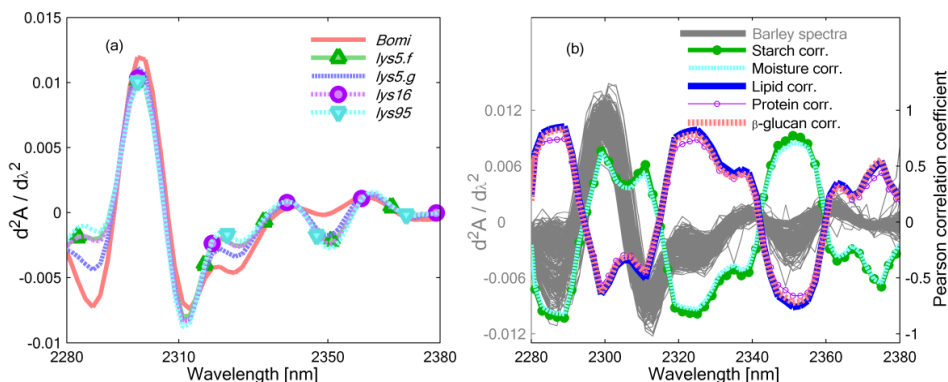


Figure 4. (a) Average second derivative spectrum for each barley genotype. (b) The second derivative spectrum shown together with the Pearson correlation coefficient calculated between each wavelength and the content of moisture,  $\beta$ -glucan, starch, protein and lipid.

The spectra of barley endosperm were compared with the oil spectra in order to investigate the influence from lipids. In Figure 5 the absorbance bands of barley and sunflower oil have their valley minimum at slightly lower wavelengths compared to the mineral oil. So the barley and sunflower oils have absorbance bands at 2312 nm and 2351 nm, and the mineral oil has absorbance bands at 2313 nm and 2352 nm. Since the absorbance bands of the oils are placed

very close to the absorbance bands in the spectra of barley endosperm it is possible that C-H vibrations from either lipids, proteins or  $\beta$ -glucans can absorb in this region. However, since the endosperm contains more starch and  $\beta$ -glucan, and less lipid and protein compared to the average content in the whole seed then it is more likely that the endosperm spectra contain information of starch at 2287 nm and 2325 nm and information on  $\beta$ -glucan at 2311 nm and 2349 nm.<sup>6,7</sup> This interpretation is in agreement with the assignment in the literature.<sup>8-10</sup>

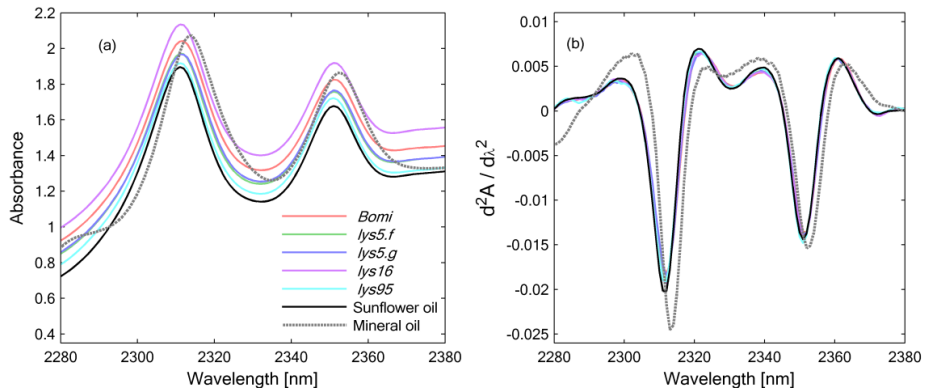


Figure 5. (a) Raw averaged oil spectra. (b) Second derivative oil spectra.

## Conclusion

It was possible to apply a supercontinuum laser in NIR transmission measurements in the region from 2260–2380 nm of one mm barley endosperm. This proof-of-concept opens the possibility to go further and measure on whole seeds. This technology could potentially be used in fast and non-destructive measurements of  $\beta$ -glucans and perhaps even more inferior compounds in intact seeds with regard to quality sorting or in plant breeding.

## Acknowledgments

The authors wish to acknowledge the generous financial support from The Danish National Advanced Technology Foundation (now Innovation Fund Denmark) to the project entitled “Light & Food”.

## References

1. Schmidt, J.; Gergely, S.; Schönlechner, R.; Grausgruber, H.; Tömösközi, S.; Salgó, A.; *Cereal Chemistry*, **2009**, 86, 398–404.
2. Seefeldt, H.F.; Blennow, A.; Jespersen, B.M.; Wollenweber, B.; Engelsens, S.B.; *Journal of Cereal Science*, **2009**, 49, 24–31.
3. Wood, P.J.; *Journal of Cereal Science*, **2007**, 46, 230–238.
4. Ringsted, T.; Dupont, S.; Ramsay, J.; Jespersen, B.M.; Sørensen, K.M.; Keiding, S.R.; Engelsens, S.B.; *Applied Spectroscopy*, in press.
5. Munck, L.; Møller, B.; Jacobsen, S.; Søndergaard, I.; *Journal of Cereal Science*, **2004**, 40, 213–222.
6. Chandra, G.S.; Proudlove, M.O.; Baxter, E.D.; *Journal of the Science of Food and Agriculture*, **1999**, 79, 37–46.
7. Neuberger, T.; Sreenivasulu, N.; Rokitta, M.; Rolletschek, H.; Göbel, C.; Rutten, T.; Radchuk, V.; Feussner, I.; Wobus, U.; Jakob, P.; Webb, A.; Borisjuk, L.; *Plant Biotechnology Journal*, **2008**, 6, 31–45.
8. Osborne, B.G.; Fearn, T.; Hindle, P.H.; *Practical NIR Spectroscopy, with applications in food and beverage analysis*, Harlow, UK, Longman Scientific and Technical, **1993**. 2<sup>nd</sup> ed.
9. Czuchajowska, Z.; Szczodrak, J.; Pomeranz, Y.; *Cereal Chemistry*, **1992**, 69, 413–418.
10. Horvath, L.; Norris, K.H.; Horvathmosonyi, M.; Rigo, J.; Hegedusvolgyesi, E.; *Acta Alimentaria*, **1984**, 13, 355–382.

---

# Posters

---



# 2D NIR-MIR correlation spectroscopy

## A useful tool to augment the interpretation of NIR spectra

T. Ringsted<sup>1</sup>, S. Dupont<sup>2</sup>, J. Ramsay<sup>2</sup>, S.R. Keiding<sup>2</sup>, S.B. Engelsen<sup>1</sup>

<sup>1</sup> Department of Food Science, University of Copenhagen, Rolighedsvej 26, 1958 Frederiksberg, Denmark

<sup>2</sup> Department of Chemistry, Aarhus University, Langelandsgade 140, 8000 Aarhus, Denmark

### Background

Barton and co-workers developed a two-dimensional technique where the correlation coefficients between near- and mid-infrared spectra are mapped in order to show how the fundamental molecular vibrations in the mid-infrared (MIR) region relates with the overtones and combination bands observed in the near-infrared (NIR).<sup>1</sup>

C-H<sub>2</sub>, C-H<sub>3</sub> and C=C bonds are important components of oils. C-H vibrations appear in both near- and mid-infrared and it is therefore possible to study how the fundamental vibrations continue into overtones and combination bands.

Bread staling is when consumer acceptance of bakery products are decreasing because of changes in the crumb and not by microorganisms. Bread ageing have been studied with infrared spectroscopy at wavenumbers which were associated with ordered starch (1047 cm<sup>-1</sup>) and amorphous starch (1022 cm<sup>-1</sup>). However, studies on bread staling by infrared spectroscopy are few and only two time points were measured.<sup>2,3</sup>

### Aim

This study presents 2D NIR-MIR correlation spectra of C-H vibrations in oil and the bread crump staling process.

### Instrument

The NIR spectra were collected in the range between 400-2500 nm using a NIR systems spectrometer model 6500 (NIR systems, Inc., Silver Springs, USA). The oils were measured in transmission mode in a 4 mm quartz cuvette and the bread samples were measured in reflectance mode. MIR spectra were collected in the range 4000-400 cm<sup>-1</sup> using a Bomem Arid-Zone MB100 FT-IR (Bomem, Quebec, Canada) interferometer equipped with an attenuated total reflectance (ATR) unit.

### Samples

48 purchased oils extracted from olives (originating from Italy, Spain, Portugal, Greece, Palestine, Tunisia), rapeseeds, sunflower seeds, sesame seeds, safflower seeds, hemp seeds, grape seeds, pumpkin seeds, rose hip seeds, linseeds, cummin, argan kernels, apricot kernels, peanuts, almonds, macadamia nuts, walnuts, hazelnuts, pecan nuts, pistachio nuts, soya beans, rice, corn, fish, cod liver.

10 identical wheat breads were made and one new bread was measured after 1, 2, 5, 6, 7, 12, 14, 19, 21 and 23 days. Each bread was measured on three slices and these three spectra were averaged in order to cover the variation within a bread.

### Acknowledgements

The authors wish to acknowledge the generous financial support from The Danish National Advanced Technology Foundation (now Innovation Fund Denmark) to the project entitled "Light & Food".

### Conclusion

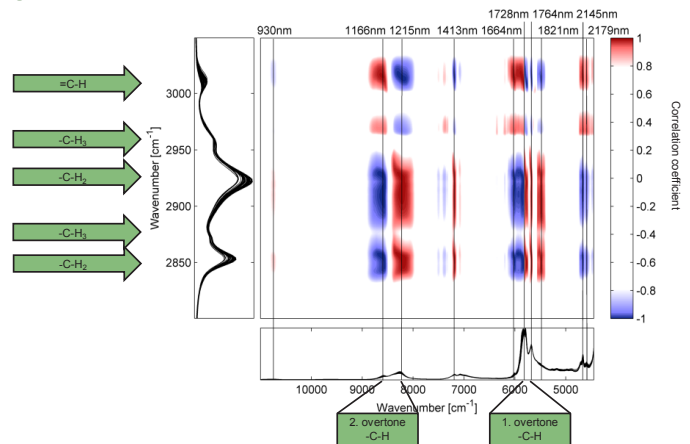
It was possible with 48 different oils to retrieve high correlation coefficients between the C-H vibrations in the mid-infrared and the overtones and combination bands in the near-infrared.

The first continuous measurements of bread aging were performed with near- and mid-infrared spectroscopy.

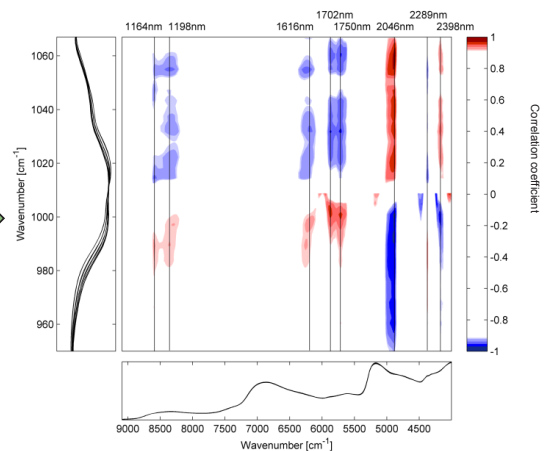
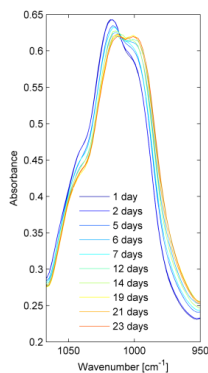
The bread spectra showed that the peaks at 999, 1018 and 1043 cm<sup>-1</sup> changed during bread storage.

### Results

1 Correlation coefficients for 48 vegetable, seed, nut and fish oils measured by near- and mid-infrared spectroscopy showed high values between fundamental C-H vibrations and their overtones and combination bands.



2 The bread spectra changed from 1 day to 23 days after baking. A decrease in absorbance was seen at 1018 and 1043 cm<sup>-1</sup>, and an increase was seen at 999cm<sup>-1</sup>. The correlation coefficients between near- and mid-infrared showed high values at the 1. and 2. overtones of C-H and combination bands.



### References:

1. F.E. Barton II, D.S. Himmelsbach, J.H. Duckworth & M.J. Smith, Two-dimensional vibration spectroscopy: correlation of mid- and near-infrared regions, *Applied Spectroscopy* (1992) 46, 420-429.
2. O. Sevenou, S.E. Hill, I.A. Farhat & J.R. Mitchell, Organisation of the external region of the starch granule as determined by infrared spectroscopy, *International Journal of Biological Macromolecules* (2002) 31, 79-85.
3. R.H. Wilson & P.S. Belfon, A Fourier-transform infrared study of wheat starch gels, *Carbohydrate Research* (1968) 180, 339-344.

# Near-infrared spectroscopy using a supercontinuum laser. Application to long-wavelength transmission spectra of barley seeds

T. Ringsted<sup>1</sup>, S. Dupont<sup>2</sup>, J. Ramsay<sup>2</sup>, S.R. Keiding<sup>2</sup>, S.B. Engelsen<sup>1</sup>

<sup>1</sup> Department of Food Science, University of Copenhagen, Rolighedsvej 26, 1958 Frederiksberg, Denmark

<sup>2</sup> Department of Chemistry, Aarhus University, Langelandsgade 140, 8000 Aarhus, Denmark

## Background

The supercontinuum laser is a new type of light source, which combines the coherent light properties of a laser with a broad spectral region.<sup>1</sup> This makes it possible to focus the light onto small samples like seeds without losing intensity and facilitate either rapid or high-precision measurements.

Barley and wheat seeds have only been studied by near-infrared (NIR) transmission in the short wavelength region up to 1100 nm. However, the long-wavelength region from 2260–2380 nm have previously shown to be particularly useful in differentiating barley phenotypes by using NIR spectroscopy in reflectance mode.<sup>2</sup>

$\beta$ -glucans are a type of fibre which is present in e.g. seeds.  $\beta$ -glucans in barley have been found to have health promoting effects but they can also cause problems in brewing processes.  $\beta$ -glucans are not well predicted in the wavelength range from 850–1050 nm, so measurements of whole seeds by long-wavelength transmission NIR spectroscopy could lead to new possibilities in ultra-fast screening of  $\beta$ -glucan.

## Aim

The aim of the present study was to establish an apparatus that provided advantageous working conditions for the supercontinuum laser and at the same time to investigate its capability to measure the barley endosperm by transmission experiments in the NIR long-wavelength region.

## Instrument

An experimental spectrometer was developed consisting of a supercontinuum laser source (NKT Photonics), a dispersive monochromator and a PbSe detector (see Figure 1)

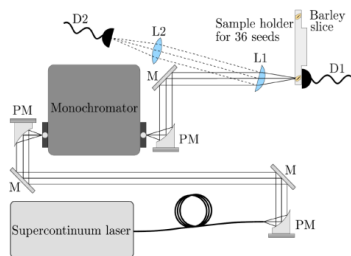


Figure 1. The supercontinuum source is launched from a fiber onto an off-axis parabolic mirror (PM) for collimation. The light is then guided by silver mirrors (M) and focused by another PM into a grating monochromator for wavelength selection. The narrow-band light is subsequently collimated with a PM before it is focused by a plano-convex CaF<sub>2</sub> lens (L1) onto the barley grain of interest. A PbSe detector (D1) is used for detection of the transmitted light. The plano-convex lens (L1) is tilted at a small angle, and the back-reflection is used as a reference, which is focused by the CaF<sub>2</sub> lens (L2) onto another PbSe detector (D2).

## Samples

350 seeds from five barley genotypes were measured in 100  $\mu$ m slices by NIR transmission from 2235–2381 nm. One barley genotype was 'normal' (Bomi) and the other four genotypes were high  $\beta$ -glucan mutants (*lys5.f*, *lys5.g*, 16 and 95). Oils from the same five barley genotypes were measured in a cuvette with a 100  $\mu$ m path length from 2003–2497 nm.

In order to increase spectral interpretation the content of moisture,  $\beta$ -glucan, starch, protein and lipid was determined for each barley genotype and the fatty acid composition were measured by GC-MS for the five barley oils.

## Acknowledgements

The authors wish to acknowledge the generous financial support from The Danish National Advanced Technology Foundation (now Innovation Fund Denmark) to the project entitled 'Light & Food'.

## Conclusion

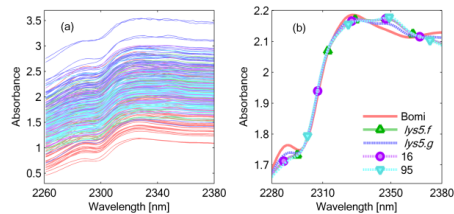
The first measurements of barley seeds by long-wavelength NIR transmission spectroscopy were performed. In future studies it is possible to improve the experimental setup with a stronger supercontinuum laser and a better suited detector which might lead to measurements on whole seeds instead of slices.

For the measurements on barley slices, this study supports the correlation between the peaks at 2287 and 2323 nm to starch, and the peak at 2349 nm to lipid and  $\beta$ -glucan content. However, it cannot be excluded that cellulose is contributing to the absorbance at 2323 and 2349 nm.

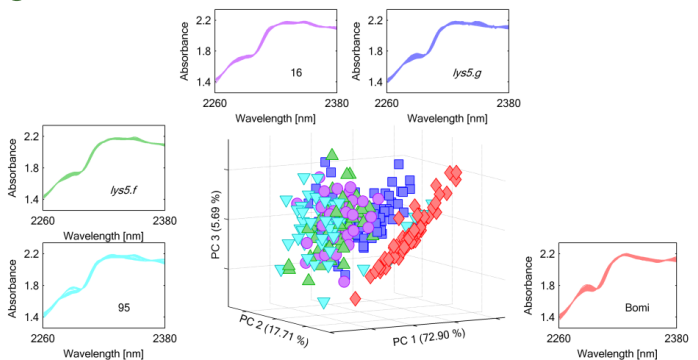
The barley oil samples showed peaks at about the same wavelengths as the barley slices. From the literature it was found that the oil peaks at 2289, 2327 and 2349 nm was due to CH<sub>2</sub>, CH<sub>3</sub> and HC=CHCH<sub>2</sub> vibrations, respectively.

## Results

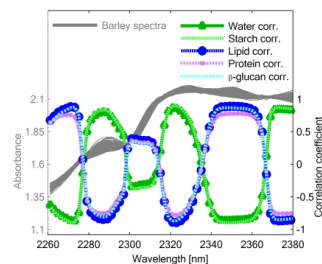
- 1 (a) Raw spectra from 279 barley slices and (b) the average spectra after preprocessing with extended multiplicative scatter correction (EMSC)



- 2 Finding differences and similarities between five barley genotypes with principal component analysis (PCA)



- 3 Interpreting the spectra by correlating with the content of moisture, starch, lipid, protein and  $\beta$ -glucan.<sup>3</sup>



## References:

- J. M. Dudley, G. Genty & S. Coen, Supercontinuum generation in photonic crystal fiber, *Reviews of Modern Physics* (2006), 78, 1135–1184.
- H.F. Seefeldt, A. Blennow, B.P. Møller, B. Wollenweber & S.B. Engelsen, Accumulation of mixed linkage (1 $\rightarrow$ 3)(1 $\rightarrow$ 4)-D- $\beta$ -glucan during grain filling in barley - A vibrational spectroscopy study, *Journal of Cereal Science* (2009), 49(1), 24–31.
- T. Skov, A.H. Honoré, H.M. Jensen, T. Næs, S.B. Engelsen, Chemometrics in foodomics: Handling data structures from multiple analytical platforms, *TRAC-Trends in Analytical Chemistry* (2014), 60, 71–79.

# 2D NIR-MIR correlation spectroscopy

## A useful tool to augment the interpretation of NIR spectra

T. Ringsted<sup>1</sup> and S.B. Engelsen<sup>1</sup>

<sup>1</sup> Department of Food Science, University of Copenhagen, Rolighedsvej 26, 1958 Frederiksberg, Denmark

### Background

Barton and co-workers developed a two-dimensional technique where the correlation coefficients between near- and mid-infrared spectra are mapped in order to show how the fundamental molecular vibrations in the mid-infrared (MIR) region relates with the overtones and combination bands observed in the near-infrared (NIR).<sup>1</sup>

### Application – Bread staling

Several chemical and physical changes occurs in bread during storage. Bread staling is a term used to describe when consumer acceptance of bakery products are decreasing because of hardness changes in the crumb and not by microorganisms. Bread staling has been studied with infrared spectroscopy at wavenumbers which were associated with ordered starch (1047 cm<sup>-1</sup>) and amorphous starch (1022 cm<sup>-1</sup>).<sup>2,3</sup> Few studies have investigated bread staling with NIR and the spectral information on ordered and amorphous starch has not been located in the NIR spectra.<sup>4</sup> This study presents 2D NIR-MIR correlation spectroscopy of the bread crumb staling process in white wheat bread. The aim is to use knowledge from the MIR to increase the interpretation of the NIR.

### Data

13 identical white wheat breads were made and one new bread was measured after 4, 6, 23, 24, 25, 27, 29, 47, 48, 49, 53, 120 and 168 hours. Each bread had the crumb measured on three slices and these three spectra were averaged in order to cover the variation within one bread. The NIR spectra were collected in reflectance mode in the range between 400-2500 nm using a NIR systems spectrometer model 6500 (NIR systems, Inc, Silver Springs, USA). MIR spectra were collected in the range 4000-400 cm<sup>-1</sup> using a Bomem Arik-Zone MB100 FT-IR (Bomem, Quebec, Canada) interferometer equipped with an attenuated total reflectance (ATR) unit. The spectra were preprocessed with extended multiplicative scatter correction (EMSC) and mean centered. The Pearson correlation coefficients were calculated between each wavenumber in the NIR and MIR spectra.

### Acknowledgements

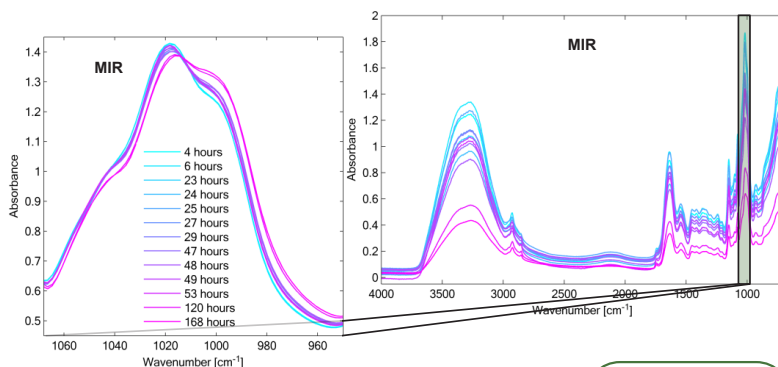
The authors wish to acknowledge the generous financial support from The Danish National Advanced Technology Foundation (now Innovation Fund Denmark) to the project entitled "Light & Food". Thanks also goes to Novozymes A/S for preparing the bread.

### Conclusions

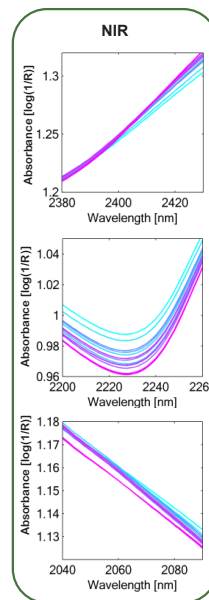
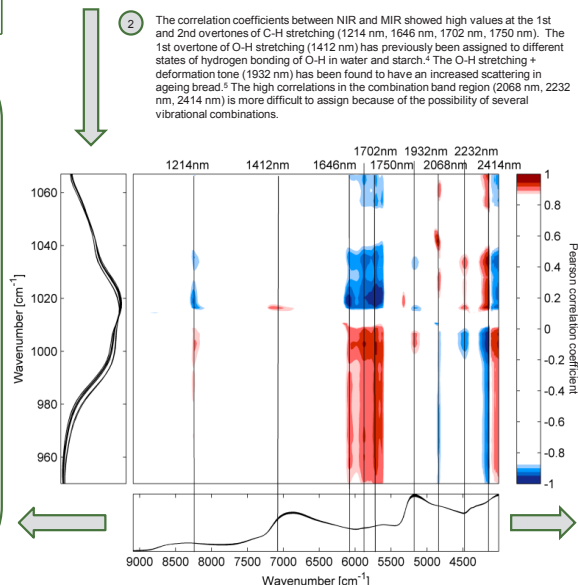
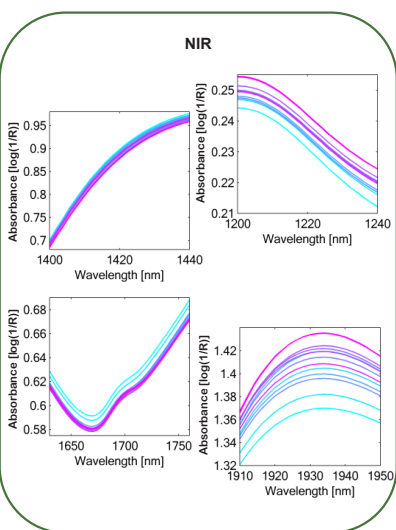
The bread crumb spectra showed that the MIR peaks at 999, 1018 and 1043 cm<sup>-1</sup> change during bread storage. The information about starch ordering in these MIR peaks was searched for in the NIR by 2D correlation spectroscopy. High correlations were found between the MIR peaks and overtones of C-H and O-H stretching vibrations as well as in combination bands of the NIR spectra. The high correlations is caused by changes in the number and strength of hydrogen bonds between hydroxyl groups in starch and water as well as physical changes caused by an increased scattering from the hardened (more crystalline) bread.

### Results

1 The bread crumb spectra from 950-1070 cm<sup>-1</sup> was selected because it contains information on ordered (crystalline amylopectin) and amorphous starch. During bread storage, a decrease was observed in the MIR spectra at 1018 and 1043 cm<sup>-1</sup>, and an increase was observed at 999cm<sup>-1</sup>.



2 The correlation coefficients between NIR and MIR showed high values at the 1st and 2nd overtones of C-H stretching (1214 nm, 1646 nm, 1702 nm, 1750 nm). The 1st overtone of O-H stretching (1412 nm) has previously been assigned to different states of hydrogen bonding of O-H in water and starch.<sup>4</sup> The O-H stretching + deformation tone (1932 nm) has been found to have an increased scattering in ageing bread.<sup>5</sup> The high correlations in the combination band region (2068 nm, 2232 nm, 2414 nm) is more difficult to assign because of the possibility of several vibrational combinations.



### References:

1. F.E. Barton II, D.S. Himmelsbach, J.H. Duckworth & M.J. Smith, Two-dimensional vibration spectroscopy: correlation of mid- and near-infrared regions, *Applied Spectroscopy* (1992) 46, 420–429.
2. O. Sevenou, S.E. Hill, I.A. Farhat & J.R. Mitchell, Organisation of the external region of the starch granule as determined by infrared spectroscopy, *International Journal of Biological Macromolecules* (2002) 31, 79–85.
3. R.H. Wilson & P.S. Belton, A Fourier-transform infrared study of wheat starch gels, *Carbohydrate Research* (1988) 180, 339–344.
4. B.G. Osborne, Near infrared spectroscopic studies of starch and water in some processed cereal foods, *Journal of Near Infrared Spectroscopy* (1996) 4, 195–200.
5. R.H. Wilson, B.J. Goodfellow & P.S. Belton, Comparison of Fourier Transform Mid Infrared Spectroscopy and Near Infrared Reflectance Spectroscopy with Differential Scanning Calorimetry for the Study of the Staling of Bread, *Journal of the Science of Food and Agriculture* (1991) 54, 471–483.

# Near-infrared spectroscopy using a supercontinuum laser

## Application to long-wavelength transmission spectra of barley seeds

T. Ringsted<sup>1</sup>, S. Dupont<sup>2</sup>, J. Ramsay<sup>2</sup>, B.M. Jespersen<sup>1</sup>, S.R. Keiding<sup>2</sup>, S.B. Engelsen<sup>1</sup>  
<sup>1</sup> Department of Food Science, University of Copenhagen, Rolighedsvej 26, 1958 Frederiksberg, Denmark  
<sup>2</sup> Department of Chemistry, Aarhus University, Langelandsgade 140, 8000 Aarhus, Denmark



### Background

The supercontinuum laser is a new type of light source, which combines the coherent light properties of a laser with a broad spectral region.<sup>1</sup> This makes it possible to focus the light onto small samples like seeds without losing intensity and facilitate either rapid or high-precision measurements.

Barley and wheat seeds have only been studied by near-infrared (NIR) transmission in the short wavelength region up to 1100 nm. However, the long-wavelength region from 2260-2380 nm have previously shown to be particularly useful in differentiating barley phenotypes by using NIR spectroscopy in reflectance mode.<sup>2</sup>

$\beta$ -glucans are polysaccharide fibres which are present in e.g. seeds.  $\beta$ -glucans in barley have been found to have health promoting effects, but they can also cause problems in the brewing processes.  $\beta$ -glucans are not well predicted in the wavelength range from 850-1050 nm, so measurements of whole seeds by long-wavelength transmission NIR spectroscopy could lead to new possibilities in ultra-fast screening of  $\beta$ -glucan content.

### Aim

The aim of the present study was to establish an apparatus that provided advantageous working conditions for the supercontinuum laser and at the same time to investigate its capability to measure the barley endosperm by transmission experiments in the NIR long-wavelength region.

### Instrument

An experimental spectrometer was developed consisting of a supercontinuum laser source (NKT Photonics), a dispersive monochromator and a PbSe detector (see Figure 1)

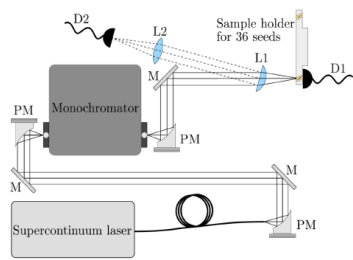


Figure 1. The supercontinuum source is launched from a fiber onto an off-axis parabolic mirror (PM) for collimation. The light is then guided by silver mirrors (M) and focused by another PM into a grating monochromator for wavelength selection. The narrow-band light is subsequently collimated with a PM before it is focused by a plano-convex CaF<sub>2</sub> lens (L1) onto the barley grain of interest. A PbSe detector (D1) is used for detection of the transmitted light. The plano-convex lens (L1) is tilted at a small angle, and the back-reflection is used as a reference, which is focused by the CaF<sub>2</sub> lens (L2) onto another PbSe detector (D2).

### Samples

A total of 105 intact whole seeds from five different barley genotypes were measured three times each by NIR transmission from 2255-2381 nm. One barley genotype was "normal" (Boni) and the other four genotypes were high  $\beta$ -glucan mutants (*lys5.f*, *lys5.g*, *lys16* and *lys95*). Subsequently the content of  $\beta$ -glucan and protein was measured for each individual barley seed.

The 315 spectra were preprocessed with extended multiplicative scatter correction (EMSC)<sup>3</sup> and mean centered before multivariate data analysis. Partial least squares (PLS) regression was applied in order to predict the content of  $\beta$ -glucan and protein. Spectra from 62 spectral outliers were removed before modeling and 253 spectra was therefore used in this analysis.

### Acknowledgements

The authors wish to acknowledge the generous financial support from the IDRC Travel Award and the Danish National Advanced Technology Foundation (now Innovation Fund Denmark) to the project entitled "Light & Food".

### References:

- J. M. Dudley, G. Genty & S. Coen, Supercontinuum generation in photonic crystal fiber. *Reviews of Modern Physics* (2006), 78, 1135–1184.
- H.F. Seefeldt, A. Blennow, B.P. Møller, B. Wollenweber & S.B. Engelsen, Accumulation of mixed linkage (1→3)-(1→4)-D- $\beta$ -glucan during grain filling in barley - A vibrational spectroscopy study. *Journal of Cereal Science* (2009), 49(1), 24-31.
- H. Martens, J.P. Nielsen & S.B. Engelsen, Light Scattering and Light Absorbance Separated by Extended Multiplicative Signal Correction. Application to Near-Infrared Transmission Analysis of Powder Mixtures, *Analytical Chemistry* (2003) 75, 394-40
- T. Ringsted, S. Dupont, J. Ramsay, B.M. Jespersen, K. M. Sørensen, S.R. Keiding, S.B. Engelsen, Near-Infrared Spectroscopy Using a Supercontinuum Laser: Application to Long Wavelength Transmission Spectra of Barley Endosperm and Oil. *Applied Spectroscopy* (2016) 70, 1176–1185.

### Conclusion

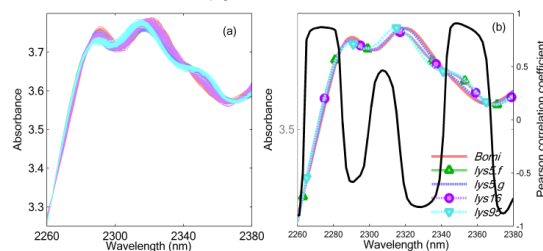
This preliminary study include the first measurements of whole intact barley seeds by long-wavelength NIR transmission spectroscopy.

In a previous study, a correlation was found between the starch content and the absorbance peaks at 2289 and 2319 nm, and between the  $\beta$ -glucan content and the absorbance peak at 2349 nm. The seed protein content also showed a correlation albeit weaker to the absorbance peak at 2349 nm.<sup>4</sup>

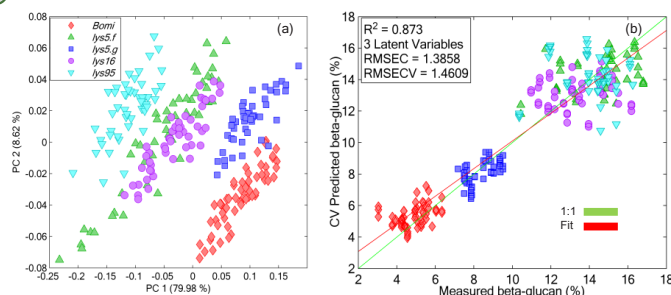
The present study, demonstrate that it is possible to predict the  $\beta$ -glucan content from the long-wavelength NIR spectra with a prediction error of only approximately 1.5%. This method has great potential for being used as a new efficient barley breeding technique or even as a fast single seed sorting sensor.

### Results

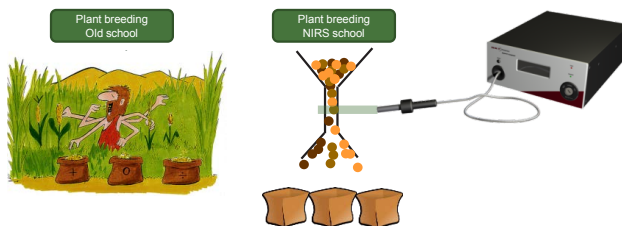
- 1 (a) EMSC preprocessed spectra from barley seeds and (b) the average EMSC preprocessed spectra of each barley phenotype together with Pearson's correlation coefficient to the  $\beta$ -glucan content.



- 2 (a) A PCA model on the EMSC preprocessed spectra and (b) a PLS model predicting the content of  $\beta$ -glucan.



### Outreach – Future applications



# 2D NIR-MIR covariance spectroscopy

## Augmenting the interpretation of NIR spectra of bread staling

T. Ringsted<sup>1</sup> and S.B. Engelsen<sup>1</sup>

<sup>1</sup> Department of Food Science, University of Copenhagen, Rolighedsvej 26, 1958 Frederiksberg, Denmark

### Background

Two-dimensional (2D) correlation spectroscopy combining near- and mid-infrared spectra shows how the fundamental molecular vibrations in the mid-infrared (MIR) region relates with the overtones and combination bands observed in the near-infrared (NIR).<sup>1,2</sup> By this method, the chemical information in the MIR spectra can be used to augment the interpretation and discover important wavelength regions in the NIR spectra.

### Application – Bread staling

Bread staling is presumably responsible for the largest single source of food waste with a significant global environmental footprint. Several chemical and physical changes occurs in bread during storage. Bread staling is a term used to describe changes in bakery product which cause a decreasing consumer acceptance because of non-microbial processes. Bread staling has been studied with infrared spectroscopy at wavenumbers which were associated with recrystallization of amylopectin (1047 cm<sup>-1</sup>) and amorphous starch (1022 cm<sup>-1</sup>).<sup>3</sup> A few studies have investigated bread staling with NIR spectroscopy and most of them have used raw spectra which contain both chemical and physical information.<sup>4,5</sup> This study presents 2D NIR-MIR correlation spectroscopy of the bread crumb staling process in white wheat bread. The aim is to use *a priori* knowledge from the MIR spectra to increase the chemical interpretation of the changes that happen in the NIR spectra.

### Data

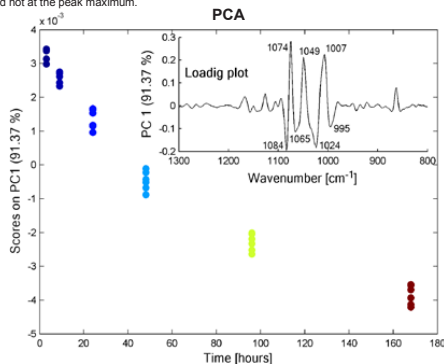
Twelve wheat breads packed in vacuum bags and stored at ambient temperature were measured with both NIR and MIR spectroscopy. Two loaves were measured at 3 hours, 9 hours, 1, 2, 4, and 7 days after baking. Three bread slices from each of the two breads resulted in 6 measurements at each time point. The NIR spectra were collected in reflectance mode in the range between 400-2500 nm using a NIRSystems spectrometer model 6500 (NIRSystems, Inc., Silver Springs, USA). MIR spectra were collected in the range 4000-400 cm<sup>-1</sup> using a Bomem Aird-Zone MB100 FT-IR (Bomem, Quebec, Canada) equipped with an attenuated total reflectance (ATR) unit. Before calculating the 2D correlation spectrum the spectra were preprocessed with extended multiplicative scatter correction (EMSC)<sup>6</sup> and mean centered. The 2D correlation spectroscopy plots were calculated as the covariance between NIR and MIR.

### Acknowledgements

The authors wish to acknowledge the generous financial support from the IDRC Travel Award and the Danish National Advanced Technology Foundation (now Innovation Fund Denmark) to the project entitled "Light & Food". Thanks also goes to Novozymes A/S for preparing the bread.

### Figure 2

A PCA on MIR spectra preprocessed with Savitzky-Golay 2. derivative showed a clear separation between different storage times. From the loading plot it was seen that old bread had a lower 2. derivative absorbance at 1074, 1049 and 1007 cm<sup>-1</sup>. The lower 2. derivative at 1074 and 1007 cm<sup>-1</sup> is caused by peak shifts. This can also be seen in Fig. 3 where there is high covariance with opposite signs at the peak sides and not at the peak maximum.



### Conclusions

The bread crumb spectra show that the MIR peaks at 1005, 1020 and 1049 cm<sup>-1</sup> change as a function of bread storage. A PCA on the MIR spectra show very systematic differences along PC1 according to the bread storage time. The information about starch ordering in these MIR peaks was searched for in the NIR by 2D correlation spectroscopy. High correlations were found between the MIR peaks and overtones of the OH stretching vibrations of the NIR spectra. The high correlations are caused by changes in the number and strength of hydrogen bonds between hydroxyl groups in starch and water caused by a more crystalline bread structure.

### Results

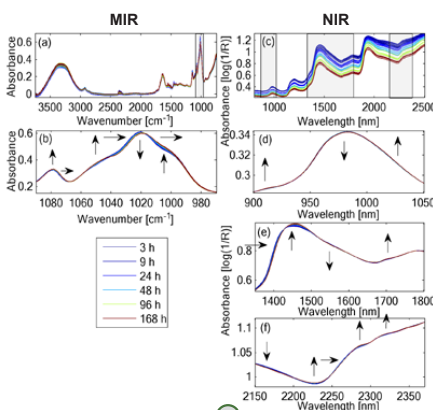
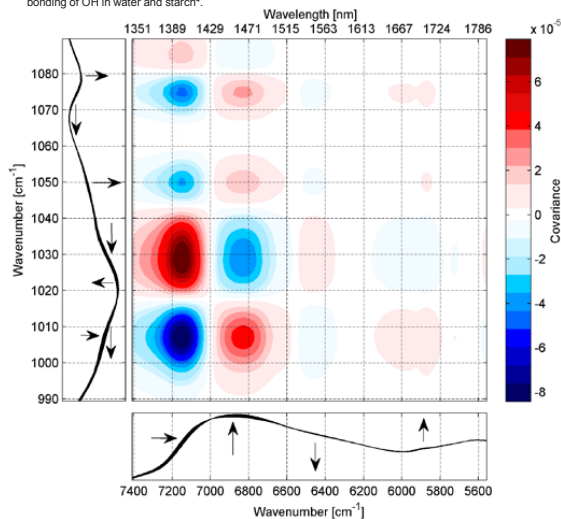


### Figure 1

From the raw MIR spectra of the bread crumb (Fig. 1a) the region from 970-1090 cm<sup>-1</sup> was selected because it contains information on ordered (crystalline amylopectin) and amorphous starch. The EMSC preprocessed spectra in Fig. 1b show that during bread storage, a decrease is observed in the MIR spectra at 1020 cm<sup>-1</sup>, and an increase is observed at 1049 and 1005 cm<sup>-1</sup>. The raw NIR spectra in Fig. 1c show a decreasing absorbance at all wavelengths from 3-168 hours after baking. Fig. 1d,e,f shows the NIR spectra after preprocessing with EMSC. The movement of water from crumb to crust is observed as a decrease at the 2. overtone of OH stretching at 980 nm, a shift at the 1. OH overtone at 1413 nm, and a fall in absorbance at the 1. OH overtone at 1540 nm. An increase in the concentration of starch, protein and fat is observed from the rise of the 3. overtone of CH stretching at 915 nm, a CH combination band at 1014 nm, the 1. overtone of OH in starch at 1466 nm, 1. overtone of CH at 1700 nm, and CH combination bands at 2262 nm and 2315 nm.

### Figure 3

The covariance between NIR and MIR spectra show high values at the 1. overtones of OH stretching (1413 nm, 1466 nm, 1540 nm). The 1. overtone of OH stretching has previously been assigned to different states of hydrogen bonding of OH in water and starch<sup>7</sup>.



### References:

1. F.E. Barton II, D.S. Himmelsbach, J.H. Duckworth & M.J. Smith, Two-dimensional vibration spectroscopy: correlation of mid- and near-infrared regions, *Applied Spectroscopy* (1992) 46, 420-429.
2. Noda, I., Ozaki, Y., Two-Dimensional Correlation Spectroscopy - Applications in Vibrational and Optical Spectroscopy, John Wiley & Sons, Weinheim (2004).
3. van Soest, J.J.G., Tournois, H., de Wit, D., Vliegthart, J.F.G., Short-range structure in (partially) crystalline potato starch determined with attenuated total reflectance Fourier-transform IR spectroscopy, *Carbohydrate Research* (1995) 279, 201-214.
4. B.G. Osborne, Near infrared spectroscopic studies of starch and water in some processed cereal foods, *Journal of Near Infrared Spectroscopy* (1996) 4, 195-200.
5. R.H. Wilson, B.J. Goodfellow & P.S. Betton, Comparison of Fourier Transform Mid Infrared Spectroscopy and Near Infrared Spectroscopy with Differential Scanning Calorimetry for the Study of the Staling of Bread, *Journal of the Science of Food and Agriculture* (1991) 54, 471-483.
6. H. Martens, J.P. Nielsen & S.B. Engelsen, Light Scattering and Light Absorbance Separated by Extended Multiplicative Signal Correction. Application to Near-Infrared Transmission Analysis of Powder Mixtures, *Analytical Chemistry* (2003) 75, 394-404.

TINE RINGSTED

## Near infrared spectroscopy of food systems using a supercontinuum laser

---



The fast and non-destructive features of near-infrared spectroscopy makes it a very useful technology for measurements of the chemical composition of food products. The supercontinuum laser is a new light source that combines the collimated beam of a laser with the broad range of wavelengths of a lamp. The supercontinuum laser is therefore different from the traditional lamps used for near-infrared spectroscopy because of its spatially coherent beam. This work set out to find possible food products that would benefit from the collimated beam of the supercontinuum laser. The chemical information retrieved from near-infrared spectroscopy can sometimes be difficult to interpret. An

additional goal was therefore to increase the spectral interpretation by correlating different near- and mid-infrared information.

The advantages of the supercontinuum laser compared to a traditional infrared lamp were investigated in three cases. (1) The supercontinuum laser was used to measure  $\beta$ -glucan through intact single barley seeds at previously un-used near-infrared wavelengths. (2) The possible gas measurements of food products were reviewed and the collimated beam was thought to give new opportunities. (3) The supercontinuum laser was combined with a 10.6 km long silica fiber to produce a new type of spectrometer. The new spectrometer showed that it can measure sugar in water and melamine in milk powder. More studies of the new spectrometer are needed to determine the possibilities for quantitative measurements.

Bread hardness is one of the unwanted processes in aging bread and near- and mid-infrared spectroscopy was used to follow this parameter. The interpretation of the near-infrared spectra was increased by correlating well-known mid-infrared information on aging bread with less understood near-infrared information and bread hardness.